I. CONSTITUTIVE RELATIONS FOR A GRANULAR MATERIAL

II. THE DISTRIBUTION OF STRESSES AND DEVELOPMENT OF FAILURE AT THE TOE OF A SLOPE AND AROUND THE TIP OF A CRACK

Thesis by

Tyzz-Dwo Lu

In Partial Fulfillment of the Requirements

For the Degree of

Doctor of Philosophy

California Institute of Technology

Pasadena, California

1973

(Submitted August 11, 1972)

ACKNOWLEDGMENTS

ABSTRACT

In the first part of this thesis, a three-dimensional rheological model was constructed to represent the deformation behavior of a granular material. The constitutive relations for a granular material were subsequently derived. The rheological model was conceived from the observed behavior of granular material from laboratory experiments and from theoretical considerations. The constitutive relations were expressed in incremental forms to account for the stress history and loading path dependency of a granular material's behavior, such as non-linearity, initial or induced anisotropy, history and path dependency, and shear dilatance.

The qualitative and quantitative behavior of a granular material such as sand under shear stress from experimental results and from the proposed constitutive relations was examined and compared. It was found that the experimental data and the proposed constitutive relations were in close agreement.

Due to the number of parameters involved, and the non-symmetrical resulting stiffness matrix in a general stress-strain formulation, it is difficult to apply the proposed constitutive in a finite element computer formulation at the present state of the art. Consequently the application of finite element methods to non-linear problems was examined in more detail as a preliminary step. The effect, or the results of the material properties, the finite element mesh size and the computational procedure was examined in detail in Part II of this thesis.

TABLE OF CONTENTS

FIGURES FOR PART I

Figure No.		Page

List of Figures in Part II

List of Figures in Part II (Cont'd.)

PART I

CONSTITUTIVE RELATIONS FOR A GRANULAR MATERIAL

CHAPTER I

INTRODUCTION AND SCOPE OF RESEARCH

I.1 Prelude

Until several years ago, nearly all the investigators in soil mechanics paid little or no attention to the general stress-strain behavior in real soils and devoted their studies almost exclusively to the peak or ultimate strengths of soils. The soils behavior was assumed to be linear up to the ultimate strength. As a consequence in classical soil mechanics, problems of stress distribution and deformation have generally been solved on the basis of linear elasticity theory [1] and problems associated with stability and limit equilibrium have been examined assuming soil to be a rigid-plastic material [2]. This school of thought was advocated by Terzaghi [2] and has dominated soil engineering in practice, despite the known fact that soil's behavior is neither linearly elastic nor has a constant yield stress after the point of failure is reached. Soil engineers have perhaps been reluctant to employ a more realistic approach because of the convenience of applying simple theories and due to the fact that a more realistic approach to represent soil behavior is difficult to arrive at and leads to computational problems.

The separation of a real soil behavior into either a linear deformation problem without regard to localized yielding, or into a failure problem in which deformations in the soil are ignored has caused many difficulties in the analysis, understanding and interpretation of the real-life behavior of soils. A proper formulation and

solution of soil mechanics boundary-value problems requires an understanding of the stress-strain relation of the material. Realistic stress-strain relations for soils behavior are necessarily complex as a result of the physical and geometrical structure of soil. A complicated stress-strain relation gives rise to analytical difficulties. However, because of the development of digital computers, a complex, realistic description of stress-strain behavior may be employed economically in solving boundary value problems in soil mechanics. At present, it appears that computer capabilities have developed beyond the state of the art of the description of soil behavior.

Consequently, the first part of this thesis is devoted to the development of a more realistic constitutive relation for a granular material. The effort is restricted to quasi-static behavior.

I.2 Definition of Terms

Confusion often arises from the lack of generally accepted terminology in the fields of rheology. It is desirable to indicate a number of definitions that have been adopted in the present work.

The term "stress" is defined in the usual engineering sense as force per unit area [1]. In the present study all the stresses are principal stresses unless otherwise mentioned, and are implied to be "effective" in soil mechanics terms. The path traced out in principal stress "space" during a test is called a "stress-path." The term "strain" is also defined in the usual engineering sense. Unless otherwise mentioned the strains in this study are principal strains. According to the usual sign convention in soil mechanics

compressive stresses and strains are considered to be positive.

The material is "isotropic" if the mechanical properties of the material are independent of direction, and is "anisotropic" if mechanical properties are dependent on direction. The term "induced anisotropy" refers to the anisotropy due to the loading and straining or due to the different slip behaviors in extension and compression.

A "principal stress" or "principal strain" space is a three-dimensional domain with three mutually perpendicular axes expressed in terms of three principal stresses or strains. A "yield criterion" is a function of stress or strain level where the material exhibits large deformations or a relatively sudden change in the stress-strain curve for a small increment of applied stress. The yield criterion defines a "yield surface" in stress or strain space. "Strain- or work-hardening" refers to yield survace which changes with deformation. A "stable" work-hardening material in the sense of Drucker [3] is defined as a work-hardening material on which the application and removal of an external force results in (1) positive work and (2) positive or zero net work over the cycle of loading and unloading.

I.3 Important Aspects of Granular Material Behavior and the Drawbacks of Previous Approaches

In the absence of a stress-strain relation proper to a granular material, it has been difficult or impossible to perform a rigorous analysis of many realistic field problems in soil mechanics. Various writers have attempted to deduce a useful mathematical description of a constitutive law for the granular media expressed in appropriate

form for subsequent analysis on the basis of linear elasticity [1] ,
or visco-elasticity [4] , of perfect plasticity [5] , or of the elastic-
plastic theory for stable work-hardening materials [6,7] . More
recently, incremental theories of non-linear elasticity [8,9] and
plasticity [10] have been employed. A general review of previous
work will be included in Chapter II.

In some cases, the above-mentioned theories and methods
may give satisfactory approximation to the behavior of a granular
material in specific circumstances. However, the main drawback
in using these theories and methods is that many important aspects
of the deformation behaviors can not be generally accounted for.
The important aspects, which must be included in the constitutive
relation for granular media are:

(a) dilatancy due to a pure shear stress increment,

(b) work-hardening behavior, and the inelastic strains during
shear deformation,

(c) dependency of strain on the stress history and path,

(d) induced anisotropy due to loading and due to the different
deformation behaviors in extension and in compression.

It is desirable to have a brief description of the general
behavior of a granular material such as sand under stress to illustrate
these important aspects. A granular material such as sand under a
given load for a period of time before removal of the load, exhibits
an overall (macroscopic) deformation behavior as shown in Fig. I.1
after Scott [11] . When the load is statically applied at time O, there
is an instantaneous deformation OA. If the load is removed immedi-

ately, the deformation becomes OE which is a permanent set. If the load is applied for a period of time, the deformation increases along AB, which for sand will rapidly flatten out to a horizontal line BB'. After the removal of the load, the deformation immediately reduces by an amount of BC. The deformation will be further reduced in time along the curve CD until a steady value is reached. This illustrates that the deformation behavior of a granular material is not elastic.

Furthermore, the deformation behavior is also non-linear; this can be demonstrated by the results of tests on sand in the conventional triaxial test apparatus. A typical conventional axial compression test result is shown in Fig. I.2 to illustrate this point [12]. If the axial stress is increased, the stress-strain curve traces along a non-linear line OA. When the axial stress is reduced at point A, the unloading curve is AB, with OB representing the plastic strain. If it is reloaded at B the stress-strain curve follows a different curve line OC, thus forming a hysteresis loop. If the load is further increased beyond the stress level of A or C, the stress-strain curve becomes more of a continuation of OA than of BC.

It is well-known that a granular material dilates at small strains (positively or negatively) under pure shear stress [13]. In addition, it has been shown by Ko and Scott [14] that a granular material, especially sand, begins to deform plastically at very small shear stress regardless of the magnitude of the hydrostatic compression. The yielding is then continuous until a final failure condition is reached. This indicates that each new stress point on a given

shear stress path is a point on the newly generated yield surface and is dragging a yield surface with it.

The last, but not the least, important aspect is anisotropic induced by the loading and resulting from the different deformation behavior in extension and in compression. Experimental data on Ottawa sand under axial compression and axial extension (stress paths are shown in Fig. IV.2) performed by Bell [15] indicate that a movement of the stress point toward an axial extension stress state leads toward yield, whereas a movement of stress point toward the axial compression stress state leads toward increased "stability." In other words, granular soil behaves differently in extension and in compression. Other experimental evidence to substantiate this point is the finding of different stress-strain curves in axial compression and axial extension as obtained in the laboratory tests on Ottawa sand by Ko [16] and Masson [17].

A study of the literature indicated that a suitable model for material behavior exhibiting all the above effects had been suggested by Iwan [18, 19]. This model appeared to show promise as a descip- tion of soil behavior and a detailed examination of it follows later.

I. 4 Research Scope

In the first part of this thesis, attempts are made to develop a rheological model to describe the deformation behavior of a granular material under various stress and strain conditions. The effort concentrates on the evidence observed in laboratory tests and theoreti- cal considerations to obtain a rheological model exhibiting a stress- strain relation closely similar to the experimental results.

From the contact stress theory [1], the relation between the tangential component of the contact force between grains and displacement is inelastic, so that the stress-strain relation should depend upon the entire loading history. Accordingly, the correct stress-strain relation for a granular material should be given as an incremental one. The constitutive relation in this thesis will be presented in incremental form to take the effect of stress history and path into consideration.

The feasibility of the incremental constitutive relation will be tested by fitting the experimental results on Ottawa sand under various stress conditions in tests performed by Ko [16] and Masson [17].

Linear soil deformation problems of complicated geometry have been tackled by means of finite element computer programs [20]. A limited number of bilinear studies have been made in attempts to examine the yield and failure situation [21,22]. The results of these studies raise some questions as to the techniques used and theoretical interpretation. Some general non-linear studies have been attempted [9,17,61,62] on a piecewise linear basis with generally unsatisfactory results either from a rigorous point of view or from viewpoints of material characterization.

The material model suggested in Part I would lead to a finite element formulation considerably more rigorous and also more complicated than any previously suggested. Due to the number of parameters involved, the nonsymmetrical resulting stiffness matrix in a general formulation, and the complicated loading and unloading process, it is

difficult for the finite element computer program at present state of the art to handle the relationships proposed. So it was decided to examine the application of finite element methods to non-linear problems in more detail as a preliminary step. For practical reasons, the problem of the conditions of stress around the toe of a slope or at the tip of a crack [23, 24] in a bilinear material is chosen for this purpose. The effect on the results of the material properties, the finite element mesh size, and the computational procedure is examined in detail in Part II of this thesis.
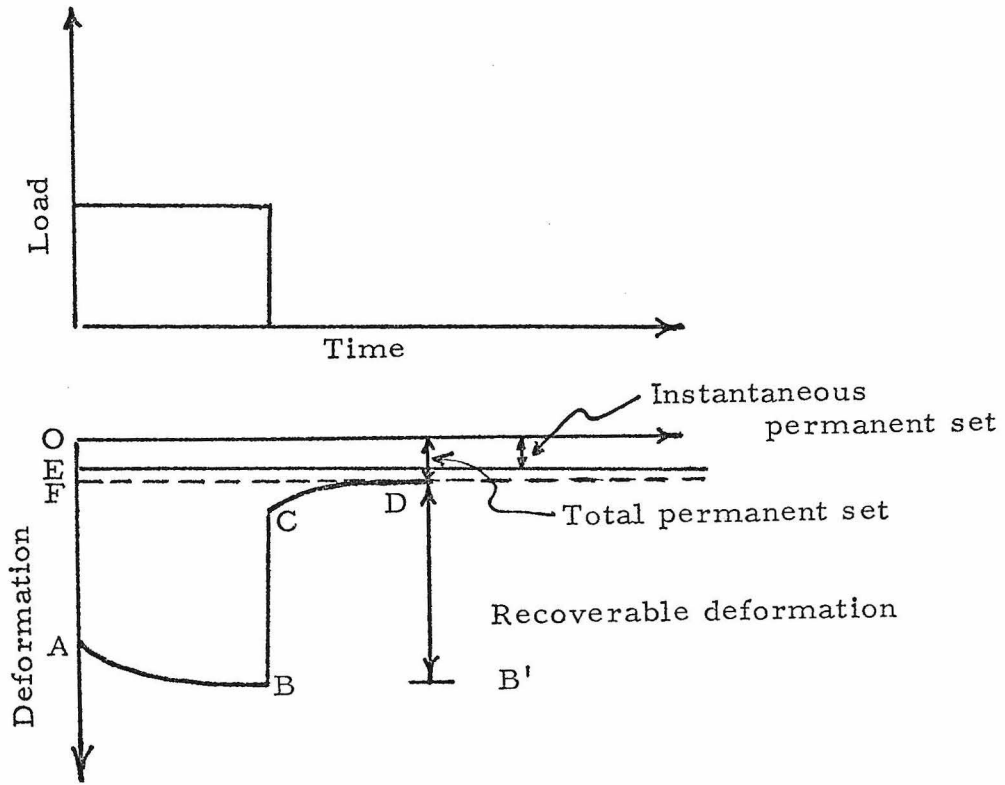
Fig. I.1. Time-dependent Soil Behavior
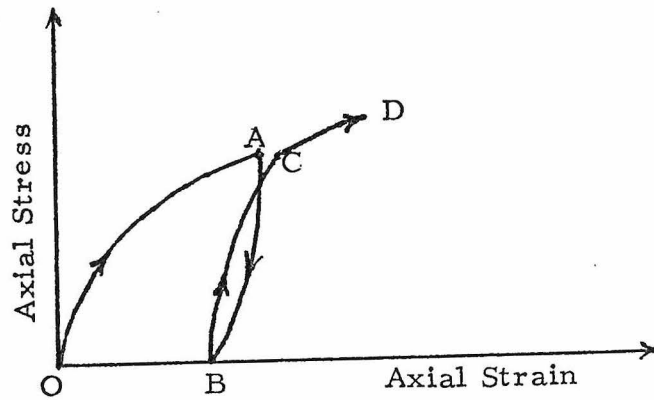
Fig. I.2. Soil Behavior in Triaxial Test

CHAPTER II

SURVEY OF PREVIOUS WORK

II.1 Prelude

The deformation behavior of granular material under stress is highly complex and extremely difficult to obtain by testing methods or to represent by mathematical descriptions. The granular material's behavior includes nonlinearity, inelasticity, anisotropy, shear dilatancy, stress and strain history dependency, random geometric packing, and time-dependency. Although a large effort has been devoted to this field by many investigators in the past few years, little advance has been achieved. Any explicit description in phenomenological or mathematical terms needs some degree of idealization of actual behavior and can not always be expected to be valid under different stress or loading conditions. Attempts to represent closely the behavior observed experimentally lead to ever increasing elaboration in detail of a mathematical or physical model. A useful mathematical or experimental description of the stress-strain relation in a material is one which can be employed as economically as possible in predicting the performance of the material under specific conditions.

In studying the constitutive relations for granular materials two types of approach are usually considered. The first studies

soils as a discrete system consisting of an orderly or random assemblage of particles. The second approach considers soils to behave as a continuum and various continuum mechanics models are employed to represent deformation behavior under specific circumstances. Both approaches are sometimes used together by some investigators in order to have a close representation of the stress-strain relationship. In addition, statistical mechanics is also employed by some investigators in conjunction with one or both above-mentioned approaches to account for the randomness in particle size and shape distribution.

One has to keep in mind that any proposed general constitutive law must be able to predict the material behavior over a wide range of stress and strain states. The legitimacy of a constitutive relation has to be confirmed by laboratory tests on soil samples under various stress and strain consitions. Theoretically, identical samples tested under identical stress or strain loadings in different testing apparatus must yield the same deformation-stress responses. However, this seldom occurs in practice due to the various limitations and constraints of testing apparatus. In describing the deformation behavior of a material in a laboratory test the influence of the constraints of the apparatus must be carefully examined and deducted from the observed material behavior.

The current concepts of stress-deformation mechanism in granular material have been reviewed by Barden and Khayatt[25], Frydman [26], Scott and Ko [27], and Masson [17]. Avoiding as

much unnecessary overlapping with the above references as possible, the previous work concerning the subject of constitutive relations for granular material will be categorically described and discussed in this chapter.

II.2 Discrete Models for Granular Materials

In investigating the deformation behavior of granular media by considering them as discrete systems, some simplification is always needed. The fundamental starting ground is the study of the particle packing phenomena. The first systematic treatment of ideal (regular) packings was due to Slichter [28]. He established various arrangements of uniform spheres and gave formulas to calculate their density. In studying the deformation behavior early attention was directed to the correlation of material density to the number of contacts (coordinate number) as first proposed and investigated by Smith, Foote and Busang [29] and by Filep [30]. Since then, various discrete models have been proposed. They usually, unless mentioned otherwise, have some common assumptions such as

(a) The grains are in direct elastic contact with each other;

(b) There are no adhesive forces between grains; the frictional forces between contact are mobilized by movements of grains only.

Based on Hertz's theory [1], the assumption (a) results in a nonlinear relation between the normal components of contact force

and displacement. Under pure normal stress, the predicted stress-strain relation is elastic and has a modulus of elasticity inversely proportional to the cubic root of normal stress. However, under assumption (b), the relation between the tangential components of contact force and displacement is not elastic and the stress-strain relation depends upon the entire loading history [31]. Accordingly, the proper constitutive relation for granular material must be expressed in incremental form. The early research in this direction was the study of elastic waves in granular substances [32], [33], [34]. These studies predicted a wave velocity proportional to the sixth root of an initially isotropic pressure (hydrostatic) and the cubic root (rather than the usual square root) of shear stress.

In the course of the development of a mathematical theory of small deformations in granular media of ideal pacings, the particle contact behaviors under different loading conditions were studied and described in a series of papers by Mindlin [35], Lubkin [36], Mindlin, et al. [37], Mindlin and Deresiewicz [31], and Mindlin [38]. The results of their analyses had been utilized in developing incremental constitutive relationships for granular media in face-centered cubic (hexagonal) array [39] and in simple cubic array [40]. In their analyses, the total stress-strain relations for ideal packings had to be obtained from a complicated integration of differential stress-strain relations along a specific stress path. This is possible only for some simple loading paths such as uniaxial and axial compression [40], [41]. Their analyses are not immediately applicable to the general three-dimensional loadings in real granular

material due to the above-mentioned shortcomings and due to the fact that real material does not consist of identical grains arranged in ideal pacing.

However, the results of the analysis for ideal pacings can be realistically applied to the randomly packed arrays by some means of correlating either the density or the coordinate number of the ideal models to the real material. One such method is by representing the assembly of real material as composed of separate clusters of cubic array (loosest possible) and hexagonal array (densest) in such a proportion as to give similar characteristics (such as density and coordinate number) of the real assembly. This was first proposed by Smith, et al. [29] and was successfully applied to the compression of granular material under hydrostatic compression by Ko and Scott [42]. A similar approach which approximates the relevant variables in a volume element containing a big number of particles by relations among the statistical expectation values from representative ensembles of "cells" each of which consists of only a few grains, was proposed and pursued by Gudehus [43]. He concluded that a realistical general three-dimensional approach must start from the contact forces and the geometrical statistics of random arrays. The same starting point was employed by Horne [44] and Neuber [45].

In recent years, statistical approaches have been taken more frequently in the study of the mechanics of granular media. In a discrete system, the influential factors are the coordinate number,

the orientation of contacts, the friction force between contacts and the mechanical properties of the grains. In a real material, most of these factors are at random due to the irregular distributions of size and shape of particles and geometrical structure. The study of ideal packing is only an idealization of nature and it is understood that the results of such an investigation must be extended to randomly oriented assemblies of particles. Furthermore since granular materials are, in fact, discrete media certain size restrictions on the infinitesimal element for analysis purposes are necessary. The element size must be such as to include a large number of grains. It is logical to employ certain statistical descriptions of the behavior of microscopic medium in leading to the macroscopic stress-strain characteristics of granular materials.

Aside from the approaches by Ko and Scott, and Gudehus, various other investigators directed their research in this direction. Murayama [46] developed a statistical model to explain the shearing behavior of sand. In his model, the orientation of slipping planes between contacts was assumed normally distributed. This eventually led to a conclusion that maximum shear strain increased proportionately to the ratio of octahedral shear stress to octahedral normal stress. Hess and Stoll [47] characterized granular material as a statistically homogeneous medium made up of cells which were regular arrays of particles and which were distributed and oriented at random with respect to the directions of principal stresses. Accounting for both the elastic deformation of the particles and inelastic deformation due to interparticle sliding,

their model was found to predict many of the features of the response of real granular materials. However, its use was limited in practical cases because the theory includes rather cumbersome volume integrals which must be evaluated numerically.

Stochastic models have also been used to study the deformation behavior of granular materials. Litwiniszyn [48] studied surface subsidence due to mine operations by a "random walk" argument and later extended this to apply to general problems in the mechanics of granular media [49]. Marsal [50] studied transient motion in the grain-skeleton during one-dimensional compression by considering the movements of particles to be the consequence of erratic impulses transferred to each grain by the neighboring ones, coupled with constant action. Smoltczyk [51] calculated the stress distribution in soil media based on a model which assumed a statistical normal distribution of stress in a particulate structure.

Marsal [52] developed a more complicated model by considering granular material as a congregation of spherical grains of different sizes distributed according to the grain-size curve of the granular soil. The contact forces between grains were treated as a random variable and found to approach asymptotically a normal distribution. The number of contacts in a grain detached by a plane was also considered as a random variable with a constant probability density for each contact occurrence. Based on these assumptions and frictional resistance considerations, Marsal obtained incremental stress-strain relations. The experimental

result of hydrostatic compression, triaxial compression, and one-dimensional compression tests were qualitatively confirmed from the incremental constitutive relations.

The concept of an analogy between grain assemblages and "macromeritic" liquids introduced by Winterkorn [53] may also provide some insight into the behavior of granular materials. With the analogy, the law of physics with respect to liquids can be applied to granular systems, giving a new direction to the research. This concept was utilized by Kezdi [54] to investigate shearing resistance and compressibility in an assemblage of rigid spheres, and to determine the lateral earth pressure coefficient from the point of view of the lateral pressure developed in an ideal packing of rigid spheres.

In contrast to the above approach, an energy method, the so-called "stress dilatancy" theory was proposed by Rowe [55], [56]. He analyzed the behavior of regular packings of uniform rigid cohesionless spheres under axially symmetrical stress states, and two-dimensional rods under plane stress state; and deduced the condition that the ratio of rate of energy dissipation in internal friction to the rate of energy supplied in the major principal effective stress direction was a minimum. An energy ratio criterion is thus established for the critical angle of sliding between particles following which stress would be transmitted to other particle contacts. The complete stress-deformation process was considered a continuous sliding accomplished by change in

geometrical structure as the internal frictional resistance decreases. Observing that a characteristic angle, α, of the regular packing arrangements was absent in his derivation of an energy ratio criterion, Rowe suggested that his theory was applicable to random arrays of particles as well as to regular arrays. This postulation and assumed deformation mechanisms with the absence of rolling effects was criticized.

Horne [44], [57] studied Rowe's theory in detail and showed that a closed packed assembly is likely to deform in large groups by a predominantly translatory rather than rotating motion. However, Horne also concluded that the packing characteristics of random assemblies must also be considered before stress or strain-ratios can be derived. Horne [44], [57] propounded a method similar to Rowe's approach for describing the state of anisotropy existing in a random assembly in terms of "mean projected solid paths" in the various coordinate directions. On the basis of these concepts, the rates of strain in the principal directions were expressed in terms of the frequency and magnitude of sliding between particles. The statistical characteristics of a random assembly of particles was thus taken into consideration for the deformation behavior. Horne showed his analysis gave results for regular arrays corresponding to those obtained by Rowe. Horne's analysis and experimental results on triaxial extension and compression tests by other investigators [58], [59] tend to substantiate Rowe's theory. However, the theory has not been tested for general three-dimensional loadings.

II.3 Continuum Mechanics Approaches

Although the particles in granular materials such as sands are relatively large in comparison with the crystals of metalic materials, the domains of boundary value problems in granular material are also relatively large. Therefore, instead of a discrete model approach, it has been more common to regard granular materials as continua in studying their behaviors. The methods and results of continuum mechanics such as elasticity theory, plasticity theory are usually employed in this approach and will be described in the following section.

II.3-1 Elasticity Theory

Elasticity theory assumes that all of the deformation is recoverable and the material returns to its initial state upon removal of the loading. There is a general discrepancy in using the theory of elasticity in describing the deformation behavior of granular materials since permanent plastic deformation inevitably makes an appearance upon the unloading of a granular material. Therefore, elasticity theory can only be applied to the case of monotonically increasing loading, or in cases where the applied and removed load causes negligible plastic strains.

The simplest continuum model for granular material behavior is linear elasticity theory. The linear theory of elasticity has been well developed in the last eighty years [1] and many solutions exist

for application to some of the practical problems such as calculation of stresses and settlements in a region of soil underlying an engineering structure. Recently, due to the development of the finite element method [60] for handling complicated boundary value problems, soil engineers find elasticity theory even more convenient than ever and are perhaps reluctant to try other approaches in representing more realistic soil behavior. Other drawbacks of linear elasticity theory are that it cannot in general represent the nonlinear and partially inelastic behavior of soil and in particular can not account for the dilatancy effect due to the application of shear stresses to soil.

Attempts to represent nonlinear behavior and dilatancy due to shear in granular media treated as elastic material can be classified into two areas. The first is an empirical process of simulating nonlinear stress-strain relations without referring to the framework of continuum mechanics theory in the formulation of constitutive relations. Figure II.1 shows three techniques in this empirical scope, which are generally employed by investigators. The quasi-linear technique as indicated in Fig. II.1(a) simulates the real homogeneous granular material (soil) in the state of stress or strain. This is done by expressing the tangent modulus of the stress-strain curve as a function of the state of stress or strain [61]. In the similar manner, the Poisson's ratio can also be expressed as a function of the stress as proposed by Girijavallabhan and Reese [62]. This technique has been widely used for solving some practical engineering problems due to its ease in adapting

into the well developed finite element methods and high speed digital computers. Evidences for this are more than abundant in engineering literature [e.g., 63]. Figure II.1(b) indicates the piecewise linear technique in which the real homogeneous material (soil) behavior is approximated by various nonlinear representations with the solutions carried out by piecewise linear approximations [64]. The third technique is to express strains explicitly in terms of stresses or vice versa. As a first step in reaching a long term aim to write a generalized three-dimensional tensional form of the stress-strain relations for soils, Konder [65] suggested an empirical hyperbolic stress strain relation for cohesive soil in the triaxial test, of the following form

$$\epsilon \sigma - \beta \epsilon + \alpha \sigma = 0 \qquad (2.1)$$

where σ is the normal principal stress difference and ϵ is axial strain. The two constants α and β are related to the initial tangent modulus and ultimate strength at large strain respectively. Aside from being without any theoretical basis, the empirical approximation yields good results only if the material under specific stress or strain condition behaves as assumed.

The second approach follows the well-developed nonlinear small-strain theory in the field of solid mechanics [66], [67] by using a higher order of deformation law comparable to Hooke's Law. The nonlinear total stress-strain relation expresses stress as a function of the existing strains (deformation gradients) measured

from some reference configuration [68]. The result is independent of the manner the total strain is reached. Chang, et al [9] argued that if such a deformation law were to be applied to a strain-history dependent material (such as granular material) under arbitrary stress paths, then the laboratory test for materials should follow proportional loading paths.

Two fundamental methods of formulating nonlinear elastic stress-strain relations are due to Green and Cauchy respectively. Green's method postulates the existence of a stored strain energy density function W for the model continuum. The strain energy density function can be taken as a function of any three independent strain invariants. According to the conservation of energy hypothesis, the constitutive relation can be expressed as

$$\sigma_{ij} = \frac{\partial W}{\partial e_{ij}} \qquad (2.2)$$

where σ_{ij} and e_{ij} are stress and strain tensors respectively. In this way, the order of nonlinearity depends on the powers of energy density function in terms of strain. For instance, an nth order stress-strain law can be obtained by expressing W as a function of n+1 powers of strain. Furthermore, a nonlinear stress-strain law may also be found by carrying out an analogous sequence of operations on the complementary energy density function U, which is defined as

$$U = \sigma_{ij} e_{ij} - W \qquad (2.3)$$

Chang, et al [9] attempted a second-order approximation of granular behavior by writing W in terms of all powers of strains up to three. Thus stresses are expressed in terms of a second order strain function with five material constants to be determined from material tests along prescribed stress paths. Chang, et al, also developed an incremental stress-strain relation for the second-order approximation in preparation for the numerical computation. From the experimental results of hydrostatic compression tests performed by Ko and Scott [14], [42], [69] in a three-dimensional triaxial test box [70], Chang, et al, obtained values of these constants and the incremental stress-strain relation; the soil's response in a triaxial shear test was simulated. It was shown that this nonlinear approximation represented many of the characteristics of granular material behavior and reasonable agreement was observed. The major weakness of the theory was the material instability innate in the second order approximation as pointed out by Chang, et al.

In observing the shape of principal stress-strain curves from shear tests on sands, Masson [17] concluded that these curves could be best approximated by odd rather than even functions and a power series in stress would be preferable to powers of strain for modeling the softening behavior of sand under shear. Therefore the complementary energy density in terms of three stress invariants with all powers of stress up to four was postulated by Masson in order to derive a third-order law. Strains were thus expressed as third-order functions of stresses with nine material constants. The

incremental stress-strain relation was also derived for hydrostatic compression (HC), triaxial compression (TC), triaxial extension (TE), radial shear (RS-60°) and conventional triaxial compression (CTC) and extension (CTE) test. (The stress paths of these tests are shown in Figs. IV.1, IV.2, and IV.8). Experimental tests on Ottawa sand along HC, TC, TE, RS-60°, CTC and CTE stress paths were performed in a three-dimensional triaxial testing apparatus to determine the nine material constants. Masson [17] found that the third-order law was capable of accounting for all essential aspects of the behavior of the material, especially the high degree of nonlinearity. Applying this third-order law to some boundary values problems, Masson also found a close correlation in comparing with the experimental results. Meissner [71] also derived a third-order stress-strain law with the postulation that the strain energy density function was a function of strain with all powers up to four. Stress was a cubic function of strains with twelve material constants. These twelve constants were exclusively determined from the conventional test data. The conclusions of Meissner were similar to Masson's findings.

A third order stress-strain relation was also derived by Chang [72] with the use of a strain energy density function approximated by two functions in polynomial form in order to avoid the possible instability in stress-strain relations due to polynomial approximation. In his constitutive relations, eleven material constants were needed. Chang's derivation was purely based on a phenomenological conjecture. No experiments were given to deter-

mine the eleven material constants or to verify its legitimacy.

It has to be pointed out that a general third-order approx-
imation yields eleven or more material constants depending on the
form of energy density function assumed. Some of these material
constants can be suppressed by requiring zero stress to imply zero
strain. It is not surprising that different numbers of material
constants are obtained by different investigators using the same
third-order approximation technique.

Aside from being invalid for the unloading case, the above-
mentioned nonlinear approximations have one thing in common that
the predicted response is symmetrical with respect to tension and
compression. In other words, exept for change of sign the con-
ventional triaxial compression and conventional triaxial extension
tests, or axial compression and axial extension, would yield identical
results as predicted by these nonlinear laws. However, experiments
on granular materials such as Ottawa sand [16], [17] have indicated
that the deformation behavior in extension and compression of
granular material is not identical.

Another point of view in nonlinear approaches is Cauchy's
method which postulates that the state of stress is a function of
the current state of strain. This is within the scope of hyper-
elasticity theory [67], since any stress-strain relation obtained
from Cauchy's method can also be derived from Green's method
with a specific chosen strain energy density function. Higher order
of nonlinear approximation may also be employed to develop a

stress-strain relation for granular material if one does not mind the complicated formulation.

Noticing that an incremental stress-strain relation is more appropriate to account for the path-dependent characteristics of granular material, Coon and Evans [73] used constitutive relations corresponding to a special case of first order theory of hypoelasticity [74] to fit the experimental data and to predict the recoverable deformation of granular materials under conventional triaxial loadings. The concept of hypoelasticity embodies a class of ideal materials whose constitutive relations are governed by the principle

$$\text{rate of stress} = f(\text{rate of strain}) \tag{2.12}$$

This was first proposed by Truesdell [74] and later studied in detail by Bernstein [75]. This may become a potentially powerful tool in describing the deformation behavior of granular material under monotonically increasing loadings since its innately incremental characteristics in principle can account for the path-dependent behavior of a granular material with a limited memory. However, as in the other analyses with granular models, the theory has not been tested for general three-dimensional loadings due to its complexity.

II. 3-2 Plasticity, Yield Surface and Flow Rules

The application of the mathematical theory of plasticity to

the stress-strain relaitionship was first suggested by Levy [76] ninety years ago. The first generalized incremental relationship between stress and strain incorporating both elastic and plastic components for the stress analaysis in metal was derived by Reuss [77] some forty years ago. Terzaghi [2] was the first one to apply plasticity theory to soil mechanics problems by approximating the behavior of soils as being rigid plastic. The typical stress-deformation pattern for a granular material is shown in Fig. II.2(a), in which the separate contributions for recoverable (elastic) deformation and irrecoverable (plastic) deformation are indicated. This typical behavior of material is ususally simplified as shown in Fig. II.2(b) for solving some boundary value problems. A material is called rigid-plastic if the recoverable deformations are small in magnitude in comparison with the overall movements consequent upon the attainment of limiting stress, and hence may be neglected. When recoverable deformations are so large that they play an important part in any stress analysis performed, the material study involved is called elastic-plastic analysis.

Terzaghi's rigid-plastic analysis applied to the stability problems deals with the conditions for the equilibrium of idealized soils immediately preceding by ultimate failure by plastic flow and gives no consideration to the corresponding state of strain. As pointed out by Smith and Kay [10] Terzaghi's analysis yields a "transition of semi-infinite masses from a state of elastic equilibrium into a state of plastic equilibrium which can only be accomplished by an imaginary process of stretching and compressing the

soil which is without any parallel in the physical world." There-
fore, Terzaghi's analysis of treating soils as rigid-plastic materials
is not rigorous.

A more rigorous plasticity approach considering both states
of stress and strain for soil mechanics problems was initially
developed in a series of papers by Drucker and Prager [78], Shield
[79], Drucker [80], and Shield [81], [82]. In the theory of plasticity,
the material is considered to behave elastically until a yield condition
is reached. The yield condition usually takes the form of a convex
surface in stress space. When the state of stress reaches a point
on the yield surface, the material yields indefinitely. The yield
surface in terms of state of stress is taken to be a plastic potential.
The rate of plastic strain occurring at yield is determined by some
flow rule associated with this plastic potential. Therefore, two
things are important in plasticity theory: namely, yield condition
and flow rule.

A considerable effort has been devoted to obtaining a work-
able form of yield surface for granular materials. The simplest
analytical representations of yield surface for cohesionless soils
(granular material) are cones or pyramids with generally hexagonal
bases as represented in an octahedral stress plane as shown in
Fig. II.3. A yield surface according to Tresca's criterion of
failure is represented by a regular hexagon; the field condition is
reached when a maximum shear stress reaches a certain level [83].
The yield condition due to von Mises states that yield occurs when

the octahedral shear stress reaches a critical value as represented by a circle in Fig. II.3. The oldest and the most widely used criterion for cohesionless soils is the Mohr-Coulomb yield condition which states that the soil will yield or fail when the obliquity of resultant stress on some plane reaches a maximum value.

Various other pyramidal yield surfaces such as the Mohr-Coulomb yield surface with tension cut-off [84], and Haythornthwaite's maximum reduced stress criterion [85], have also been suggested. Paul [86] has reviewed the experimental results on brittle metal, rocks, granular materials, and soil and developed a generalized pyramidal yield criterion, with a yield surface as shown in Fig. II.4. Many of the yield surfaces proposed for various materials are only special cases of Paul's generalized pyramidal yield surface.

The presence of corners in a pyramidal yield surface is not a law of nature in soil's behavior and creates difficulties in analytical applications. A continuous closed-form yield surface is more desirable. The condition of isotropy requires any cross section of a yield surface projected on an octahedral stress plane to show the threefold type of symmetry as shown in Fig. II.5. It seems to the author that the simplest continuous form for this cross section is a cylindrical function with the following relation:

$$\rho = \frac{A}{1 - B\cos 3\theta} \tag{2.4}$$

where ρ is the distance from the hydrostatic axis to any point on the yield surface whose radius intersects the major principal axis

on a hydrostatic plane with an angle θ as shown in Fig. II.5. A and B in Eq. (2.4) are constants to be determined later.

Let σ_1, σ_2, and σ_3 be three principal effective stresses, then the first effective stress invariant J_1 equals $(\sigma_1 + \sigma_2 + \sigma_3)$. If the hydrostatic component of stress at a point is subtracted from each of the principal stresses, the deviatoric stress system $(\sigma'_1, \sigma'_2, \sigma'_3)$ arises

$$\sigma'_1 = \sigma_1 - \frac{\sigma_1 + \sigma_2 + \sigma_3}{3} = \sigma_1 - J_1/3$$

$$\sigma'_2 = \sigma_2 - J_1/3 \qquad (2.5)$$

$$\sigma'_3 = \sigma_3 - J_1/3$$

From Eq. (2.5), the three deviatoric stress invariants J'_1, J'_2 and J'_3 can be obtained [27] as follows

$$J'_1 = (\sigma_1 - \frac{J_1}{3}) + (\sigma_2 - \frac{J_1}{3}) + (\sigma_3 - \frac{J_1}{3}) = 0$$

$$J'_2 = -\frac{1}{6}\left[(\sigma_1 - \sigma_2)^2 + (\sigma_2 - \sigma_3)^2 + (\sigma_3 - \sigma_1)^2\right] \qquad (2.6)$$

$$J'_3 = \frac{1}{27}(2\sigma_1 - \sigma_2 - \sigma_3)(2\sigma_2 - \sigma_1 - \sigma_3)(2\sigma_3 - \sigma_1 - \sigma_2)$$

It can also be shown [27] that ρ and θ are given by the following relations

$$\rho = \sqrt{2}\,(-J'_2)^{1/2}$$

$$\theta = \tfrac{1}{3}\cos^{-1}\left[\frac{3\sqrt{3}}{2}\ \frac{J'_3}{(-J'_2)^{3/2}}\right] \tag{2.7}$$

Let a and b denote the values of ρ at $\theta = 0°$ and at $\theta = 60°$ respectively as shown in Fig. II.4, then A and B can be obtained from Eq.(2.4) and are expressed as follows

$$A = \frac{2ab}{a+b}$$

$$B = \frac{a-b}{a+b} \tag{2.8}$$

From Eqs. (2.4), (2.7) and (2.8), the yield surface on an octahedral plane can be obtained and expressed as follows

$$f = \frac{1}{\sqrt{2}}\,(\tfrac{1}{a}+\tfrac{1}{b})(-J'_2)^{1/2} - \frac{3\sqrt{3}}{2\sqrt{2}}\,(\tfrac{1}{b}-\tfrac{1}{a})\,\frac{J'_3}{(-J'_2)} - 1 = 0 \tag{2.9}$$

For a granular material, the effect of the hydrostatic effective pressure (J_1) in yielding is known to be significant at usual working stresses, so that it can be expected that a generalized yield surface should be described as

$$f(J_1, J'_2, J'_3) = 0 \tag{2.10}$$

Therefore, it can be expected that a and b values should be, at

least, functions of J_1 and material properties such as the void ratio of the granular material. The exact relation of a and b with J_1 and void ratio is not known and more research is necessary towards this end. However, from the available experimental results by Ko and Scott [69], the yield surface suggested by the author seems to give a simple and excellent approximation as shown in Fig.II.6 and Table II.1.

It can be seen from Eq. (2.9) that if a = b the yield surface becomes a circle of von Mises type. Observing the test results on Brasted sand, Bishop [87] found that the von Mises yield criterion (circular yield surface) failed to predict meaningful results. Furthermore, Bishop [87] illustrated some portion of circular yield surface in principal effective stress space was in a state of negative effective stress. For a cohesionless soil (sand) this is meaningless. Therefore, it can be expected that a circular yield surface (a = b) is not suitable for granular material. This implies that the condition of a > b has to be observed in the yield function indicated by Eq. (2.9).

For some values of a and b, some region in the cross section of yield surface may become concave, which is not possible for the class of materials known as stable work hardening materials classified by Drucker [88]. However, if we are concerned with fracture or with the failure of a granular material, rather than plastic flow, the materials may not fall into a stable work-hardening classification in the sense of Drucker [3].

Granular material exhibits work-hardening behavior which implies that the position of the yield surface changes with the increase of stress. Drucker, Gibson and Henkel [89] took the Mohr-Coulomb yield criterion as a limit surface and closed the open ends with a family of hemispheres. The hemispherical surfaces were assumed to be the family of yield loci and the material was always at yield as a stress path moved out until it finally reached the Mohr-Coulomb limit or failure surface.

Roscoe and Schofield [90] and Roscoe, Schofield and Thurrairajah [91] proposed a yield surface for "wet" clay in a (p, q, e) space; where $p = (\sigma_1 + \sigma_2 + \sigma_3)/3$, $q = (\sigma_1 - \sigma_3)$ and e is the void ratio. For the triaxial data an additional stress parameter q_w, which is obtained from the observed deviatoric stress q by application of a boundary energy correction and an elastic energy correction is needed for a unique yield surface under drained and undrained (no volume change) condition. They took the critical void ratio as a limiting surface and closed the open ends with a family of bullet-shaped yield loci. Although they claimed considerable success for their theory in producing a stress-strain theory for "wet" clay, the application to granular material remains to be examined.

A yielding model including no possibility of tension and transition between Mohr-Coulomb and von Mises criterion has been proposed [92], [93] to study wave propagation in soils and qualitative success has been claimed. Numerous other forms of yield surfaces for strain-hardening materials are also possible. Koiter

[94] represented the yield function (plastic potential) by a family of Tresea yield surfaces. Prager [95] suggested a family of von Mises yield surfaces. Weidler and Paslay [96] incorporated density effects in terms of specific volume into a family of von Mises conditions in strain space to derive a constitutive relation for a granular medium. Their analysis was compared with experimental results in direct shear tests with qualitative agreement. However, one has to point out that direct shear tests are not good for comparison purpose. The main drawbacks of using such tests for the evaluation of constitutive relations are: the nonuniform deformation in the samples and the uncertainty in the boundary stress condition.

Most investigators associate the plastic strain with the plastic potential by a normality condition which states that the direction of the plastic strain rate vector is given by the normal to the yield surface. In a mathematical expression, the normality condition can be expressed as

$$\dot{\epsilon}^{p}_{ij} = \lambda \frac{\partial f}{\partial \sigma_{ij}} \tag{2.11}$$

where $\dot{\epsilon}^{p}_{ij}$ is the plastic strain rate tensor, σ_{ij} the stress tensor, f the plastic potential on yield function, and λ is a proportionality constant which can be varied with the state of stress or strain.

Equation (2.11) is called the "associated flow rule" since it associates plastic strain rate with stresses by a normality condition. It has been pointed out that the normality of the plastic strain

increment vector to the yield is not a law of nature of soil's behavior [97], [98]. While, for some materials, normality may have been observed, it is not necessarily applicable to all materials. Normality condition requires that the granular material must expand volumetrically, plastically at yield if the soil's yield surface depends and increases with the hydrostatic stress. From the experimental results on Ottawa sand, Ko and Scott [69] found that soils tended to expand at yield, but it was not sufficient to make the plastic strain increment vector normal to the failure surfaces. The question on the lack of normality for soils was first raised by de Jong [99]. For a granular material whose deformational mechanism is primarily associated with a frictional system, normality does not hold in general.

This lack of normality for granular material has been substantially supported by experimental investigations on sands by Weidler [100]; Poorooshasb, Holubec, and Sherbourne [101]; Barden and Khayatt [102]; and Ko and Scott [14]. However, because of the nature of soil behavior it is not clear how sensitive soil is to the nature of the tests devised to investigate normality. Further examination of the relevance of normality condition to plastic analysis of granular materials is needed.

For granular material, it would seem that certain non-associated flow rules may be appropriate. Weidler and Paslay [96] derived a nonassociated flow rule from energy considerations and later applied it to triaxial tests for verification [103]. Although

certain important aspects such as mode of deformation, the analytical and numerical results appear to agree with experience in soil testing. However, more research is needed for a workable non-associated flow rule to yield a quantitative evidence of its usefulness.

The most important features of granular materials are elasticity, frictional elasticity and work-hardening. It is possible to study the deformation behavior by rheological models. The elastic behavior caused by the Hertz effect can be represented by a nonlinear spring. The frictional behavior can be easily symbolized by a slip (St. Venant) element. The simple form of the rheological model for granular material would be a series of spring-slip elements as suggested by Smoltezyk [104] and shown in Fig. II.7(a). Brown [105] represented the deformation behavior of frictional system by a model (Fig. II.7(b)) which did not satisfy the criterion of a stable work-hardening material in the sense of Drucker. A two-dimensional model as shown in Fig. II.7(c) was used by Palmer [106]. Palmer showed that the yield condition $P = \mu Q$ (Fig. II.7(c)) was not a plastic potential and the normality condition did not hold. In other words, the yield condition is homogeneous in the stress component and the direction of plastic deformation is also a homogeneous function of stress but does not obey the normality condition.

Iwan [18], [19] used the distributed element model of Fig. II.7(d) to study the yielding behavior of continuous and composite

systems. Iwan's model led to stress-strain relations which exhibited anisotropic strain-hardening (Bauschinger effect). The concept of the one-dimensional class of models was extended to three dimensions and led to a subsequent generalization of the customary concepts of the incremental theory of plasticity. The built-in distributed characteristics in Iwan's model can be easily adapted with certain statistical parameters to account for the randomness of packing, and size and shape distribution of particles in a granular system. Iwan's model of yield behavior was adapted by Chang [107] who derived a refined incremental plasticity stress-strain law by a collection of generalized Mohr-Coulomb yield surfaces to describe the plastic behavior of soil in shear. The main drawback in Chang's deviation was that it would be very difficult if not impossible to fit it to test data. One possible remedy for this drawback is to use some distributed characteristics in the family of yield loci. Some more research is necessary to verify this point.

Wells and Paslay [108] used a model (Fig. II. 7 (e)) similar to Iwan's model (Fig. II. 7(d)) to develop a stress-strain relation with the yield surfaces expressed in strain space for a specific type of material characterized by coplanar motion of dislocations. The concept of a one-dimensional model was extended to establish a three-dimensional family of yield functions in principal strain space $(\epsilon_1, \epsilon_2, \epsilon_3)$, whose axes, ϵ_1, ϵ_2, and ϵ_3 are aligned with the principal stress σ_1- , σ_2- , and σ_3- axes.

It is also possible to develop a more complicated model

which simultaneously allows for different effects to have an increasing similarity with the deformation behavior of real material. Unlike other types of models, the stress-strain relation is usually obtained solely from the mechanism of this type of model without conjunction with any other assumptions or hypotheses. One of these models was due to Yandell [109], [110]. Yandell simulated a long section of a pavement under plane stress condition by a two-dimensional mechanical lattice analogy (Fig. II. 8(a)) made up by a family of identical mechanical models as shown in Fig. II. 8(b). The elastic elements (linear springs in Fig. II. 8(b)) exhibited one stiffness in loading path and a higher stiffness in unloading path. The stiffness coefficients of spring elements (A, S, V) were calculated by frame analysis for the representation of a non-buckling plate of unit thickness [110]. A possible load-deflection path exhibited by a unit element is shown as in Fig. II. 8(c). With this analogy, Yandell was able to predict the behavior of an elasto-plastic pavement during repeated loading by traveling rollers.

TABLE II.1

Comparison of Experimental Data and Predictions by Eq. (2.9)

(a) For void ratio e = 0.61

θ \ ρ	Ko's data[*]	Prediction
0°	10.5	10.5[**]
15°	9.54	10.3
30°	8.75	9.35
45°	8.45	8.7
60°	8.3	8.3[**]

(b) For void ratio e = 0.52

θ \ ρ	Ko's data[*]	Prediction
0°	13.1	13.1[**]
15°	11.4	12.3
30°	10.1	10.65
45°	9.2	9.45
60°	9	9[**]

[*]Measured from Fig. II.6, 1 cm = 1 .

[**]Taken as the value of Ko's data.
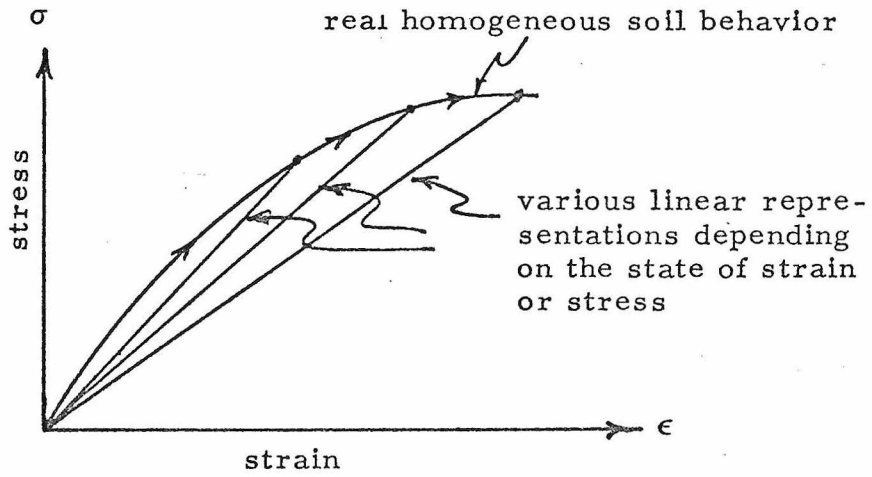
(a) Quasi-linear Technique
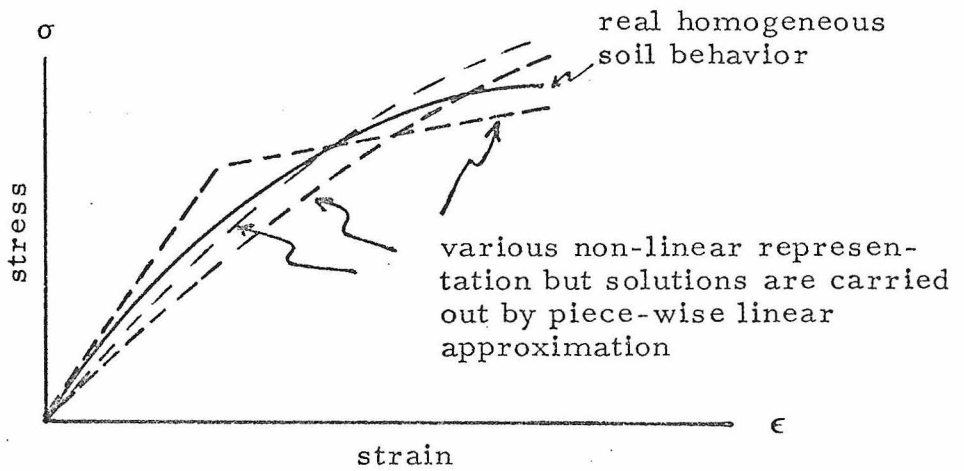
(b) Piece-wise Linear Approximation

Fig. II.1. Various Empirical Techniques for the Soil Behavior
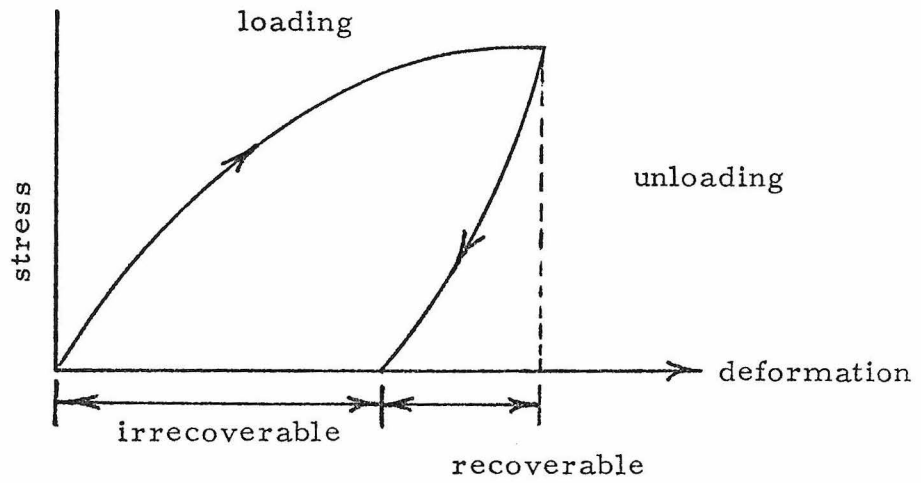
(a) Real Homogeneous Soil Behavior
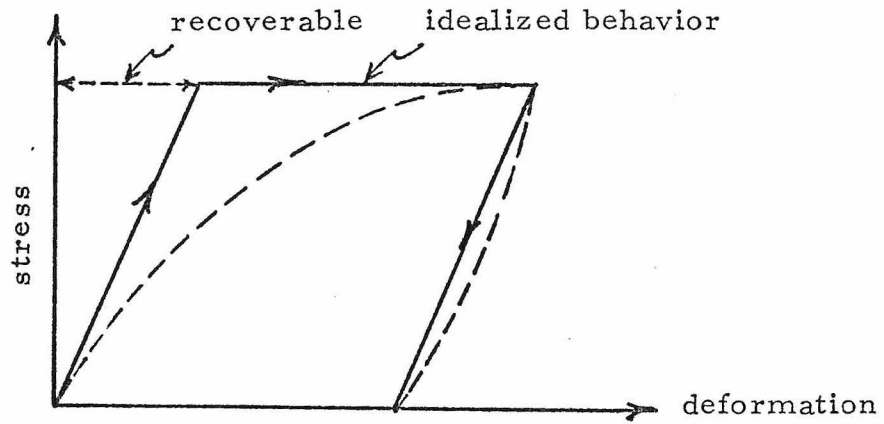
(b) Idealized Soil Behavior

Fig. II.2. Real Homogeneous Soil Behavior and Idealization

a. PRINCIPAL STRESS SPACE

b. INTERSECTION OF TYPICAL
ANALYTICAL FAILURE THEORIES
WITH π PLANE
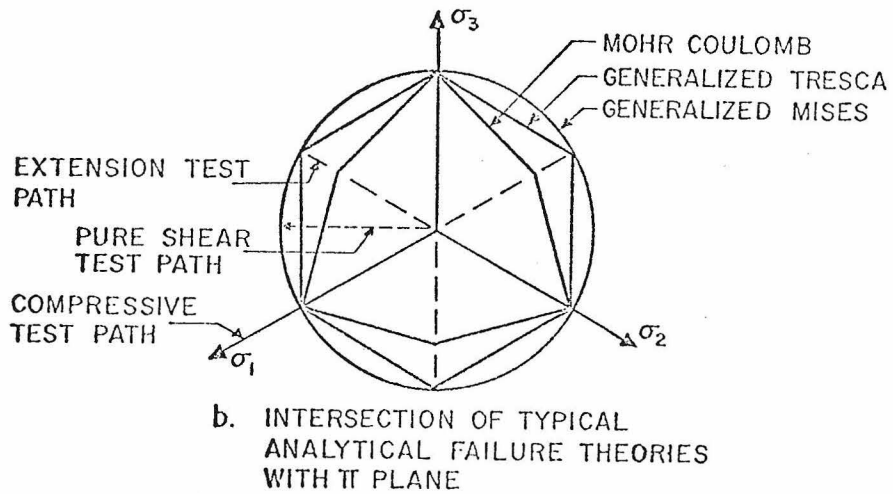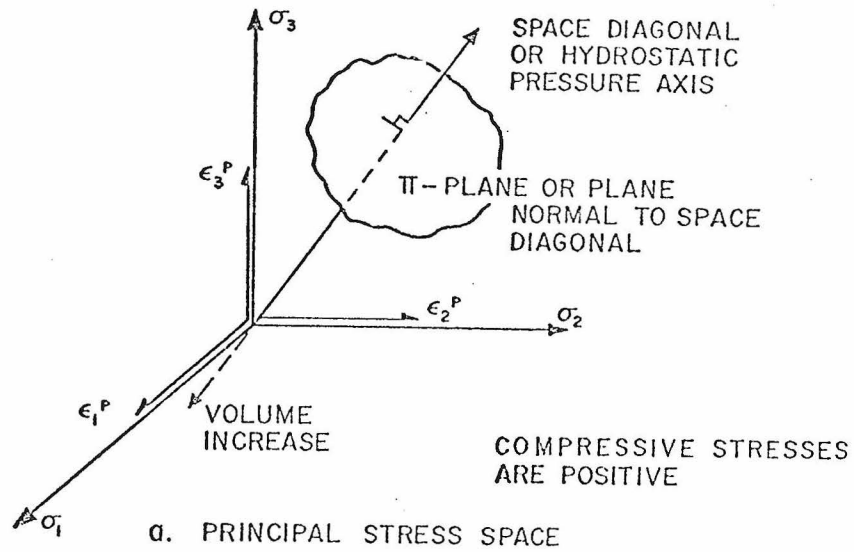
Fig. II.3. Principal Stress Space and Failure Theories
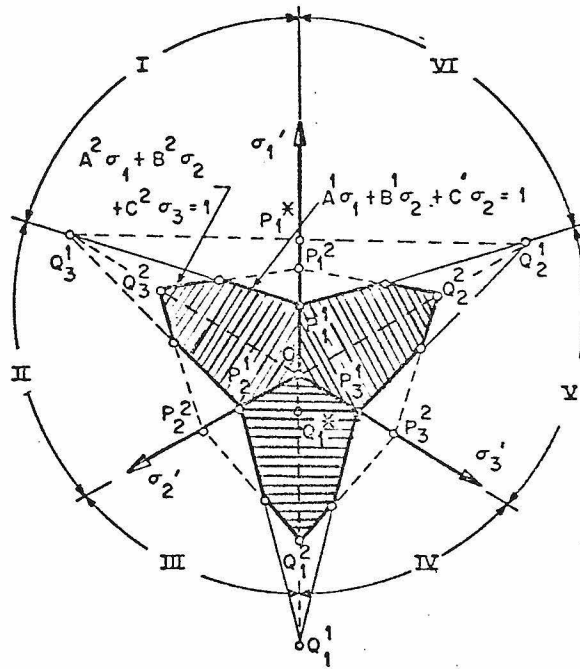
Notes: (1) The twelve-sided polygon (shaded) represents a piece-wise linear failure surface on an octahedral plane.

(2) Each of the twelve sides is represented by an equation of the form

$$A\sigma_1 + B\sigma_2 + C\sigma_3 = 1.$$

Fig. II.4. Paul's Generalized Pyramidal Failure Surface
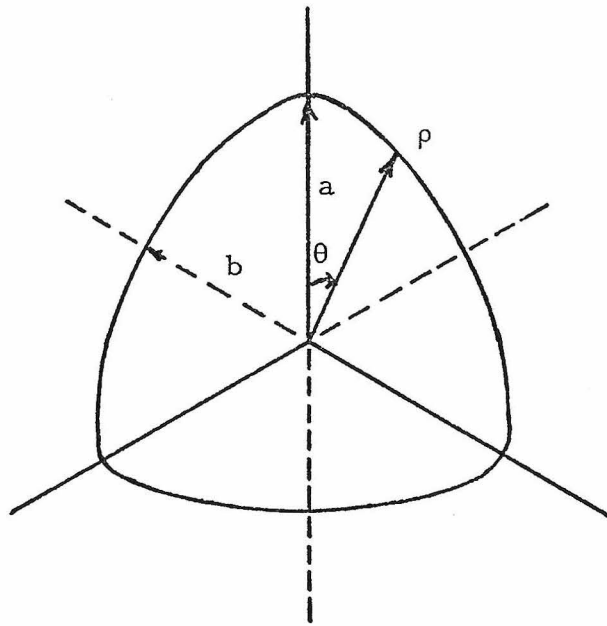
(a) Regular shape
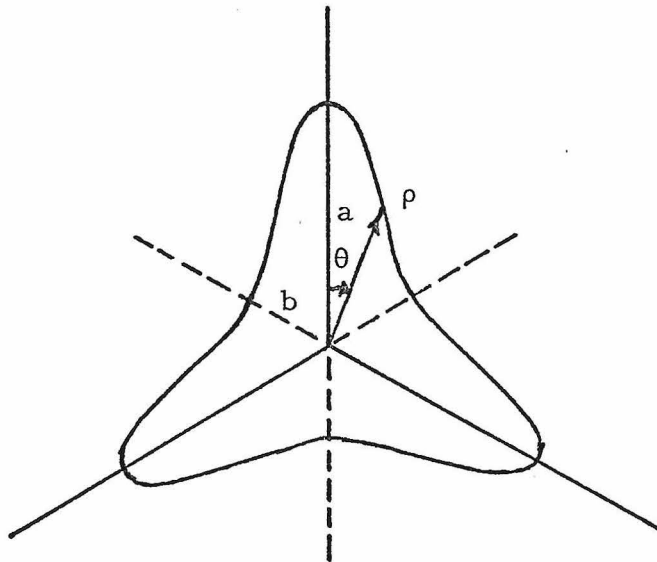
(b) concave shape

Fig. II.5. Continuous Yield Surface in Eq. (2.9)
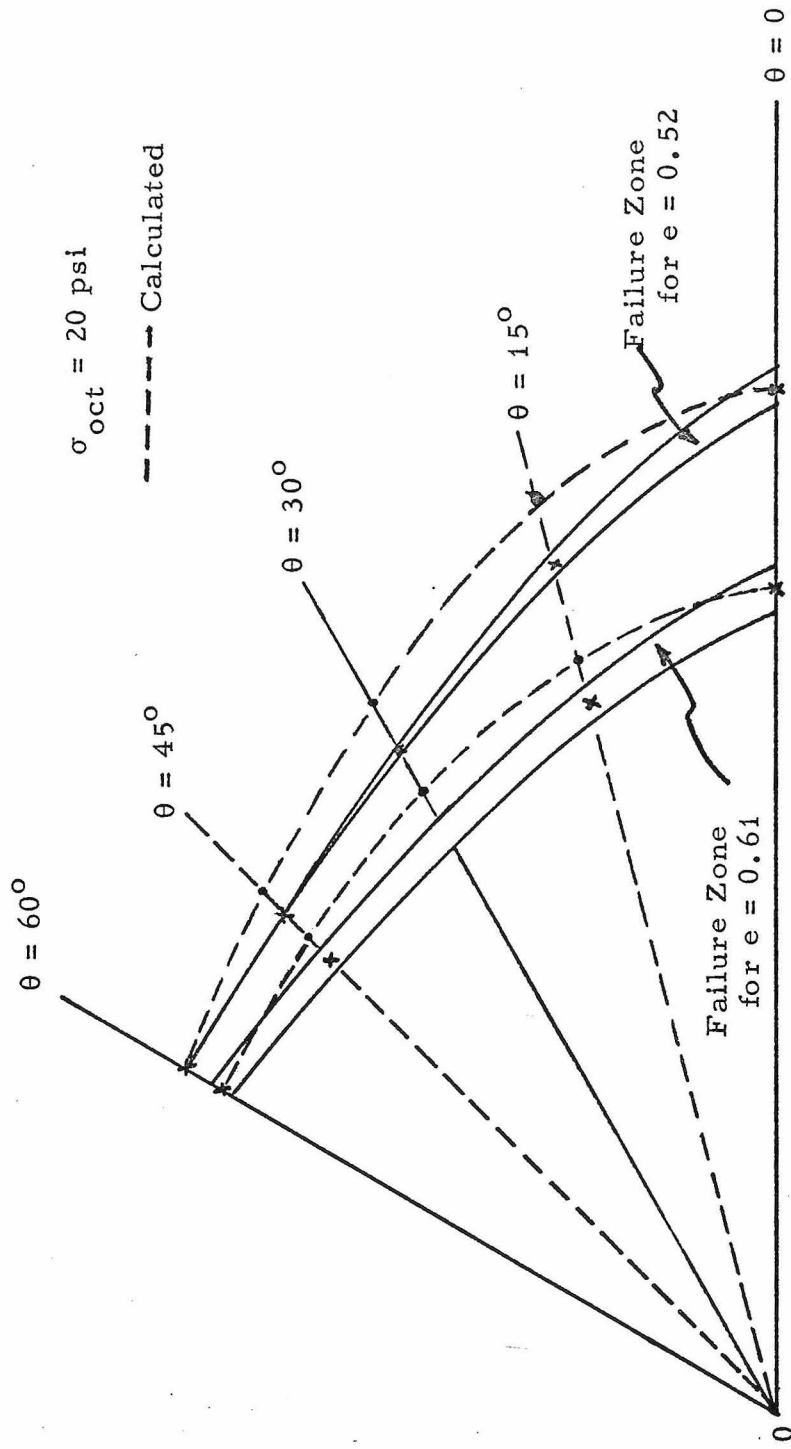
Fig. II.6. Failure Envelopes, Experimental Data and Prediction by Eq. (2.9) for Ottawa Sand [16]
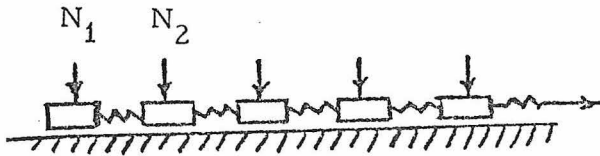
(a) Smoltezyk's Model
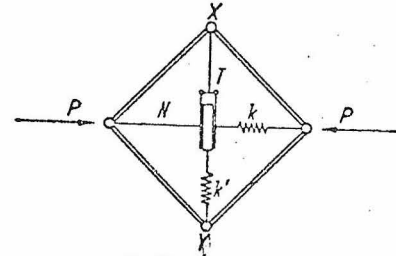
(b) Brown's Model

Positive T tensile
Positive N compressive
Member XY initially s_0 too long
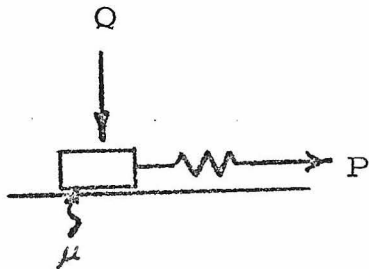
(c) Palmer's Model
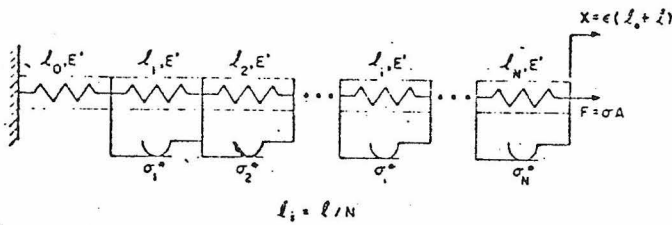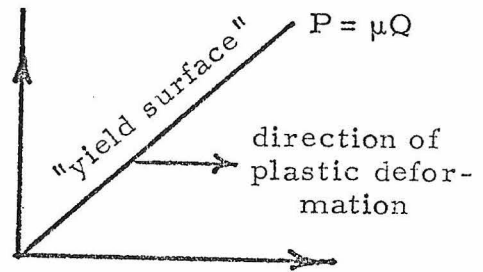
(d) Iwan's series-parallel Model[*]

[*]Iwan's parallel-series model shown in Fig. III.3
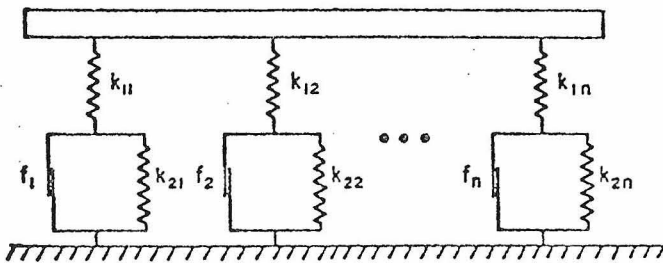
(e) Well's and Paslay's Model

Fig. II.7. Various Rheological Models
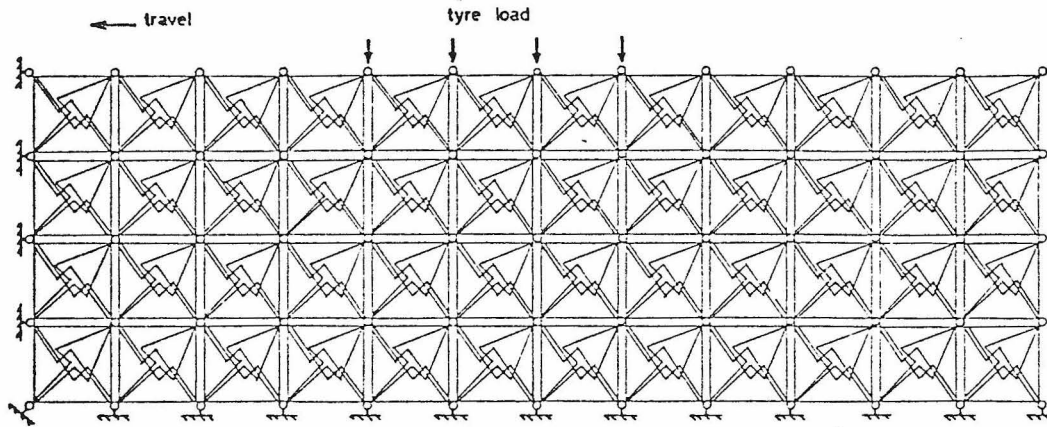
(a) An assembly of units to simulate a long section of an elastoplastic pavement experiencing plane stress.

A— horizontal and vertical elements
S— shear elements ; V— volume elements
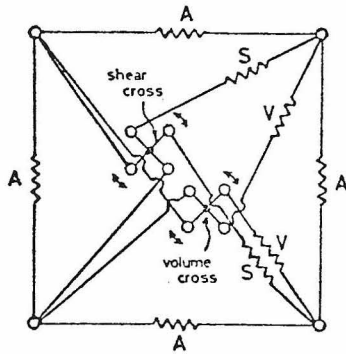
Elements exhibit a higher compliance when loading than when unloading

(b) A unit of the lattice structure simulating the behavior of the soil.
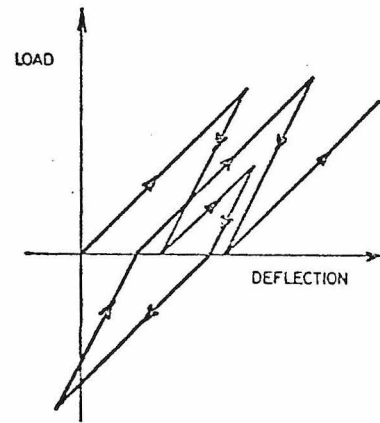
(c) Possible load-deflection behavior of an element or model.

Fig. II.8. Yandell's Model

CHAPTER III

RHEOLOGICAL MODELS AND GENERAL THEORY

III.1 One-Dimensional Model and General Concepts

A granular medium consists of irregularly shaped and sized grains packed randomly together. The number of contacts per unit volume depends on the porosity, the shape and size distribution of grains, and the state of stress. A change in the state of stress will cause a change in the interparticle forces between contacts which, in turn, causes the grains to move or slip with respect to each other. A recovery of the state of stress would recover a certain portion of the deformation but not all of it because most of the grain slips at contacts can not be totally recovered. We will first consider the one-dimensional case.

When a granular material is under external stresses or loadings, each grain is subjected to a resultant stress or force through the contacts with neighboring grains. The movement or deformation of each grain can be assumed to be a function of this resultant force. When this force reaches a certain level, the grain slips with respect to the neighboring grains. The movement or deformation of each grain can be assumed to be a function of this resultant force. When this force reaches a certain level, the grain slips with respect to the neighboring grain. This level of stress varies from grain to grain and is dependent on the contacts, the shape and grain distribution of the granular medium. Experimental results on Ottawa sand by Ko [16] and Masson [17] had clearly indicated that granular material

behaved differently under axial compression and axial extension stress conditions. Therefore, it is likely that this force level as such slip occurs may be different for each grain in compression and extension.

As one approach to mathematical analysis, the above behavior of a grain may be represented by a mechanical model consisting of a spring and two slip elements as shown in Fig. III.1. The spring represents the elastic behavior before the grain slips at the contact. The two slip elements with stops represent the slip stress level in compression and extension respectively. The slip elements represent the summation of slip behavior of all the contacts in a grain in a granular material. Thus the model presented here is a homogeneous elastically isotropic body containing a number of randomly oriented contacts slipping at certain critical stress. In this mechanical model it can be seen that when the resultant stress in this grain is less than σ_t^* in extension or σ_c^* in compression, the grain behaves elastically. However if the stress level exceeds σ_t^* in extension or σ_c^* in compression, the grain slips and plastic strains thus develop.

In the one-dimensional case, the behavior of the granular medium consisting of an assemblage of grains is represented by a mechanical model containing a large number of these spring-slip elements in parallel as shown in Fig. III.2. The properties of the elements are distributed in some fashion to be determined to represent the field characteristics of each individual grain of the granular medium. Some postulations for σ_c^* and σ_t^*, and the stress-strain relations for this one-dimensional model will be demonstrated in Section III. 1-2.

III.1-1 Simple Model

Before discussing the detail of our one-dimensional model for granular material, it is advisable to examine a simpler class of model as shown in Fig. III.3. The constitutive relation for this simpler model is not difficult to derive and will eventually lead to the constitutive derivation for our more complicated model with some modification. This model was used by Iwan [18,19] to describe the yielding behavior of continuous and composite systems. A similar model was also used by Wells and Paslay [103] for the analysis of the Bauschinger effect in some engineering alloys. For illustrative purposes, this simple model shown in Fig. III.3 is defined as Model A. The more complicated model shown in Figs. III.1 and III.2 is classified as Model B in this study. As shown in Fig. III.3, Model A has a large number of elements in parallel; each element consists of a spring and a slip element in series. The hysteresis loop of this simple model can be divided into three parts, namely, initial loading path, unloading path and reloading path as shown in Fig. III.4. The derivation is after Iwan [18,19]:

(a) Initial loading path

For a discrete model, the constitutive relation can be expressed as

$$\sigma = \frac{F}{A} = \sum_{i=1}^{n} \frac{E_i}{N} \epsilon + \sum_{i=n+1}^{N} \frac{\sigma_i^*}{N} \qquad (3.1)$$

where σ_i^* is the limit (critical) stress for the ith element to slip, and E_i is the Young's modulus of the spring for the ith element.

The first part of the right-hand side of Eq. (3.1) represents those elements which remain elastic during the loading process, and the second part represents those elements which have yielded. In general, σ_i^* and E_i can be regarded as distributed parameters. Thus Eq. (3.1) can be rewritten as:

$$\sigma = \int_{E\epsilon}^{\infty} E\epsilon\phi(\sigma^*)d\sigma^* + \int_0^{E\epsilon} \sigma^*\phi(\sigma^*)\,d\sigma^* \qquad (3.2)$$

where $\phi(\phi^*)$ is the distributed function and $\phi(\sigma^*)\,d\sigma^*$ represents the fraction of total elements having limit stress between σ^* and $\sigma^* + d\sigma^*$. Statistically speaking, $\phi(\sigma^*)$ represents the probability density function of the spring-slip element which slip at a corresponding stress level σ^*. Equation (3.2) can be further rearranged as

$$\sigma = \int_0^{\infty} E\epsilon\phi(\sigma^*)\,d\sigma^* - \int_0^{E\epsilon}(E\epsilon - \sigma^*)\phi(\sigma^*)\,d\sigma^* \qquad (3.3)$$

(b) Unloading path

When the medium is initially loaded to a state of σ_u and ϵ_u, the stress-strain curve for the unloading path can be expressed as:

$$\sigma = \int_{E\epsilon_u}^{\infty} E\epsilon\phi(\sigma^*)\,d\sigma^* + \int_{E(\epsilon_u-\epsilon)/2}^{E\epsilon_u}(E\epsilon - E\epsilon_u + \sigma^*)\,d\sigma^*$$

$$- \int_0^{E(\epsilon_u-\epsilon)/2} \sigma^*\phi(\sigma^*)\,d\sigma^* \qquad (3.4)$$

The first part of the right-hand side of Eq. (3.4) represents the behavior of the unyielded elements, the second part represents that of elements which yielded upon initial loading but behave elastically

upon unloading, and the third part represents those elements which yield upon initial loading and now yield again but in an opposite sense.

It can be proved after some mathematical manipulation that if $\int_0^\infty \phi(\sigma^*)\, d\sigma^* = 1$, the loading stress-strain relationship becomes:

$$\sigma = \sigma_u - E(\epsilon_u - \epsilon) + \int_0^{E(\epsilon_u - \epsilon)/2} [E(\epsilon_u - \epsilon) - 2\sigma^*]\phi(\sigma^*)\, d\sigma^* \qquad (3.5)$$

(Note: this also assumes that E is independent of σ^*.)

(c) Reloading path

When a material is unloaded to a state of σ_R and ϵ_R (where $|\epsilon_R| \leq |\epsilon_u|$) and then is reloaded, the stress-strain relationship can be represented as

$$\sigma = \int_0^{E(\epsilon - \epsilon_R)/2} \sigma^*\phi(\sigma^*)\, d\sigma^* + \int_{E(\epsilon - \epsilon_R)/2}^{E(\epsilon_u - \epsilon_R)/2} (E\epsilon - E\epsilon_R - \sigma^*)\phi(\sigma^*)\, d\sigma^*$$

$$+ \int_{E(\epsilon_u - \epsilon_R)/2}^{E\epsilon_u} (E\epsilon - E\epsilon_u + \sigma^*)\, d\sigma^* + \int_{E\epsilon_u}^\infty E\epsilon\phi(\sigma^*)\, d\sigma^* \qquad (3.6)$$

After some manipulation, Eq. (3.6) can be rewritten as

$$\sigma = \sigma_R + \int_0^\infty E(\epsilon - \epsilon_R)\phi(\sigma^*)\, d\sigma^* - \int_0^{E(\epsilon - \epsilon_R)/2} [E(\epsilon - \epsilon_R) - 2\sigma^*]\phi(\sigma^*)\, d\sigma^*$$

$$(3.7)$$

In the derivation of the hysteresis loop for the simple model, it is assumed that the stress-strain characteristics for compressive and tensile loadings are the same. This may be true to a certain extent for some engineering materials such as steel and its alloys.

However, for materials such as concrete or a granular medium, the stress-strain characteristics are different in compression and extension, the simple model thus fails to represent this behavior correctly. Therefore, to correct this, two slip elements are needed to represent the behavior of granular material under compression and extension as shown in Fig. III.2. The more realistic mechanical model yields a much more complicated hysteresis loop as can be expected. However, the derivation of loading, unloading and reloading stress-strain relations is similar to that for the simple model.

III.1-2 One-dimensional Analysis of Model B Used in This Thesis

The distribution functions for the critical yield stress in extension, σ_t^*, and compression, σ_c^*, are $\phi_t(\sigma_t^*)$ and $\phi_c(\sigma_c^*)$ respectively. These functions are not necessarily the same. For a granular material it is expected that $\phi_t(\sigma_t^*)$ and $\phi_c(\sigma_c^*)$ would be different. Here we also speculate that the following conditions should be observed:

$$\int_0^\infty \left| \phi_t(\sigma_t^*) \, d\sigma_t^* \right| = 1$$

and
(3.8)

$$\int_0^\infty \phi_c(\sigma_c^*) \, d\sigma_c^* = 1 \ .$$

Equation (III.8) implies that a granular material would totally slip or yield under infinite compression or extension. Usually, when a granular material is subjected to compression then extension, a portion of the elements will yield in compression and some other

portion will yield in extension. This implies that the hysteresis loop would be much more complicated than the one shown in Fig. III.4. Generally, the stress-strain relation of our new model to represent the one-dimensional behavior of a granular material can be illustrated as in Fig. III.5(a). The stress-strain curves shown in Fig. III.5 are qualitatively drawn to demonstrate the possible loading paths for Model B in the one-dimensional case. They are not attempted to quantitatively represent any experimental data. The stress and strain at any point x on the stress-strain curve are denoted by σ_x and ϵ_x respectively. As demonstrated in Eqs. (3.1) to (3.7), the rheological Models A and B always lead to stress-strain relation in a form which gives stress as a function of strain. The loading history and the slip behavior of elements are all expressed in terms of strain. The following derivations are referred to Fig. III.5(a).

(a) From origin to point a

This is a compression initial loading path. The stress-strain relation can be expressed as:

$$\sigma = E\epsilon - \int_0^{E\epsilon} (E\epsilon - \sigma_c^*)\phi_c^*(\sigma_c^*)\, d\sigma^* \tag{3.9}$$

so that at point a, the following stress-strain relation is obtained:

$$\sigma_a = E\epsilon_a - \int_0^{E\epsilon_a} (E\epsilon_a - \sigma_c^*)\phi_c(\sigma_c^*)\, d\sigma_c^* \tag{3.10}$$

(b) Path a → b → c (where $\epsilon \gtrless 0$)

This is the initial compressive unloading path along which the strain is decreasing but still remains positive (compressive).

Equation (3.5) can be used to express the stress-strain relation, i.e.

$$\sigma = \sigma_a - E(\epsilon_a - \epsilon) + \int_0^{E(\epsilon_a - \epsilon)/2} [E(\epsilon_a - \epsilon) - 2\sigma_c^*] \phi_c^*(\sigma_c^*) \, d\sigma_c^* \qquad (3.11)$$

Notice that at point c, $\epsilon_c = 0$. Therefore

$$\sigma_c = \sigma_a - E\epsilon_a + \int_0^{E\epsilon_a/2} (E\epsilon_a - 2\sigma_c^*) \phi_c^*(\sigma_c^*) \, d\sigma_c^* \qquad (3.12)$$

(c) Path $c \rightarrow d$ where $-\epsilon_d = \epsilon_a$ and $E < 0$

This is a combination of an initial compressive unloading and an initial extensive loading paths along which the strain is negative (extension) and has absolute value smaller than ϵ_a. As demonstrated in the stress-strain derivation for Model A, the fraction of yielded element upon compressive straining to $\epsilon = \epsilon_a$ would be $\int_0^{E\epsilon_a} \phi(\sigma_c^*) \, d\sigma_c^*$. Therefore, the unyielded fraction u of the element after initial compressive loading to $\epsilon = \epsilon_a$ and initial compressive unloading to $\epsilon = 0$, would be

$$u = 1 - \int_0^{E\epsilon_a} \phi(\sigma_c^*) \, d\sigma_c^* \qquad (3.13)$$

As the strain becomes negative, some portion of u would yield under extension while the remaining (1 - u) would continue its compressive unloading process. The stress-strain relation for path c to d can thus be written as:

$$\sigma = u\left\{ E\epsilon + \int_0^{|E\epsilon|} (|E\epsilon| - \sigma_t^*)\phi_t(\sigma_t^*) \, d\sigma_t^* \right\} - \int_0^{E(\epsilon_a - \epsilon)/2} \sigma_c^* \phi_c^*(\sigma_c^*) \, d\sigma_c^*$$

$$- \int_{E(\epsilon_a - \epsilon)/2}^{E\epsilon_a} [E(\epsilon_a - \epsilon) - \sigma_c^*] \phi(\sigma_c^*) \, d\sigma_c^* \qquad (3.14)$$

At point d, $\epsilon_d = -\epsilon_a$. Therefore the stress at point d can be obtained from Eqs. (3.12) and (3.14) as:

$$\sigma_d = \sigma_c + E\epsilon_d \left(1 - \int_0^{E\epsilon_a/2} \phi_c(\sigma_c^*)\, d\sigma_c^*\right) + u\int_0^{|E\epsilon_d|} (|E\epsilon_d| - \sigma_t^*)\phi_t\, d\sigma_t^*$$

$$+ u\int_{E\epsilon_a/2}^{E\epsilon_a} E\epsilon_a - 2\sigma_c^*\, \phi_c(\sigma_c^*)\, d\sigma_c^* \tag{3.15}$$

(d) Path $d \rightarrow e \rightarrow f \rightarrow \epsilon$ where $|\epsilon| \leq \epsilon_a$ and $\epsilon_g = \epsilon_a$

This is a combined path of initial compressive reloading and initial extensive unloading along which the strain increases and has an absolute value smaller than ϵ_a. The stress-strain relation can be written as:

$$\sigma = u\left\{\int_0^{E(\epsilon-\epsilon_d)/2} \sigma_t^*\phi_t(\sigma_t^*)\, d\sigma_t^* + \int_{E(\epsilon-\epsilon_d)/2}^{|E\epsilon_d|} [E(\epsilon-\epsilon_d) - \sigma_t^*]\phi_t\, d\phi_t^* \right.$$

$$\left. + E\epsilon\int_{|E\epsilon_d|}^{\infty} \phi_t(\sigma_t^*)\, d\sigma_t^*\right\}$$

$$+ \int_0^{E(\epsilon-\epsilon_d)/2} \sigma_c^*\phi_c(\sigma_c^*)\, d\sigma_c^* + \int_{E(\epsilon-\epsilon_d)/2}^{E(\epsilon_a-\epsilon_d)/2} [E(\epsilon-\epsilon_d) - \sigma_c^*]\phi_c(\sigma_c^*)\, d\sigma_c^*$$

$$+ \int_{E(\epsilon-\epsilon_d)/2}^{E\epsilon_a} [E(\epsilon-\epsilon_a) + \sigma_c^*]\phi_c(\sigma_c^*)\, d\sigma_c^* \tag{3.16}$$

At point g, $\epsilon_g = \epsilon_a$, so the stress at point g can be obtained from Eq. (3.16) as:

$$\sigma_g = u\left\{\int_0^{|E\epsilon_d|} \sigma_t^*\phi_t(\sigma_t^*)\, d\sigma_t^* + E\epsilon_a\int_{|E\epsilon_d|}^{\infty} \phi_t(\sigma_t^*)\, d\sigma_t^*\right\} + \int_0^{E\epsilon_a} \sigma_c^*\phi_c(\sigma_c^*)\, d\sigma_c^*$$

$$\tag{3.17}$$

Comparing Eq. (3.17) with Eq. (3.14), the following relation can be observed:

$$\sigma_g = \sigma_a - u \int_0^{|E\epsilon_d|} (E\epsilon_a - \sigma_t^*) \phi_t(\sigma_t^*) \, d\sigma_t^* \tag{3.17a}$$

In general, the hysteresis loop indicates that the stress-strain relation depends on the maximum strain magnitude previously reached and the number of loading reversals. From Eq. (3.17a), it can be seen that the stress level in compression decreases by an amount of $u \int_0^{|E\epsilon_d|} (E\epsilon_a - \sigma_t^*) \phi_t(\sigma_t^*) d\sigma_t^*$ after the first loading cycle. From a compressive stress point of view, the granular material is softening after the initial cycle of loading.

(e) Path $g \to h \to i \to j$ where $\epsilon_j = -\epsilon_g = -\epsilon_a$

This is a combined path of cyclic compressive unloading and cyclic extensive reloading. The stress-strain relation can be written as:

$$\sigma = u \left\{ \int_0^{E(\epsilon_a - \epsilon)/2} \sigma_t^* \phi_t(\sigma_t^*) \, d\sigma_t^* + \int_{E(\epsilon_a - \epsilon)/2}^{E(\epsilon_a - \epsilon_d)/2} [E(\epsilon - \epsilon_a) - \sigma_t^*] \phi_t(\sigma_t^*) \, d\sigma_t^* \right.$$

$$\left. + \int_{E(\epsilon_d - \epsilon_a)/2}^{E\epsilon_d} [E(\epsilon - \epsilon_d) + \sigma_t^*] \phi_t(\sigma_t^*) \, d\sigma_t^* + E\epsilon \int_{|E\epsilon_d|}^\infty \phi_t(\sigma_t^*) \, d\sigma_t^* \right\}$$

$$- \int_0^{E(\epsilon_a - \epsilon)/2} \sigma_c^* \phi_c^* \, d\sigma_c^* - \int_{E(\epsilon_a - \epsilon)/2}^{E\epsilon_a} [E(\epsilon_a - \epsilon) - \sigma_c^*] \phi_c^*(\sigma_c^*) \, d\sigma_c^* \tag{3.18}$$

Since $\epsilon_j = \epsilon_d = -\epsilon_a$, we can compare Eq. (3. 8) and Eq. (3. 4) and conclude that

$$\sigma_j = \sigma_d \tag{3.19}$$

In other words, point j and point d coincide.

(f) Path $j \to k \to g$

From the condition shown in Eq. (3.19) we conclude that the stress-strain relation for loading path $j \to k \to g$ is the same as the loading path $d \to e \to f \to g$.

From the above derivation and conclusion, a unique hysteresis loop is thus established for cyclic loading. This unique hysteresis loop is represented by a close loop defghid as shown in Fig. III.5(a).

III.2 Statistical Approaches to Distribution Parameters

The main purpose of a statistical approach is to determine the distributed characteristics for the parameters $(E, \sigma_c^* \text{ and } \sigma_t^*)$ involved in the slip-spring elements. As mentioned before, the distribution of these parameters depends on the geometrical configuration, the contact force, and the physical properties of the granular material such as the porosity and nature of friction between contacts. A more general approach must start from the consideration of statistical geometry of packing and the statistical distribution of contact forces and friction characteristics under a general loading condition.

In general, E, σ_c^* and σ_t^* can all be distributed parameters. However, consideration is given to the case that σ_c^* and σ_t^* are distributed while the elastic modulus E remains constant over a range of stress (if E is assumed to be distributed then the derivation for this model would become very complicated). Let $\phi_c^*(\sigma_c^*)$

and $\phi_t^*(\sigma_t^*)$ denote the distribution functions of σ_c^* and σ_t^* respectively. Then $\phi_c(\sigma_c^*) \, d\sigma_c^*$ or $\phi_t(\sigma_t^*) \, d\sigma_t^*$ are the fractions of the total slip elements having a slip stress between σ_c^* and $\sigma_c^* + d\sigma_c^*$, and between σ_t^* and $\sigma_t^* + d\sigma_t^*$ respectively. In this section, several types of distribution functions are considered. The feasibility of applying these functions to different materials are also briefly discussed. To illustrate the general situation only simple compression or extension loading paths are considered in this section.

Of all the possible distribution functions for $\phi_c(\sigma_c^*)$ and $\phi_t(\sigma_t^*)$, the rectangular distribution is probably the simplest. A rectangular distribution of $\phi_c(\sigma_c^*)$ or $\phi_t(\sigma_t^*)$ implies that the probability for the grain contacts to slip is uniform over a range of stress until a critical stress is reached. A critical stress is here defined as the minimum stress level which cause all the contacts to slip completely. Similarly, a triangular distribution of $\phi_c(\sigma_c^*)$ and $\phi_t(\sigma_t^*)$ implies that the probability for grain contacts to slip increases linearly with the increase of stress to a certain level then decreases to zero. In an effort to simulate the behavior of a granular material under hydrostatic stress, Ko and Scott [42] used a triangular distribution of gap widths with respect to hydrostatic pressure in their model consisting of simple cubic arrays and face-centered cubic array.

For ideal packings such as simple cubic and face-centered cubic arrays of a granular medium, rectangular or triangular function may be considered as acceptable for deformation behaviors due to the orderly formation of grain contacts. As mentioned over and over again, a granular medium in nature consists of irregular shaped and

sized grain packed randomly together. The distribution of the slip behavior of grain contacts can not always be expected to be as simple as rectangular or triangular. However rectangular or triangular distribution of $\phi_c(\sigma_c^*)$ or $\phi_t(\sigma_t^*)$ should be able to provide at least qualitatively some understanding of the deformation behavior of real granular material.

It should also be pointed out that certain orderness in a randomly packed real granular material may exist in nature for a distributed function of $\phi_c(\sigma_c^*)$ and $\phi_t(\sigma_t^*)$. Gaussian (normal) distribution is one of the simple forms of probability functions and most likely occur in nature. For example, the frequency distribution of a random noise is well known to be normally distributed. Therefore, Gaussian distribution of $\phi_c(\sigma_c^*)$ and $\phi_t(\sigma_t^*)$ should be considered as a most likely possibility. This may sound philosophical. However, certain physical grounds and advantages of representing slip behavior of granular materials by Gaussian distribution will be discussed later in this section.

Some of the stress-strain relation derivations and properties of using rectangular, triangular and Gaussian distributions to represent $\phi_c(\sigma_c^*)$ or $\phi_t(\sigma_t^*)$ for Models A and B will be given as follows:

III. 2-1 Rectangular distribution of slip behavior

$\phi_c(\sigma_c^*)$ or $\phi_t(\sigma_t^*)$ is a rectangular distribution. As shown in Fig. III.6, let

$$\phi(\sigma^*) = \frac{1}{x} \quad \text{if} \quad 0 \leq \sigma^* \leq x$$

$$= 0 \quad \text{if} \quad \sigma^* > x$$

(3.20)

such that

$$\int_0^\infty \phi(\sigma^*) \, d\sigma^* = 1 \tag{3.20a}$$

where x is the critical stress level and has dimension of E. $\phi(\sigma^*)$ represents either $\phi_c(\sigma_c^*)$ or $\phi_t(\sigma_t^*)$ and has a dimension of $1/E$.

The stress-strain relation can be obtained by substituting Eq. (3.20) into Eqs. (3.2), (3.5) and (3.7) or into Eqs. (3.10) to (3.18). For illustrative purposes only the stress-strain relation for a simple model (Model A) will be presented as follows.

(i) Loading path (substituting Eq. (3.20) into Eq. (3.2))

$$\sigma = E\epsilon \left(1 - \frac{E\epsilon}{2x}\right) \qquad \text{if} \qquad E\epsilon \leq x$$

$$\sigma = 0.5x \qquad \text{if} \qquad E\epsilon > x \tag{3.21}$$

(ii) Unloading path (unloading at σ_u and ϵ_u)

$$\sigma = \sigma_u - E(\epsilon_u - \epsilon)\left[1 - \frac{E(\epsilon_u - \epsilon)}{4x}\right] \quad \text{if} \quad 0 \leq E(\epsilon_u - \epsilon) \leq 2x$$

$$\sigma = -0.5x \qquad \qquad \text{if} \quad E(\epsilon_u - \epsilon) > 2x \tag{3.22}$$

(iii) Reloading path (reloading at σ_R and ϵ_R)

$$\sigma = \sigma_R + E(\epsilon - \epsilon_R)\left[1 - \frac{E(\epsilon - \epsilon_R)}{4x}\right] \quad \text{if} \quad 0 \leq E(\epsilon - \epsilon_R) \leq 2x$$

$$\sigma = 0.5x \qquad \qquad \text{if} \quad E(\epsilon - \epsilon_R) \geq 2x \tag{3.23}$$

A dimensionless plot, in which σ is expressed in terms of x, is shown in Fig. III.7. Observing the results, the following remarks can be made:

1. For all loading paths, σ is a 2nd order function of ϵ. That is to say the $\sigma - \epsilon$ plot is a parabolic curve.

2. When $E\epsilon = x$, the resulting stress is half of the value obtained from a linear analysis.

3. Due to the simplicity of this rectangular distribution, it is easy to express the stress-strain relation in incremental form by simply taking the derivative of σ with respect to ϵ.

III. 2-2 Triangular distribution of slip behavior

$\phi_c(\sigma_c^*)$ or $\phi_t(\sigma_t^*)$ is a triangular distribution. As shown in Fig. III.8, let

$$\phi(\sigma^*) = \frac{4\sigma^*}{x^2} \qquad \text{if} \quad 0 \leq \sigma^* \leq \frac{x}{2}$$

$$= \frac{4(x-\sigma^*)}{x^2} \qquad \text{if} \quad \frac{x}{2} \leq \sigma^* \leq x \qquad (3.24)$$

$$= 0 \qquad \text{elsewhere}$$

such that

$$\int_0^\infty \phi(\sigma^*) \, d\sigma^* = 1 \qquad (3.24a)$$

where the definitions and dimensions of x and ϕ are the same as in previous derivations.

The stress-strain relations for different loading paths for Model A can be illustrated as follows.

(i) Loading path

Substituting Eq. (3.24) into Eq. (3.2), the stress-strain

relation for loading path can be expressed as

$$\sigma = E\epsilon \left\{ 1 - \frac{2(E\epsilon)^2}{3x^2} \right\} \qquad\qquad \text{for } E\epsilon \leq \frac{x}{2}$$

$$= E\epsilon \left\{ 1 - \frac{(E\epsilon)}{3x^2} \right\} + \frac{4}{3x^2}(E\epsilon - 0.5x) \quad \text{for } \frac{x}{2} \leq E\epsilon \leq x \quad (3.25)$$

$$= 0.5\,x \qquad\qquad\qquad\qquad \text{elsewhere}$$

(ii) Unloading path (unloading at σ_u and ϵ_u, $\epsilon_u-\epsilon = 0$ and $|\epsilon| < \epsilon_u$)

Substituting Eq. (3.24) into Eq. (3.5) the stress-strain relation

for unloading path can be expressed as

$$\sigma = \sigma_u - E(\epsilon_u-\epsilon)\left\{ 1 - \frac{[E(\epsilon_u-\epsilon)]^2}{6x^2} \right\} \qquad \text{for } 0 \leq E(\epsilon_u-\epsilon) \leq x$$

$$= \sigma_u - 2E(\epsilon_u-\epsilon) + \frac{[E(\epsilon_u-\epsilon)]^2}{x} - \frac{[E(\epsilon_u-\epsilon)]^3}{6x^2} + \frac{x}{3} \quad \text{for } x \leq E(\epsilon_u-\epsilon) \leq 2x$$

$$= -0.5\,x \qquad\qquad\qquad\qquad\qquad\qquad \text{for } E(\epsilon_u-\epsilon) \geq 2x$$

$$(3.26)$$

(iii) Reloading path (reloading at σ_R and ϵ_R, $\epsilon-\epsilon_R > 0$ and $|\epsilon| \leq \epsilon_u$)

Substituting Eq. (3.24) into Eq. (3.7), the stress-strain for

reloading path can be expressed as

$$\sigma = \sigma_R + E(\epsilon-\epsilon_R)\left\{ 1 - \frac{[E(\epsilon-\epsilon_R)]^2}{6x^2} \right\} \qquad \text{for } 0 \leq E(\epsilon-\epsilon_R) \leq x$$

$$= \sigma_R + 2E(\epsilon-\epsilon_R) - \frac{[E(\epsilon-\epsilon_R)]^2}{x} + \frac{[E(\epsilon-\epsilon_R)]^3}{6x^2} - \frac{x}{3}$$

$$\text{for } x \leq E(\epsilon-\epsilon_R) \leq 2x$$

$$= 0.5\,x \qquad\qquad\qquad\qquad \text{for } E(\epsilon-\epsilon_R) \geq 2x$$

$$(3.27)$$

The dimensionless plot of stress-strain curve for both loading and unloading is shown in Fig. III.9. From the above derivations and results, the following remarks can be made:

1. For all loading paths, stress is a 3rd order function of strain. That is to say the σ-ϵ plot is a cubic curve.

2. Let x denote the critical stress level at which all the grain contacts slip completely. Then for any loading path the stress is within the range of $x/2$ and $-x/2$.

3. Like the rectangular distribution, the triangular description of slip behavior yields simple forms of stress-strain relation. It is easy to express the stress-strain relation in incremental form by simply taking the derivatives of stress with respect to strain.

III. 2-3 Further comments for both rectangular and triangular distributions of $\phi(\sigma^*)$

From the stress-strain curves for rectangular and triangular distributions of $\phi(\sigma^*)$, it can be observed that the material represented by Models A and B behaves like a perfectly plastic medium as the strain reaches a magnitude of x/E, while the stress-strain relation differs a little bit from the linear case when the strain is small. This type of deformation behavior can be approximated by a perfectly elasto-plastic material.

The purpose of a one-dimensional analysis established here is not an attempt to fit or predict the one-dimensional deformation behavior of granular material. A true one-dimensional test in granular material is very difficult it not impossible to perform due

to difficulty of controlling the stresses and strains in the other two dimensions at zero level. Instead, the purpose of one-dimensional analysis is to establish a stress-strain model whose behavior is in close resemblance with the deformation behavior of a granular material in three-dimensional cases. It is hoped that this one-dimensional model will eventually lead to a general three-dimensional description of a granular material's behavior.

A typical experimental data of Ottawa sand under axial shear test (the stress path is indicated in Fig. IV.2 in the next chapter) performed by Ko [16] in a cubic triaxial testing apparatus is chosen for comparison purposes. Ko's Tca-1 test results (page 112 of Ref. [16]) of stress-strain in major principal direction are plotted in dotted lines as shown in Figs. III.10 and III.11. To simulate this test data, the E and x values for both rectangular and triaxial distribution of $\phi(\sigma^*)$ are measured from the curve of test data. E is measured as the initial slope of the curve of test data, and x is taken to be $\frac{1}{2}$ of the value of maximum stress level of the testing stress-strain curve. The simulated stress-strain curves for rectangular distribution and triangular distribution of $\phi(\sigma^*)$ in Model A and B are shown in solid lines in Figs. III.10 and III.11 respectively.

It can be seen that the loading and unloading curves for both distributions are quite similar to the testing curves. The loading curves of both distributions all indicate a sharper change of slope in comparison with the experimental stress-strain curve which has a smoother and more subtle change of slope. The unloading stress-

strain curves for both distributions are almost straight compared to the curved test cuves. However, the magnitude of the stress-strain relation for both unloading curves are very similar to that of the Tca-1 test.

In observing the overall stress-strain loading and unloading curves for both distributions functions and the Tca-1 test curve, it can be noticed that the simulation by both distributions is not at all a bad fit in comparison with the stress-strain curves obtained by the presently existing theories and methods. This manifests the potential of using slip-spring elements to represent the granular material's behavior since, as shown here, they can apparently describe the fundamental aspects of the stress-strain behavior of a granular material even when a simple distribution function for slip behavior is used.

III. 2-4 Gaussian (normal) distribution of slip behavior

As shown in Fig. III.12, let

$$\phi(\sigma^*) = \frac{t}{\sqrt{2\pi}\, s} \exp\left[- \frac{1}{2}\left(\frac{\sigma^*-m}{s}\right)^2\right] \tag{3.28}$$

where

$$t = 1 / \left\{ 1 - \int_{-\infty}^{0} \frac{1}{\sqrt{2\pi}} \exp\left[- \frac{1}{2}\left(\frac{\sigma^*-m}{s}\right)^2\right] ds^* \right\} \tag{3.28a}$$

s is the standard, slip-stress deviation and

m is the mean of the Gaussian distribution

(notice that m and s have dimension of stress and $\phi(\sigma^*)$ has dimension of $(\text{stress})^{-1}$) such that

$$\int_{0}^{\infty} \phi(\sigma^*)\, d\sigma^* = 1 \tag{3.28b}$$

The stress-strain relations for different leading paths for Model A can be illustrated as follows.

(i) Initial loading path

Substituting Eq. (3.28) into Eq. (3.2) the stress-strain relation for loading path can be expressed as

$$\sigma = E\epsilon - \frac{t}{\sqrt{2\pi}\ s} \int_0^{E\epsilon} (E\epsilon - \sigma^*) \exp\left[-\frac{1}{2}\left(\frac{\sigma^* - m}{s}\right)^2\right] d\sigma^* \qquad (3.29)$$

(ii) Unloading path (unloading at σ_u and ϵ_u, and $|\epsilon| < \epsilon_u$)

Similarly, the stress-strain relation for unloading path can be obtained by substituting Eq. (3.28) into Eq. (3.5), and expressed as

$$\sigma = \sigma_u - E(\epsilon_u - \epsilon) \ \frac{2t}{\sqrt{2\pi}\ s} \int_0^{E(\epsilon_u - \epsilon)/2} \left[\frac{E(\epsilon_u - \epsilon)}{2} - \sigma^*\right] \exp\left[\frac{1}{2}\left(\frac{\sigma^* - m}{s}\right)^2\right] d\sigma^*$$

$$(3.30)$$

(iii) Reloading path (reloading at σ_R and ϵ_R, $|\epsilon| \leq \epsilon_u$

Substituting Eq. (3.28) into Eq. (3.7), the stress-strain relation for reloading path can be obtained as

$$\sigma = \sigma_R \ E(\epsilon - \epsilon_R) - \frac{2t}{\sqrt{2\pi}\ s} \int_0^{E(\epsilon - \epsilon_R)/2} \left[\frac{E(\epsilon - \epsilon_R)}{2} - \sigma^*\right] \exp\left[-\frac{1}{2}\left(\frac{\sigma^* - m}{s}\right)^2\right] d\sigma^*$$

$$(3.31)$$

The resulting plots of the stress-strain relation for the Gaussian distribution function for several values of s and m, along with the test results of Ko's Tca-1 test [16] are shown in Fig. III.13. Here, E is again obtained from the magnitude of initial slope of stress-strain curve of Tca-1 test. From these results, the follow-

ing conclusions can be made:

(1) In assuming a Gaussian distribution for $\phi(\sigma^*)$, there are several parameters, namely m and s, which need to be considered. It is noticed that m and s values can be different in compression and extension. If the modulus E is assumed to be constant then its value may be determined from the initial slope of a stress-strain plot. The values of m and s can be determined from fitting the experimental data or may be obtained from physical considerations. More parameters mean more freedom to fit a set of data. However, they also mean that more experimental data and more complicated procedure are required to closely determine the necessary quantities. The advantages may be outweighed by the disadvantages.

(2) From the loading path of the stress-strain plot for the Gaussian distribution function, it can be seen that a higher mean, m, results in a steeper slope for small strain and a flatter slope when strain becomes larger. The influence of the standard deviation, s, is in the level of stress. Higher standard deviation values result in a higher stress level at the same amount of strain.

(3) The combined influence of m and s or the stress-strain relation enable us to obtain good fits to almost any experimental data available at present.

As mentioned before, the stress-strain behavior of a granular material depends on a number of factors. A more general approach must start from the statistical geometry of the packing, the corresponding contact force and friction, and an incremental expression for stress-strain relation. The number of contacts and grain size

distribution are important factors to describe the stress-strain behavior of a granular material. In other words, the porosity or void ratio of the granular material is most important in governing the stress-strain relation. Smith, Foote, and Busang [29] have determined the experimental and theoretical relation between porosity and the number of contacts per grain for randomly packed homogeneous spheres. Their findings are shown in Fig. III.14. It can be seen that there exists a Gaussian-like distribution of the number of contacts for a particular value of porosity. In a similar manner, it can be speculated that the contact force and orientation are also distributed in Gaussian fashion. It seems, therefore, that the assumption of a Gaussian distribution function of slip stress for slip-spring elements is a reasonable one for describing the stress-strain behavior of a granular material. This couples with the ability of the Gaussian distribution function to describe closely almost any stress-strain curve as mentioned above, making the slip-spring elements model very attractive for a granular material. Furthermore, the rectangular distribution and triangular distribution can be approximated by a Gaussian distribution with a specific choice of the value of the mean and standard deviation. In this thesis, the Gaussian distribution of the slip stress for the slip-spring elements will be developed further.

III.3 Constitutive Relations for Granular Media in Two- and Three-
       Dimensional Cases

III.3-1 Preliminary Consideration

To represent more realistically and accurately the deforma-
tion behavior of a granular material, a one-dimensional model is
insufficient because it does not lead to a general three-dimensional
formulation. Although the slip and spring elements in a one-dimen-
sional model do represent in some degree the elastic-plastic behavior
of a material, the one-dimensional model fails to satisfy the following
important characteristics for the general behavior of a granular
material:

 (a) The dilatancy due to a shear stress increment,

 (b) The work hardening behavior and inelastic strains during
   shear deformation,

 (c) The quantitative influence of loading path and history on
   the stress-strain relation.

As can be expected the geometric structure of a granular
material is usually very complicated due to the irregular distribution
of different shapes and sizes of granular particles. Even for a
uniformly packed medium, the isotropy and homogeneity can be con-
sidered only from a macroscopic point of view. Moreover anisotropy
and non-homogeneity can often result from loading an initially iso-
tropic and homogeneous material[35] . From the contact stress
theory, the relation between the tangential component of the contact
force (between particles) and displacement is inelastic [31] , so
that the stress-strain relationship should depend upon the entire

loading history of the medium. Accordingly, the correct stress-
strain relation should be given as an incremental one; the purpose
of a three-dimensional model is to represent and predict the stress-
strain response of a granular material that has been subjected to an
arbitrary loading and unloading process. The model should not be
too complicated to be practical in use. In the long run, it is hoped
that the derived stress and strain relation could be applied to some
boundary value problems in soil mechanics by finite element
analysis [60].

To extend the one-dimensional model to two- or three-
dimensional stress-strain formulations requires the assessment of
the quantittative relation of stresses and strains in one direction to
the stresses and strains in other directions. In a granular medium,
the contacts between particles and the forces between contacts
dominate its deformation behaviors. They also provide the links
for the interdependence of stresses and strains in different directions
in the multi-dimensional case. For simplicity of derivation and
analysis, only principal stresses and strains are considered. For
illustrative purposes, we start with a two-dimensional homogeneous
and isotropic model and gradually develop a general anisotropic
three-dimensional model and formulation. In the two-dimensional
case, the one-dimensional model shown in Fig. III.2 can be used in
each direction to represent part of the elastic strain and all of the
plastic strain in each principal direction, if we inter-connect these
two one-dimensional models by stiffness springs with a modulus E_s
as shown in Fig. III.15. These springs provide the links between

stresses and strains in both directions. As mentioned in Chapter II, a similar two-dimensional rheological model (Fig. II.8b) was used by Yandell [110] to simulate a long section of a pavement under plane stress conditions.

At a first glance, it seems the two-dimensional model shown in Fig. III.15 has assumed that the interdependence of stresses and strains in different directions is purely elastic. However, this is not so, because the springs affect the stresses and strains in each direction which, in turn, influence the deformation behavior of the spring-slip elements. As mentioned before, a correct stress-strain relation should be given in incremental form. Due to the complexity of the stress-strain relation for the spring and slip elements, while in one direction it may follow a given loading path, the other direction may be subjected to another different loading path. This increases the need for an incremental constitutive formulation. Before beginning the derivation of the two-dimensional formulation, it is advisable to obtain the incremental form for the spring-slip elements.

III.3-2 Incremental forms for spring-slip elements

The stress and strain increments are denoted by $\Delta\sigma$ and $\Delta\epsilon$ respectively. The loading paths will all be referred to Fig. III.16. Due to the length of the derivation, only the final results will be shown here. The following derivations are applicable to any types of $\phi_c(\sigma_c^*)$ and $\phi_t(\sigma_t^*)$ distributions. $\phi_c(\sigma_c^*)$ and $\phi_t(\sigma_t^*)$ will be abbreviated as ϕ_c and ϕ_t respectively.

(a) Initial loading path $0 \rightarrow a$

$$\Delta\sigma = E\Delta\epsilon \left(1 - \int_0^{E\epsilon} \phi_c \, d\sigma_c^* \right) - \int_{E\epsilon}^{E(\epsilon+\Delta\epsilon)} [E(\epsilon+\Delta\epsilon-\sigma_c^*)]\phi_c \, d\sigma_c^* \qquad (3.32)$$

(b) Unloading path $a \rightarrow b \rightarrow c$ (unloading at $\epsilon = \epsilon_a$; $\Delta\epsilon < 0$)

$$\Delta\sigma = E\Delta\epsilon \left(1 - \int_0^{E(\epsilon_a-\epsilon)/2} \phi_c \, d\sigma_c^* \right)$$

$$- \int_0^{E(\epsilon_a-\epsilon-\Delta\epsilon)/2} [E(\epsilon_a-\epsilon-\Delta\epsilon)-2\sigma_c^*] \phi_c \, d\sigma_c^* \qquad (3.33)$$

(c) Compression unloading and extension loading path, $c \rightarrow d$ ($\Delta\epsilon < 0$ and $\epsilon < 0$)

$$\Delta\sigma = E\Delta\epsilon \left(1 - \int_0^{E(\epsilon_a-\epsilon)/2} \phi_c \, d\sigma_c^* \right)$$

$$- \int_{E(\epsilon_a-\epsilon)/2}^{E(\epsilon_a-\epsilon-\Delta\epsilon)/2} [E(\epsilon_a-\epsilon-\Delta\epsilon)-2\sigma_c^*] \phi_c \, d\sigma_c^*$$

$$- u \left\{ E\epsilon \int_0^{|E\epsilon|} \phi_t \, d\sigma_t^* + \int_{|E\epsilon|}^{|E(\epsilon+\Delta\epsilon)|} [E(\epsilon+\Delta\epsilon) - \sigma_t^*] \phi_t \, d\sigma_t^* \right\}$$

$$(3.34)$$

where

$$u = 1 - \int_0^{E\epsilon_a} \phi_c \, d\sigma_c^* \qquad (3.34a)$$

(d) Extension loading path $d \rightarrow D$ ($|\epsilon| > \epsilon_a$, $\Delta\epsilon < 0$, $\epsilon < 0$)

$$\Delta\sigma = u \left\{ E\Delta\epsilon \left(1 - \int_0^{|E\epsilon|} \phi_t \, d\sigma_t^* \right) - \int_{|E\epsilon|}^{|E(\epsilon+\Delta\epsilon)|} [|E(\epsilon+\Delta\epsilon)|-\sigma_t^*] \phi_t^* \, d\sigma_t^* \right\}$$

$$(3.35)$$

(e) Extension unloading and compression reloading path $d \to e \to f \to g$

$(\Delta\epsilon > 0, \ |\epsilon| < |\epsilon_a|)$

$$\Delta\sigma = \left\{ E\Delta\epsilon \left(1 - \int_0^{E(\epsilon-\epsilon_d)/2} \phi_c \, d\sigma_c^* \right) \right.$$

$$- \int_{E(\epsilon-\epsilon_d)/2}^{E(\epsilon+\Delta\epsilon-\epsilon_d)/2} [E(\epsilon+\Delta\epsilon-\epsilon_d) - 2\sigma_c^*] \phi_c \, d\sigma_c^* \right\}$$

$$- u \left\{ E\Delta\epsilon \int_0^{E(\epsilon-\epsilon_d)/2} \phi_t \, d\sigma_t^* \right.$$

$$+ \int_{E(\epsilon-\epsilon_d)/2}^{E(\epsilon+\Delta\epsilon-\epsilon_d)/2} [E(\epsilon+\Delta\epsilon-\epsilon_d) - 2\sigma_t^*] \dot{\phi}_t \, d\sigma_t^* \right\} \qquad (3.36)$$

(f) Extension unloading path $D \to E \to E_1$ $(\epsilon < 0, \ \Delta\epsilon > 0, \ |\epsilon| \geq |\epsilon_a|)$

$$\Delta\sigma = u \left\{ E\Delta\epsilon \left(1 - \int_0^{E(\epsilon-\epsilon_D)/2} \phi_t \, d\sigma_t^* \right) \right.$$

$$- \int_{E(\epsilon-\epsilon_D)/2}^{E(\epsilon+\Delta\epsilon-\epsilon_D)} [E(\epsilon+\Delta\epsilon-\epsilon_D) - 2\sigma_t^*] \dot{\phi}_t \, d\sigma_t^* \right\} \qquad (3.37)$$

(g) Extension unloading and compression reloading path $E_1 \to F \to G$

$(\Delta\epsilon > 0, \ |\epsilon| \geq |\epsilon_d|$

$$\Delta\sigma = \left\{ E\Delta\epsilon \left(1 - \int_0^{E(\epsilon-\epsilon_d)/2} \phi_c \, d\sigma_c^* \right) \right.$$

$$- \int_{E(\epsilon-\epsilon_d)/2}^{E(\epsilon+\Delta\epsilon-\epsilon_d)/2} [E(\epsilon+\Delta\epsilon-\epsilon_d) - 2\sigma_c^*] \dot{\phi}_c \, d\sigma_c^* \right\}$$

$$- u \left\{ E\Delta\epsilon \int_0^{E(\epsilon-\epsilon_D)/2} \phi_t \, d\sigma_t^* \right.$$

$$\int_{E(\epsilon-\epsilon_D)/2}^{E(\epsilon+\Delta\epsilon-\epsilon_D)/2} [E(\epsilon+\Delta\epsilon-\epsilon_D) - 2\sigma_t^*] \sigma_t \, d\sigma_t^* \right\} \qquad (3.38)$$

(h) Cyclic reloading path where $g \to g'$ $(\Delta\epsilon > 0, \ \Delta\epsilon > \epsilon_a = \epsilon_g)$

$$\Delta\sigma = v\left\{ E\Delta\epsilon\left(1 - \int_0^{E\epsilon} \phi_c \ d\sigma_c^*\right) - \int_{E\epsilon}^{E(\epsilon+\Delta\epsilon)} [E(\epsilon+\Delta\epsilon) - \sigma_c^*]\phi_c \ d\sigma_c^* \right\} \quad (3.39)$$

where

$$v = 1 - \int_0^{\left|E\epsilon_d\right|} \phi_t \ d\sigma_t^* \quad (3.39a)$$

(i) Compression loading path $G \to G'$ $(\Delta\epsilon > 0, \ \epsilon > \epsilon_g)$

$$\Delta\sigma = u\left\{ E\Delta\epsilon(1 - \int_0^{E(\epsilon-\epsilon_D)/2} \phi_t \ d\sigma_t^* \right.$$

$$\left. - \int_{E(\epsilon-\epsilon_D)/2}^{E(\epsilon+\Delta\epsilon-\epsilon_D)/2} [E(\epsilon+\Delta\epsilon-\epsilon_D) - 2\sigma_t^*]\phi_t \ d\sigma_t^* \right\}$$

$$- v\left\{ \int_{E\epsilon_a}^{E\epsilon} \phi_c \ d\sigma_c^* + \int_{E\epsilon}^{E(\epsilon+\Delta\epsilon)} [E(\epsilon+\Delta\epsilon) - \sigma_c^*]\phi_c \ d\sigma_c^* \right\} \quad (3.40)$$

or

$$\Delta\sigma = v\left\{ E\Delta\epsilon\left(1 - \int_0^{E\epsilon} \phi_c \ d\sigma_c^*\right) - \int_{E\epsilon}^{E(\epsilon \ \Delta\epsilon)} [E(\epsilon+\Delta\epsilon) - \sigma_c^*]\phi_c \ d\sigma_c^* \right\}$$

$$- u\left\{ E\Delta\epsilon \int_0^{E(\epsilon-\epsilon_D)/2} \phi_t \ d\sigma_t^* \right.$$

$$\left. - \int_{E(\epsilon-\epsilon_D)/2}^{E(\epsilon+\Delta\epsilon-\epsilon_D)/2} [E(\epsilon+\Delta\epsilon-\epsilon_D) - 2\sigma_t^*]\phi_t \ d\sigma_t^* \right\} \quad (3.40a)$$

III. 3-3 Two-dimensional model

For a two-dimensional model shown in Fig. III.15, the incremental stress $\Delta\sigma$ corresponding to incremental strain $\Delta\epsilon$ can be divided into two parts. The first part is contributed by the spring-slip element where the stress increment is a function of both stress history and the strain increment as shown in the previous section. The second part is contributed by the stiffness springs connecting the two one-dimensional spring-slip elements, and is recoverable. The following derivations are all devoted to this second part. Referring to Fig. III.15, let the principal stresses in the 1- and 2-direction due to stiffness springs with modulus E_s be denoted by $(\sigma_e)_1$ and $(\sigma_e)_2$ respectively, then it can be shown that the stress in the 1-direction due to the stiffness spring elements can be expressed as:

$$(\sigma_e)_1 = E_s\left\{\frac{(1+\epsilon_1)}{\sqrt{2}} - \frac{(1+\epsilon_1)}{[(1+\epsilon_1)^2+(1+\epsilon_2)^2]^{1/2}}\right\} \qquad (3.41)$$

After principal strain increments $\Delta\epsilon_1$ and $\Delta\epsilon_2$ in the 1- and 2-directions are applied, the following relation holds:

$$(\sigma_e)_1 + (\Delta\sigma_e)_1 = E_s\left\{\frac{(1+\epsilon_1+\Delta\epsilon_1)}{\sqrt{2}} - \frac{(1+\epsilon_1+\Delta\epsilon_1)}{[(1+\epsilon_1)^2+(1+\epsilon_2)^2]^{1/2}}\right\} \qquad (3.42)$$

where $(\Delta\sigma_e)_1$ denotes the part of the incremental stress in the 1-direction due to the spring element and can be obtained by applying Taylor's expansion theorem and neglecting the higher order terms, i.e.,

$$(\Delta\sigma_e)_1 = E_s \left\{ \frac{1}{\sqrt{2}} - \frac{(1+\epsilon_1)^2}{[(1+\epsilon_1)^2+(1+\epsilon_2)^2]^{3/2}} \right\} \Delta\epsilon_1$$

$$+ E_s \left\{ \frac{(1+\epsilon_1)(1+\epsilon_2)}{[(1+\epsilon_1)^2+(1+\epsilon_2)^2]^{3/2}} \right\} \Delta\epsilon_2 \quad (3.43)$$

Note that Eq. (3.43) is obtained by assuming the stiffness spring modulus, E_s, is constant. However, as will be seen later, the stiffness spring modulus for granular material unfortunately is not a constant, and is instead a function of the state stress. Equation (3.43) is valid only if the strain and stress increments are small.

Due to symmetry, the stress increment in any direction due to the interconnected springs can be expressed as

$$(\Delta\sigma_e)_i = E_s \left\{ \frac{1}{\sqrt{2}} - \frac{(1+\epsilon_i)^2}{[(1+\epsilon_i)^2+(1+\epsilon_j)^2]^{3/2}} \right\} \Delta\epsilon_i$$

$$+ E_s \left\{ \frac{(1+\epsilon_i)(1+\epsilon_j)}{[(1+\epsilon_i)^2+(1+\epsilon_j)^2]^{3/2}} \right\} \Delta\epsilon_j \quad (3.44)$$

where

$$i,j = 1,2; \quad i \neq j$$

Let $(\Delta\sigma_p)_i$ be the portion of stress increment due to the spring-slip elements in the ith principal direction. Then $(\Delta\sigma_p)_i$ can be obtained from Eqs. (3.33) to (3.40). $(\Delta\sigma_p)_i$ depends upon the magnitudes of $\Delta\epsilon_i$, and the loading history. Generally, $(\Delta\sigma_p)_i$ can be expressed as

$$(\Delta\sigma_p)_i = p_i \Delta\epsilon_i \quad (3.45)$$

where p_i equals the right-hand sides of Eqs. (3.33) to (3.40) divided

by $\Delta\epsilon_i$. As can be seen from Eqs. (3.33) to (3.40) and Eq. (3.45), p_i is strongly influenced by the loading history, and can be considered as an indicator of the influence of loading history to the stress-strain relationship.

The total stress increments $\Delta\sigma_i$ in the ith principal direction can be written as

$$\Delta\sigma_i = (\Delta\sigma_e)_i + (\Delta\sigma_p)_i \qquad (3.46)$$

This two-dimensional model can also approximately represent the linear elastic constitutive relation if the slip element is ignored or the yield stress is set to be infinite. From the elasticity theory, the following incremental relation is observed:

$$\Delta\sigma_i = \lambda(\Delta\epsilon_i + \Delta\epsilon_j) + 2\mu\Delta\epsilon_i \qquad (3.47)$$

where λ, μ are Lamé's constants in classical elasticity theory [1], and $i, j = 1, 2; \ i \neq j$.

If the slip component in the spring-slip element is absent (i.e., the slip mechanism is removed and the spring slip element becomes only a spring with modulus E) or the yield stress is set so high that no slip occurs in the range of stress considered, then from Eqs. (3.33) to (3.40) and Eq.(3.45), it can be observed that $p_i = E$ in each of the principal directions. If the strain field is small, the values of $(1+\epsilon_i)$ and $(1+\epsilon_j)$ can be approximated to be 1. If the above assumptions hold, the following relation can be obtained from Eqs. (3.44), (3.45) and (3.46):

$$\Delta\sigma_i = \frac{1}{2\sqrt{2}} E_s(\Delta\epsilon_i + \Delta\epsilon_j) + E\Delta\epsilon_i \tag{3.48}$$

where

$$i = j; \quad i,j = 1,2$$

Comparing Eqs. (3.47) and (3.48) the following relationship is reached:

$$\lambda = \frac{1}{2\sqrt{2}} E_s \tag{3.49a}$$

$$\mu = \frac{1}{2} E \tag{3.49b}$$

Let ν be Poisson's ratio for the material, then

$$\nu = \frac{E_s}{2\sqrt{2} E + 2E_s} \tag{3.50}$$

By varying the values of E and E_s, the ν values can be set anywhere between 0 and 0.5. The corresponding Young's modulus, E_y, would be:

$$E_y = E\left(\frac{2\sqrt{2} E + 3E_s}{2\sqrt{2} E + 2E_s}\right) \tag{3.51}$$

Note that if E_s or E is set to be infinite then the material is incompressible. The above illustration demonstrates the justification of using this two-dimensional model to represent the general behavior of a class of material behaviors. For a granular material, the slip stress is set to be low enough to account for the plastic strain even at small stress. For nearly elastic material, the yield stress is set to be high enough so that the plastic strain can be negligible.

As can be seen, all the stress-strain relationships are given in incremental form. Notice that the two-dimensional model does not have any indication of whether it represents a plane strain or plane stress cases. However, this is not important for the time being because the purpose of this two-dimensional model is to demonstrate the relevance of using the slip-spring and spring element. The model serves as a guide to the formulation of a more realistic and acceptable three-dimensional model from which a plane stress or plane strain formulation can be derived.

III.3-4 Three-dimensional model and formulation

Having demonstrated the use of the two-dimensional model, the derivation of the behavior of a general three-dimensional model for a granular material follows naturally as the next step. The two-dimensional model in Fig. III.15 leads to a three-dimensional model as shown in Fig. III.17. Again, in this three-dimensional model, the contribution to the stress-strain relation is divided into two parts. The first part is due to the slip-spring element and has been demonstrated in section III.3-2. The second part is partly elastic and is contributed by the interconnecting spring elements. Let $(\sigma_e)_i$ $(i = 1, 2, 3)$ denote the principal stresses due to the elastic springs E_s. It can be shown that

$$(\sigma_e)_i = 2E_s(1+\epsilon_i)\left\{\frac{2}{\sqrt{2}} - \frac{1}{\left[(1+\epsilon_i)^2+(1+\epsilon_j)^2\right]^{1/2}}\right.$$
$$\left. - \frac{1}{\left[(1+\epsilon_j)^2+(1+\epsilon_k)^2\right]^{1/2}}\right\} \qquad (3.52)$$

where

$$i \neq j \neq k ; \quad i,j,k = 1,2,3$$

Then the stress increment $(\Delta\sigma_e)_i$ due to the stiffness springs E_s after strain increments $\Delta\epsilon_i$ ($i = 1,2,3$) can be obtained as

$$(\Delta\sigma_e)_i = 2E_s \Delta\epsilon_i \left\{ \frac{2}{\sqrt{2}} - \frac{(1+\epsilon_j)^2}{[(1+\epsilon_i)^2+(1+\epsilon_j)^2]^{3/2}} - \frac{(1+\epsilon_k)^2}{[(1+\epsilon_i)^2+(1+\epsilon_j)^2]^{3/2}} \right\}$$

$$+ 2E_s \Delta\epsilon_j \left\{ \frac{(1+\epsilon_i)(1+\epsilon_k)}{[(1+\epsilon_i)^2+(1+\epsilon_j)^2]^{3/2}} \right\}$$

$$+ 2E_s \Delta\epsilon_k \left\{ \frac{(1+\epsilon_i)(1+\epsilon_k)}{[(1+\epsilon_i)^2+(1+\epsilon_k)^2]^{3/2}} \right\} \tag{3.53}$$

where

$$i \neq j \neq k; \quad i,j,k = 1,2,3$$

Notice that Eq. (3.53) is obtained from Taylor's expansion theorem by neglecting the higher-order terms and by assuming that E_s is constant. In the case of a granular material, E_s is dependent on the state of stress, since the material becomes stiffer when the hydrostatic stress is increased or when the deviatoric stress is reduced [16] . A cohesionless granular material can not support any deviatoric stress in the absence of a state of hydrostatic compression. If E_s is taken to be a variable, the derivation of the proposed stress-strain relation becomes very complicated. Thus, further simplification is needed. Since the proposed constitutive relation is expressed in incremental forms, it can be assumed that the E_s value is a constant during each stress or strain increment if the stress or

strain increment is small. Unless otherwise mentioned, the E_s value for a particular increment will therefore be taken herein to be the average of the E_s values for the state of stress before and after the increment in question. As will be discussed in the next chapter, the E_s value will be expressed in terms of the state of stress.

Again, the total stress increment can be expressed as

$$\Delta\sigma_i = (\Delta\sigma_e)_i + (\Delta\sigma_p)_i \tag{3.46}$$

where $(\Delta\sigma_p)$ can be obtained from Eqs. (3.33) to (3.40).

In matrix form, the proposed constitutive relation can be expressed as

$$\left\{\Delta\sigma\right\} = A\left\{\Delta\epsilon\right\} \tag{3.54a}$$

or

$$\left\{\begin{array}{c} \Delta\sigma_1 \\ \Delta\sigma_2 \\ \Delta\sigma_3 \end{array}\right\} = \left\{\begin{array}{ccc} a_{11} & a_{12} & a_{23} \\ a_{21} & a_{22} & a_{23} \\ a_{31} & a_{32} & a_{33} \end{array}\right\} \left\{\begin{array}{c} \Delta\epsilon_1 \\ \Delta\epsilon_2 \\ \Delta\epsilon_3 \end{array}\right\} \tag{3.54b}$$

where

$$a_{11} = 2E_s \left\{\frac{2}{\sqrt{2}} - \frac{(1+\epsilon_2)^2}{[(1+\epsilon_1)^2+(1+\epsilon_2)^2]^{3/2}} - \frac{(1+\epsilon_3)^2}{[(1+\epsilon_1)^2+(1+\epsilon_3)^2]^{3/2}}\right\} + P_1$$

$$a_{12} = a_{21} = 2E_s\left\{\frac{(1+\epsilon_1)(1+\epsilon_2)}{[(1+\epsilon_1)^2+(1+\epsilon_2)^2]^{3/2}}\right\}$$

$$a_{13} = a_{31} = 2E_s\left\{\frac{(1+\epsilon_1)(1+\epsilon_3)}{[(1+\epsilon_1)^2+(1+\epsilon_3)^2]^{3/2}}\right\}$$

$$a_{22} = 2E_s \left\{ \frac{2}{\sqrt{2}} - \frac{(1+\epsilon_1)^2}{[(1+\epsilon_1)^2+(1+\epsilon_2)^2]^{3/2}} - \frac{(1+\epsilon_3)^2}{[(1+\epsilon_2)^2+(1+\epsilon_3)^2]^{3/2}} \right\} + p_2$$

$$a_{23} = a_{32} = 2E_s \left\{ \frac{(1+\epsilon_2)(1+\epsilon_3)}{[(1+\epsilon_2)^2+(1+\epsilon_3)^2]^{3/2}} \right\}$$

$$a_{33} = 2E_s \left\{ \frac{2}{\sqrt{2}} - \frac{(1+\epsilon_1)^2}{[(1+\epsilon_1)^2+(1+\epsilon_3)^2]^{3/2}} - \frac{(1+\epsilon_2)^2}{[(1+\epsilon_2)^2+(1+\epsilon_3)^2]^{3/2}} \right\} + p_3$$

and

$$p_i = \frac{(\Delta\sigma_p)_i}{\Delta\epsilon_i} \qquad (3.55)$$

Up to now, the constitutive relations for all models in this study are of the form where stress increment is expressed in terms of strain increment. Sometimes it is more useful and desirable to express strain increment in terms of stress increment. This conversion process will involve matrix inversion and can be derived as follows:

$$\left\{ \Delta\epsilon \right\} = A^{-1} \left\{ \Delta\epsilon \right\} \qquad (3.56a)$$

or $\Delta\epsilon_i$ can be expressed explicitly as:

$$\Delta\epsilon_i = \frac{1}{\det A} \left\{ (a_{jj}a_{kk} - a_{jk}a_{kj})\Delta\sigma_i + (a_{ik}a_{kj} - a_{kk}a_{ij})\Delta\sigma_j \right.$$

$$\left. + (a_{ij}a_{kj} - a_{jj}a_{ik})\Delta\sigma_k \right\} \qquad (3.54b)$$

where

$$i \neq j \neq k; \quad i,j,k = 1,2,3$$

and

$$\det A = a_{11}a_{22}a_{33} + a_{21}a_{13}a_{32} + a_{31}a_{12}a_{23} - a_{11}a_{23}a_{32}$$

$$- a_{22}a_{13}a_{31} - a_{33}a_{12}a_{21} \tag{3.57}$$

Solving Eqs. (3.56) and (3.57) for the strain increments will require using a trial and error method since the coefficients are also functions of the strain increments. If the following iteration scheme is used the process is found to converge rapidly.

1. If the loading or unloading or reloading steps are the same as in the previous load process, the previous strain increments are used as the first trial values. If the loading path is different from that in the previous loading increment (i.e., changing from loading to unloading, or from unloading to reloading, or reloading to unloading or loading), the first trial strain increments will be taken to be zero.

2. Calculate the a_{ij}'s from Eqs. (3.33) to (3.40) and Eq. (3.55), and compute the strain increments according to Eqs. (3.56) and (3.57).

3. Use the calculated increments as the new trial values and repeat step 2.

4. Repeat steps 2 and 3 until a convergent solution is reached.

In most cases, the solution converges after two or three trials.

III. 3-5 Anisotropic model and formulation

The deformation behavior of a granular material might some-
times exhibit certain degrees of anisotropy [15]. There are evidences
that anisotropy exists even in a carefully prepared laboratory sample.
One example is Ko's experimental results on Ottawa sand tested in
a cubical triaxial testing apparatus [16]. Presumably if the sample
was initially homogeneous and isotropic, the principal deformations
in the three perpendicular directions should be equal under isotropic
loading such as hydrostatic compression. However, Ko observed
that the vertical deformation was sometimes greater.than the two
horizontal deformations which were always equal or nearly equal.

In the previous derivation, the proposed model was considered
to represent an initially homogeneous and isotropic granular material
containing randomly distributed grains and packings. Anisotropy
would be induced after straining anisotropically due to loading other
than isotropic stress path such as hydrostatic compression or exten-
sion. To account for the possible existence of initial anisotropy in a
granular medium, certain revision of the proposed model is needed.
Physically speaking anisotropy arises from the geometrical packing
in such a way that particle formation in one direction is more
susceptible to deformation than the other directions.

Of course, the initial anisotropy can be taken into considera-
tion by changing the modulus of every stiffness spring and spring-slip
element. However, this would make the derivation of the stress-
strain relation extremely complicated since there are too many
moduli of stiffness spring and spring-slip elements involved in the

proposed model. It is more desirable to employ a simpler model imposing a fictitious factor of anisotropy denoted by n_i in each of the three principal directions to account for the necessary variation of stiffness in all the stiffness spring and spring-slip elements due to initial anisotropy. It is postulated that the stresses are computed from a fictitious strain with a magnitude of $n_i \epsilon_i$ according to the configuration of the anisotropic model shown in Fig. III.18. However, the real quantity of strain corresponding to the ith principal direction is still designated as ϵ_i. It has to point out that the proposed anisotropic model is only a postulation for the behavior of an anisotropic granular material. Its validity has to be determined by certain experimental results.

As before, the stress strain relation can be derived into two parts. The first part is the contribution due to the stiffness spring elements and can be derived in the same fashion as the isotropic model in previous sections. As before, let the stress due to the stiffness springs E_s in the ith principal direction be denoted by $(\sigma_e)_i$, then it can be proved from the configuration of mechanical model shown in Fig. III.18 that

$$(\sigma_e)_i = \frac{n_i(1+\epsilon_i)}{(n_i^2+n_j^2)^{1/2}} + \frac{n_i(1+\epsilon_i)}{(n_i^2+n_k^2)^{1/2}} - \frac{n_i(1+\epsilon_i)}{[n_i^2(1+\epsilon_i)^2+n_j^2(1+\epsilon_j)^2]^{1/2}}$$

$$- \frac{n_i(1+\epsilon_i)}{[n_i^2(1+\epsilon_i)^2+n_k^2(1+\epsilon_k)^2]^{1/2}} \tag{3.58}$$

$$i \neq j \neq k; \qquad i,j,k = 1,2,3$$

After a strain increment of $(\Delta\epsilon_1, \Delta\epsilon_2, \Delta\epsilon_3)$, $(\sigma_e)_i$ increases with an amount of $(\Delta\sigma_e)_i$. After some mathematical manipulation, the following relation is obtained:

$$
(\Delta\sigma_e)_i) = \Delta\epsilon_i \left\{ \frac{n_i}{(n_i^2 + n_j^2)^{1/2}} + \frac{n_i}{(n_i^2 + n_k^2)^{1/2}} - \frac{n_i n_j^2 (1+\epsilon_j)^2}{[n_i^2(1+\epsilon_i)^2 + n_j^2(1+\epsilon_j)^2]^{3/2}} \right.
$$

$$
\left. - \frac{n_i n_k^2 (1+\epsilon_k)^2}{[n_i^2(1+\epsilon_i)^2 + n_k^2(1+\epsilon_k)^2]^{3/2}} \right\}
$$

$$
+ \left\{ \frac{n_i n_j^2 (1+\epsilon_i)(1+\epsilon_k)}{[n_i^2(1+\epsilon_i)^2 + n_j^2(1+\epsilon_j)^2]^{3/2}} \right\} \Delta\epsilon_j
$$

$$
+ \left\{ \frac{n_i n_k^2 (1+\epsilon_i)(1+\epsilon_k)}{[n_i^2(1+\epsilon_i)^2 + n_j^2(1+\epsilon_j)^2]^{3/2}} \right\} \Delta\epsilon_k \tag{3.59}
$$

The second part is the contribution due to the spring-slip elements. The stress σ_p and stress increments $(\Delta\sigma_p)_i$ in the ith principal direction due to these elements can be easily obtained by substituting ϵ_i and $\Delta\epsilon_i$ in Eqs. (3.33) to (3.40) with $n_i\epsilon_i$ and $n_i\Delta\epsilon_i$ respectively.

The procedures of carrying out the stress-strain computation are similar to the isotropic model shown in the previous section and will not be elaborated on here.
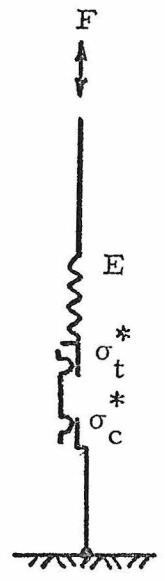
Fig. III.1. Mechanical Model Representing a
Contact Between Grains
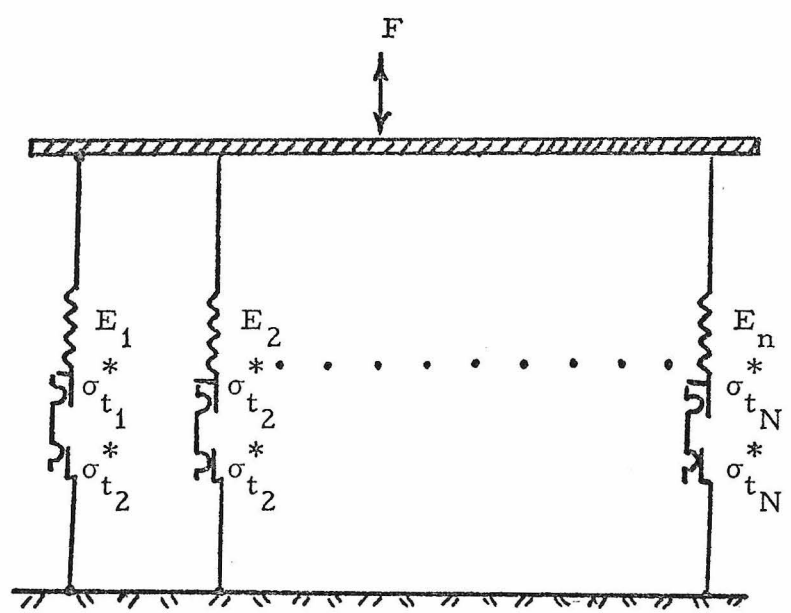
Fig. III.2. One-dimensional Mechanical Model
Representing the Material
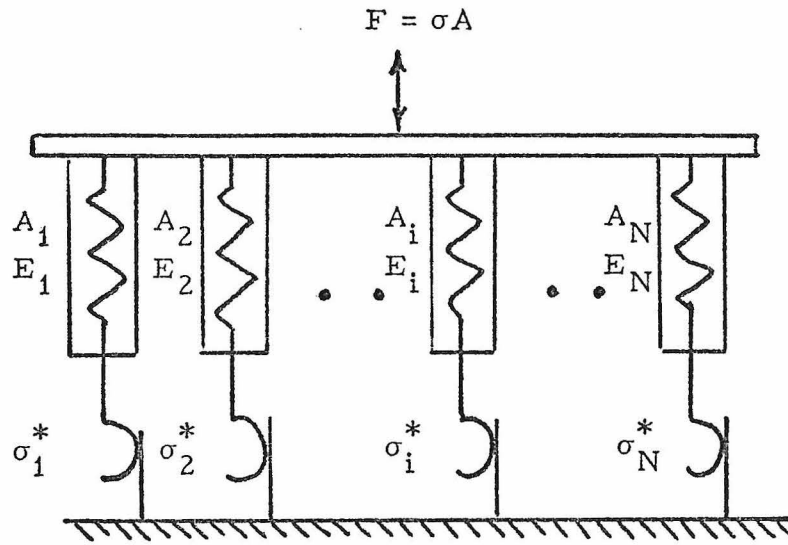
Fig. III.3. Simpler One-dimensional Model (Model A) after Iwan [19]
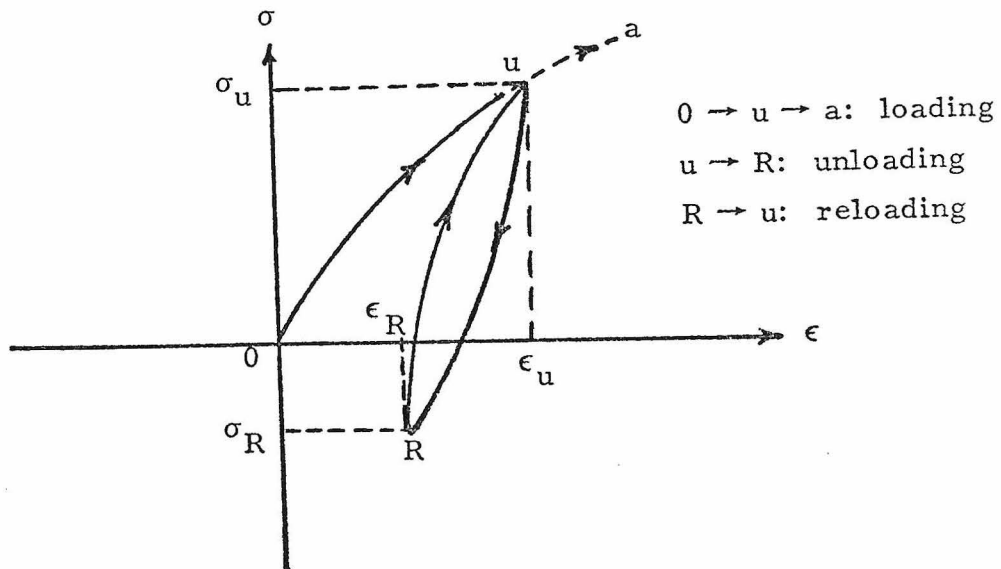
Fig. III.4. Stress-strain Loading Paths for Model A
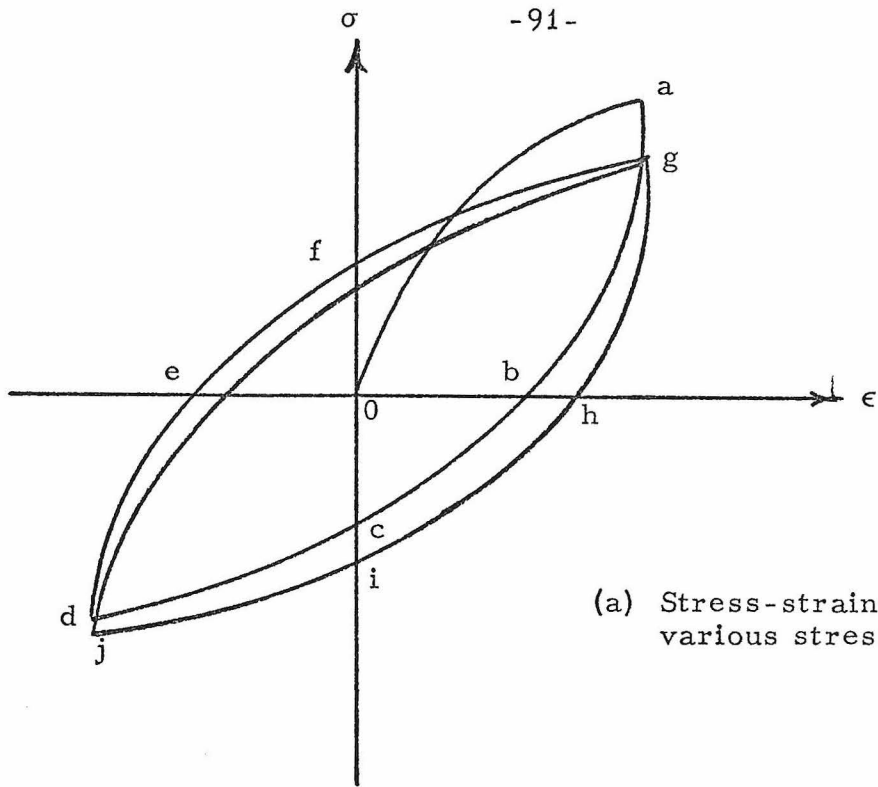
(a) Stress-strain curve for
     various stress parts
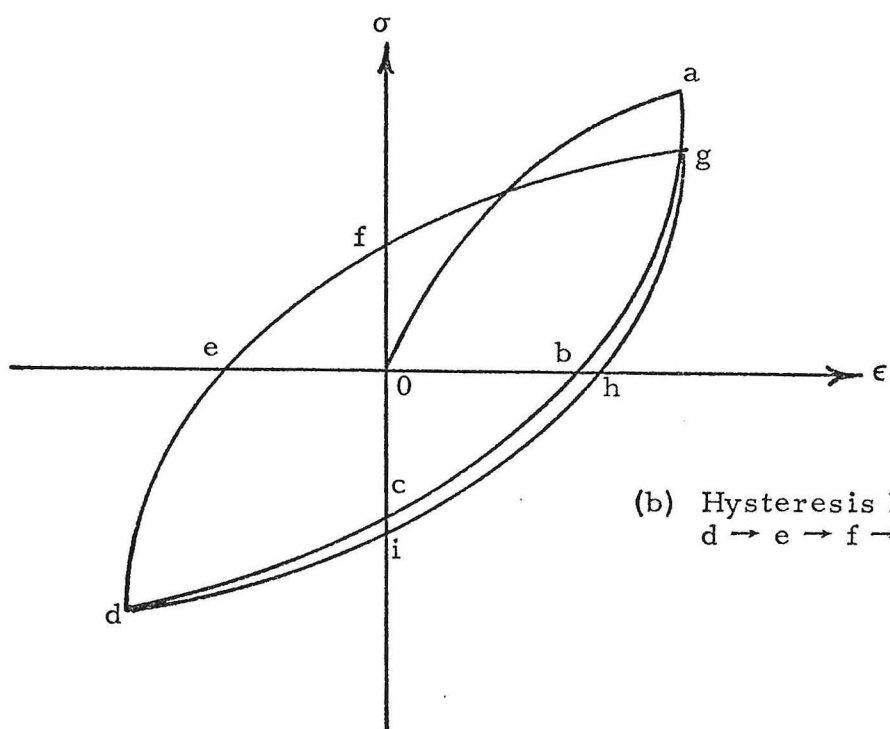
(b) Hysteresis loop
     d → e → f → g → h → i → d

Fig. III.5. Stress Paths and Hysteresis Loop for
             One-dimensional Model (Model B)
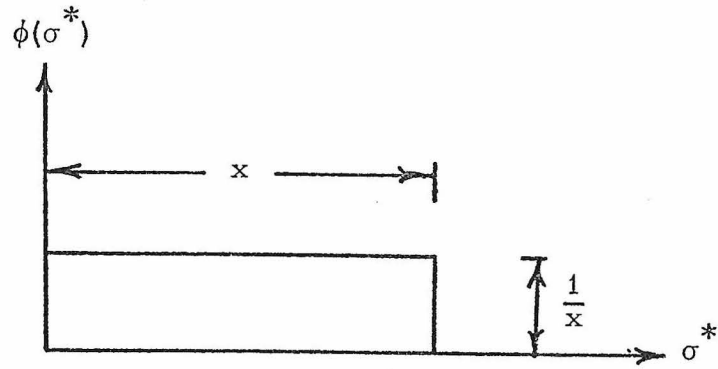
Fig. III.6. Rectangular Distribution of σ^*
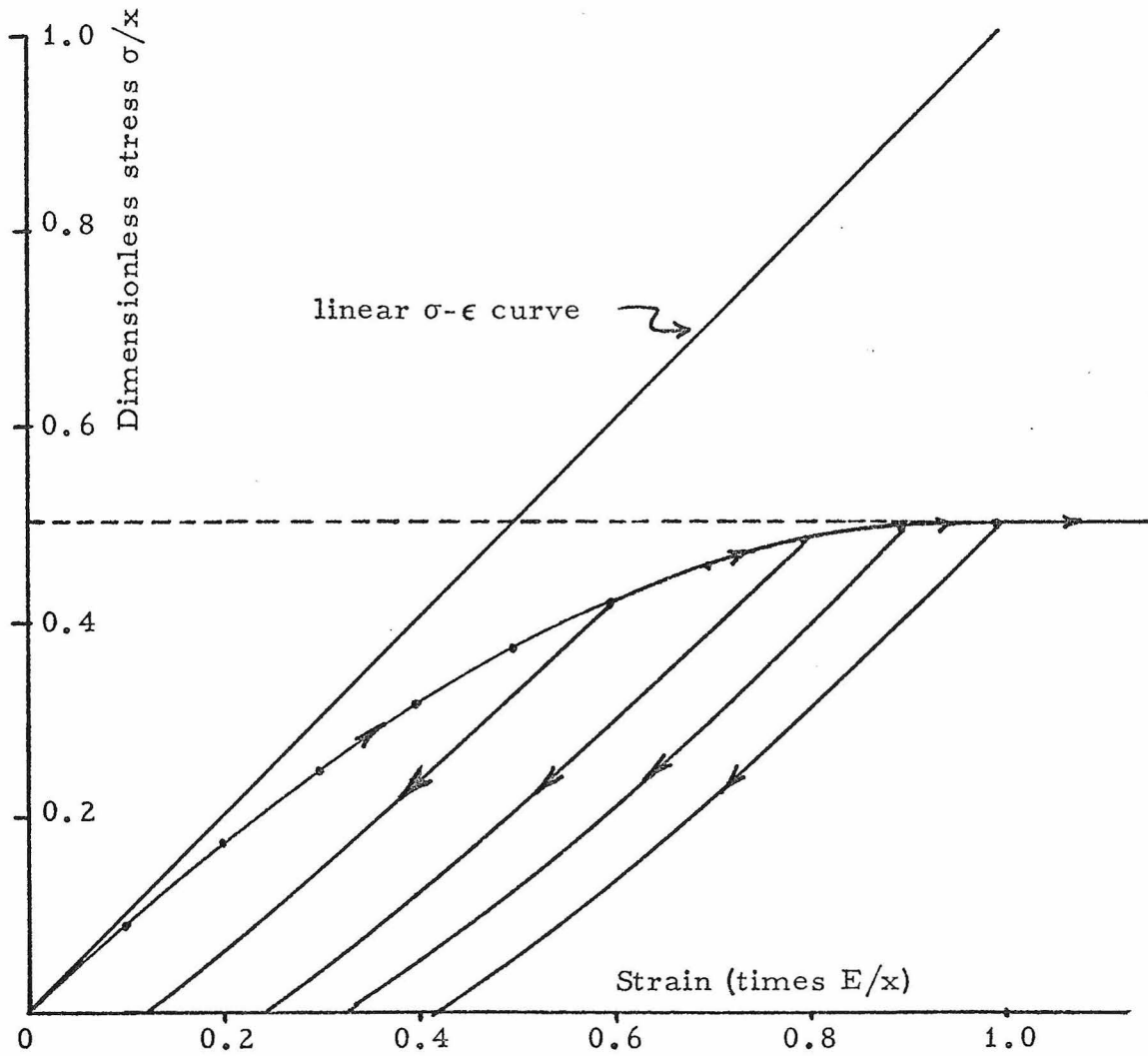
Fig. III.7. Dimensionless Stress-strain Relation for
Rectangularly Distributed $\phi(\sigma^*)$
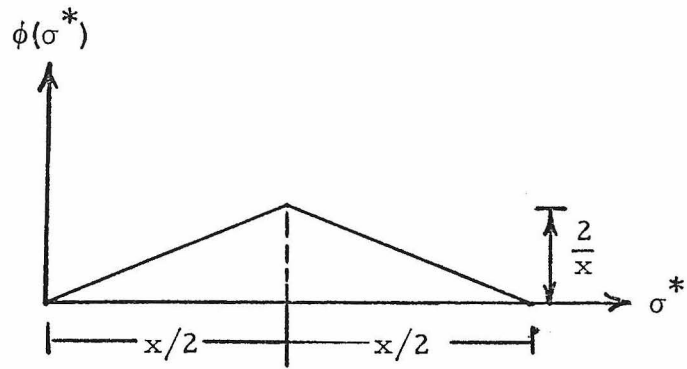
Fig. III.8. Triangular Distribution of σ^*
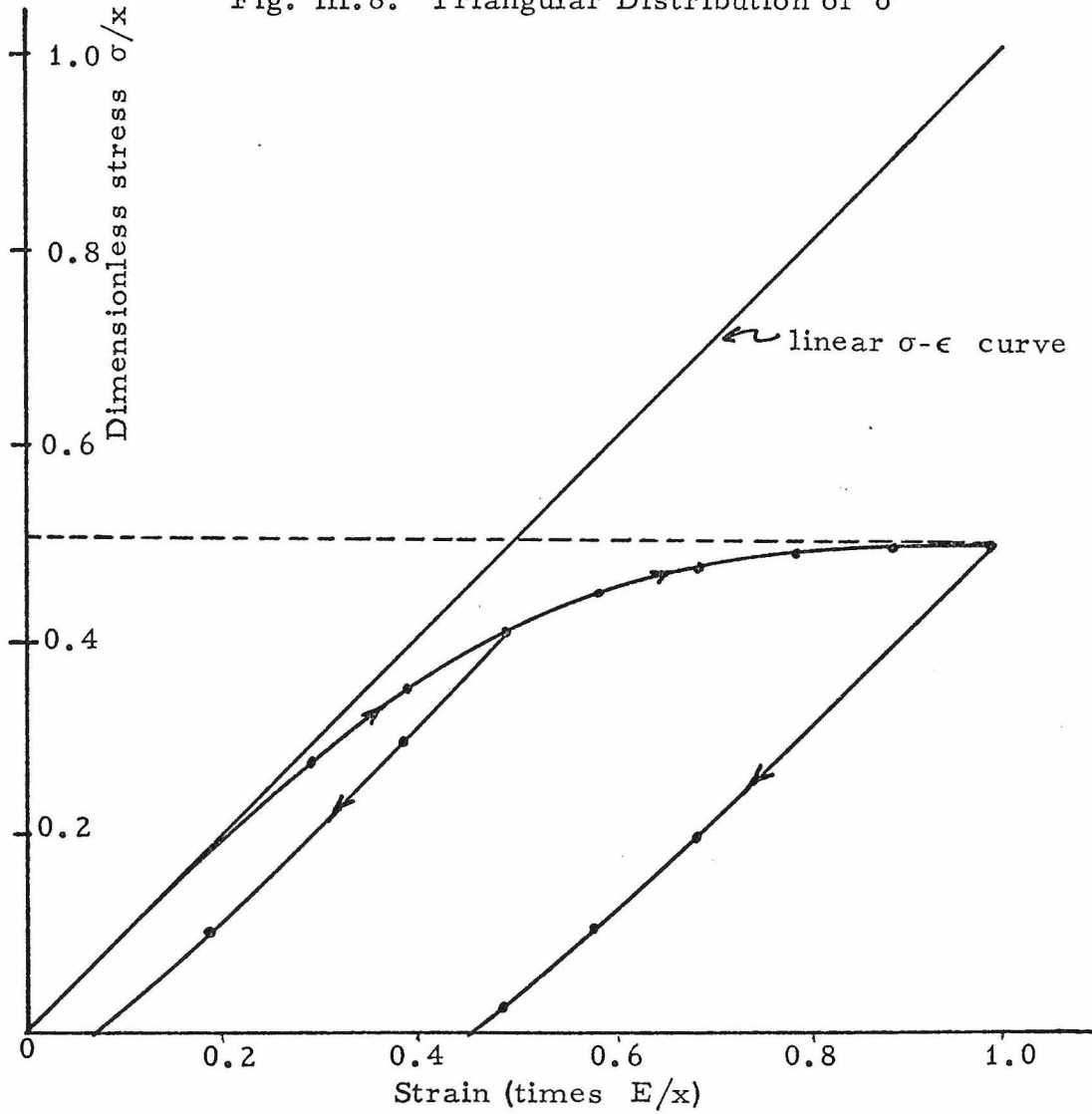
Fig. III.7. Dimensionless Stress-strain Relation for
Triangularly Distributed $\phi(\sigma^*)$
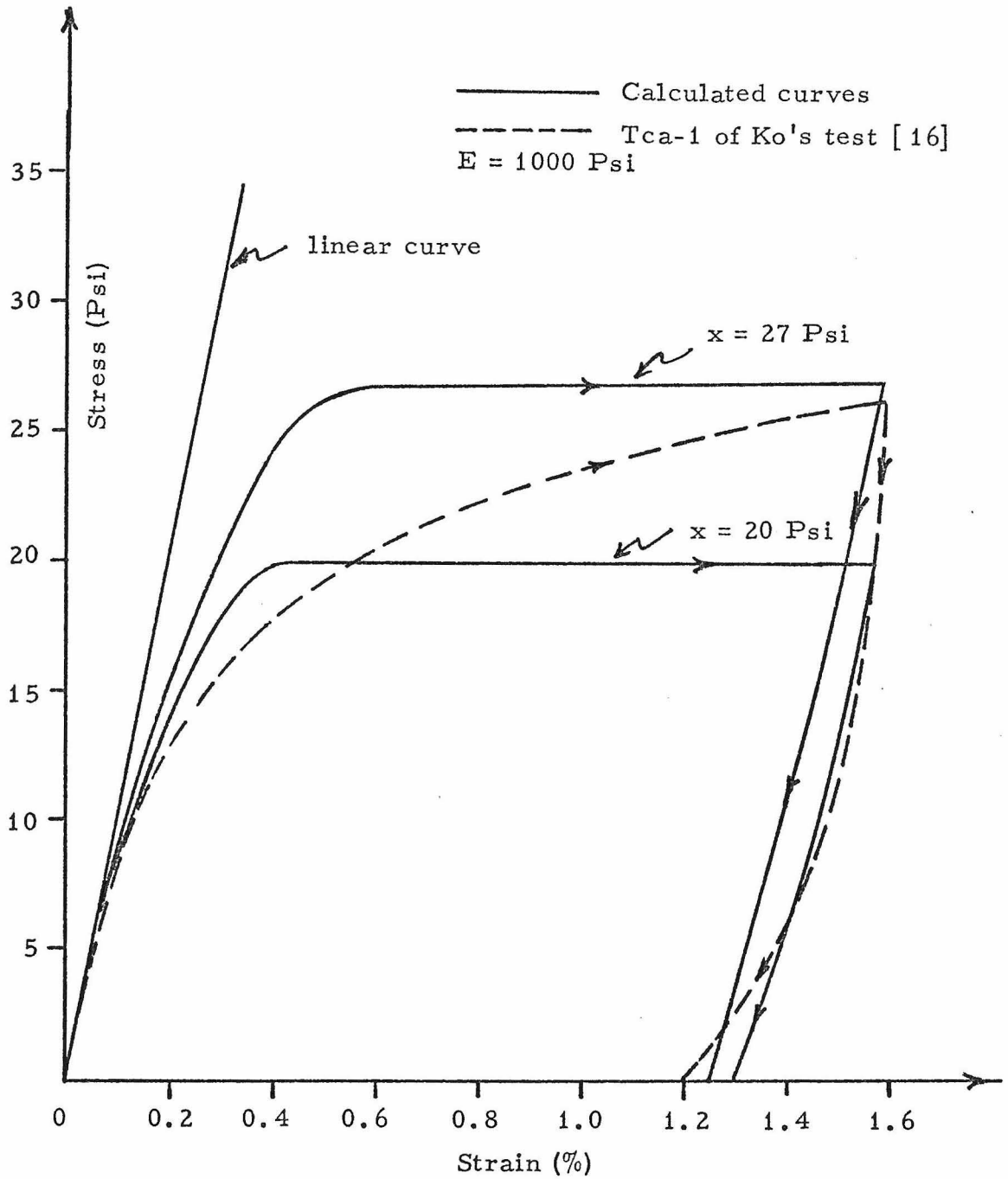
Fig. III.10. Stress-strain Curves for Rectangularly
Distributed $\phi(\sigma^*)$ and Comparison with
$\sigma_1 - \epsilon_1$ Curve of Ko's Tca-1 Test
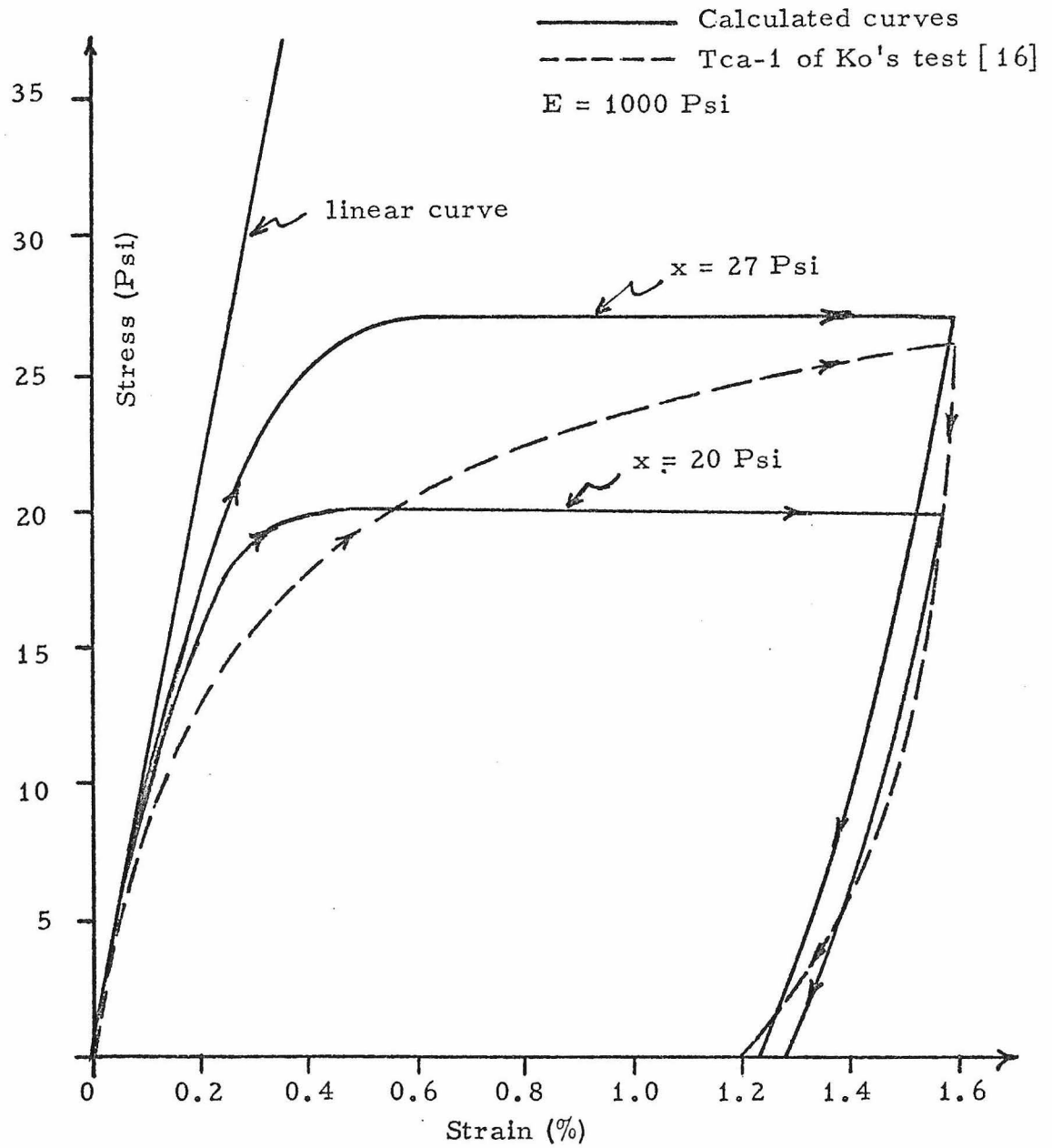
Fig. III.11. Stress-strain Curves for Triangularly
Distributed $\phi(\sigma^*)$ and Comparison with
$\sigma_1 - \epsilon_1$ Curve of Ko's Tca-1 Test
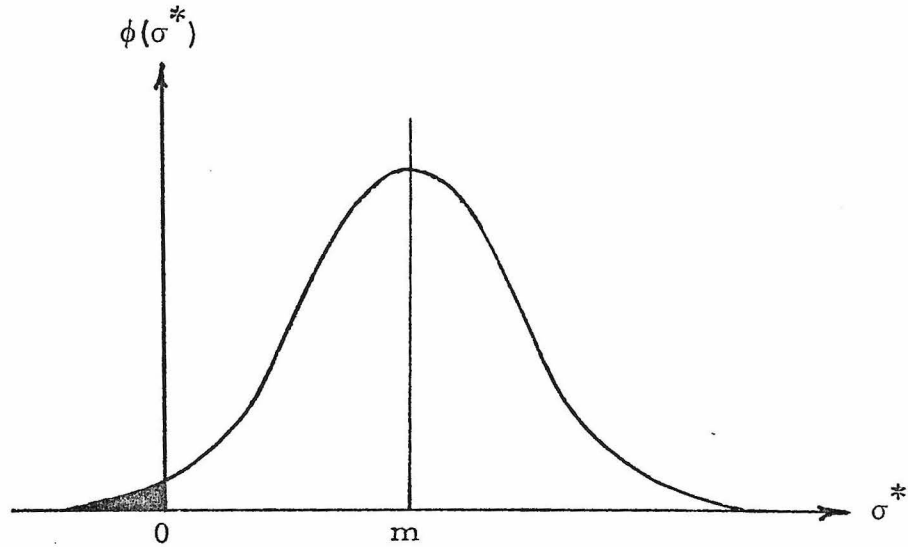
$$\phi(\sigma^*) = \frac{t}{\sqrt{2\pi}\,s} \; \exp\left[-\frac{1}{2}\left(\frac{\sigma^*-m}{s}\right)^2\right] \qquad \text{for} \quad \sigma^* \geq 0$$

$$\phi(\sigma^*) = 0 \qquad\qquad\qquad\qquad\qquad\qquad \text{for} \quad \sigma^* < 0$$

$$t = 1\Big/ \left\{1 - \int_{-\infty}^{0} \frac{1}{\sqrt{2\pi}\,s} \; \exp\left[-\frac{1}{2}\left(\frac{\sigma^*-m}{s}\right)^2\right] d\sigma^*\right\}$$

m = mean of Gaussian distribution

s = standard deviation of Gaussian distribution

Fig. III.12. The Type of Gaussian Distribution
Considered in This Thesis
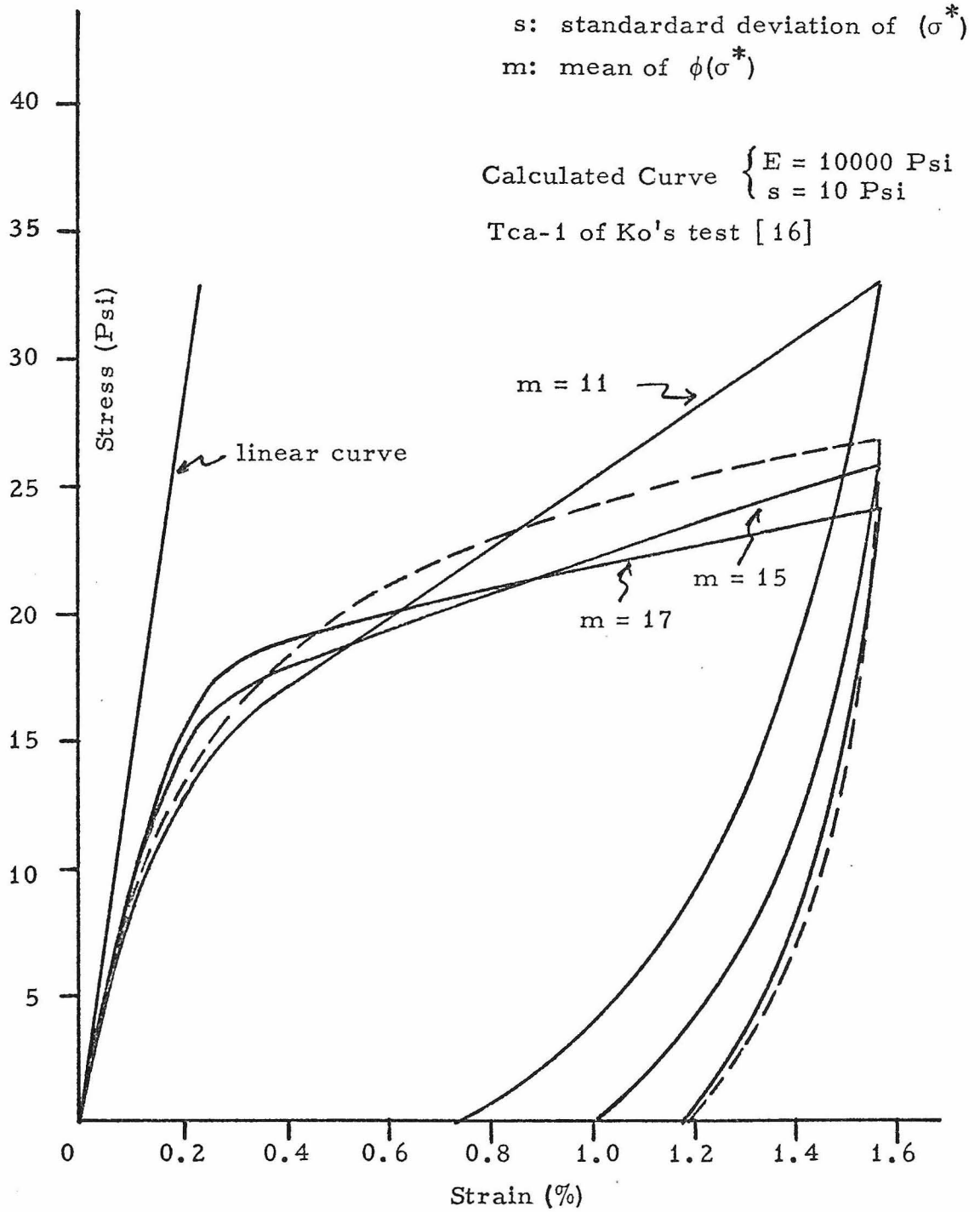
Fig. III.13. Stress-strain Curves for Gaussian-distributed
$\phi(\sigma^*)$ and Comparison with $\sigma_1 - \epsilon_1$ Curves of
Ko's Tca-1 Test
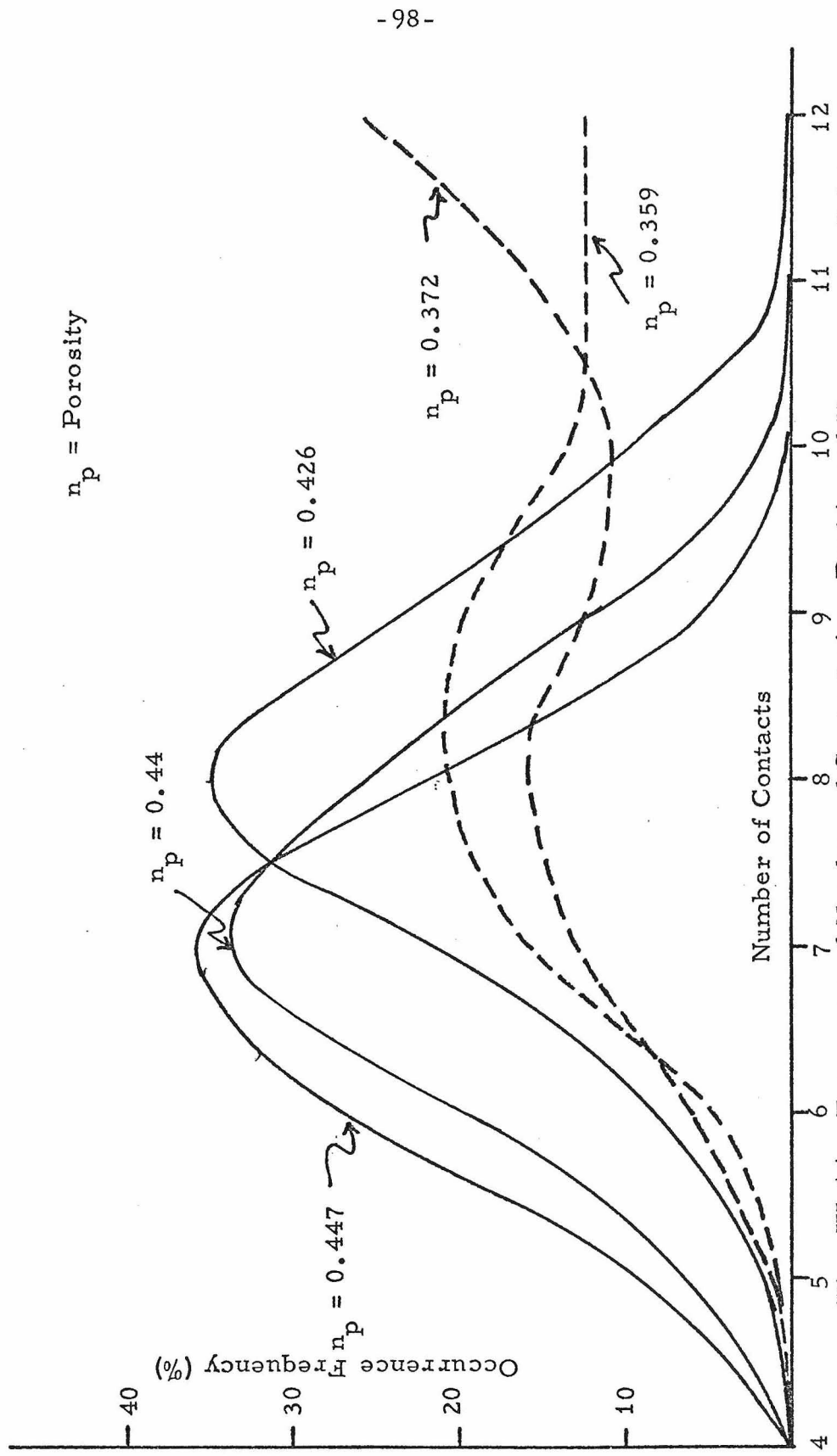
Fig. III.14. Frequency of Number of Contacts in a Packing of Homogeneous Spheres after Smith, Foote and Busang [29]
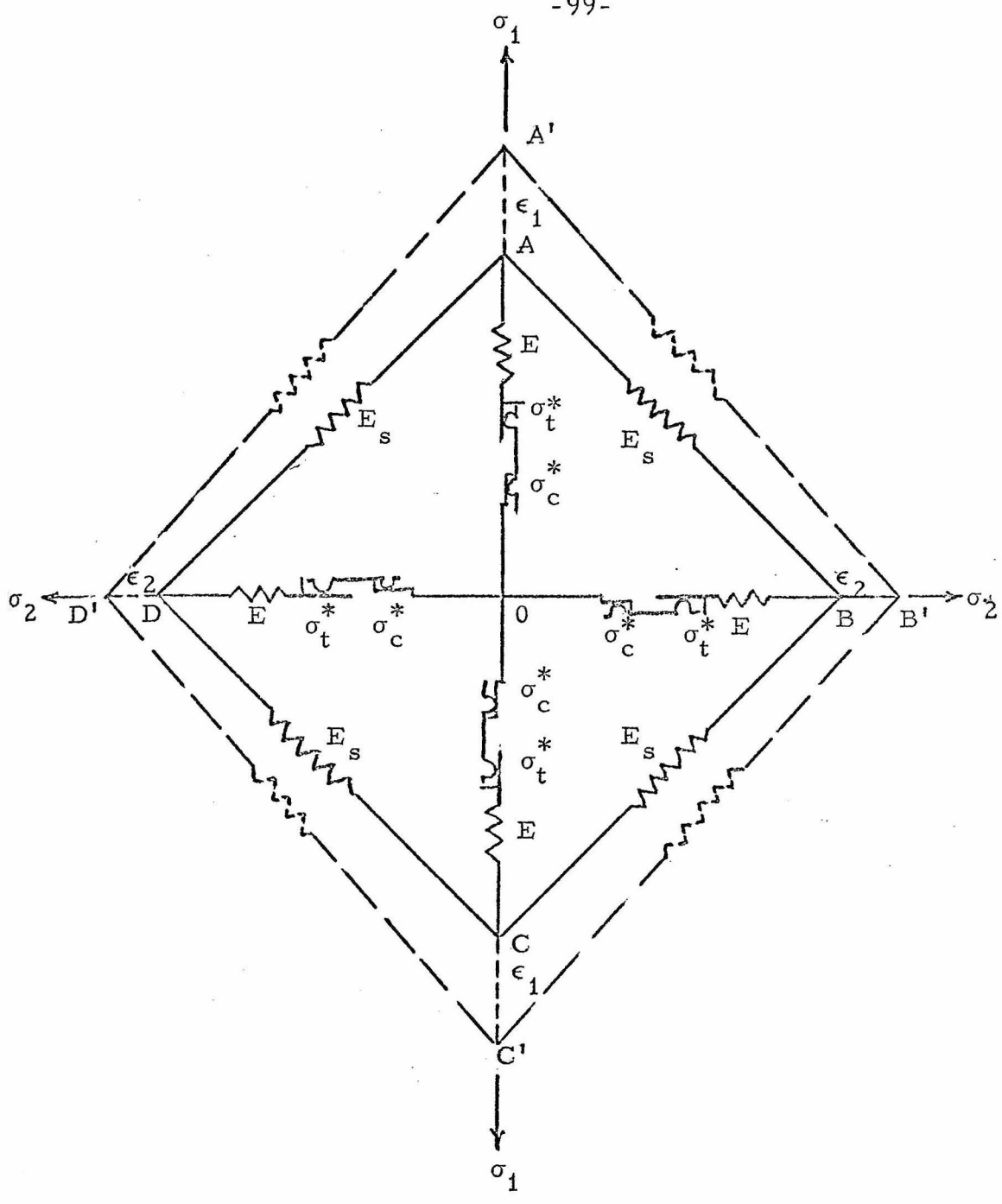
Fig. III.15. Two-dimensional Mechanical Model
Representing Granular Material
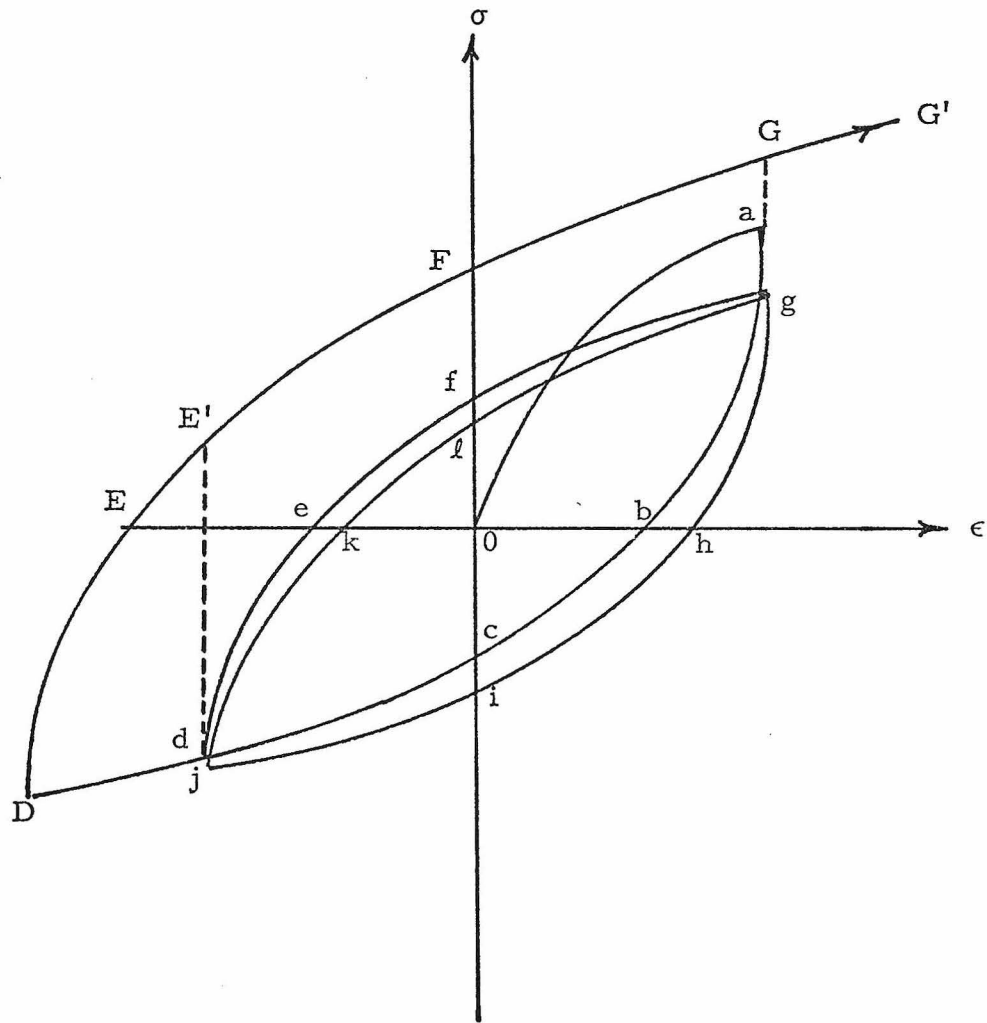
Fig. III.16. Stress-strain Paths for the Slip-spring
Elements in the Proposed Model
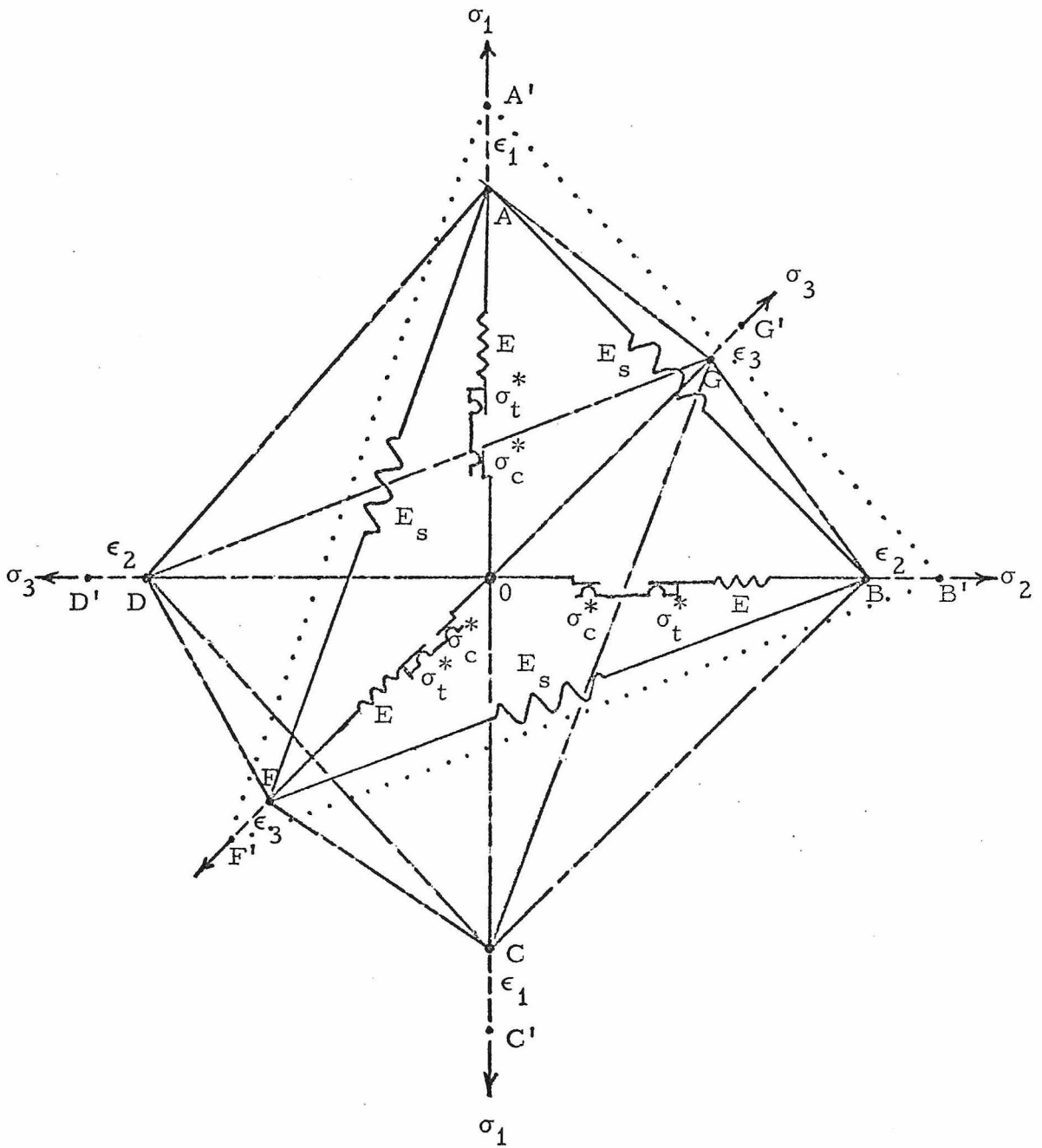
Note: 1. Due to the symmetry of this model, only the elements in
OA, OB, OF and AB, BG, GA are shown with corresponding
parameters.
2. Dotted lines represent the shape of 1/8 of the model at a
state of strain $(\epsilon_1, \epsilon_2, \epsilon_3)$.

Fig. III.17. Three-dimensional Model Representing
Granular Material's Behavior
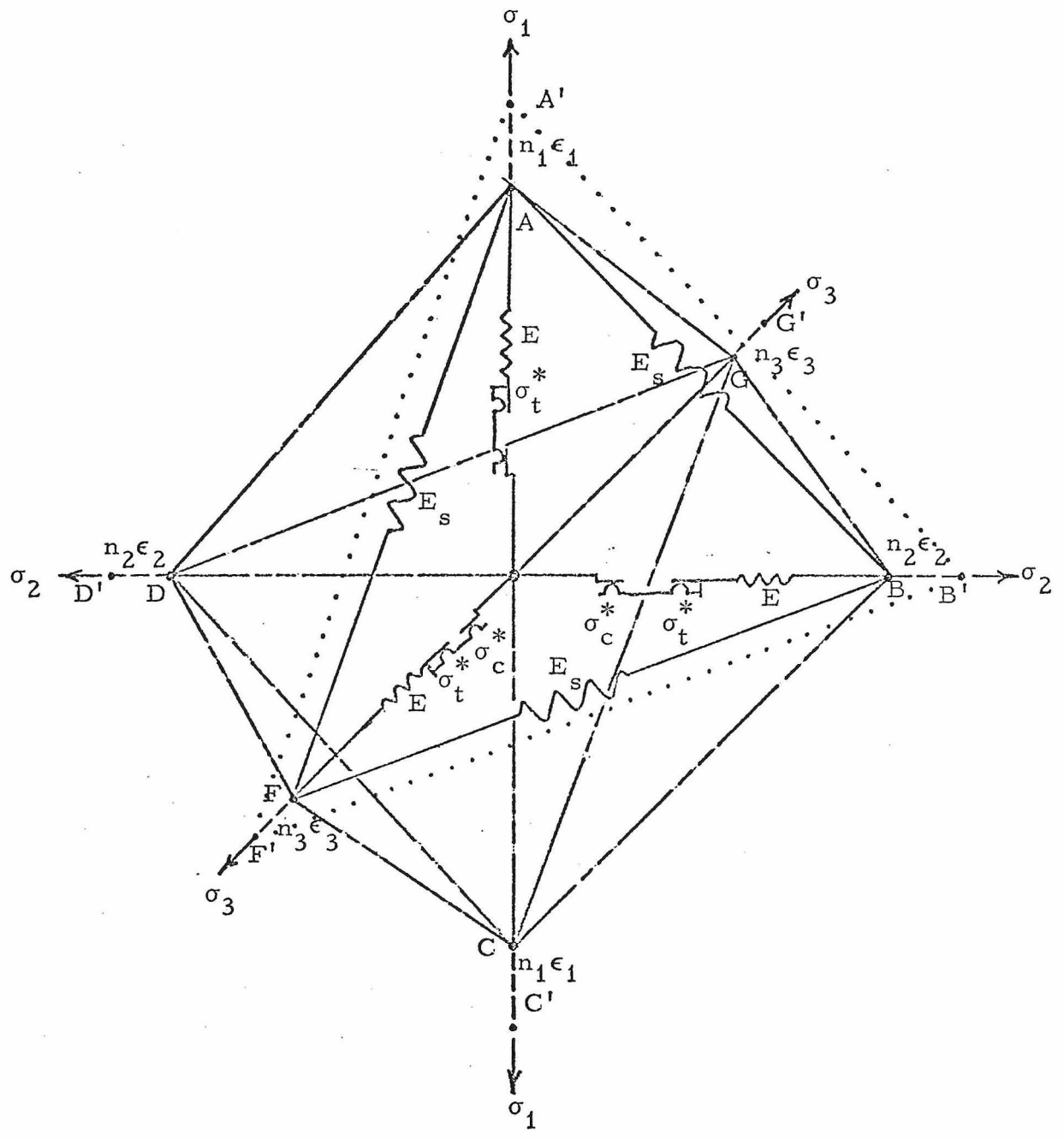
Note: 1. Due to the symmetry of this model, only the elements in
      OA, OB, OF and AB, BG, GA are shown with
      corresponding parameters.

   2. Dotted lines represent the shape of 1/8 of the model at
      a state of strain $(\epsilon_1, \epsilon_2, \epsilon_3)$.

Fig. III.18. Three-dimensional Model for Anisotropic Material

CHAPTER IV

SPECIAL CASES, DETERMINATION OF MATERIAL PARAMETER,
REPRESENTATION OF EXPERIMENTAL DATA

IV.1 Special Cases

The proposed model is derived in such a way that the stress-strain relation for any arbitrary stress-path can be obtained if the material properties are known. The material properties involved in the proposed constitutive relations are E_s, E, m_c, m_t, s_c, and s_t which, in turn, have to be determined from experimental data. In the following section, several special stress paths and the simulation of experimental data will be presented. They are taken to serve the following purposes:

(i) To provide a basis, in conjunction with the experimental results, for measuring the material properties involved in the proposed contitutive relations for a granular material.

(ii) To assess the suitability and accuracy of the proposed constitutive relations in representing the essential features of the behavior of the granular material.

(iii) To predict qualitatively and quantitatively the stress-strain relations of arbitrary stress-paths by using the material properties obtained from the experimental data in special cases.

(iv) To provide some insight on the dependency of some material parameters involved in the proposed constitutive relations with the state of stress and loading history and the mechanical properties of the material, such as the void ratio or density of the

soils.

IV.1-1 Loading paths with proportional stress increments

These loading paths are here defined to be stress paths which produce a principal effective stress state $(\sigma_1, \sigma_2, \sigma_3)$ whose three principal stress increments are proportional to each other, i.e., $\Delta\sigma_1 : \Delta\sigma_2 : \Delta\sigma_3 = \gamma : \alpha : \beta$ where γ, α and β are constants. In addition, the principal axes are not permitted to rotate. It is worth pointing out that this type of loading path is different from the conventional concept of proportional loading or straining [9] , whose three principal effective stresses or principal strains are proportional to each other. In a sense, loading paths with proportional stress increments cover a much broader area than the proportional loading. Proportional loading is only one type of the loading paths with proportional stress increments. However, the reversal is not true.

Loading paths with proportional stress increments are stress controlled processes. Most of the existing three-dimensional soil test devices are of these types. Completely strain-controlled three-dimensional tests have been reported [124] . But it is believed that the mechanical difficulties associated with these tests have prevented their successful use [17] . Since the parameters involved in the proposed constitutive relations have to be determined by experimental testing data, the understanding of loading paths with proportional stress increments is important.

The proposed constitutive relations as demonstrated in the

previous chapter are derived from a rheological model under strain-control. However, through the matrix inversion, the stress-controlled version can be obtained without difficulty. One of the special characters of a granular material, like most other materials, is its softness under shear stress. One disadvantage of using a stress-controlled path is that a large strain increment is obtained under a small stress increment when the deformation is large. This might lead to some false impression about the accuracy of the proposed constitutive relations in simulating or predicting the experimental data. This point will be illustrated in detail in later sections of this work.

(i) Hydrostatic compression

In this stress path, the three principal stresses are kept equal to each other and the three principal stress increments are the same ($\gamma = \alpha = \beta = 1$). The stress path can be readily represented in principal stress space as shown in Fig. IV.1. The hydrostatic stress, denoted by σ_{oct}, is equal to $1/\sqrt{3}$ times the distance of the stress point along the hydrostatic axis. For an isotropic material under hydrostatic compression, the three principal strains, denoted by ϵ, are also equal to each other. Let $\Delta\sigma$ and $\Delta\epsilon$ denote the principal stress and strain increments, respectively, then it can be seen from Eqs. (3.44) and (3.46) that for the model used herein,

$$\Delta\sigma = \left(\frac{4}{\sqrt{2}} E_s + p\right) \Delta\epsilon \tag{4.1}$$

where $p = p_i$, $i = 1, 2, 3$ and p_i can be obtained from Eqs. (3.33)

to (3.40) in the previous chapter.

For a granular material, the stiffening effect in the volume change due to the increase of hydrostatic compression stress is well known [1,42]. Therefore the coefficient $\left(\dfrac{4}{\sqrt{2}} E_s + p \right)$ in the right-hand side of Eq. (4.1) is evidently a function of hydrostatic stress and can not be regarded as constant. The purpose of this hydrostatic compression test is to find out what proportion of the volumetric strain is elastic and how the coefficients E_s and p vary with hydrostatic stress. Since p represents the slip behavior of the granular material, if the strain is small, the yield portion would be negligible in comparison with the elastic strain. This leads to the conclusion that the stress-strain behavior of a granular material under hydrostatic compression is essentially elastic but nonlinear if the volumetric strain is small.

(ii) Proportional stress increments with constant octahedral stress

(a) Axial shear stress path

The stress path here is either a triaxial extension (TE) or a triaxial compression (TC). For an axial shear stress path the octahedral normal stress is always kept constant throughout the stress path. The axial shear stress path can be illustrated in the principal stress space as shown in Fig. IV.1 or on an octahedral stress space as shown in Fig. IV.2. For a triaxial compression ($\gamma = 1$, $\alpha = \beta = -\dfrac{1}{2}$) or a triaxial extension ($\gamma = \alpha = 1$, $\beta = -2$) stress path, the loading starts at initially hydrostatic stress state at H (Fig. IV.1) and then

the stresses vary according to proportional stress increments so that the stress point remains on the octahedral plane through H. As the stress point moves along the projection of principal stress axis on octahedral plane and away from point H, the octahedral shear stress increases from zero. One purpose of performing tests along an axial shear stress path is to determine the shear deformation under change of shear stress, with constant hydrostatic pressure, with the shear being the only influence of stress history. The other purpose is to determine the influence of the stress direction (compression and extension) on the shear deformation. By setting $\Delta\sigma_1 = \gamma\Delta\sigma$, $\Delta\sigma_2 = \alpha\Delta\sigma$ and $\Delta\sigma_3 = \beta\Delta\sigma$ the following incremental stress-strain relation can be obtained from Eq. (3.54).

$$
\begin{Bmatrix} \Delta\epsilon_1 \\ \Delta\epsilon_2 \\ \Delta\epsilon_3 \end{Bmatrix} = \frac{\Delta\sigma}{\det A}
\begin{Bmatrix}
a_{22}a_{33}-a_{23}a_{32} & a_{13}a_{32}-a_{33}a_{12} & a_{12}a_{23}-a_{22}a_{13} \\
a_{31}a_{23}-a_{33}a_{21} & a_{11}a_{33}-a_{13}a_{31} & a_{21}a_{13}-a_{11}a_{23} \\
a_{21}a_{33}-a_{22}a_{31} & a_{31}a_{12}-a_{11}a_{32} & a_{11}a_{22}-a_{12}a_{21}
\end{Bmatrix}
\begin{Bmatrix} \gamma \\ \alpha \\ \beta \end{Bmatrix}
$$

(4.2)

where the coefficients a_{ij} (i,j = 1, 2, 3) are shown in Eq. (3.55).

The influence of stress history due to the constant hydrostatic pressure can be investigated without difficulty. If the stress history influence is neglected and it is assumed that the strains have little effect on the determination of a_{ij}, then Eq. (4.2) becomes:

$$
\begin{Bmatrix} \Delta\epsilon_1 \\ \Delta\epsilon_2 \\ \Delta\epsilon_3 \end{Bmatrix} \overset{\cdot}{=} \frac{\Delta\sigma_1}{\det A}
$$

$$
\times \begin{bmatrix} \dfrac{3E_s^2}{2}+\sqrt{2}\,E_s(p_2+p_3)+p_2p_3 & -\dfrac{E_s^2}{2}-\dfrac{1}{\sqrt{2}}E_sp_3 & -\dfrac{E_s^2}{2}-\dfrac{1}{\sqrt{2}}E_sp_2 \\[2em] -\dfrac{E_s^2}{2}-\dfrac{1}{\sqrt{2}}E_sp_3 & \dfrac{3E_s^2}{2}+\sqrt{2}\,E_s(p_3+p_1)+p_1p_3 & -\dfrac{E_s^2}{2}-\dfrac{1}{\sqrt{2}}E_sp_1 \\[2em] -\dfrac{E_s^2}{2}-\dfrac{1}{\sqrt{2}}E_sp_2 & -\dfrac{E_s^2}{2}-\dfrac{1}{\sqrt{2}}E_sp_1 & \dfrac{3E_s^2}{2}+\sqrt{2}\,E_s(p_1+p_2)+p_1p_2 \end{bmatrix}
$$

$$
\times \begin{Bmatrix} \gamma \\ \alpha \\ \beta \end{Bmatrix} \tag{4.3}
$$

i.e.

$$
\begin{Bmatrix} \Delta\epsilon_1 \\ \Delta\epsilon_2 \\ \Delta\epsilon_3 \end{Bmatrix} = \frac{\Delta\sigma}{\det A} \begin{Bmatrix} \dfrac{E_s^2}{2}(3\gamma-\alpha-\beta)+\sqrt{2}\,E_s(\gamma-\frac{1}{2}\beta)p_2+\sqrt{2}\,E_3(\gamma-\frac{\alpha}{2})p_3+\gamma p_2p_3 \\[1.5em] \dfrac{E_s^2}{2}(3\alpha-\beta-\gamma)+\sqrt{2}\,E_s(\alpha-\frac{1}{2}\beta)p_1+\sqrt{2}\,E_s(\alpha-\frac{\gamma}{2})p_3+\alpha p_1p_3 \\[1.5em] \dfrac{E_s^2}{2}(3\beta-\alpha-\gamma)+\sqrt{2}\,E_s(\beta-\frac{1}{2}\alpha)p_1+\sqrt{2}\,E_s(\beta-\frac{\gamma}{2})p_3+\beta p_1p_3 \end{Bmatrix}
$$

$$
\tag{4.4}
$$

In the TC stress path, $\alpha = -1/2$ and $\beta = -1/2$. If the p_i's are assumed to have the same order of magnitude then Eq. (4.4) indicates:

$$
\frac{\Delta\epsilon_1}{\Delta\epsilon_3} = \frac{\gamma}{\beta} = \frac{\Delta\sigma_1}{\Delta\sigma_3} = -2 \tag{4.5}
$$

Similarly, for a TE stress path $(\gamma = 1, \alpha = 1, \beta = -2)$ Eq. (4.4) yields again:

$$\frac{\Delta\epsilon_1}{\Delta\epsilon_3} = \frac{\gamma}{\beta} = \frac{\Delta\sigma_1}{\Delta\sigma_3} = -\frac{1}{2} \qquad (4.6)$$

Equations (4.5) and (4.6) imply that along the axial shear path, proportional stress and strain increments are roughly interchangeable if there is no stress history influence. As mentioned before, the axial shear stress path initially starts at a hydrostatic compression stress σ_{oct} and a corresponding strain ϵ_{oct} and then follows a stress path according to the specific proportional stress increment. If the differences between the present state and initial hydrostatic state of stress and strains are taken to be the coordinates of the stress-strain curves, Eqs. (4.5) and (4.6) can be qualitatively illustrated as shown in Fig. IV.3. Therefore, if the influence of stress history and stress (or strain) path is excluded or neglected, the stress-strain relationship should exhibit the following characteristics:

(1) Loading with proportional stress increment induces proportional strain increment. The slope in the strain/strain plot starts at the value achieved in initial hydrostatic compression. The slope in the smaller stress (absolute value) direction becomes flatter than in the larger stress direction as indicated in Fig. IV.3.

(2) For an isotropic material, the $\sigma_1 - \epsilon_1$ curve in a TC path is identical with the $\sigma_3 - \epsilon_3$ curve in the TE path if they are plotted in the coordinate system shown in Fig. IV.3. Similarly

$\sigma_3 - \epsilon_3$ curve in the TC path is identical with the $\sigma_1 - \epsilon_1$ curve in the TE path.

However, the above characteristics are not observed in tests of the stress-strain behavior of a granular material. According to experimental test results on Ottawa sand by Ko [16] and Masson [17], the behavior of a granular material along the axial shear stress path can be qualitatively illustrated in Fig. IV.4. Due to the influence of hydrostatic stress history and stress path, the stress-strain behaviors under the TC and TE stress path have the following characteristics:

(1) Along the TC stress path, the $\sigma_3 - \epsilon_3$ curve exhibits higher slope when the strain is small but it eventually indicates flatter slope with a sharper change of slope at some stress-strain state in comparison with the proportional strain increment $\sigma_3 - \epsilon_3$ curve (broken lines in Fig. IV.4(a)) obtained by one and one correspondence from the $\sigma_1 - \epsilon_1$ curve.

(2) Along the TE stress path, the $\sigma_1 - \epsilon_1$ curve exhibits a smaller slope when the strain is small but eventually reaches a higher slope with a smoother change of slope at some stress-strain state in comparison with the proportional straining $\sigma_1 - \epsilon_1$ curve (broken lines in Fig. IV.4(b)) obtained by one and one correspondence from the $\sigma_3 - \epsilon_3$ curve.

(3) In comparing the $\sigma_1 - \epsilon_1$ curve along the TC stress path and the $\sigma_3 - \epsilon_3$ curve along the TE stress path, the difference is evident; the latter curve has a higher initial slope but eventually reaches a lower ultimate stress level with sharper change of slope.

All of these indicate that the stress history, the stress-strain path, and the difference of slip characteristics in compression and in extension play important roles in the behavior of a granular material. All of the above-mentioned characteristics lead to one conclusion--that the granular material behaves differently in compression and in extension. However, previous investigation and theory [9,17] have never taken these facts into consideration. The proposed rheological model offers a satisfactory description of all these observed behaviors. They can be interpreted as follows:

The axial shear stress path always starts with an initial hydrostatic compression state with stress and strain corresponding to σ_{oct} and ϵ_{oct}. This means the material is initially loaded to a compression strain ϵ_{oct}. If proportional stress increments are applied according to the axial shear stress path, $\Delta\sigma$ is positive (compression) and $\Delta\sigma_3$ is negative (extension). Then the $\sigma_1 - \epsilon_1$ curve continues its compressive loading process which yields a p_1 value progressively smaller than the p_1 value of previous stress increment. At the instant of applying the first stress increment, the $\sigma_3 - \epsilon_3$ curve starts its compressive unloading process, the p_3 value is equal to E as can be seen from Eqs. (3.34) and (3.45). As the stress increments are being continuously applied, the p_3 value continuously decreases along a compressive unloading path but with a smaller rate than p_1 in the $\sigma_1 - \epsilon_1$ curve due to compressive loading. This is clearly indicated by Eqs. (3.33), (3.34) and (3.45) in the previous chapter. Therefore, at early stages of loading along the axial shear stress path, p_3 is larger than p_1. The slope of a

stress-strain curve in this study is contributed by stiffness springs E_s and p_i (i = 1, 2, 3). The influence of E_s on both $\sigma_1 - \epsilon_1$ and $\sigma_3 - \epsilon_3$ curves is approximately the same order of magnitude for small strain as can be seen from Eq. (3.53). The presence of p_3 being larger than p_1 makes the $\sigma_3 - \epsilon_3$ curve always exhibit a higher slope value than that of the $\sigma_1 - \epsilon_1$ curve in the early part of the axial shear stress loading path. As the axial shear stress loading continues, ϵ_1 decreases. At a certain stage and beyond, ϵ reaches a zero value and further becomes negative (extension), then the $\sigma_3 - \epsilon_1$ curve undergoes the process of extension unloading as shown in Fig. III.16. Thus p_3 decreases rapidly because the slip characteristics of a granular material is more susceptible to extension than compression. At a certain level of straining along an axial shear stress path, p_3 will be less than p_1. Thus in the later part of the axial shear stress path, the slope of the $\sigma_3 - \epsilon_1$ curve is flatter than the slope of the $\sigma_1 - \epsilon_1$ curve.

(b) Radial shear stress path

As shown in Fig. IV.2, the radial shear stress path lies somewhere in between the TE and TC stress paths on an octahedral stress plane. The stress path extends radially from the hydrostatic axis O and makes an angle θ^o with the horizontal axis. It will be called an RS-θ^o stress path following Ko's definition [16]. The axial stress path is essentially a particular kind of radial shear stress path, thus the TE stress path can be defined as RS-30° and the TC stress path as RS-90°. The other radial shear stress paths

lie between the TE and TC stress paths as shown in Fig. IV.2.

The stress path RS-60° is particularly interesting, since σ_2 is kept constant in this stress path. Therefore, the RS-60° stress path represents a special kind of plane stress condition. For the RS-60° stress path, experimental results on Ottawa sand performed by Ko [16] and Masson [17] showed that the strain in the σ_2 direction is small in comparison with the strains in the other two directions. It can therefore be speculated that the plane strain condition lies in the neighborhood of the RS-60° stress path although it is not necessarily represented by a straight line stress path. It can also be speculated that the stress-strain curves for a radial shear stress path should fall in between the stress-strain curves of the TE and TC stress path as shown in Fig. IV.5. The experimental results on Ottawa sand by Ko [16] and Masson [17] (shown in Figs. IV.6 and IV.7) seem to substantiate this speculation. The purpose of performing tests along a radial stress path is to investigate the stress-strain relations of granular materials under general three-dimensional stress states and also to use the proposed constitutive relation to the model and experimental results.

(iii) Proportional stress increments with variable σ_{oct}

In the previously discussed shear stress path, the octahedral normal stress was kept constant, and the influence of the stress path or the strain path was through the shear stress change. However in the conventional triaxial tests the octahedral normal stresses change along the stress path. Therefore the purpose of performing

tests following conventional triaxial stress paths is to investigate
the quantitative influence of changes in both shear and octahedral
stresses on the stress-strain behavior of a granular material and,
of course, to investigate the failure envelope. All the conventional
triaxial stress paths follow the rule of loading with proportional
stress increments with the change of octahedral stress along their
stress paths and can be illustrated in principal stress space as
shown in Fig. IV.8. The conventional triaxial stress paths always
start at an initially hydrostatic stress state, and then the stresses
vary according to proportional stress increments. If the effect of
stress history and stress path on the stress-strain behavior in an
isotropic material is again neglected, the following relations are
obtained from Eq. (4.4):

(a) CTC stress path ($\gamma = 1$, $\alpha = 0$, $\beta = 0$; $\Delta\sigma_1 = \Delta\sigma$,

$\Delta\sigma_2 = \Delta\sigma_3 = 0$; $\Delta\epsilon_2 = \Delta\epsilon_3$ and $p_2 = p_3 = p_T$)

$$\Delta\epsilon_1 = \frac{\Delta\sigma}{\det A}\left[\frac{1}{2}(E_s^2 + \sqrt{2}\,E_s p_T)\left(3 + \frac{\sqrt{2}\,p_T}{E_s}\right)\right] \tag{4.7a}$$

and

$$\Delta\epsilon_2 = \Delta\epsilon_3 = \frac{\Delta\sigma}{\det A}\left[-\frac{1}{2}(E_s^2 + \sqrt{2}\,E_s p_T)\right] \tag{4.7b}$$

Thus,

$$\left|\frac{\Delta\epsilon_1}{\Delta\epsilon_2}\right| = \left|\frac{\Delta\epsilon_1}{\Delta\epsilon_3}\right| = \left(3 + \frac{\sqrt{2}\,p_T}{E_s}\right) \tag{4.8}$$

(b) CTC-A stress path ($\gamma = 0$, $\alpha = \beta = -1$; $\Delta\sigma_1 = 0$, $\Delta\sigma_2 = \Delta\sigma_3 = -\Delta\sigma$; $\Delta\epsilon_2 = \Delta\epsilon_3$; $p_1 = p_c$, $p_2 = p_3 = p_T$)

$$\Delta\epsilon_1 = \frac{\Delta\sigma}{\det A} \quad E_s^2 + \sqrt{2} E_s p_T \tag{4.9a}$$

and

$$\Delta\epsilon_2 = \Delta\epsilon_3 = \frac{\Delta\sigma}{\det A} \left[-(E_s^2 + \sqrt{2} E_s p_T) \left(1 + \frac{\sqrt{2}}{2} \frac{p_c}{E} \right) \right] \tag{4.9b}$$

Thus,

$$\left| \frac{\Delta\epsilon_1}{\Delta\epsilon_2} \right| = \left| \frac{\Delta\epsilon_1}{\Delta\epsilon_3} \right| = \frac{1}{1 + \frac{\sqrt{2}}{2} \frac{p_c}{E}} \tag{4.10}$$

(c) CTE stress path ($\gamma = 0$, $\alpha = 0$, $\beta = -1$; $\Delta\sigma_1 = \Delta\sigma_2 = 0$, $\Delta\sigma_3 = -\Delta\sigma$; $\Delta\epsilon_1 = \Delta\epsilon_2$; $p_1 = p_2 = p_c$)

$$\Delta\epsilon_1 = \Delta\epsilon_2 = \frac{\Delta\sigma}{\det A} \left[\frac{1}{2} (E_s^2 + \sqrt{2} E_s p_c) \right] \tag{4.11a}$$

$$\Delta\epsilon_3 = \frac{\Delta\sigma}{\det A} \left[-\frac{1}{2} (E_s^2 + \sqrt{2} E_s p_c) \left(3 + \frac{\sqrt{2} \, p_c}{E_s} \right) \right] \tag{4.11b}$$

Thus,

$$\left| \frac{\Delta\epsilon_1}{\Delta\epsilon_2} \right| = \left| \frac{\Delta\epsilon_1}{\Delta\epsilon_3} \right| = \frac{1}{3 + \frac{\sqrt{2} \, p_c}{E_s}} \tag{4.12}$$

(d) CTE-A stress path ($\gamma = 1$, $\alpha = 1$, $\beta = 0$; $\Delta\sigma_1 = \Delta\sigma_2 = \Delta\sigma$, $\Delta\sigma_3 = 0$; $\Delta\epsilon_2 = \Delta\epsilon_3$; $p_1 = p_2 = p_c$, $p_3 = p_T$)

$$\Delta\epsilon_1 = \Delta\epsilon_2 = \frac{\Delta\sigma}{\det A} \left[(E_s^2 + \sqrt{2} E_s p_c) \left(1 + \frac{\sqrt{2}}{2} \frac{p_T}{E_s} \right) \right] \tag{4.13a}$$

$$\Delta\epsilon_3 = \frac{\Delta\sigma}{\det A}\left[-(E_s^2 + \sqrt{2}\,E_s p_c)\right] \tag{4.13b}$$

Thus

$$\left|\frac{\Delta\epsilon_1}{\Delta\epsilon_3}\right| = \left|\frac{\Delta\epsilon_2}{\Delta\epsilon_3}\right| = \left(1 + \frac{\sqrt{2}}{2}\frac{p_T}{E_s}\right) \tag{4.14}$$

Let σ_{oct}^o and ϵ_{oct}^o be the initial hydrostatic stress and strain, the stress-strain relations in Eqs. (4.7) to (4.14) can be illustrated as shown in Fig. IV.9. It can be seen that the stress-strain behavior is strongly dependent on the stress path even though the effects of stress history and strain characteristics are disregarded. The true stress-strain behavior of a granular material will be different from the one shown in Fig. IV.9 due to the influence of stress history and the different slip characteristics in compression and extension. As demonstrated in the stress-strain relation along the axial shear stress path, the influence of stress history and slip characteristic would again be reflected in a $\sigma_{oct} - \epsilon_3$ (extension) curve having a higher initial slope but eventually reaching a lower stress with sharper change of slope in comparison with the stress-strain relations shown in Fig. IV.9.

(iv) The stress paths for all the above-mentioned loading with proportional stress increments can be summarized in Table IV.1.

TABLE IV.1

Stress path	γ	α	β	$\Delta\sigma_{oct}$	$\Delta\tau_{oct}$
HC	1	1	1	1	0
TC	1	-1/2	-1/2	0	$1/3\sqrt{2}$
TE	1/2	1/2	-1	0	$1/3\sqrt{2}$
RS-60°	1	0	-1	0	$\sqrt{2}/\sqrt{3}$
CTC	1	0	0	1/3	$\sqrt{2}/3$
CTC-A	0	-1	-1	-2/3	$\sqrt{2}/3$
CTE	0	0	-1	-1/3	$\sqrt{2}/3$
CTE-A	1	1	0	2/3	$\sqrt{2}/3$

IV.1-2 Plane strain-stress path

In soil mechanics problems, the plane strain case is most frequently encountered. In order to apply the constitutive relations developed here to boundary value problems in soil mechanics, a general two-dimensional constitutive relation formulation in terms of σ_x, σ_y, τ_{xy}, ϵ_x, ϵ_y and γ_{xy} is needed and will be treated in detail in the next chapter. Here only some general aspects of the plane strain case in terms of principal stresses and strains will be discussed. By setting the intermediate principal strain and strain increment equal to zero, the constitutive relation in Eq. (3.54) becomes

$$\begin{bmatrix} \Delta\sigma_1 \\ \Delta\sigma_3 \end{bmatrix} = \begin{bmatrix} a_{11} & a_{13} \\ a_{31} & a_{33} \end{bmatrix} \begin{bmatrix} \Delta\epsilon_1 \\ \Delta\epsilon_3 \end{bmatrix} \qquad (4.15a)$$

and

$$\Delta\sigma_2 = a_{21}\Delta\epsilon_1 + a_{23}\Delta\epsilon_3 \qquad (4.15b)$$

where the a_{ij}'s can be obtained from Eq. (3.55) with $\epsilon_2 = 0$. If the influence of stress history and the slip characteristics are again disregarded, Eq. (4.15) can be approximately rewritten as follows:

$$\begin{bmatrix} \Delta\sigma_1 \\ \Delta\sigma_3 \end{bmatrix} = \left\{ \begin{array}{l} (\sqrt{2}\,E_s + p_1)\Delta\epsilon_1 + \dfrac{\sqrt{2}}{2}E_s\Delta\epsilon_3 \\ \dfrac{\sqrt{2}}{2}E_s\Delta\epsilon_1 + (\sqrt{2}\,E_s + p_1)\Delta\epsilon_3 \end{array} \right\} \qquad (4.16a)$$

and

$$\Delta\sigma_1 + \Delta\sigma_2 + \Delta\sigma_3 = (2\sqrt{2}\,E_s + p_1)\Delta\epsilon_1 + (2\sqrt{2}\,E_s + p_2)\Delta\epsilon_3 \qquad (4.16b)$$

If the octahedral normal stress is kept constant in the plane strain-stress path, the right-hand side of Eq. (4.16b) is equal to zero. Therefore, $\Delta\epsilon_3$ is approximately equal to $-\Delta\epsilon_1$, which in turn implies $\Delta\sigma_3$ is approximately equal to $-\Delta\sigma_1$ (RS-60° stress path). In other words, the plane strain stress path approximately coincides with the plane stress case on the same octahedral stress plane if the effect of stress history and slip-strain characteristics is neglected. However, in the real behavior of granular material, the latter effects must be recognized so that in reality the plane strain stress path will lie in the neighborhood of the plane stress case (RS-60°) but will be represented by a curved line rather than a straight line.

IV.2 Theoretical and Experimental Consideration of Parameters

Involved in the Proposed Constitutive Relations

IV.2-1 Relation of E_s to σ_{oct}

In the proposed model the stiffening spring with modulus E_s represents the elastic strain and volume changes of granular material under stress. The stiffening effect due to the increase of octahedral normal stress means that E_s increases with σ_{oct}. Some investigators [16,42] have tried to predict the compressibility of granular material by using Hertz's contact theory applied to spherical grains. Thus, the volumetric strain ϵ_{oct} is expressed as a two-thirds power function of σ_{oct}. In other words, the slope of $\sigma_{oct} - \epsilon_{oct}$ would be a one-third power function of σ_{oct} if Hertz's theory is applied. However, experimental results obtained by Ko and Scott

on Ottawa sand indicate that in a granular material such as sand, this relationship does not hold. The sand soil becomes stiffer more rapidly than predicted by Hertz's theory. Ko [16] and Masson [17] have performed hydrostatic compression tests on medium-dense Ottawa sand using two different but similar versions of cubit triaxial testing apparatus. Their results are shown in Figs. IV.10 and IV.11.

As derived in Eq. (4.1), the proposed stress-strain relation for hydrostatic compression would be approximated as:

$$\Delta\sigma_{oct} = \left(\frac{4}{\sqrt{2}}E_s + p\right)\Delta\epsilon_{oct} \qquad (4.1a)$$

Therefore, the terms $\frac{4}{\sqrt{2}}E_s + p$ represent the slope of the stress-strain curve under hydrostatic compression and can be deter-

mined from the experimental data. The term p denotes, as before, the stiffness portion due to the slip-spring elements with modulus E. The slip-spring elements represent the slip characteristics between contacts of a granular medium with a certain geometric packing. Therefore, p is presumably a function of the number of contacts and thus of the void ratio of a granular material.

Under hydrostatic compressure in the normal pressure range (say, 0 - 100 psi) the deformation is small in comparison with the deformation due to shear. This point is clearly indicated from Ko [16] and Masson's [17] experimental results on Ottawa sand shown in Figs. IV.6, IV.7, IV.10 and IV.11. If the slip is assumed to be negligible during the hydrostatic compression test then the p value is approximately equal to the modulus E. If it is further assumed that the void ratio or geometric packing change due to the hydrostatic pressure in the normal pressure range is insignificant, then E can be regarded as constant throughout the hydrostatic compression test.

In the case of a granular material, it can not support any deviatoric stress in the absence of a state of hydrostatic compression. Therefore, the slope of $\sigma_{oct} - \epsilon_{oct}$ curve at zero octahedral normal stress should be totally due to the modulus E of the slip-spring element since E_s at $\sigma_{oct} = 0$ is equal to zero. From Eq. (4.1) the slope of the curve is equal to $\frac{4}{\sqrt{2}} E_s + p$. The value can be separated by subtracting the p value from the slope of $\sigma_{oct} - \epsilon_{oct}$ curve. p can be assumed to be equal to E for all of the hydrostatic curves since:

(a) if ϵ_{oct} is small, only a negligible fraction of slip-spring elements has yielded and therefore p is approximately equal to E,

(b) if ϵ_{oct} is large, the difference between p and E would be negligible in comparison with the high value of $\frac{4}{\sqrt{2}} E_s$ as σ_{oct} becomes large.

The statement in the above paragraph may seem to be a presumptuous postulation. Further explanation is needed if the proposed model is to represent the deformation behavior of a granular material; it must have the property of being unable to support any shear stress in the absence of hydrostatic compression (i.e. $\sigma_{oct} = 0$). The only possibility for the proposed model to do so is by setting $E_s = 0$ at $\sigma_{oct} = 0$. In the absence of the stiffness springs E_s ($E_s = 0$) at $\sigma_{oct} = 0$, the proposed model consists of only three mutually-perpendicular slip-spring elements hinged together at the centroid (point 0 in Fig. III.17), and can not support any shear stress, since the presence of any small amount of shear would make the proposed model undergo continuous shear deformation and finally collapse. However, the slip mechanism is due to the contacts between grains and the slip mechanism should still exist in the three mutually-perpendicular principal direction even though σ_{oct} and E_s are both zero.

The hydrostatic compression tests on medium dense sand by Ko [16] and Masson [17] have already been shown in Figs. IV.10 and IV.11. To investigate the variation of E_s vs. σ_{oct}, the slopes of the σ_{oct}- ϵ_{oct} curves of their hydrostatic compression results must be calculated with respect to different levels of σ_{oct} stress.

In Ko's hydrostatic compression test [16], an arbitrary datum pressure was chosen at 4 psi, because at smaller pressures an uncertainty exists as to the sample's boundary condition in a soil test box. Therefore, Ko's testing results under hydrostatic compression have to be extrapolated to zero state of stress and strain. The corrected σ_{oct}-ϵ_{oct} curve is denoted by dotted lines as shown in Fig. IV. 0. The E_s values at various σ_{oct} stress levels for both Ko's and Masson's test results on Ottawa sand are tabulated in Tables IV.2 and IV.3

TABLE IV.2

E_s and E values from HC-test on medium dense
Ottawa sand by Ko[16]

σ_{oct}	ϵ_{oct}	$\frac{4}{\sqrt{2}} E_s + p$	Estimated $\frac{4}{\sqrt{2}} E_s$
(psi)	(%)	(psi)	(psi)
0	0	8000 (= E)	0
5	0.023	24250	16250
10	0.06	26670	18670
15	0.07	32000	24000
20	0.09	36370	28370
30	0.113	42100	36100
40	0.131	53300	45300
50	0.152	66670	58670

TABLE IV.3

E_s and E values from HC-test on medium dense
Ottawa sand (e = 0.524) by Masson [17]

σ_{oct}	ϵ_{oct}	$\frac{4}{\sqrt{2}} E_s + p$	Estimated $\frac{4}{\sqrt{2}} E_s$
(psi)	(%)	(psi)	(psi)
0	0	7500	0
5	0.041	20000	12500
10	0.062	24240	17140
15	0.08	28570	21070
20	0.095	33400	25900
30	0.122	33400	25900
40	0.146	48500	41000

If the estimated $\frac{4}{\sqrt{2}} E_s$ values are plotted against σ_{oct} as shown in Fig. IV.12, it is found that E_s increases with σ_{oct}. Both experimental data by Ko and Masson indicate that there exists a bilinear relation between E_s and σ_{oct} as illustrated in Fig. IV.12. For σ_{oct} larger than 5 psi, the E_s can be taken as a linear function of σ_{oct} rather than the one-third power function of σ_{oct} obtained from Hertz's theory.

IV.2-2 E_s vs. octahedral shear stress (τ_{oct})

When a granular material is subjected to a pure shear stress increment, there is usually observed a partially inelastic behavior with failure occurring when the shear stress reaches a certain level. From Eq. (3.46), it seems that the elastic stress component due to the stiffness spring elements with modulus E_s always exists in the

loading or unloading process. As indicated by Eqs. (3.33) to (3.40) and Eq. (3.46) in the previous chapter, when the strain level is large, the portion of stress increments due to slip-spring elements in the proposed model would be very small since most of the slip-spring elements have already yielded at large strain level. If E_s is assumed to be independent of octahedral shear stress then no failure will occur at large strain since the material behavior becomes predominantly elastic if the strain becomes large. This is a contradiction to the observed experimental data such as the test results of Ottawa sand under axial shear stress loading obtained by Ko [16] and Masson [17] (Figs. IV.6 and IV.7). Therefore, if the proposed three-dimensional model really represents the correct behavior of a granular material, it is inevitable that E_s be dependent on the octahedral shear stress. It can be postulated that the E_s value decreases with the increase of octahedral shear stress.

Some substantial complications in the formulation of stress-strain relations also develop thereby. However, this complication can be avoided by treating the E_s as a piecewise linear constant during each stress or strain increment. Since the constitutive relation is derived in incremental form, the error due to this linear approximation of E_s will be negligible if the stress or strain increment is kept at a small value.

An analytical expression of E_s in terms of octahedral shear stress may be proven to be difficult if not impossible. However, one might find the numerical relation between E_s and octahedral shear stress by simulating the axial shear stress path experimental

data and from some theoretical consideration of the deformation behavior of contacts between grains in a granular behavior.

Thurston and Deresiewicz [41] analyzed a face-centered cubic array of uniform spheres (the densest regular packing) and found the following relations for two spheres in contact.

(a) Loading curve

$$\delta = \frac{3(2-\nu)fN}{8\mu a}\left[1 - (1 - \frac{T}{fN})\right]^{2/3} \tag{4.17}$$

where

δ = relative tangential displacement of distinct points

f = coefficient of friction

T = tangential force

N = normal force

$a = \left[\frac{e(1-\nu)RN}{8\mu}\right]^{1/3}$ by Hertz's theory

R = radius of spheres

μ = shear modulus of grain

ν = Poisson's ratio of grain

or

$$\delta = \omega(fN)^{2/3}\left[1 - (1 - \frac{T}{fN})^{2/3}\right] \tag{4.17a}$$

where

$$\omega = \frac{3(2-\nu)f^{1/3}}{4[3R(1-\nu)\mu^2]^{1/3}} \tag{4.18}$$

Suppose N is constant then

$$\frac{dT}{d\delta} = (fN)^{1/3}(1 - \frac{T}{fN})^{1/3}\bigg/\frac{2}{3}\omega \tag{4.19}$$

(b) Unloading curve and reloading curve

A relation similar to Eq. (4.19) exists for both the unloading and the reloading case.

Equation (4.19) indicates that the slope of the T-δ curve is a one-third power function of shear force for two spheres in contact in the one-dimensional case. If an analogy can be postulated between Eq. (4.19) and the proposed three-dimensional model, it would seem that E_s decreases with a one-third power function of the difference between one and the ratio of τ_{oct} to σ_{oct}. However, the macroscopic behavior of randomly packed granular material as a whole under shear stress may not be represented by a simple relation derived from two spheres at contact. The true relation between E_s and σ_{oct} can only be determined from an examination of experimental data.

As indicated in section IV.2-1, E_s is a linear function of σ_{oct} rather than the one-third power function of σ_{oct} obtained from Hertz's theory. If this analogy can be applied to the relation between E_s and shear stress, it would be expected that E_s decreases with certain power functions of the difference between one and the ratio of τ_{oct} to σ_{oct}. As will be shown in the next section, if E_s is taken as a square function of the difference between one and τ_{oct}/σ_{oct}, the Tca-2 stress-strain curve of Ko's experimental results on Ottawa sand (Fig. IV.6 and Ref. [16]) can be closely simulated (Fig. IV.17). However, if the same relation is used to predict Ko's TE-1 test curve, the correlation between this proposed model and experimental data is not very good (Fig. IV.18).

Although the expression of E_s as a certain power function of $[1 - (\tau_{oct}/\sigma_{oct})]$ does not predict closely the experimental data of Ottawa sand under TE tests, nevertheless, some qualitative agreement between the shape of the stress-strain curves calculated by the proposed constitutive relation and that of the experimental results is apparently reached. In order to reach a better agreement between the proposed model and the deformation behavior of a granular material under various loading conditions, more effort in searching for a relationship between E_s and τ_{oct} is needed.

In establishing a workable relation between E_s and τ_{oct}, another factor must be taken into consideration. That is the fact that the E_s value can not be less than zero. For if $E_s < 0$, it would be possible to have a positive strain in the direction perpendicular to the direction along which a positive strain exists with a corresponding compressive stress, which is impossible for an isotropic material. If E_s is expressed as a power function of $[1 - (\tau_{oct}/\sigma_{oct})]$ along certain stress paths where τ_{oct}/σ_{oct} may have a value larger than one (such as the CTC stress path in Table IV.1), then E_s may become negative.

As indicated before, E_s has to decrease with the increase of τ_{oct}, and E_s increases with the increase of σ_{oct} according to the theoretical considerations and experimental results. The simplest relation to meet the above requirement and the condition of $E_s > 0$ is to express E_s as a certain power function of the ratio of σ_{oct} to the sum of σ_{oct} and τ_{oct}, i.e.,

$$E_s \propto \left(\frac{\sigma_{oct}}{\sigma_{oct} + \tau_{oct}} \right)^n \tag{4.20}$$

where n = constant.

Let $(E_s)_{\tau=0}$ denote the E_s value corresponding to $\tau_{oct} = 0$. Then Eq. (4.20) can be rewritten as

$$\frac{E_s}{(E_s)_{\tau=0}} = \left(\frac{\sigma_{oct}}{\sigma_{oct} + \tau_{oct}} \right)^n \tag{4.21}$$

The proposed model involves the stiffness spring modulus E_s and the slip-spring elements whose contribution to the stress-strain curve is indicated by the value p_i. The slope of the stress-strain curve must be the reflection of the influences of E_s and p_i on the stress-strain behavior. If the influences of E_s and p_i on the stress-strain curve are further assumed to be the same order of magnitude along a shear stress path (TC, TE or RS-θ^o), then the slope of a stress-strain curve will serve as an indication of how the E_s value varies with τ_{oct}.

Let S_e and $(S_e)_{\tau=0}$ denote the slope of an experimental stress-strain curve at $\tau_{oct} \neq 0$ and $\tau_{oct} = 0$ respectively. Then the ratio of S_e to $(S_e)_{\tau=0}$ can be plotted with the stress level for comparison purposes. For illustrative purposes, this plot will be called the "stiffness ratio curve" hereafter. The right-hand side of Eq. (4.21) for various n values can also be plotted with the stress level along the same stress path as the experimental data. Compare these plots and the plot from the stiffness ratio curve, and the n

value for a specific material can be estimated. For example, the stiffness ratio curves of the $\sigma_1 - \epsilon_1$ curve in the TCa-2 test and the $\sigma_3 - \epsilon_3$ curve in the TEa-2 test of Ko's experimental data on medium dense Ottawa sand are plotted in Figs. IV.13 and IV.14. A value of n = 5 is estimated when these stiffness ratio curves are compared with the plots of the right-hand side of Eq. (4.21) vs. stress level for various n values as shown in Figs. IV.13 and IV.14.

A word of caution is warranted. Due to the influence of the testing apparatus, the same material tested under the same stress conditions may yield different results from different apparatus. Since the relation of E_s and τ_{oct} is experimentally obtained, n values may be different for the same material tested in different apparatus.

IV.3 Representation of Experimental Data on Ottawa Sand

There are six material parameters, namely E_s, E, m_c, s_c, m_t, s_t to be determined. Ideally, it would be most desirable if they can be determined by six independent experimental data. Due to the complexity of the proposed constitutive relations and the complex stress-strain behavior of a granular material, it is impractical to set up tests along six independent stress paths. Although E_s and E can be estimated and the relation between E_s and octahedral and octahedral shear stresses can be concluded from hydrostatic compression tests and axial shear tests as shown in the previous section, there are still four other statistical parameters to be determined. In this thesis, the four statistical parameters are

determined by fitting the TC-stress path experimental data. Usually, there are several different combinations of these four parameters to describe the TC-stress path stress-strain behavior equally well. However, there is one combination of these which can best represent the stress-strain relation observed along the TE stress path. This combination is selected to represent the soil behavior. At first glance, it would seem that this procedure is highly arbitrary and tedious to follow. However, there are certain properties of the four statistical parameters that can be very helpful in determining the right combination. These properties can be observed from the properties of the Gaussian type distribution function and from the experimental data to be simulated. These properties are:

(1) Due to the difference in slip characteristics in compression and in extension the values of m_c and s_c are always larger than the respective values of m_t and s_t in extension. This means that the granular material is more susceptible to strain in extension as indicated by the observed experimental results [15, 16, 17].

(2) The values of m_c and m_t determine the slope of the axial shear stress path at small strain. Higher m_c and m_t values result in a steeper slope at small strain because of the higher mean level of slip stress for the material as indicated by the Gaussian distribution function or by Eqs. (3.33) to (3.40).

(3) The values of s_c and s_t dictate the smoothness of slope changes in a stress-strain curve. A sharper change of slope at some strain level is the indication of a smaller s_c or s_t

value. This is due to the properties of a Gaussian type distribution function. A small standard deviation means the slip stress distribution is more concentrated around the mean stress level. In other words, its distribution is closer to a triangular distribution. As the value of s_c increases, the slip stress distribution is further spreading more evenly out toward a rectangular distribution function.

A Fortran IV computer program is set up to calculate the stress and strain under arbitrary stress conditions of the proposed constitutive relation. A computer plot subroutine is also set up to present the computed results. Figs. IV.15 and IV.16 show some examples illustrating the above discussion.

As mentioned in the previous section, if the relation between E_s and the octahedral shear stress is taken to be

$$\frac{E_s}{(E_s)_{\tau=0}} = \left(1 - \frac{\tau_{oct}}{\sigma_{oct}} \right)^n \tag{4.22}$$

then it is found by the trial method that $n = 2$ would closely simulate the results of the TCa-2 test data by Ko on medium dense sand (Fig. IV.6 and Ref. [18]) as shown in Fig. IV.17. However, as shown in Fig. IV.18, if the same parameters are used to simulate Ko's TEa-2 test data on Ottawa sand with similar void ratios, it is found that the simulation is not as desirable as was hoped. Equation (4.22) is subsequently discarded.

Equation (4.21) mentioned in the previous section is used for the relation between E_s and τ_{oct} in simulating the experimental

data on medium dense sand obtained by Ko [16] and Masson [17] (Figs. IV.6 and IV.7). All the stress increments used in computing the stress-strain relation are taken exactly according to the stressing process in the specific experimental data to be simulated.

For Ko's data as shown in Fig. IV.6, all the axial shear stress and radial shear stress are approximated at the same magnitude of void ratio and all have been subjected to 20 psi of hydrostatic compression pressure. The corresponding strain is $\epsilon_{oct} = 0.009$ as shown in Fig. IV.10. The E_s and E values are obtained from Table IV.2, Fig. IV.12 and Eq. (4.21). The involved parameters found to be able to closely simulate Ko's TCa-2 tests are indicated in Fig. IV.19. It can be seen from Fig. IV.19 that the simulation is excellent considering the compexity and the uncertainty of a granular material's behavior.

The same parameters are used to predict the experimental stress-strain curve of Ko's TEa-2, RS-45°, RS-60°-1 and RS-75°-1 tests shown in Fig. IV.6. Figures IV.20 to IV.23 are the results predicted by the proposed constitutive relation. Again all the predictions except the RS-75°-1 test are extremely close to the experimental data. The failure of predicting the RS-75°-1 test is probably due to the irregularity in the test results. As can be seen from Figs. IV.5 and IV.6, the qualitative description of the proposed constitutive relation agrees with the experimental stress-strain behavior along shear stress paths except in the stress path of RS-75°. If the prediction by the proposed constitutive law can predict most of the experimental data closely, there is no reason for an experimental

stress-strain data point along a particular shear stress path to be an exception.

The same procedures are also used to simulate Masson's test data shown in Figs. IV.7, IV.11 and Table IV.3. Again, a close simulation is indicated as shown in Figs. IV.24 to IV.27.

IV.4 Remark

From the simulation and prediction results of the test data on Ottawa sand by Ko [16] and Masson [17] shown in Figs. IV.19 to IV.26 it can be seen that the experimental results and the proposed constitutive relations are in close agreement. It can be concluded that the proposed constitutive relations are much more realistic than any other theories and models at the present state of the art in describing the deformation behavior of a granular material.

The ultimate purpose of having a realistic constitutive relation is to be able to apply it to solve some field problems in soil mechanics. The field problems in soil mechanics usually have complicated geometries in the boundaries. The usual way of dealing with this type of problem is the use of finite element analysis taking the corresponding constitutive relations into consideration. As will be shown in the next chapter, the most general forms of the constitutive relations derived from this model in general three-dimensional stress-strain formulation have a non-symmetrical stiffness matrix once the shear stresses and strains are present. This couples with the complexity of the proposed constitutive relations, and the loading and unloading process is

beyond the capability in the present state of the art in finite element computer formulations. In recent years, the finite element analysis has been vastly employed and the solution technique has been vastly improved. This is no reason to believe that a workable scheme to solve a problem with non-symmetrical stiffness matrix is unreachable in the near future. More effort is needed in this direction in order to apply the proposed constitutive relations for a granular material to some boundary value problems in soil mechanics.
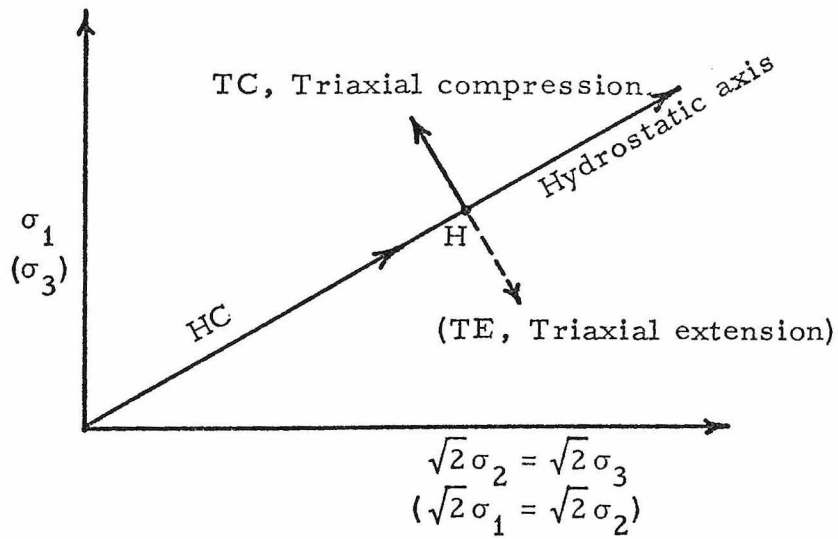
Fig. IV.1. Hydrostatic Compression and Axial Shear
Stress Paths in Principal Stress Space
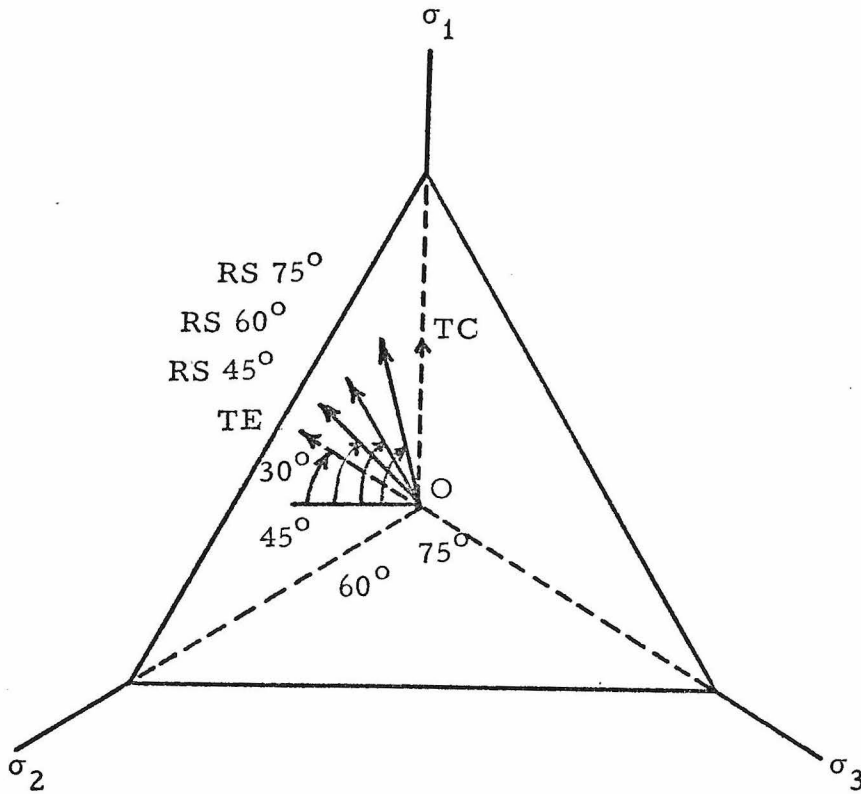
Fig. IV.2. Axial and Radial Shear Stress Paths
on an Octahedral Plane

Fig. IV.3. Identical Stress-Strain Curves for Proportional Stress Increment Stress Path and Proportional Increment Stress Path, Disregarding the Effect of Stress History and Strain Characteristics

(a) TC Stress Path

(b) TE Stress Path

(c) Comparison between TC and TE Stress Paths
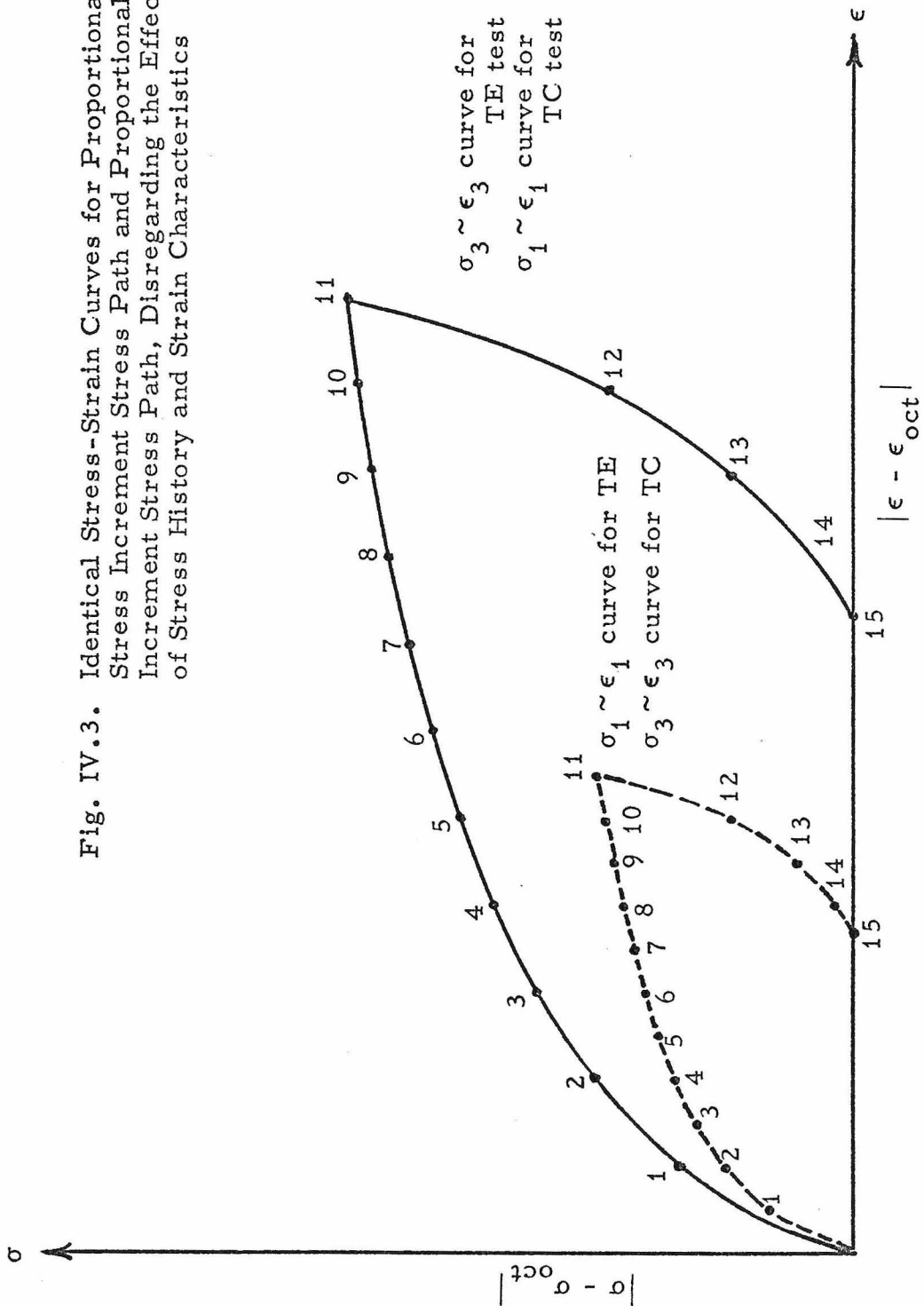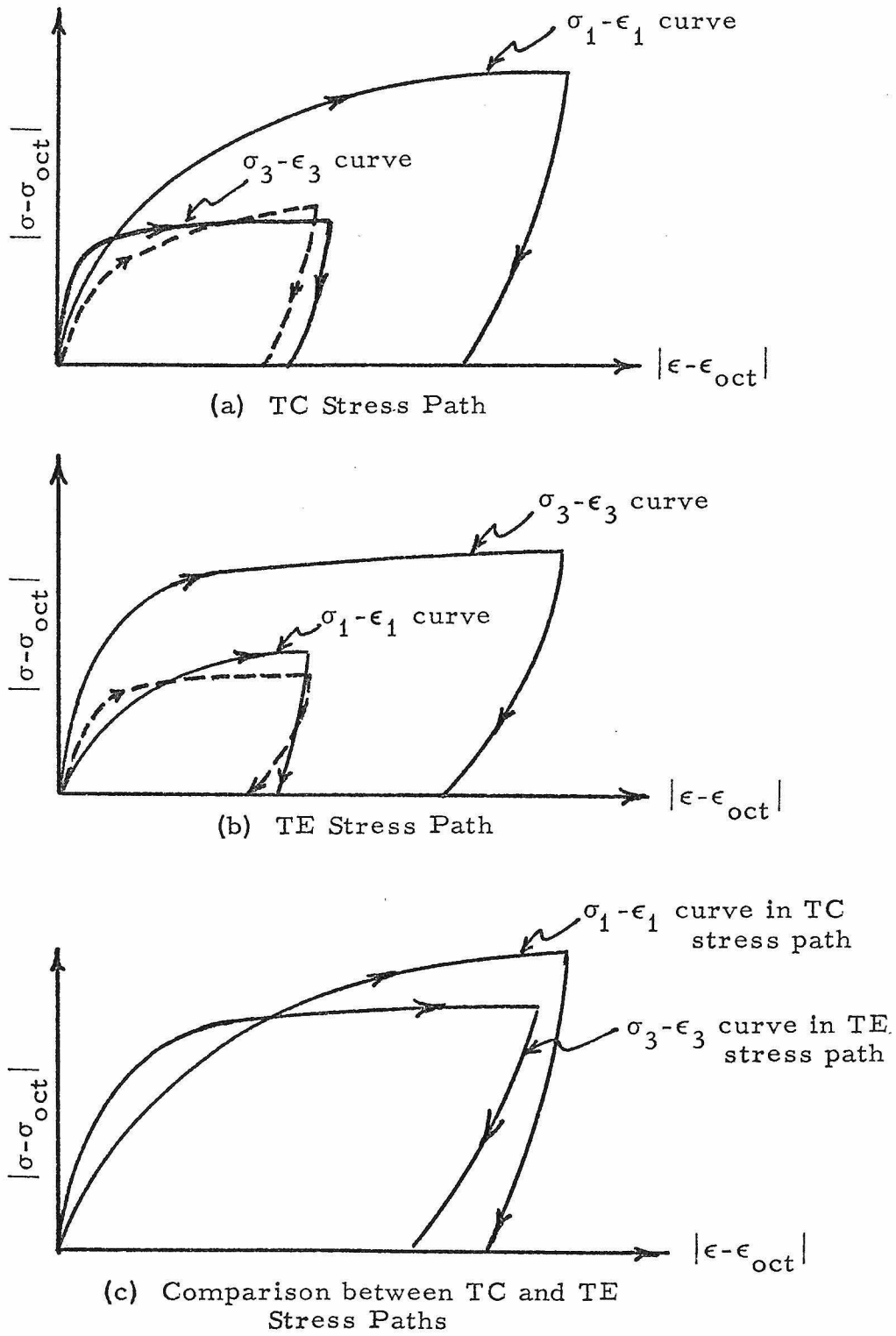
Fig. IV.4. Granular Material's Qualitative Stress-Strain Behaviors Along Axial Shear Stress Paths
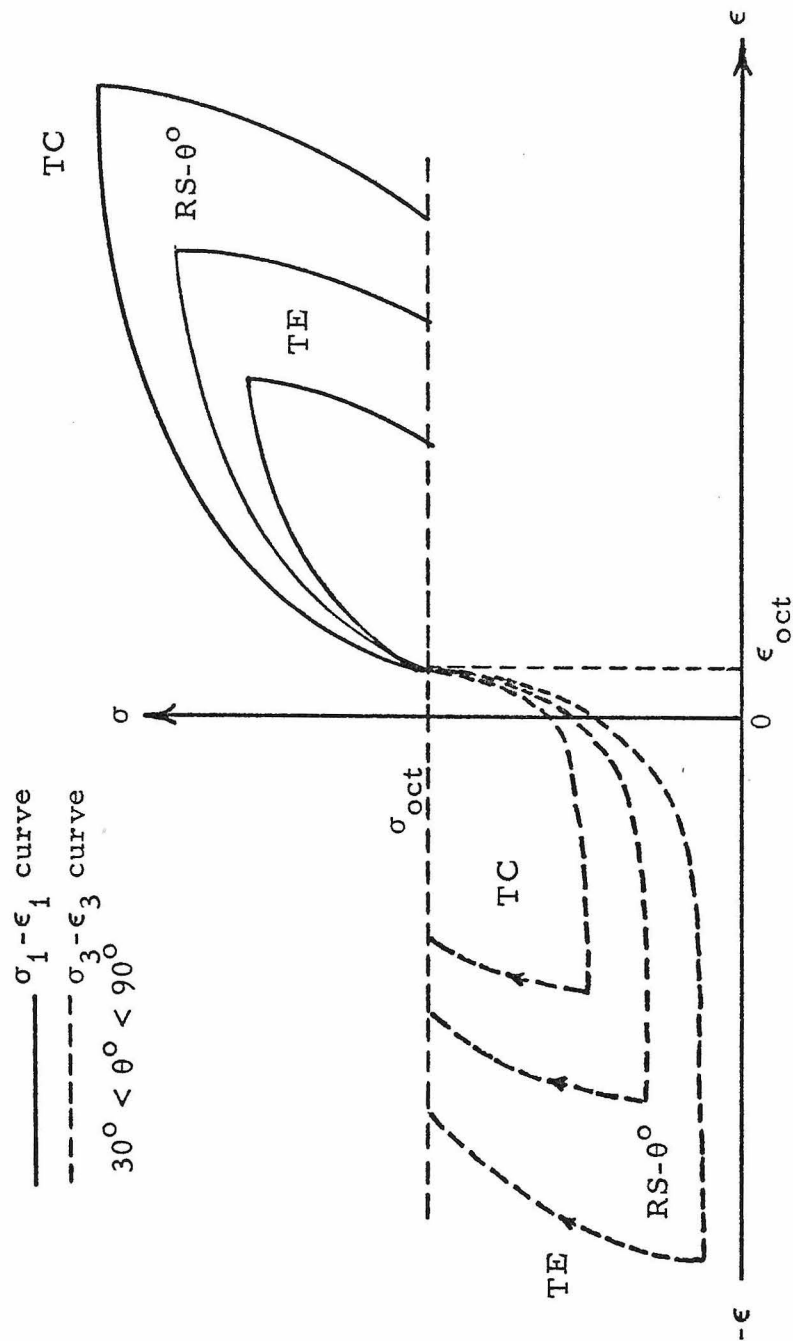
Fig. IV.5. Qualitative Stress-Strain Relation Between
Axial Shear and Radial Shear Stress Paths
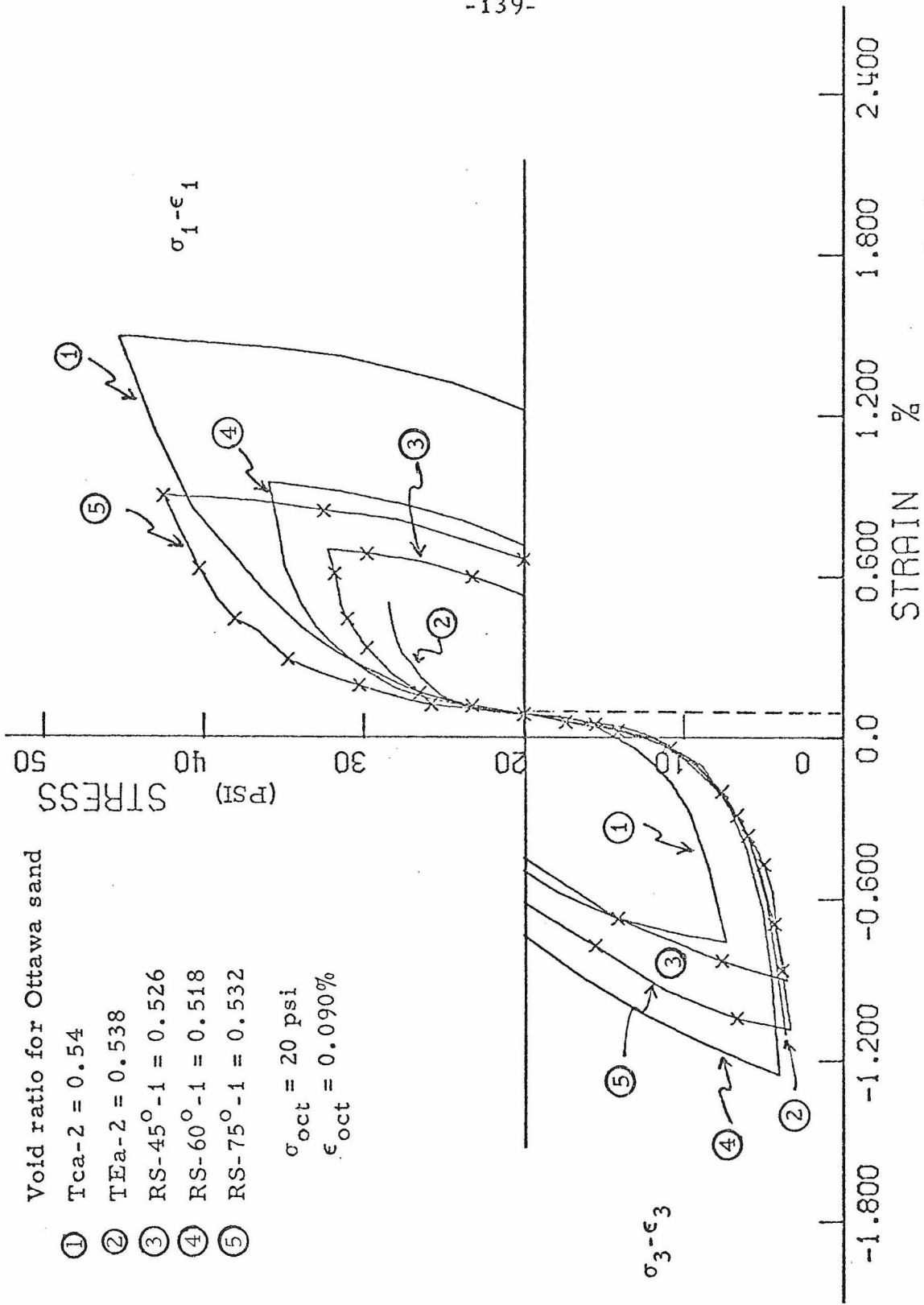
Fig. IV.6. Experimental Data under Shear Stress Paths Obtained by Ko [16]
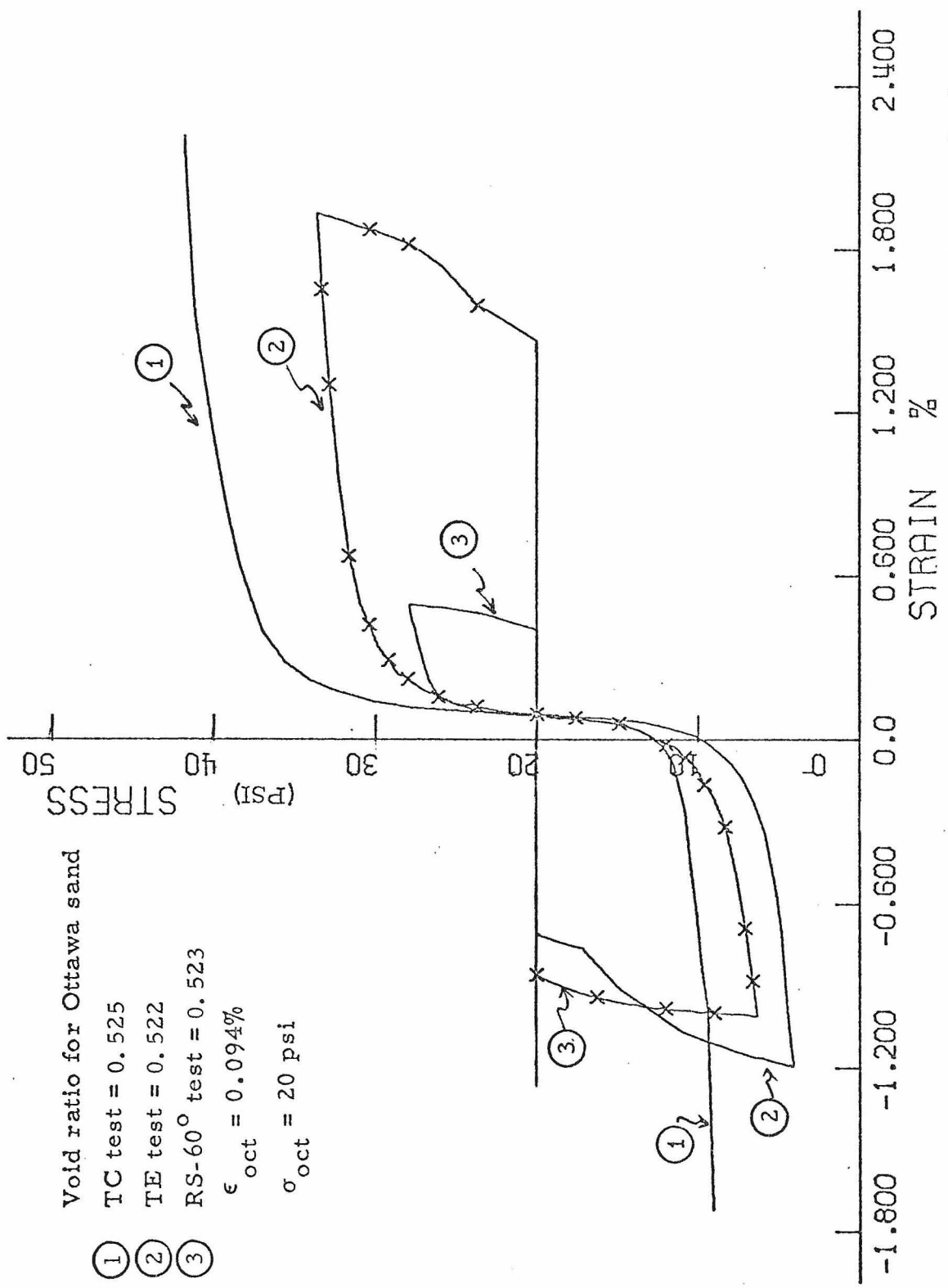
Fig. IV.7. Experimental Data under Shear Stress Paths Obtained by Masson [17]
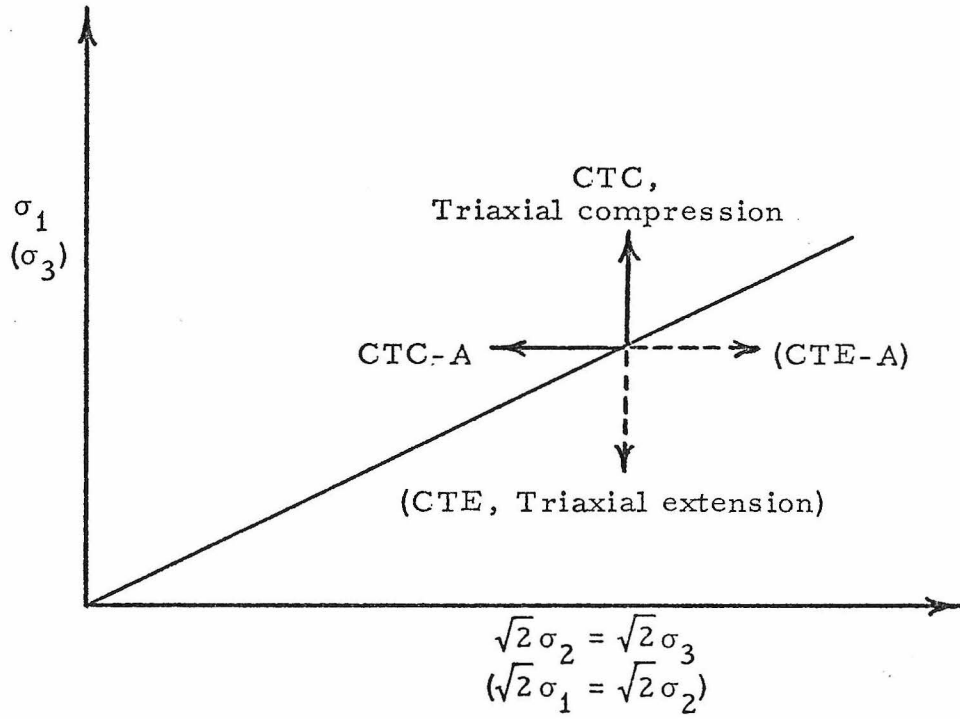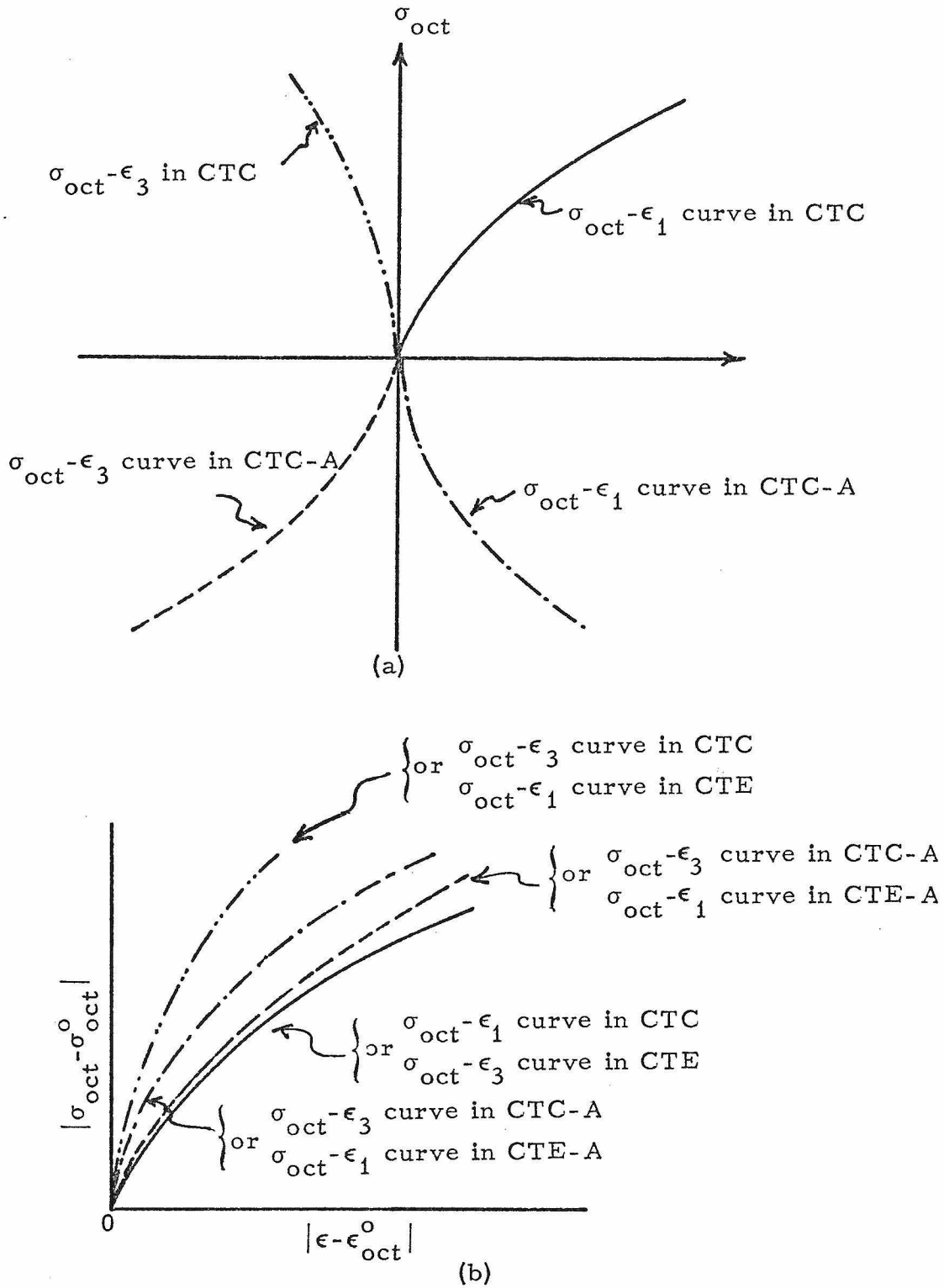
Fig. IV.8. Conventional Triaxial Stress Paths in Principal Stress

σ_{oct}

$\sigma_{oct}-\epsilon_3$ in CTC

$\sigma_{oct}-\epsilon_1$ curve in CTC

$\sigma_{oct}-\epsilon_3$ curve in CTC-A

$\sigma_{oct}-\epsilon_1$ curve in CTC-A

(a)

$\left\{ or \begin{array}{l} \sigma_{oct}-\epsilon_3 \text{ curve in CTC} \\ \sigma_{oct}-\epsilon_1 \text{ curve in CTE} \end{array} \right.$

$\left\{ or \begin{array}{l} \sigma_{oct}-\epsilon_3 \text{ curve in CTC-A} \\ \sigma_{oct}-\epsilon_1 \text{ curve in CTE-A} \end{array} \right.$

$\left\{ or \begin{array}{l} \sigma_{oct}-\epsilon_1 \text{ curve in CTC} \\ \sigma_{oct}-\epsilon_3 \text{ curve in CTE} \end{array} \right.$

$\left\{ or \begin{array}{l} \sigma_{oct}-\epsilon_3 \text{ curve in CTC-A} \\ \sigma_{oct}-\epsilon_1 \text{ curve in CTE-A} \end{array} \right.$

$|\sigma_{oct}-\sigma^o_{oct}|$

0

$|\epsilon-\epsilon^o_{oct}|$

(b)

Fig. IV.9. Qualitative Stress-Strain Relations for Conventional Triaxial Stress Paths Disregarding the Effect of Stress History and Strain Characteristics
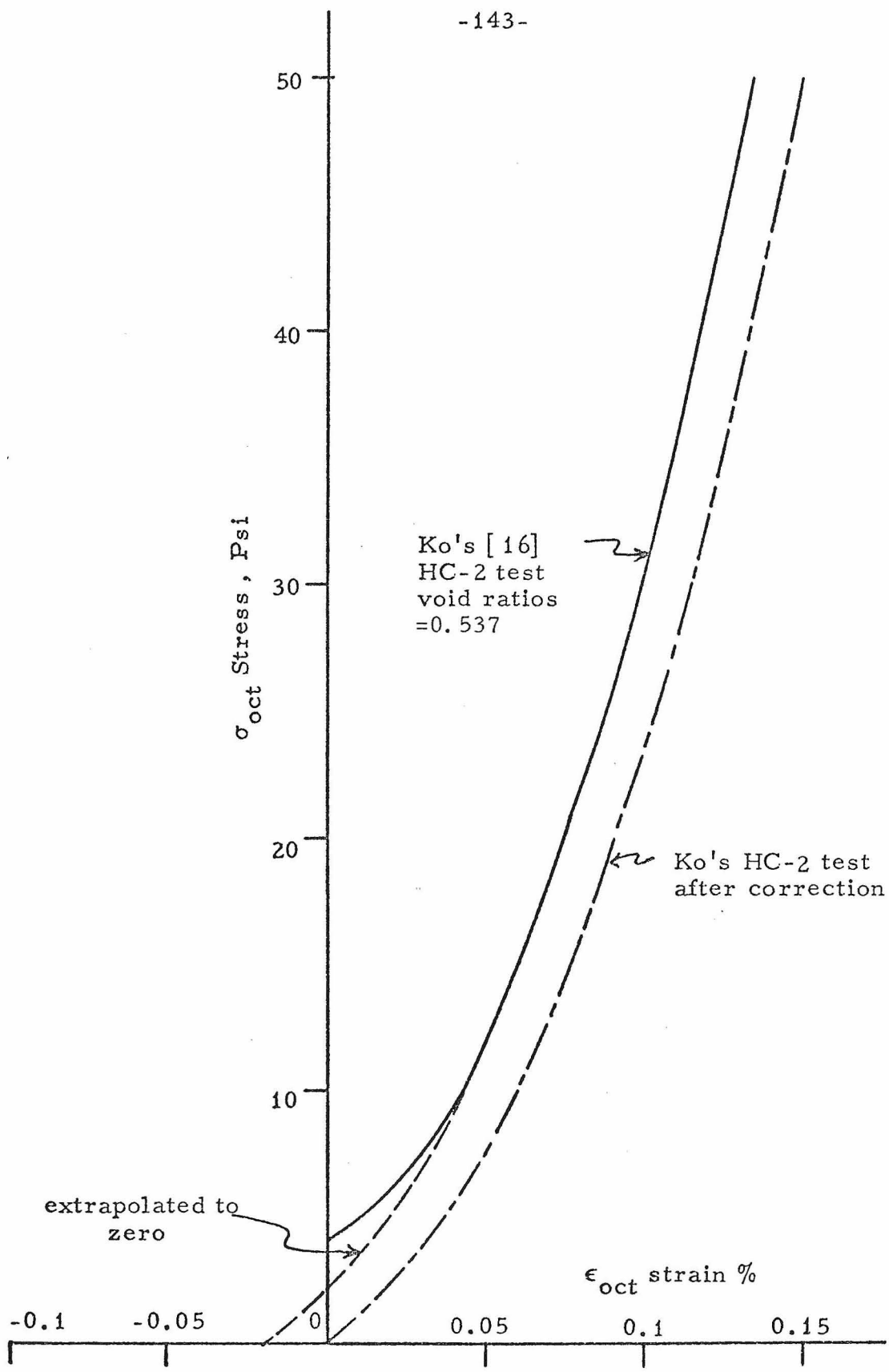
Fig. IV.10. Ko's [16] Experimental Data of Hydrostatic Compression on Medium Dense Ottawa Sand

Masson's [17] HC test
on dense sand

void ratio =0.524
$\epsilon_{oct} = \frac{1}{3} (\epsilon_1 + \epsilon_2 + \epsilon_3)$
$\sigma_{oct} = \frac{1}{3} (\sigma_1 + \sigma_2 + \sigma_3)$
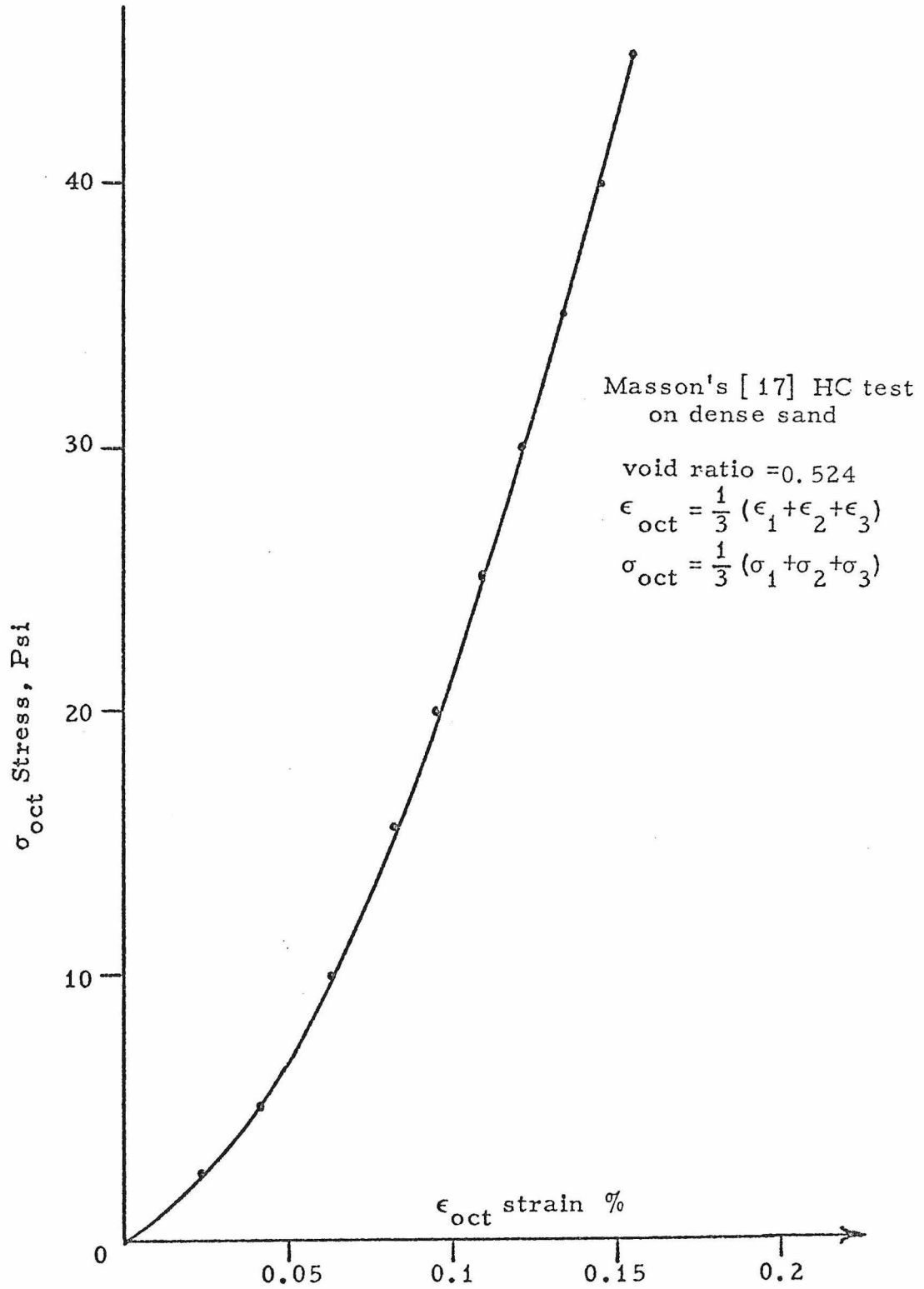
Fig. IV.11. Masson's [17] Experimental Data of Hydrostatic Compression on Dense Ottawa Sand
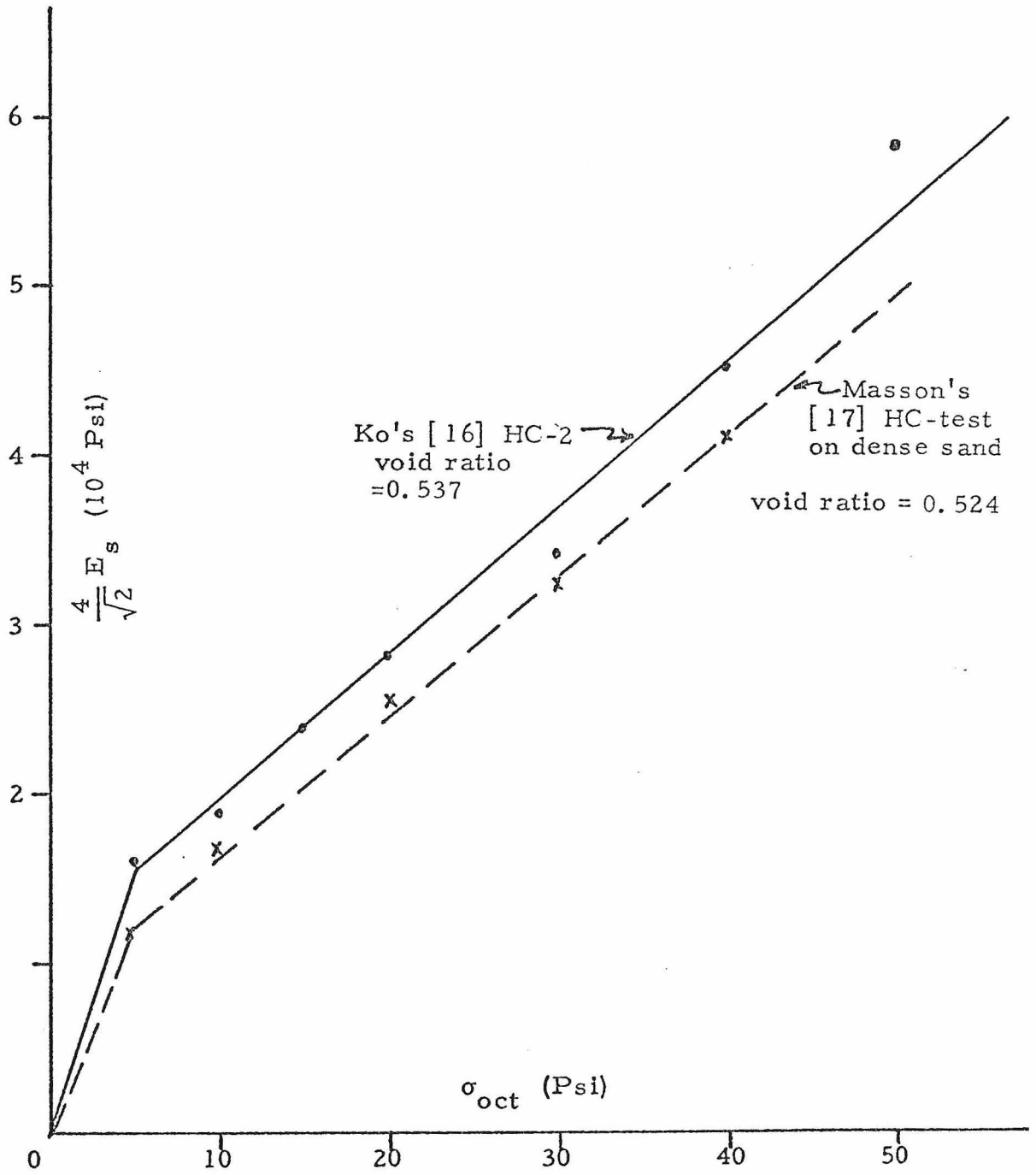
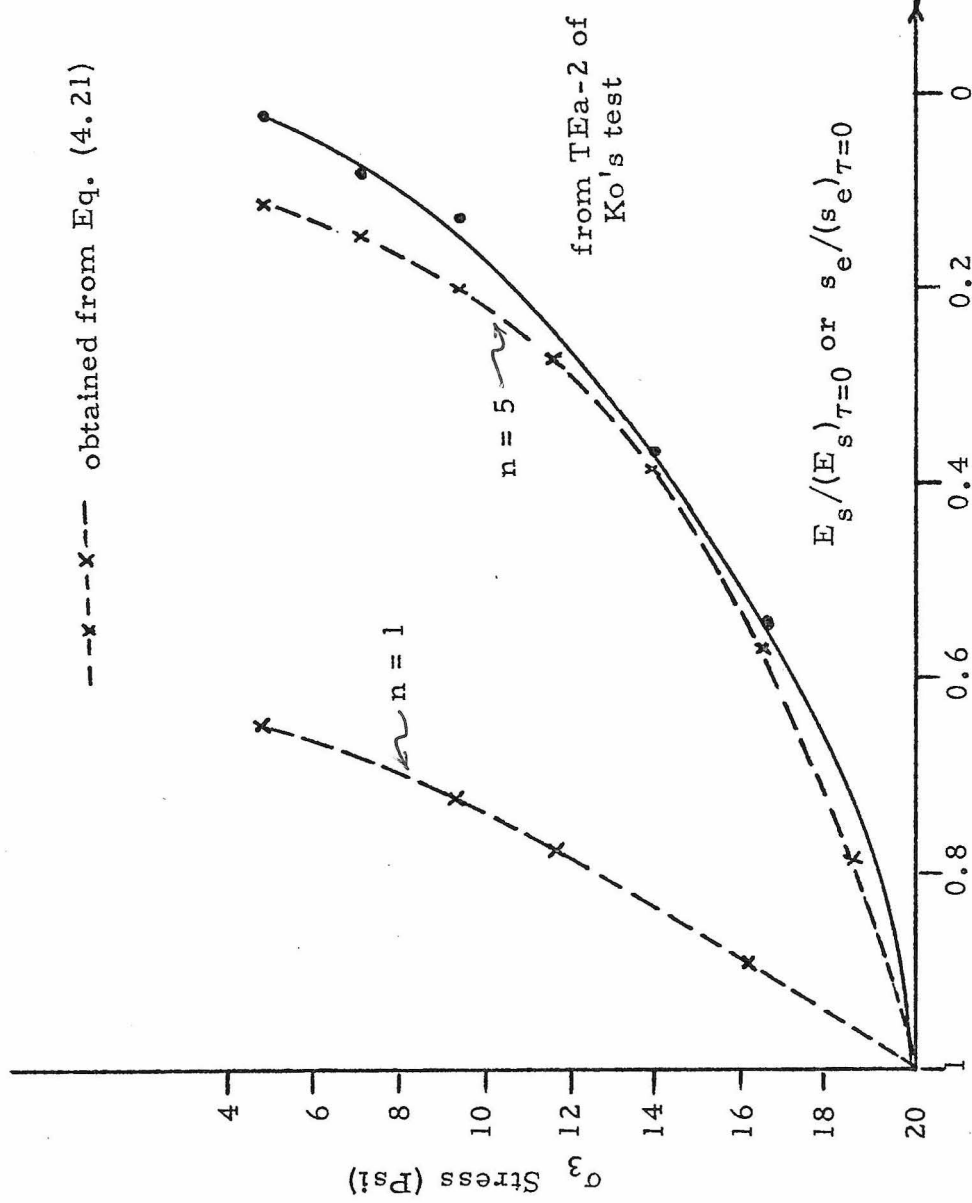Fig. IV.12. Experimental E_s Values vs. Hydrostatic Compression Stress

Fig. IV.14. Comparison of $E_s/(E_s)_{\tau=0}$ in Eq. (4.21) and $s_e/(s_e)_{\tau=0}$ from Experimental Data
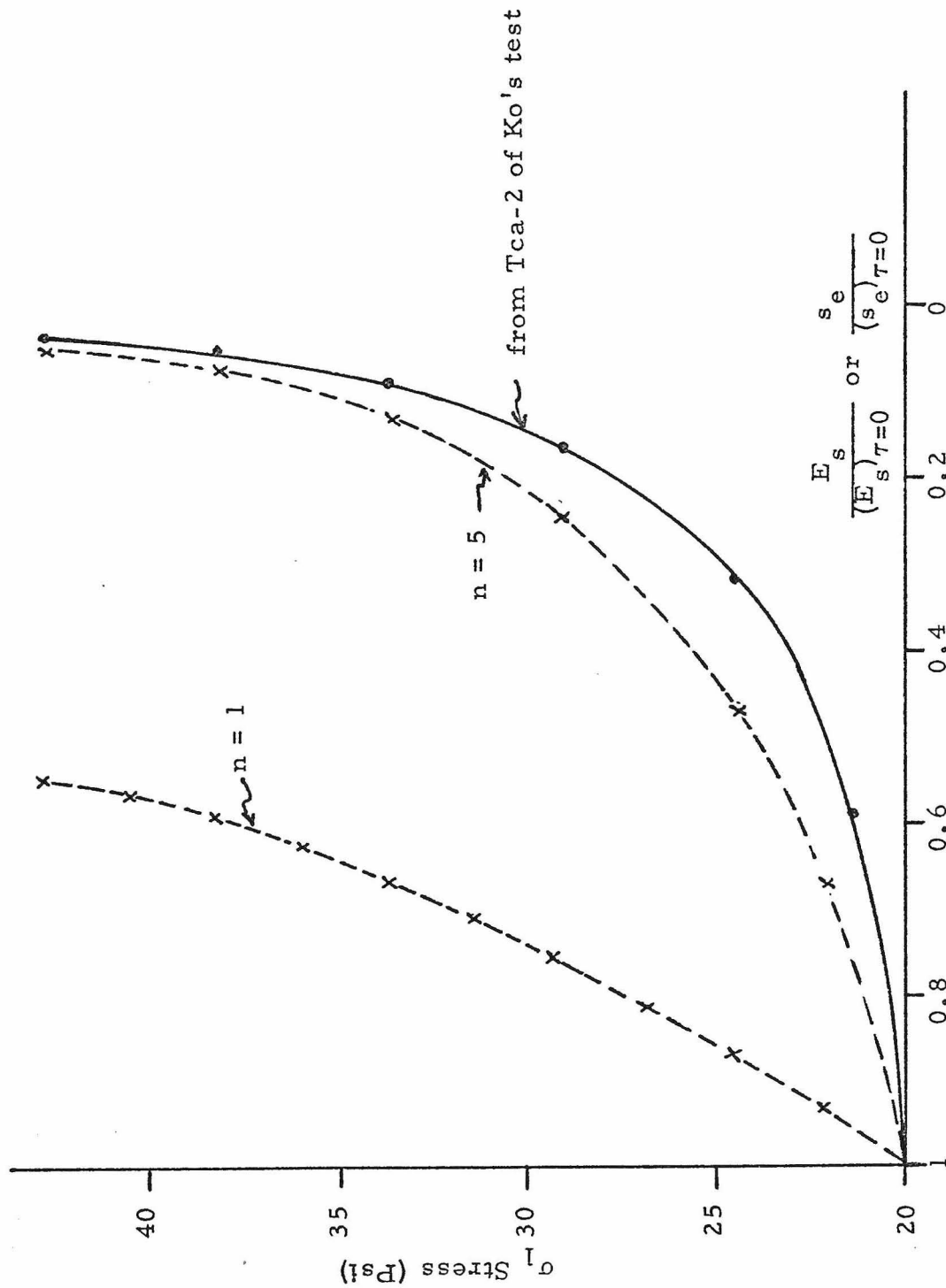
Fig. IV.13. Comparison of $E_s/(E_s)_{\tau=0}$ in Eq. (4.21) and $s_e/(s_e)_{\tau=0}$ from Experimental Data
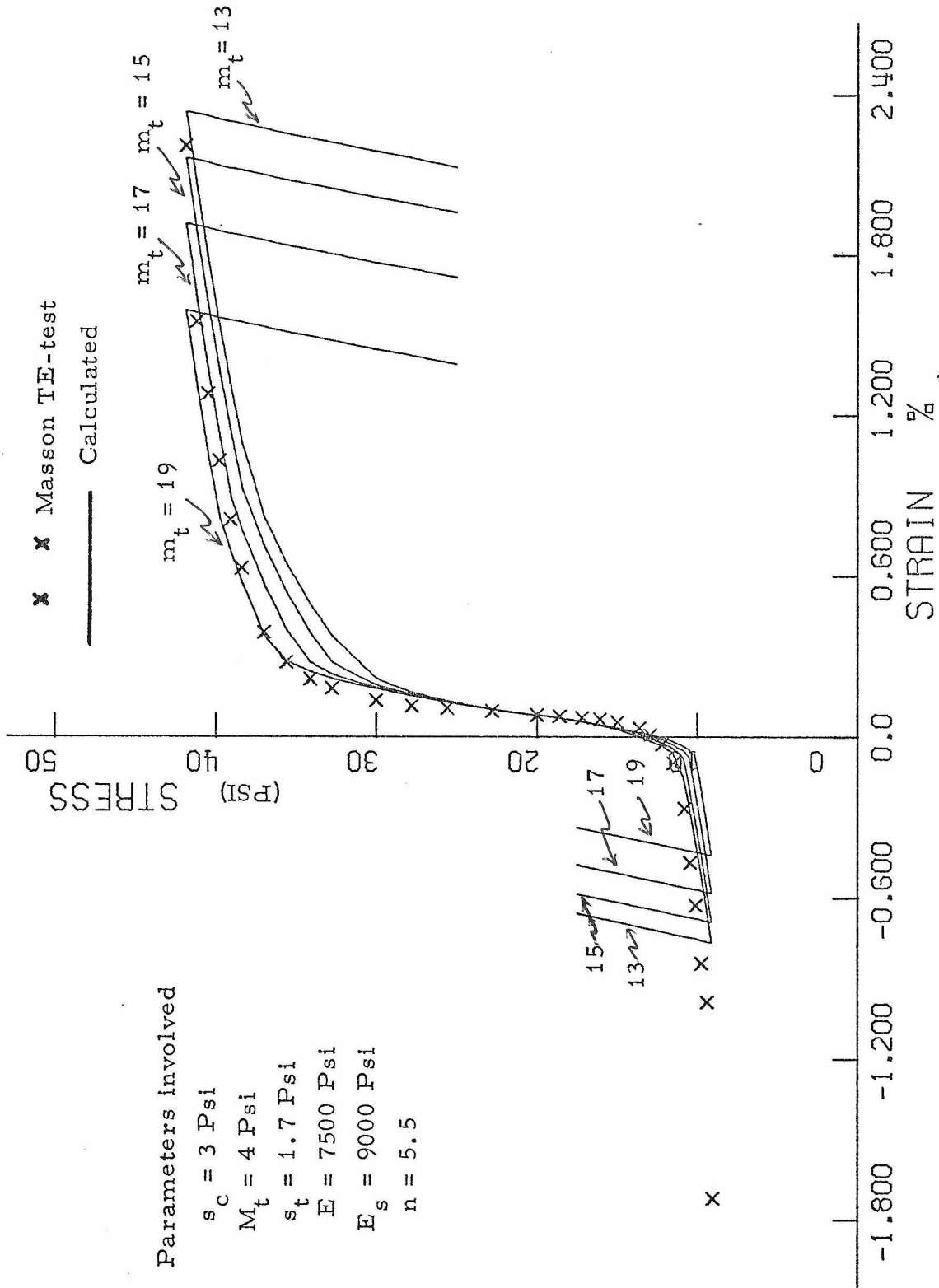
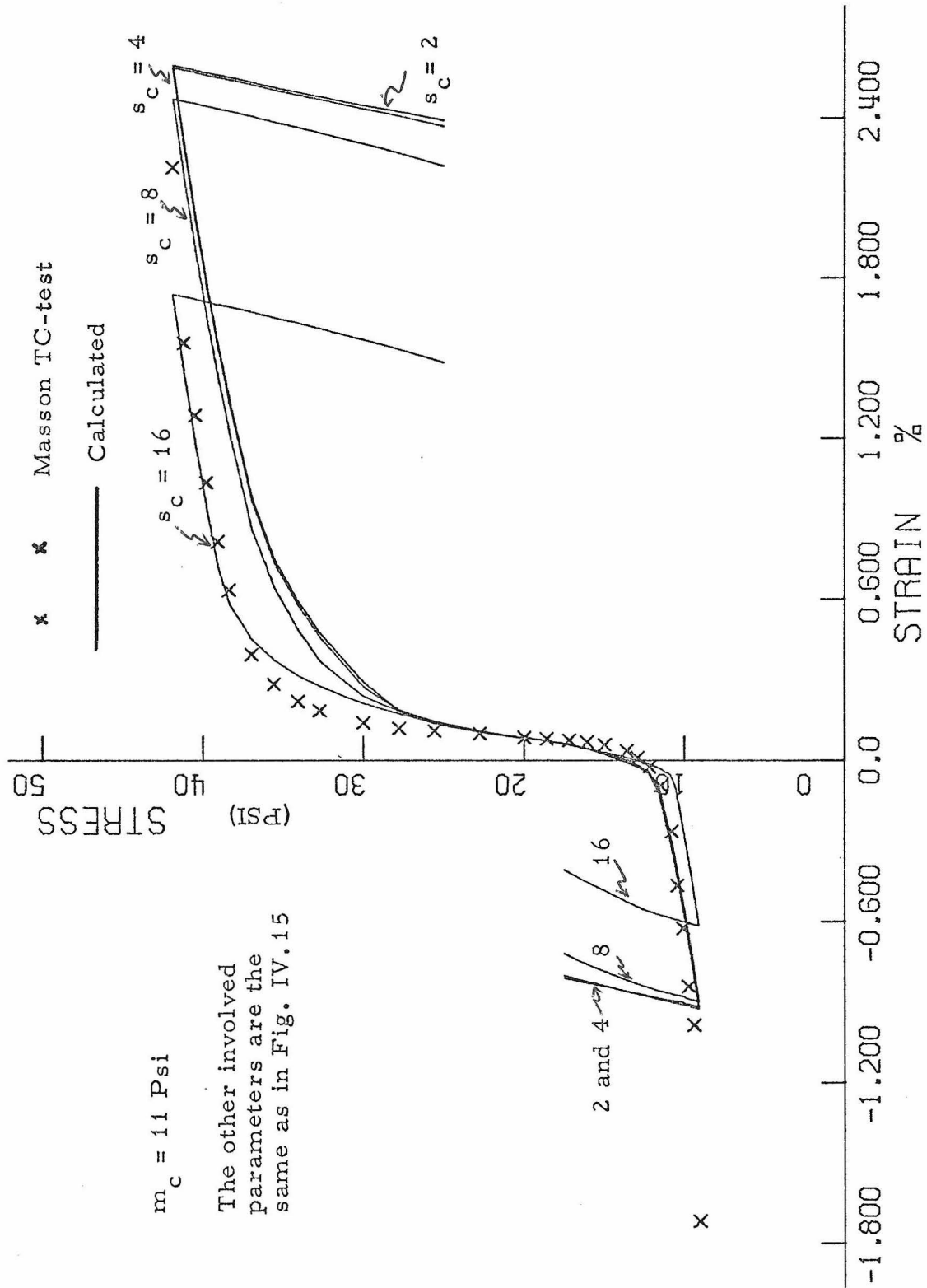Fig. IV.15. The Influence of Various Means of a Gaussian Type $\phi(\sigma^*)$ on the Stress-strain Curve

Fig. IV.16. The Influence of Various Standard Deviations of a Gaussian Type $\phi(\sigma^*)$ on Stress-strain Curve
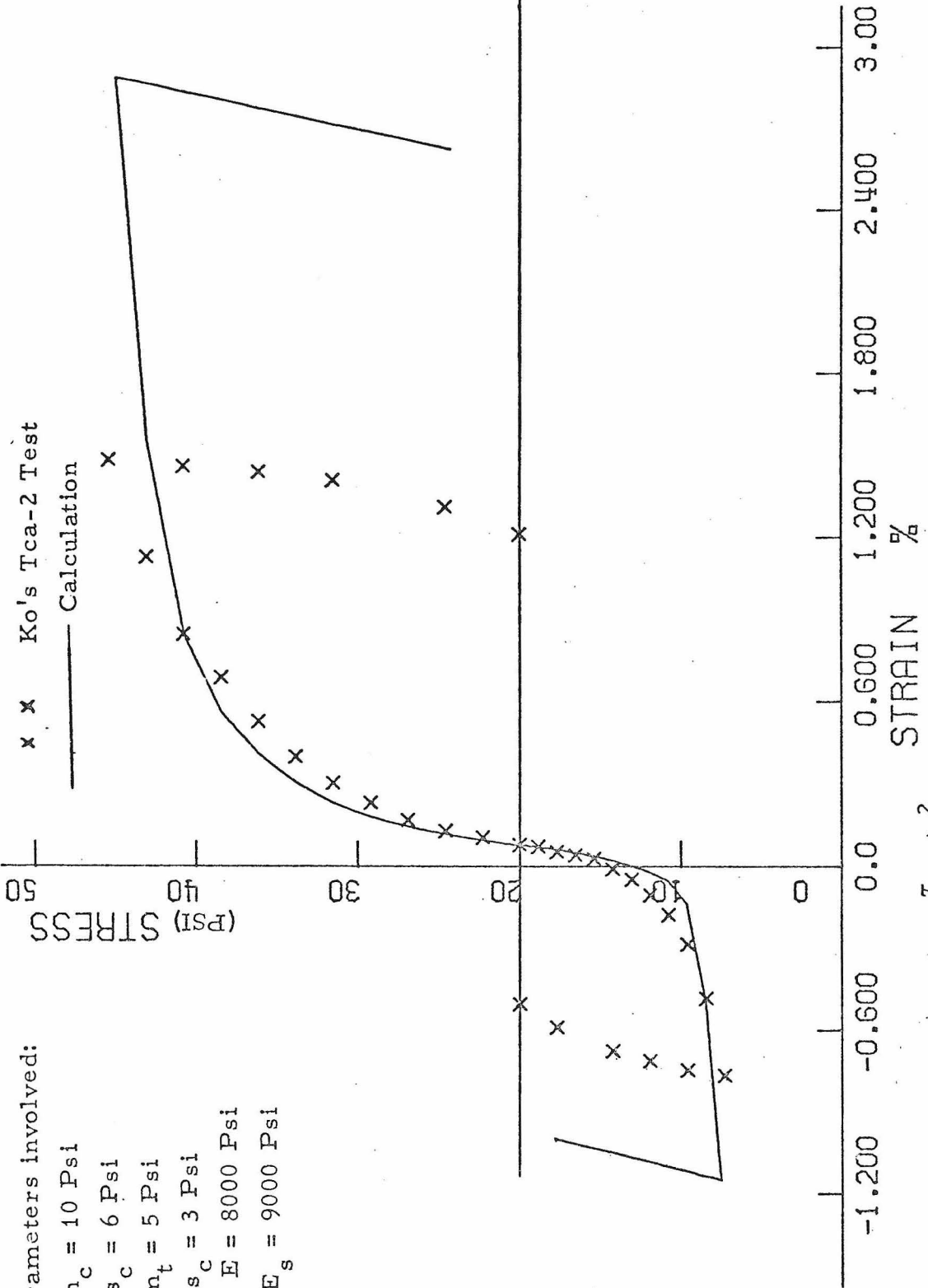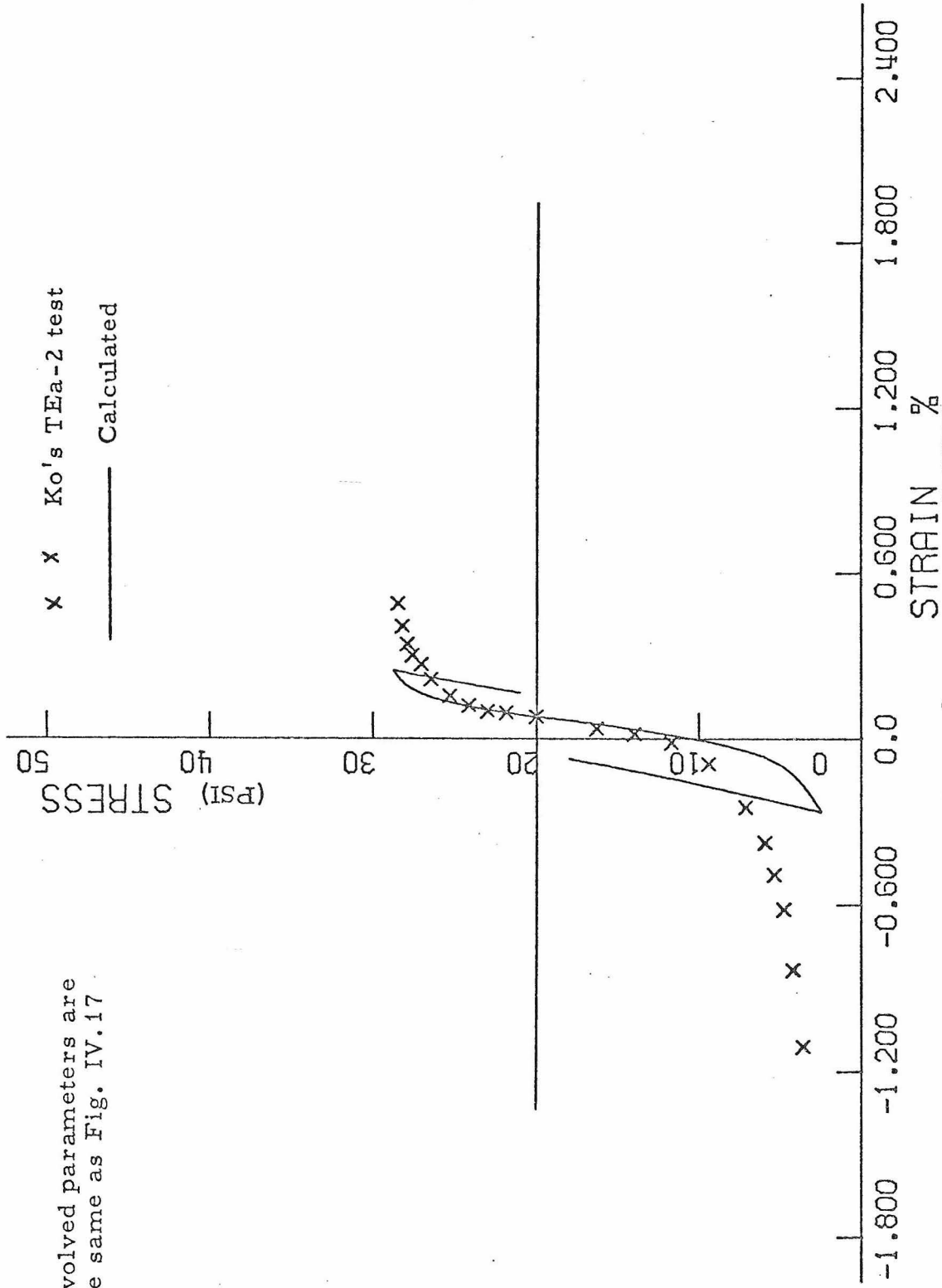
Fig. IV.17. $E_s \propto \left(1 - \dfrac{\tau_{oct}}{\sigma_{oct}}\right)^2$ Predicts Closely Ko's Tca-2 Test

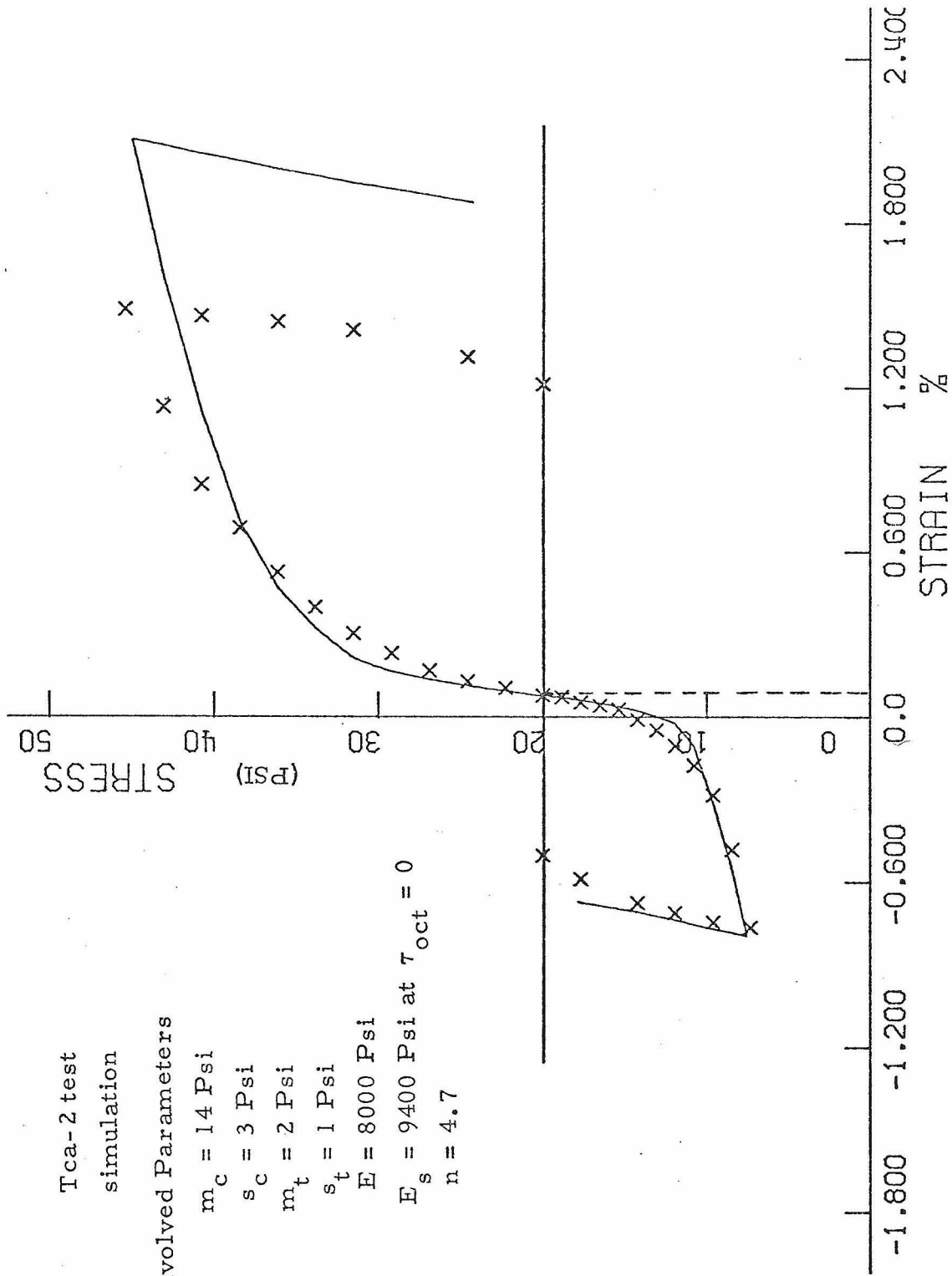Fig. IV.18 $E_s \propto \left(1 - \dfrac{\tau_{oct}}{\sigma_{oct}}\right)^2$ Fails to Predict Ko's TEa-2 Test
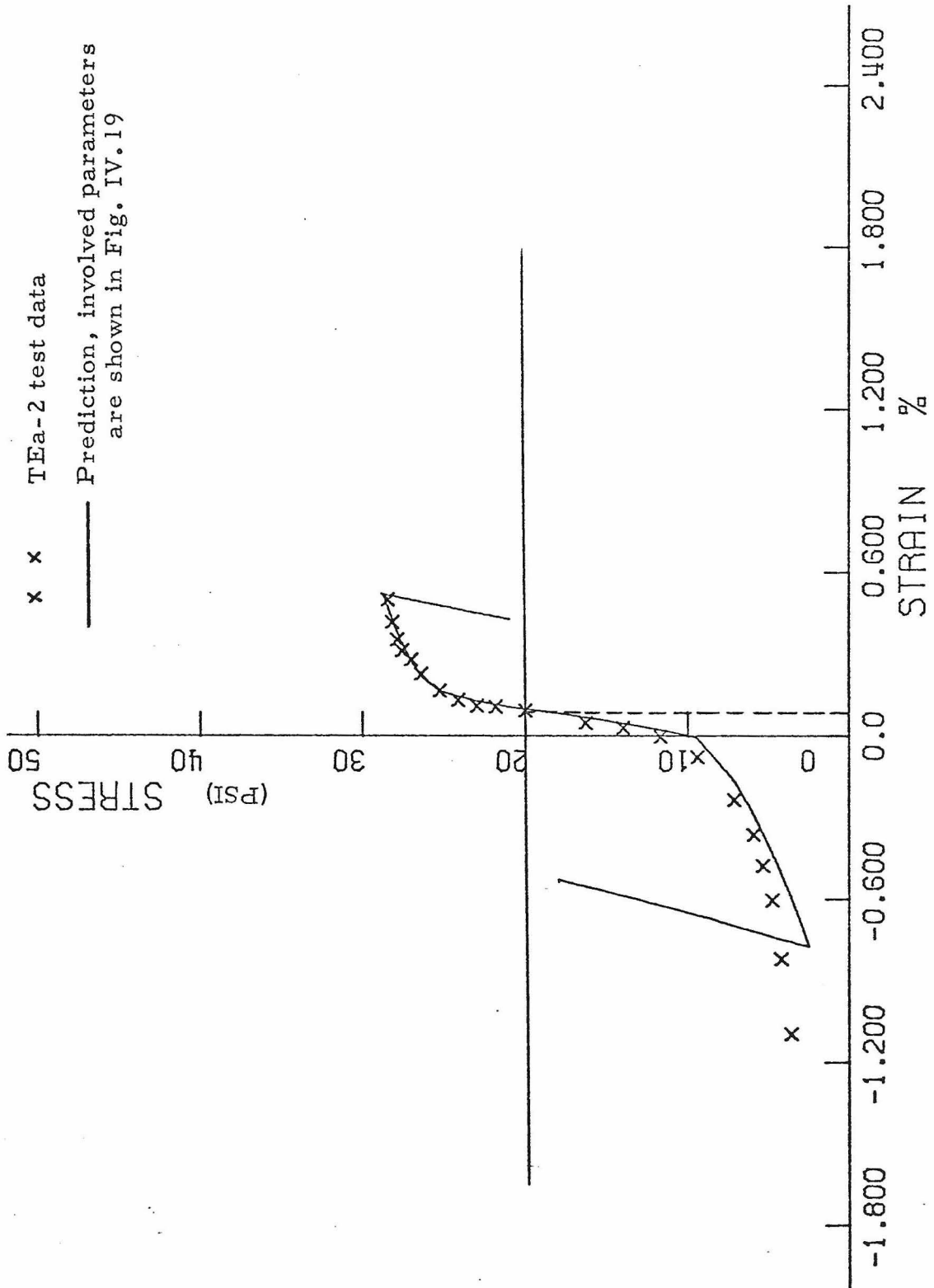
Fig. IV.19. Simulation of Ko's Tca-2 Test

Tca-2 test
simulation

Involved Parameters

$m_c = 14$ Psi
$s_c = 3$ Psi
$m_t = 2$ Psi
$s_t = 1$ Psi
$E = 8000$ Psi
$E_s = 9400$ Psi at $\tau_{oct} = 0$
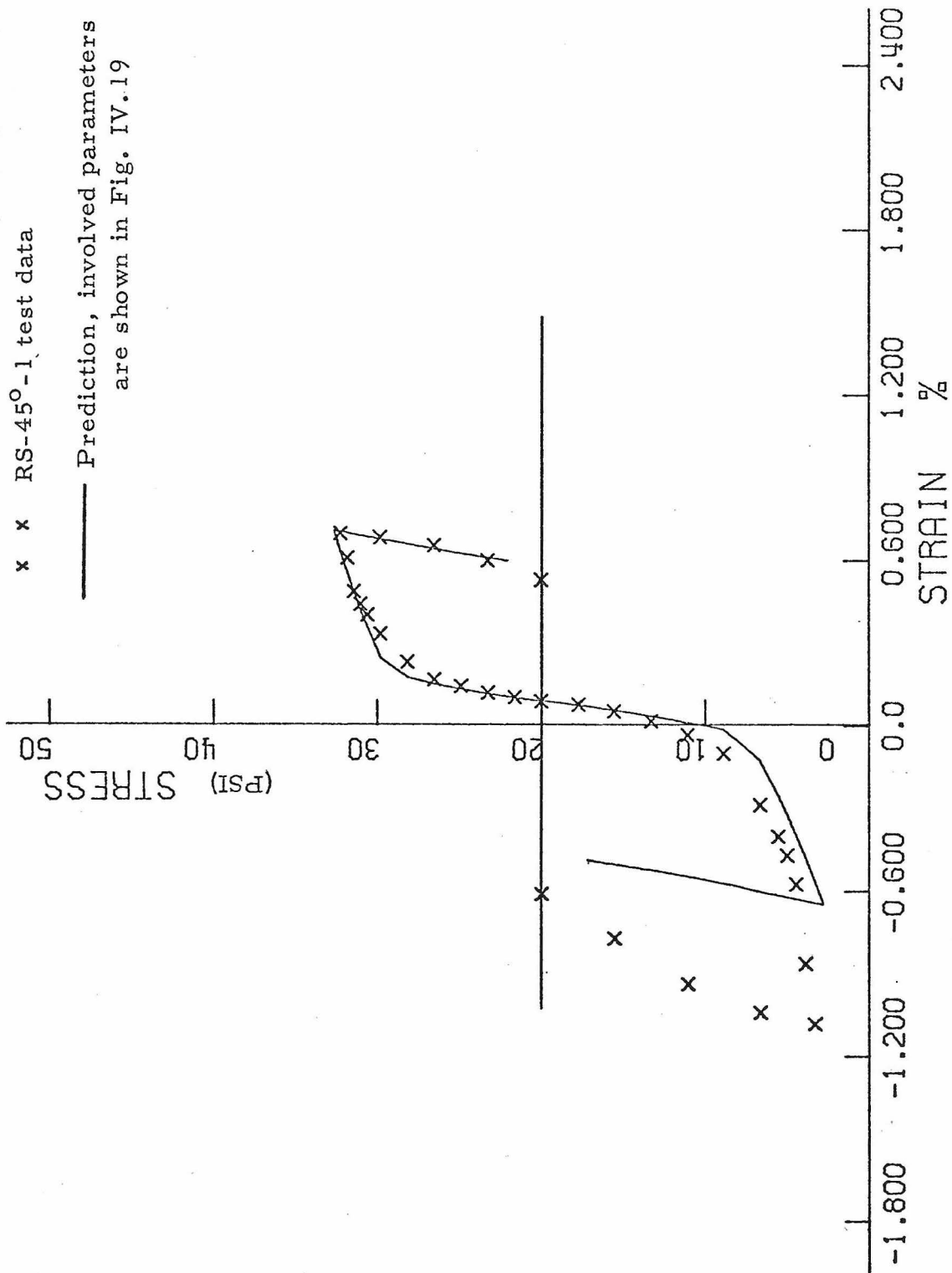$n = 4.7$

Fig. IV.20. Prediction of Ko's TEa-2 Test

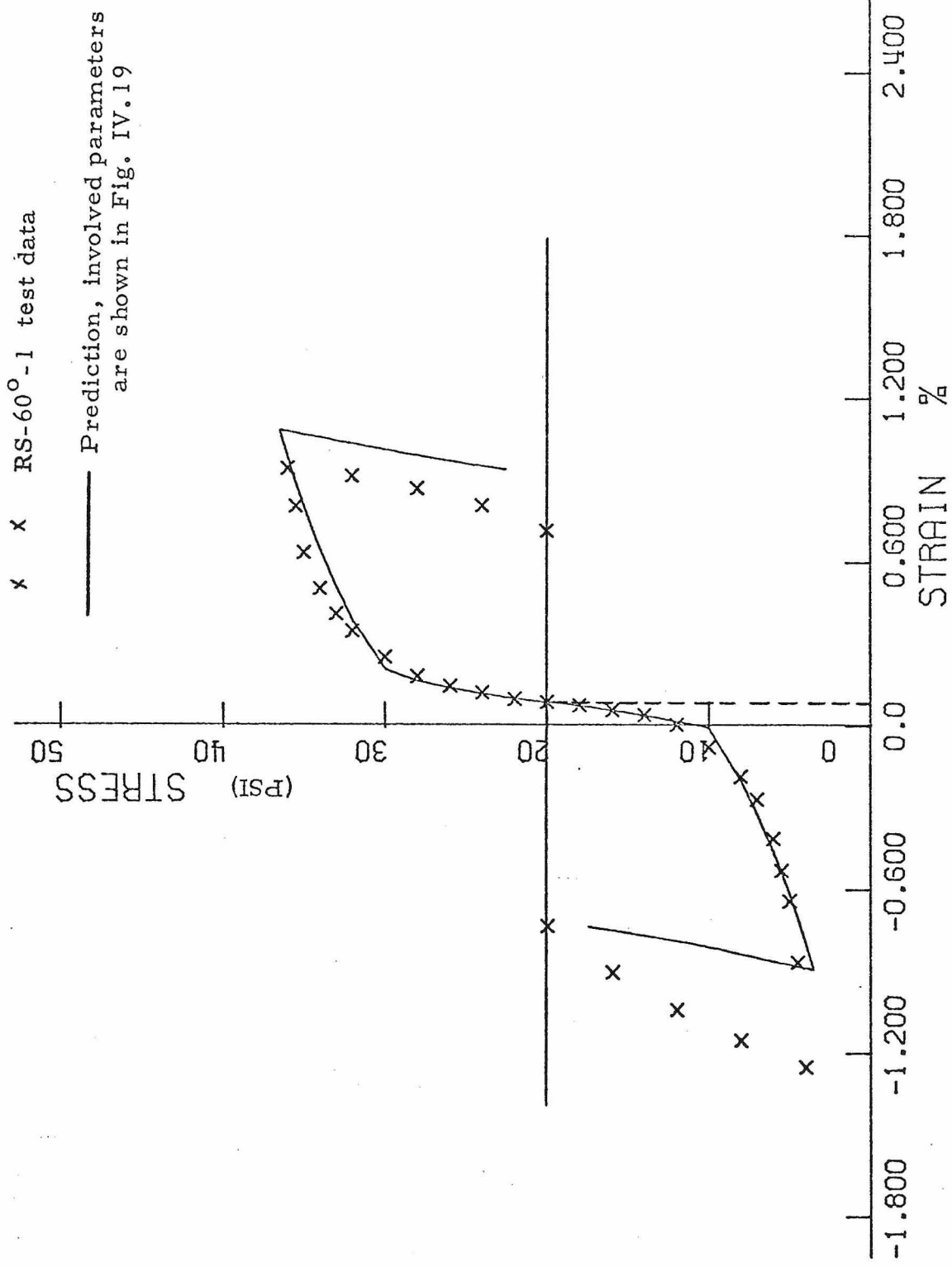Fig. IV-21. Prediction of Ko's RS-45°-1 Test

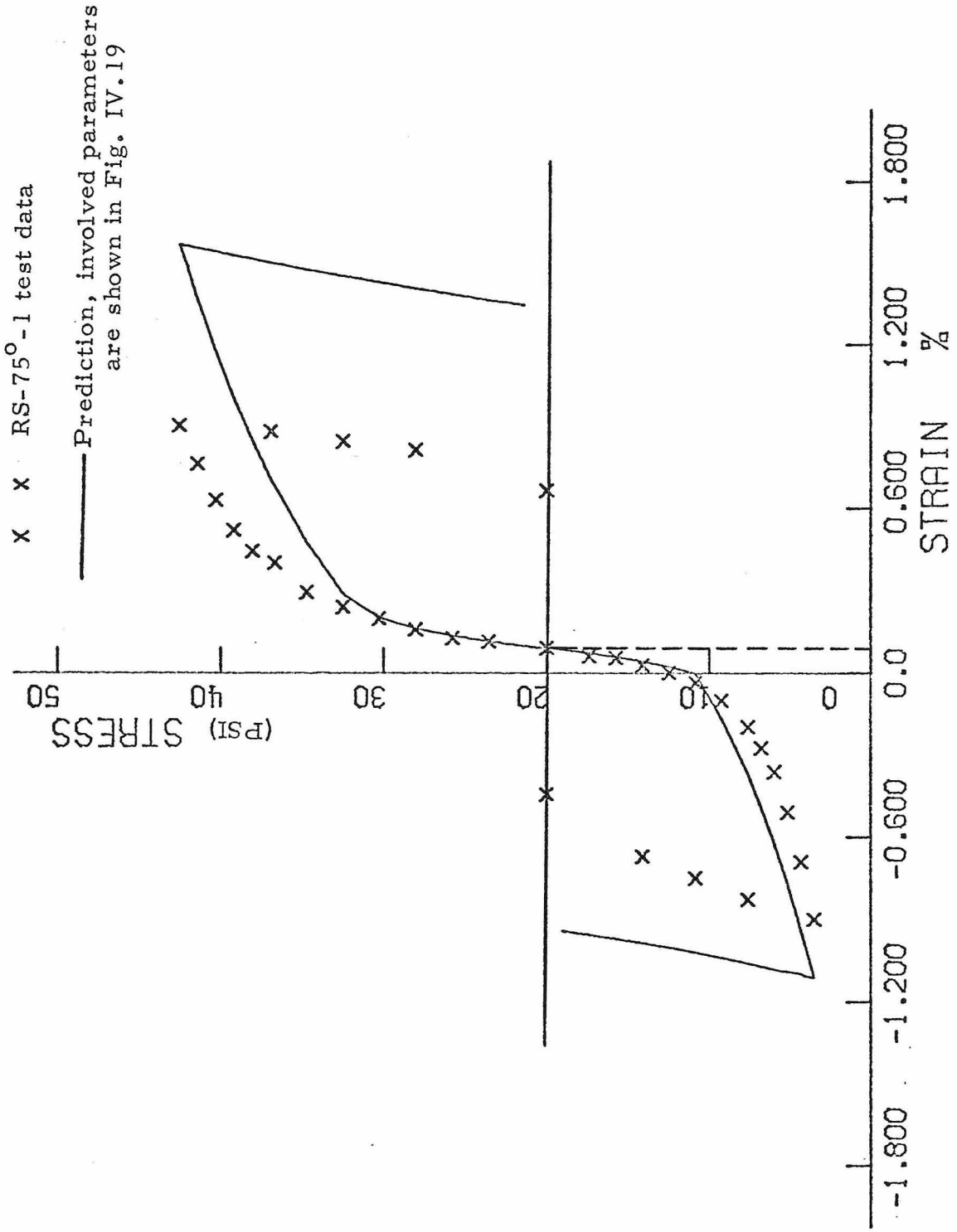Fig. IV.22. Prediction of Ko's RS-60°-1 Test
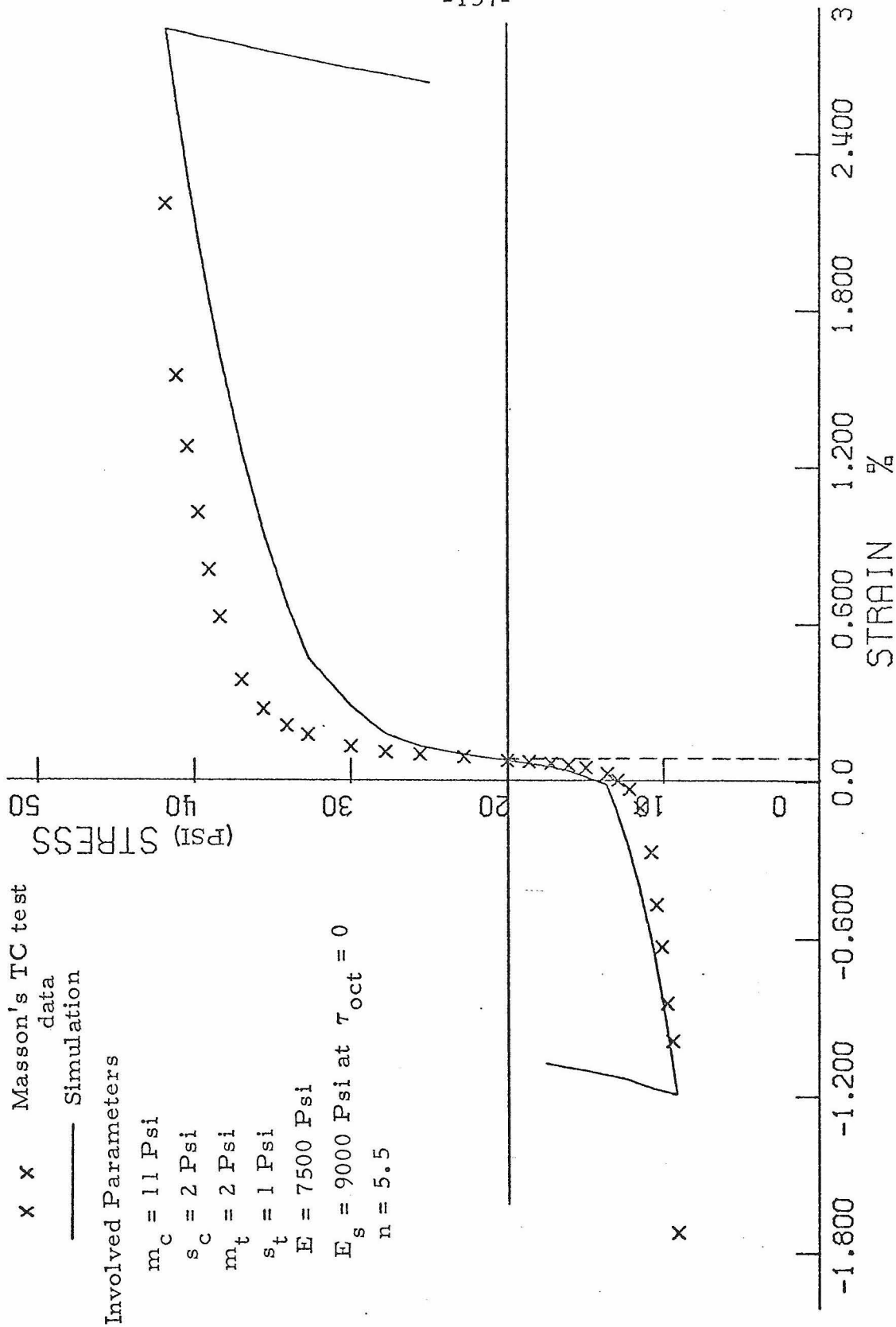
Fig. IV.23. Prediction of Ko's RS-75°-1 Test

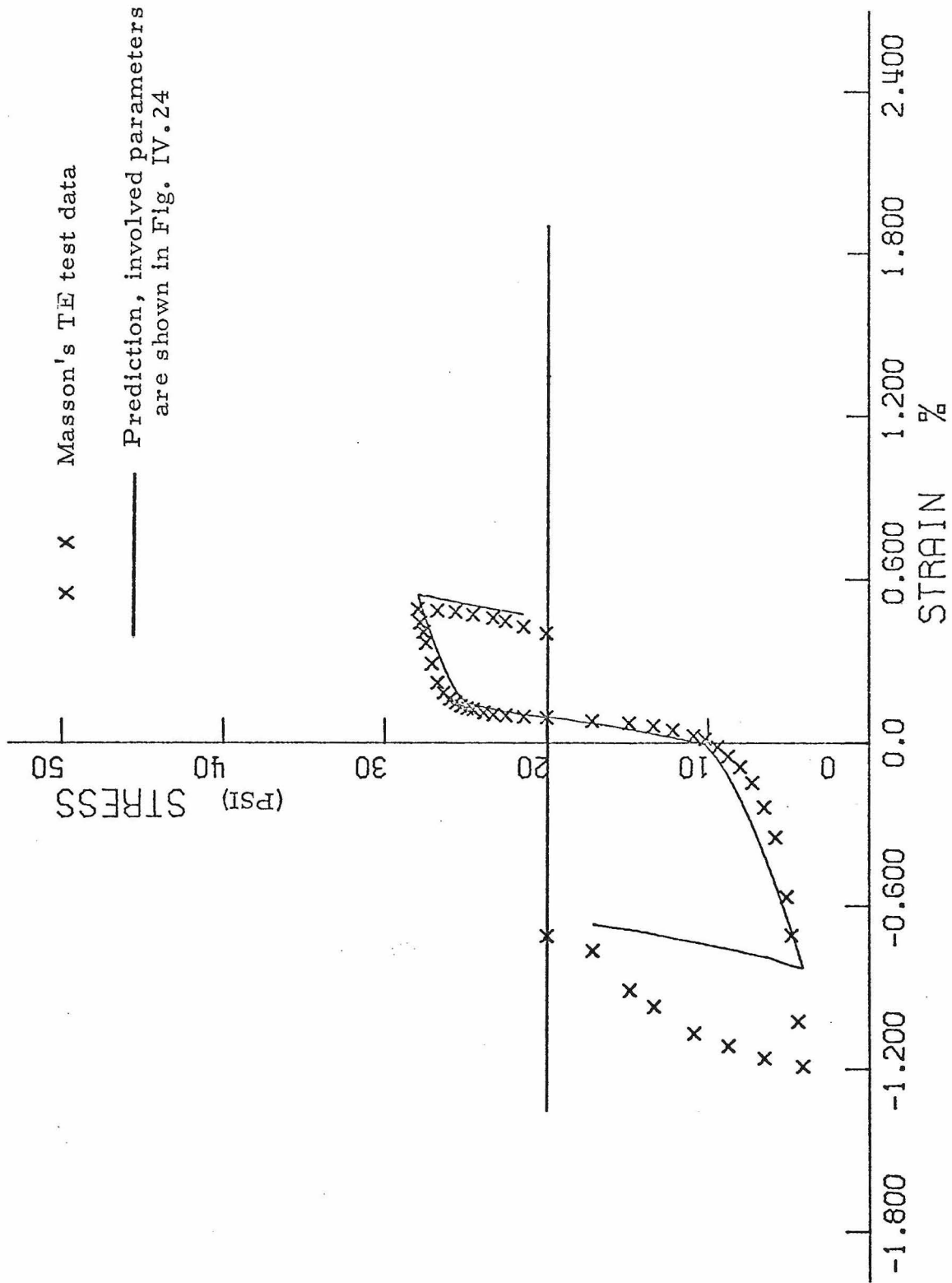Fig. IV.24. Simulation of Masson's [17] TC Test
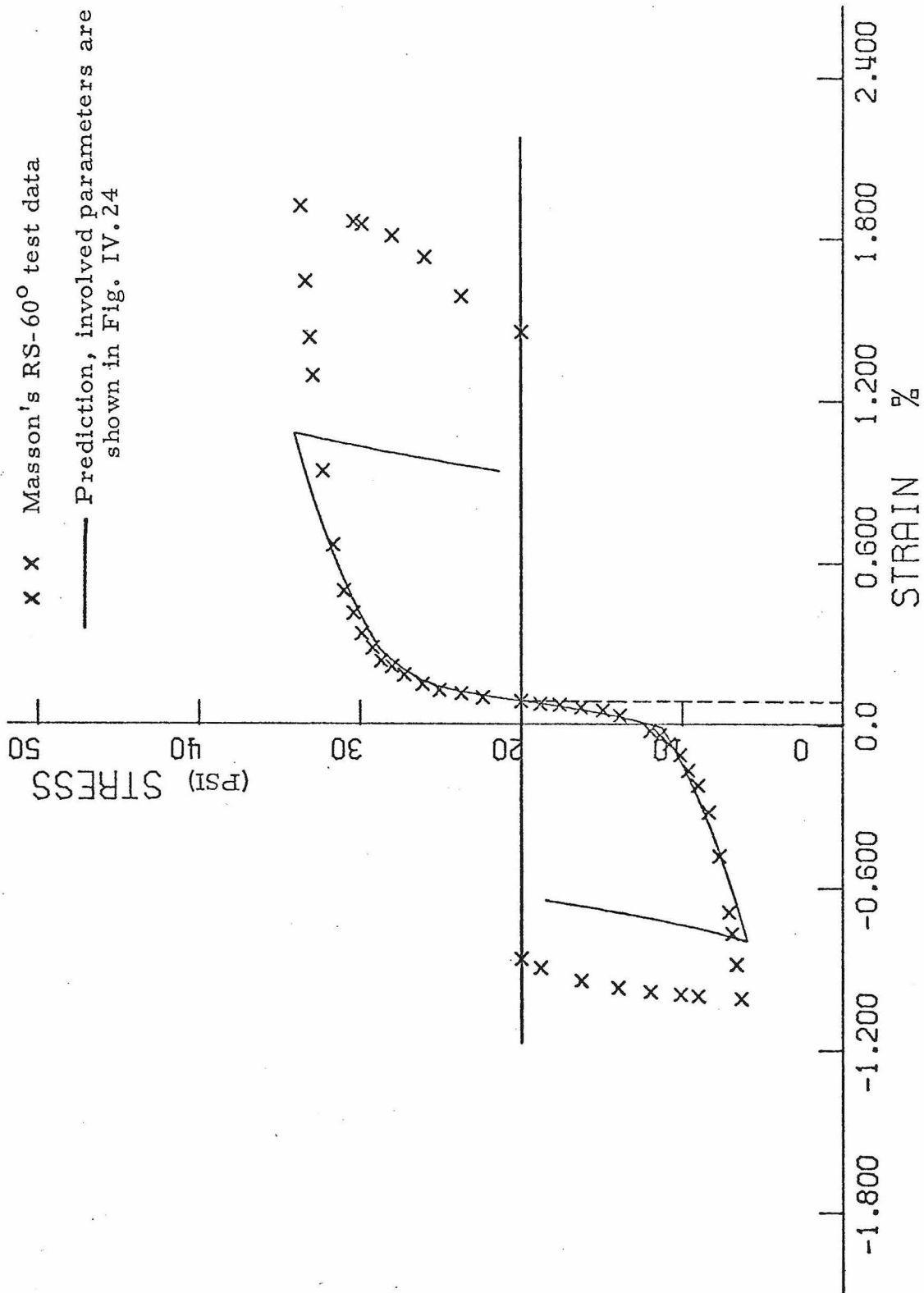
Fig. IV.25. Prediction of Masson's TE Test

Fig. IV.26. Prediction of Masson's RS-60° Test

CHAPTER V

SUMMARY AND CONCLUSIONS OF PART I
AND RECOMMENDATIONS FOR FUTURE WORK

V.1 Summary and Conclusion

In the first part of this thesis, attempts have been made to develop a rheological model to describe the deformation behavior of a granular material under various stress and strain conditions. An acceptable rheological model must be able to yield a constitutive law which can include many important aspects of a granular material's behavior observed in nature or in laboratory tests. The important aspects of granular materials behaviors are stated in Chapter I.

To develop a rheological model for granular media, consideration must also be given to the geometry of grain packing and the mechanical behavior of contacts between grains. Since granular material in nature is packed randomly together by irregularly sized and shaped particles, these properties must be described statistically. Certain physical aspects such as number of contacts and their orientations, and deformation behaviors upon loading must be considered as random variables. A rheological model for granular materials must have certain distributed characteristics which can statistically describe these random variables.

Previous work on constitutive relation for a granular material is reviewed in Chapter II. Some comments and suggestions are also given in the hope that future investigators can take them into consideration to arrive at more realistic constitutive relations which can more closely describe the deformation behavior of a granular material and can be practically applied to solve some boundary value problems in soil mechanics.

Rheological models consisting of spring and slip elements are often used to simulate some of the important features of granular material behavior, such as non-linearity in stress-strain behavior, slip of contacts between grains due to shear. Most rheological models [18], [19] are used in the hope that they will eventually lead to a general three dimensional formulation. Other types of rheological models such as the one shown in Fig. II. 8 [99), [100] are used to obtain the stress-strain relation solely from the mechanism exhibited by the model without consideration of of any other assumptions or hypothesis. The rheological model developed in this thesis is of this type.

In the course of developing a rheological model to represent the deformation behavior for a granular material, consideration is first given to the contact behavior. A rheological model consisting of slip and a spring elements in series suggested by Iwan [19] is used to represent the grain contact behavior. A one dimensional model is constructed by a group of these slip-spring elements in parallel (Fig. III. 3) and is employed to represent the granular

material's behavior. The critical (slip) stress level at which the element slips can be considered as a distributed function on account of the irregularity in size and shape of grains and the randomness of the packing of the material.

The purpose of a one-dimensional model is to demonstrate that its stress-strain relation bears some resemblance to the deformation behavior of a granular material. A simple rectangularly or trangularly distributed function is assumed for the critical stress level and produced a good resemblance to the experimental data obtained by Ko [16] on Ottawa sand under the axial stress condition (Figs. III. 3. 10 and 3. 11). This manifests the potential of using slip-spring elements to represent the granular material's behavior since they can apparently describe some fundamental aspects of the stress-strain behavior of a granular material even when a simple slip stress distribution function is used. However, throughout this thesis, a Gaussian type of distribution function is employed due to its similarity to the distribution of coordinate number (number of contact) in a granular material (Fig. III. 14) and due to the fact that it can closely describe almost any stress-strain curve by simply varying its mean and standard deviation. Furthermore, depending on the magnitude of its standard deviation, the Gaussian distribution can approximately represent either the triangular or rectangular distributions.

In observing the experimental results on Ottawa sand by Bell [15], Ko [16], Ko and Scott [14], and Masson [17], it seems that a granular

material exhibits different characteristics in compression and extension. If a rheological model is to closely describe the behavior of a granular material, the slip-spring elements must consist of two slip elements and a spring element in series as shown in Fig.III.1, and the one-dimensional model is therefore constructed as shown in Fig.III.2. From this one-dimensional model, a unique hysteresis loop is found and shown in Fig.III.5b.

To extend the one-dimensional model to multi-dimensional stress-strain formulations requires the assessment of the quantitative relation of stress and strain in one-dimension to the stresses and strains in other directions. A two-dimensional model is constructed by placing slip-spring elements along two perpendicular directions and interconnecting them with stiffness spring elements as shown in Fig.III.15. It is demonstrated that the simplest case of this model can approximately simulate the classical two-dimensional linearly elastic material by discarding the slip elements. The stress or strain increments in this model can be divided into two parts. The first part is the contribution due to stiffness spring elements and the second part is the contribution due to the slip-spring elements. The constitutive relations are expressed in incremental forms to account for stress or strain history and path dependency.

A three-dimensional model shown in Fig.III.17 is subsequently constructed in a similar manner. The constitutive relation obtained by the three-dimensional expresses the stress increments in terms

of strain and strain increments. This is equivalent to a strain-controlled stress path. Most of the three-dimensional soil test devices now in use, are of the stress-controlled type [16],[17]. Although, completely strain-controlled test devices have been reported [123], [124], it is believed that the mechanical problems associated with these devices have prevented their successful use. In order to simulate and predict laboratory test data, it would be advisable to express the strain increments in terms of stress increments in the constitutive relations. This is achieved by matrix inversion as shown in Eq.(3.54) to (3.56). All the subsequent laboratory test data simulation and prediction by this three-dimensional model are obtained in this fashion.

The consitutive law derived from the proposed model is derived in such a way that the stress-strain relation for any arbitrary stress-path can be obtained if the material properties are shown. The material properties involved in the proposed constitutive relations are the moduli of the stiffness springs and the spring in the slip-spring elements, and the slip stress distribution parameters m_c, m_t, s_c and s_t which, in turn, have to be determined from experimental data. Before the determination of these parameters, the qualitative description of the stress-strain relations under different stress-paths by the proposed model is represented and compared with the stress-strain curves observed in the experimental data on Ottawa sand by Ko [16] and Masson [17].

The most frequently used stress-paths in a stress-controlled

test are loading paths with proportional stress increments, in which the three principal stress increments are proportionate to each other ($\Delta\sigma_1 : \Delta\sigma_2 : \Delta\sigma_3 = \gamma : \alpha : \beta$) as shown in Table III.2. These stress paths include bydrostatic compression, axial shear, radial shear and conventional triaxial test stress-paths as shown in Figs.IV.1, IV.2 and IV.7. The hydrostatic compression stress-path is used to determine the relation between the modulus of stiffness spring, E_s , and the octahedral normal stress, σ_{oct}.

For an isotropic material, it is concluded a loading path with proportional stress increments would approximately imply proportional strain increments if the stress-strain relation is independent of the loading history and if the slip behavior is the same for both compression and extension. This point has been illustrated in Eqs.(4.3) to (4.14). However, this is not observed in the experimental data on Ottawa sand shown in Figs.IV.6, IV.7, IV.10 and IV.11. If the effect of the loading history and the difference of slip behavior in compression and in extension are considered, the proposed constitutive relations can qualitatively describe the deformation behavior observed in laboratory tests on Ottawa sand by Ko and Masson.

There are several parameters involved in the proposed model. They have to be determined by experimental data. The modulus E for the slip-spring elements is assumed to be constant for a specific packing of material and can be obtained from the hydrostatic compression test data. The modulus E_s is found to be

a function of σ_{oct} and τ_{oct}. E_s increases with the increase of σ_{oct}, and decreases with the increase of τ_{oct}. From Ko and Masson's hydrostatic compression test on medium dense Ottawa sand (Figs. IV.10 and IV.11) it is found that E_s increases linearly with the increase of σ_{oct} (for $\sigma_{oct} > 5$ psi as shown in Fig.IV.12) instead of the 1/3 power function of σ_{oct} as predicted by Hertz' theory [1],[16].

From the slip behavior of contacts between grains, it is found the relation between E_s and τ_{oct} can be expressed in Eq. (4.22). However, it is found unsuitable for simulating and predicting the experimental results on Ottawa sand as shown in Figs. IV.17 and IV.18. It is further found that Eq.(4.22) would lead to negative E_s value for certain stress paths, which contradicts granular materials behavior. It is thus concluded that Eq.(4.22) does not represent the true relation between E_s and τ_{oct}.

From the theoretical consideration and evidences observed from the axial shear stress test, it is found that Eq.(4.21) can best describe the relation between E_s and τ_{oct}. The order of power, n, in the right hand side of Eq.(4.21) has to be determined from experimental data. Different materials have different n values.

The distributed parameters, m_c , m_t , s_c , s_t have certain specific meanings and influence on the stress-strain curves due to the properties of Gaussian distribution function used. The influence of m_c , s_c , and s_t on the shape of stress-strain curve is illustrated in Figs.IV.15 and IV.16. Generally these distributed

parameters can be determined from simulation of test data along an axial shear stress path.

Figs. IV. 19 to IV. 26 illustrate the simulations and prediction results of Ko [16] and Masson's [17] test data on Ottawa sand by the proposed constitutive relations. It can be concluded that the proposed constitutive relations are much more realistic than any other theories and models at the present state of the art in describing the deformation behavior of a granular material. They are warranted for further application to the boundary layer problems in soil mechanics. However, the constitutive relations derived from the proposed model in general three-dimensional stress-strain formulation have a non-symmetrical stiffness matrix as will be shown in the next section. The present state of the art in finite element computer formulation cannot solve this. More effect toward a workable solving technique in finite element computer formulation is urged.

V. 2 Recommendations for Future Work

1. More experimental data for granular media of various densities similar to Ko [16] and Masson's [17] tests in a triaxial cube box are needed. The purpose of this is to correlate the involved parameters E_s, E, m_c, m_t, s_c and s_t with the mechanical properties such as the void ratio or density of the material. Furthermore, experimental data along an arbitrary stress-path areneeded so that the eligibility of applying the proposed constitutive relations to general three-dimensional stress or strain

conditions can be further certified.

2. The proposed constitutive relations are generally applicable to the type of materials which exhibit plastic strains comparable with the elastic strains under loading. This type of materials includes concretes, polycrystalline materials (such as steel or nickel-base alloy) and structural materials of continuous and composite systems as mentioned in Ref. [19].

3. The proposed model can be further modified to include the viscous or viscoelastic deformation behavior of a material by adding creep or damping elements to the proposed model. Further work is necessary for this purpose.

4. All the derivations of proposed constitutive relations in part I of of this thesis involve only the stresses and strains in principal directions. For the purpose of applying the proposed constitutive relations to some boundary value problems in soil mechanics, a general stress-strail formulation is needed. This can be achieved by applying normal and shear stresses and strains to the model. Due to the complexity involved in deriving a general three-dimensional constitutive relation, only the generalized formulation for plane strain case will be considered here.

A plane strain model is shown in Fig. V.1 (the elements in and connected with the z-direction where strains = 0 are not shown). The symbols for stresses and strains, and the following derivations are all referred to Fig. V.1, unless mentioned otherwise.

Again, as before, the stress and strain increments can be separated into two parts. The first part is due to the stiffness springs E_s and is denoted by $(\ )_e$. The second part is due to the slip-spring elements and is denoted by $(\ )_p$. Thus,

$$\Delta \sigma_x = \Delta(\sigma_x) + \Delta(\sigma_x)_p = \Delta(\sigma_x)_e + p_x \Delta \epsilon_x$$

$$\Delta \sigma_y = \Delta(\sigma_y)_e + \Delta(\sigma_y)_p = \Delta(\sigma_y)_e + p_y \Delta \epsilon_y$$

$$\Delta \tau_{xy} = \Delta(\tau_{xy})_e + \Delta(\tau_{xy})_p = \Delta(\tau_{xy})_e + \gamma_{xy} p_x \Delta \epsilon_x$$

$$\Delta \tau_{yx} = \Delta(\tau_{yx})_e + \Delta(\tau_{yx})_p = \Delta(\tau_{yx})_e + \gamma_{yx} p_y \Delta \epsilon_y$$

(5.1)

where p_x and p_y can be obtained by substituting ϵ_x and ϵ_y respectively into ϵ's in Eqs. (3.33) to (3.40) depending on the loading paths.

$\Delta(\ )_e$ terms can be obtained as follows:

$$\Delta(\sigma_x)_e = E_s \left\{ \left[\frac{4}{\sqrt{2}} - \frac{(v-x)^2}{A} - \frac{(v+x)^2}{B} - \frac{2}{(1+u^2)^{3/2}} \right] \Delta \epsilon_x \right.$$

$$+ \left[\frac{(u-y)(v-x)}{A} + \frac{(u+y)(v+x)}{B} \right] \Delta \epsilon_y$$

$$+ \left[- \frac{(u-y)(v-x)}{A} + \frac{(u+y)(v+x)}{B} \right] \Delta \gamma_{xy}$$

$$+ \left. \left[\frac{(v-x)^2}{A} - \frac{(v+x)^2}{B} \right] \Delta \gamma_{yx} \right\}$$

(5.2)

$$\Delta(\sigma_y)_e = E_x \left\{ \left[\frac{(u-y)(v-x)}{A} + \frac{(u+y)(v+x)}{B} \right] \Delta\epsilon_x \right.$$

$$+ \left[\frac{4}{\sqrt{2}} - \frac{(u-y)^2}{A} - \frac{(u+y)^2}{B} - \frac{2}{(1+v^2)^{3/2}} \right] \Delta\epsilon_y$$

$$+ \left[\frac{(u-y)^2}{A} - \frac{(u+y)^2}{B} \right] \Delta\gamma_{xy}$$

$$+ \left. \left[-\frac{(u-y)(v-x)}{A} + \frac{(u+y)(v+x)}{B} \right] \Delta\gamma_{yx} \right\} \qquad (5.3)$$

$$\Delta(\tau_{xy})_e = E_s \left\{ \left[-\frac{(v-x)(u-y)}{A} + \frac{(v+x)(u+y)}{B} \right] \Delta\epsilon_x \right.$$

$$+ \left[\frac{(u-y)^2}{A} - \frac{(u+y)^2}{B} \right] \Delta\epsilon_y$$

$$+ \left[\frac{4}{\sqrt{2}} - \frac{2}{\sqrt{1+u^2}} - \frac{(u-y)^2}{A} - \frac{(u+y)^2}{B} \right] \Delta\gamma_{xy}$$

$$+ \left. \left[\frac{(u-y)(v-x)}{A} + \frac{(u+y)(v+x)}{B} \right] \Delta\gamma_{yx} \right\} \qquad (5.4)$$

$$\Delta(\tau_{yx})_e = E_s \left\{ \left[\frac{(v-x)^2}{A} - \frac{(v+x)^2}{A} \right] \Delta\epsilon_x \right.$$

$$+ \left[-\frac{(u-y)(v-x)}{A} + \frac{(u+y)(v+x)}{B} \right] \Delta\epsilon_y$$

$$+ \left[\frac{(u-y)(v-x)}{A} + \frac{(u+y)(v+x)}{B} \right] \Delta\gamma_{xy}$$

$$+ \left. \left[\frac{4}{\sqrt{2}} - \frac{2}{\sqrt{1+v^2}} - \frac{(v-x)^2}{A} - \frac{(v+x)^2}{B} \right] \Delta\gamma_{yx} \right\} \qquad (5.5)$$

where

$$u = 1 + \epsilon_x$$

$$v = 1 + \epsilon_y$$

$$x = \gamma_{xt}(1 + \epsilon_x) \tag{5.6}$$

$$y = \gamma_{yx}(1 + \epsilon_y)$$

$$A = \left[(u-y)^2 + (v-x)^2 \right]^{1/2}$$

$$B = \left[(u+y)^2 + (v+x)^2 \right]^{1/2}$$

From Eqs. (5.1) to (5.5) the increments of stresses and strains can be expressed as

$$
\begin{Bmatrix}
\Delta\sigma_x \\
\Delta\sigma_y \\
\Delta\tau_{xy} \\
\Delta\tau_{yx}
\end{Bmatrix}
= A
\begin{Bmatrix}
\Delta\epsilon_x \\
\Delta\epsilon_y \\
\Delta\gamma_{xy} \\
\Delta\gamma_{yx}
\end{Bmatrix}
\tag{5.7}
$$

with the condition $\Delta\tau_{xy} = \Delta\tau_{yx}$.

As can be seen from Eqs. (5.1) to (5.5), the stiffness matrix A is non-symmetrical. This non-symmetrical stiffness matrix couples with the complexity of the proposed constitutive relations, and the loading and unloading process is beyond the capability in the present stage of the art in finite element computer formulation [60]. More research is needed toward a workable computer scheme for solving a problem with non-symmetrical stiffness matrix.
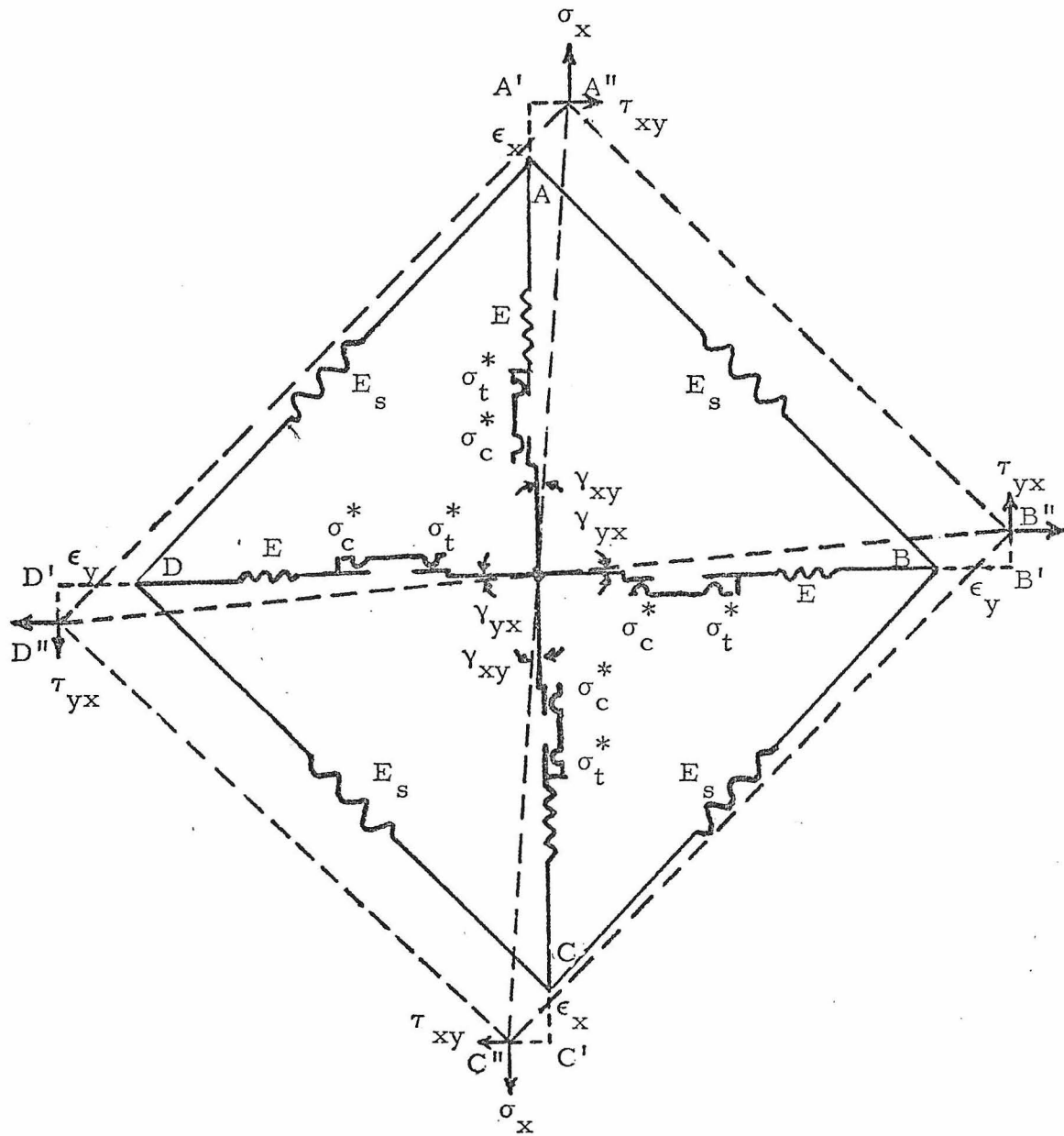
Note: 1. Elements along and connected with the third direction are not shown.

2. $\tau_{xy} = \tau_{yx}$, $\gamma_{xy} \neq \gamma_{yx}$.

Fig. V.1. Three-dimensional Model for General Stress-strain Formulation

PART II

THE DISTRIBUTION OF STRESSES AND DEVELOPMENT
OF FAILURE AT THE TOE OF A SLOPE AND AROUND
THE TIP OF A CRACK

CHAPTER VI

PROBLEMS TREATED AND BILINEAR FINITE ELEMENT ANALYSIS

VI.1 Introduction; problems treated.

Due to the complexity of material properties and boundary conditions, many problems in the soil mechanics and geophysical sciences are difficult to idealise and thus cannot be solved analytically. However, the widely applied finite element analysis [60] provides engineers and geophysicists with a simple and effective means to tackle some problems which they would otherwise be unable to solve satisfactorily. One of these problems is the determination of the stress and deformation distribution in and ultimately the stability of a slope or an embankment. With the assumption of isotropic rigid-plastic material and ignoring the strain-deformation field totally, a number of classical methods of slope stability analysis can be found in the engineering literature [11], [111]. In dealing with the failure problems of a slope or embankment, most of these classical methods have been widely used and proved to be quite satisfactory in many cases in engineering practice. However, analyses by these methods do not represent the behavior of a slope except at failure.

Acceptable factors of safety in a well-designed slope or embankment are low enough that the soil is not everywhere in even

an approximately linearly elastic state. The states of stress and displacement and the extent of regions of yield even in a stable slope may be important to the performance of a slope and location of adjacent structures. The classical linear elasticity theory can provide the stress and displacement results only for some uncomplicated wedges with relatively simple boundary and loading conditions [112], [113]. If a linear elastic analysis, whether it be performed analytically or by the finite element method, is applied to the problem of a finite slope, high stresses in some regions and tensile stresses in others will be found. It can be expected that failure will develop from these regions.

Local yielding causes some degree of relaxation in the state of stress and deformation in the entire slope region. Stress-strain redistribution and the development of failure around a slope have been studied by various investigators [21], [22] with the application of a bilinear finite element method. The finite element grid around the toe has not generally been taken small enough to clearly indicate the stress concentration there. In addition, the boundaries to the region are seldom placed far enough away from the toe to prevent their interference with the problem area. Consequently, the previous investigations indicated that failure sometimes develops in some area other than the toe of the slope [22].

In fracture theory [24] the stress-strain field in the vicinity of a crack is of vital interest. The stress concentration and development of failure around the toe of the slope should be considered to be a similar problem. It is instructive, therefore, to

study the crack problem first before examining the behavior of a slope or embankment. In the past numerous investigators have applied the linear theory of elasticity to the crack problem with the assumption that the strains are infinitesimal and that the boundary condition of the crack surface is undisturbed and pre-described [23]. From the use of the linear theory of elasticity, the stress concentration at the tip of a crack has been evaluated. This theory has been applied to the analysis of crack development in brittle materials. However, in dealing with fracture in ductile materials, plastic flow (or strain) occurs in this region, to relieve the high stress developed. It has been argued that the occurrence of plastic strain will not result in a significant difference from linear results used in the calculation of relevant quantities [114] such as stored elastic energy. However, the question of the influence of plastic strains on the stress field near a crack is still being pursued. No results in the field of fracture mechanics suitable for immediate application to the slope stability problem have been found in their investigation. In order to consider the crack problem, therefore, linear and bilinear finite element methods were applied in this study for the following purposes:

1. To assess the finite element method in this analysis by comparing the resulting stress field with the analytical solution from the linear theory.

2. To establish the quantitative influence of plastic strain on the stress field near the tip as in the vicinity of the crack.

3. To investigate the influence of the crack surface's shape

on the stress field.

The linear and bilinear finite element computer program used in this study is adapted and revised from Wilson's original program [20] for two-dimensional plane strain analysis. Computer plotting subroutines were also set up to plot displacements, stress fields, and the contours of stresses to aid in the interpretation of the results. All the displacement and stress field plots are capable of indicating both direction and magnitude.

Three types of problems will be investigated in the Part II of this thesis. The first problem is devoted to the crack problem as mentioned above. The second problem deals with the study of the stress and displacement distributions in slopes or embankments. The last one concerns the development of failure in and the stability of a slope.

VI. 2 Bilinear Finite Element Analysis.

VI. 2.1 Functional Consideration.

The principles of linear finite element methods are well known and can be found in many engineering references [115]. Bilinear and non-linear variations of the basic method have been described [115]. In the present application a bilinear representation as shown in Fig. IV.1, is used because of the lack of knowledge of a workable constitutive relation for real soils. Note that the bi-linear relation is valid as an approximation to the material

properties only if a monotonic increase in stresses or in certain stress invariants in the simulated problem occurs. Usually, the bilinear stress-strain relationship is expressed in terms of stress and strain invariants as shown in Fig.1, where

$$\bar{\sigma} = \frac{1}{\sqrt{2}} \sqrt{(\sigma_1 - \sigma_2)^2 + (\sigma_2 - \sigma_3)^2 + (\sigma_3 - \sigma_1)^2}$$

and (6.1)

$$\bar{\epsilon} = \frac{1}{\sqrt{2}} \sqrt{(\epsilon_1 - \epsilon_2)^2 + (\epsilon_2 - \epsilon_3)^2 + (\epsilon_3 - \epsilon_1)^2}$$

If Von Mises' yield criterion is used, the bilinear stress-strain relation can be expressed in equivalent linear form as

$$G_i = Gn + \frac{\sigma_y}{\bar{\epsilon}_i} (1-n)$$ (6.2)

where G is the shear modulus, G_i is the shear modulus corresponding to $\bar{\epsilon}_i$, n the elasticity ratio, and σ_y is the stress as shown in Fig.1. In the above, ϵ_1, σ_1 etc., stand for the principal strain and stress components. The usual failure criterion for soil is, of course, that of Mohr-Coulomb, with the yield stress depending on the hydrostatic stress through the parameter of friction angle. The latter criterion is more difficult to implement in finite element analysis, and the Von Mises criterion was used in the present preliminary investigation. For monotonic loading paths, the criteria can be made essentially identical when the friction angle is taken to be zero. A generalized Von Mises criteria for Mohr-Coulomb type material for plane strain condition has been established

[116][*] to include both friction angle ϕ and cohesion c into consideration. The yield stress can be expressed as

$$\sigma_y = \frac{3c + (\sigma_1 + \sigma_2 + \sigma_3)\tan\phi}{\sqrt{3 + 4\tan^2\phi}} \tag{6.3}$$

From Eq.(6.3), it can be seen higher deviatoric yield stress is required for higher cohesion and friction angle values for the development of failure.

Usually a bilinear finite element analysis is solved by one of the following methods, namely, direct-iterative method, incremental stress or strain method [116] or by incremental plasticity theory [117]. The direct iterative method is illustrated in Fig. VI. 2. The process of calculation can be described as follows:

1. A linear analysis is performed to determine the stresses and strains based on initial G and ν values.

2. The computed stresses and strains are used to determine a new G and ν for each element by means of Fig. VI. 2(a) or Fig. VI. 2(b).

3. The new E and ν are then used to carry out another linearly elastic analysis.

4. Repeat step 2 and step 3.

---

[*]Normality condition is involved in deriving this relation. Volume change is small if ϕ is small.

The number of trials depends on the value of n, the iterative method used and the type of problem considered. The iterative scheme has been found empirically to be convergent for most cases. If n is small, the method in Fig. VI. 2(b) would converge faster. If n is large, the method in Fig. VI. 2(a) would be more suitable. However, it is to be noticed that any process will be considered as legitimate providing the stress state in each element at the final solution lies on the given bilinear stress-strain function. Thus at any intermediate stage during the iterative process, either of the techniques in Figs. VI. 2(a) or VI. 2(b), or the combination of these two can be used depending on the problem considered.

VI. 2. 2 Preliminary Example

Since this study concerns the stress concentration and the development of failure around the toe of a slope and in the vicinity of a crack, it is preferable to start with a preliminary problem to demonstrate the level of stress concentration which does occur and that the bilinear finite element approach gives a convergent solution. The problem configuration and prescribed boundary conditions as shown in Fig. VI. 3 are taken for this purpose. The element size is made smaller in the vicinity of the toe in order to show adequately the degree of stress concentration. In a mathematical analysis the toe is a singular point. This problem can be considered to be similar to the region around the toe of an excavated 90° slope with the exception that, in this case, the boundary and loading conditions are restricted as shown in Fig. VI. 3. The

constraint due to the boundary conditions considered tend to lessen the degree of stress concentration at this singular point.

The results of a linear analysis by finite element method of this problem in terms of resulting principal stresses, displacements and major principal stress contours, in the shaded portion of Fig. VI.3, are plotted in Figs. VI.4, VI.5 and VI.6 respectively. The stress concentration around the corner is evident. A bilinear relation as shown in Fig. VI.7(a) with the iterative scheme of Fig. VI.2(a) was also used to solve this problem; the resulting major principal stresses in the corner elements are plotted in Figs. VI.7(b) and VI.7(c). It can be concluded that the number of approximations required to give an adequate representation depends on the yield stress σ_y, the elastic ratio n and the characteristics of the problem considered. For this specific type of problem, the errors are small after three approximations for n = 0.5 and after four approximations for n = 0.2. Generally, the number of approximations required increases with the decrease of elastic ratio n, i.e., as the material model approaches the ideal elastic-plastic condition more closely.
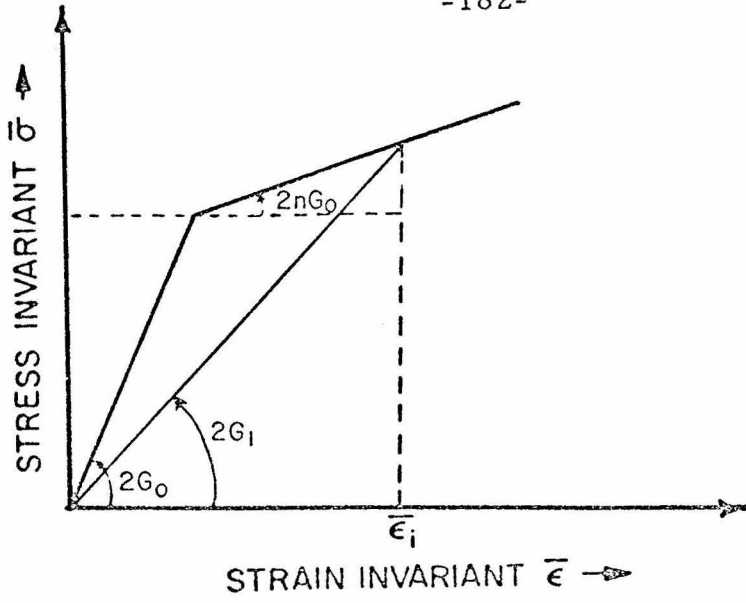
Fig. VI.1   Bilinear Stress-Strain Relation
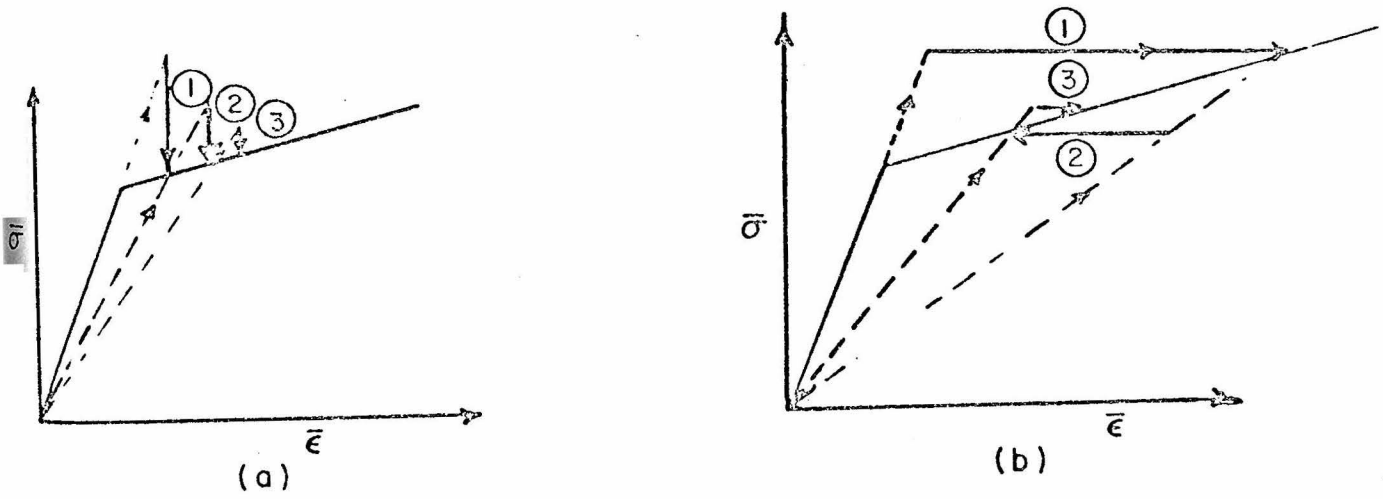
Fig. VI.2   Iterative Scheme

No. of Nodal points = 190
No. of Elements = 162

$E = 2 \times 10^6$ psf

$\nu = 0.3$

OA = AB = DE = OE = 90 ft

BC = 180 ft

Boundary conditions

(a) Along AB and CD: Zero horizontal
    displacement

(b) Along BC and DE: Zero vertical
    displacement

(c) Along OA and EO: 100 psf
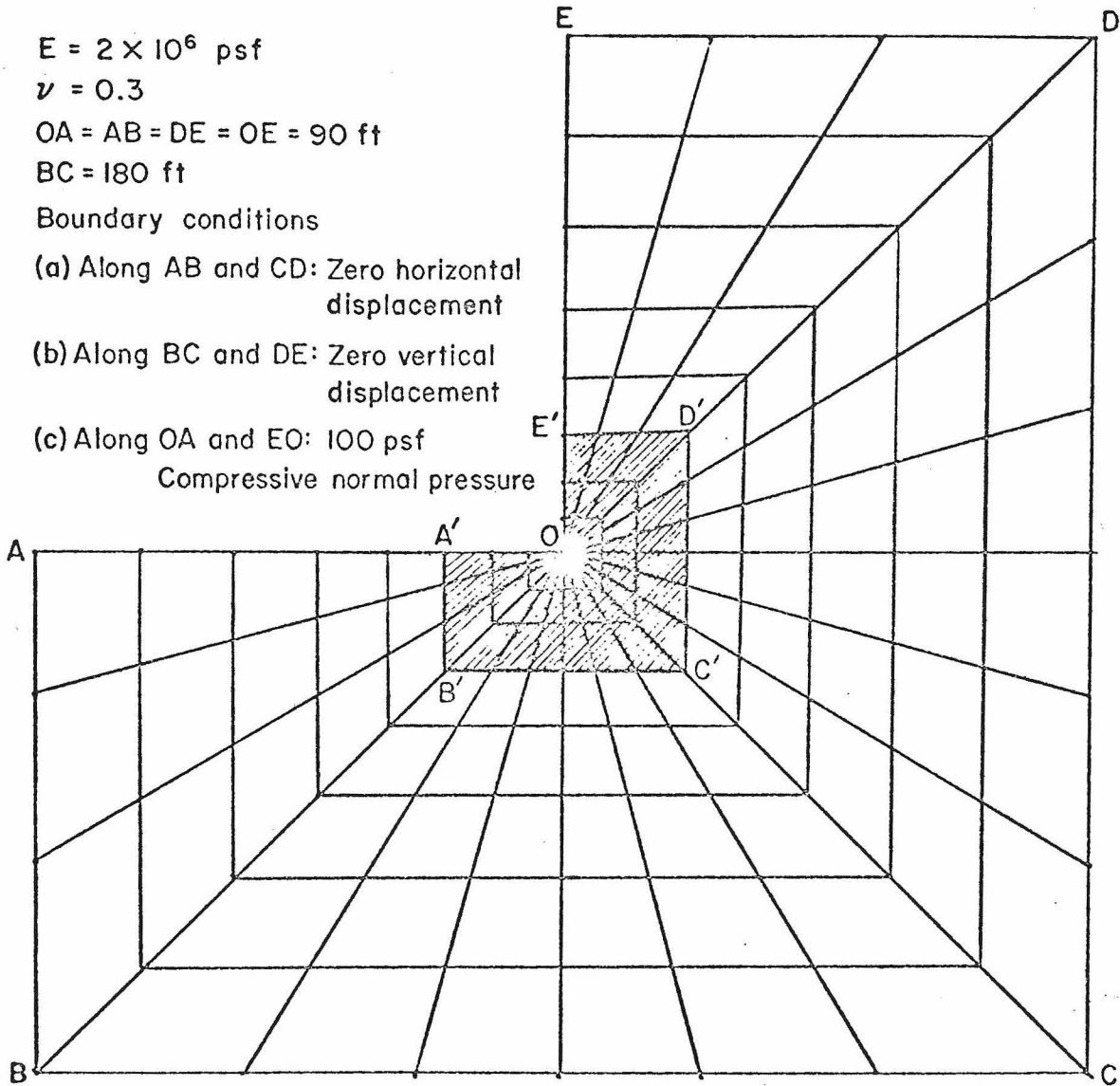   Compressive normal pressure

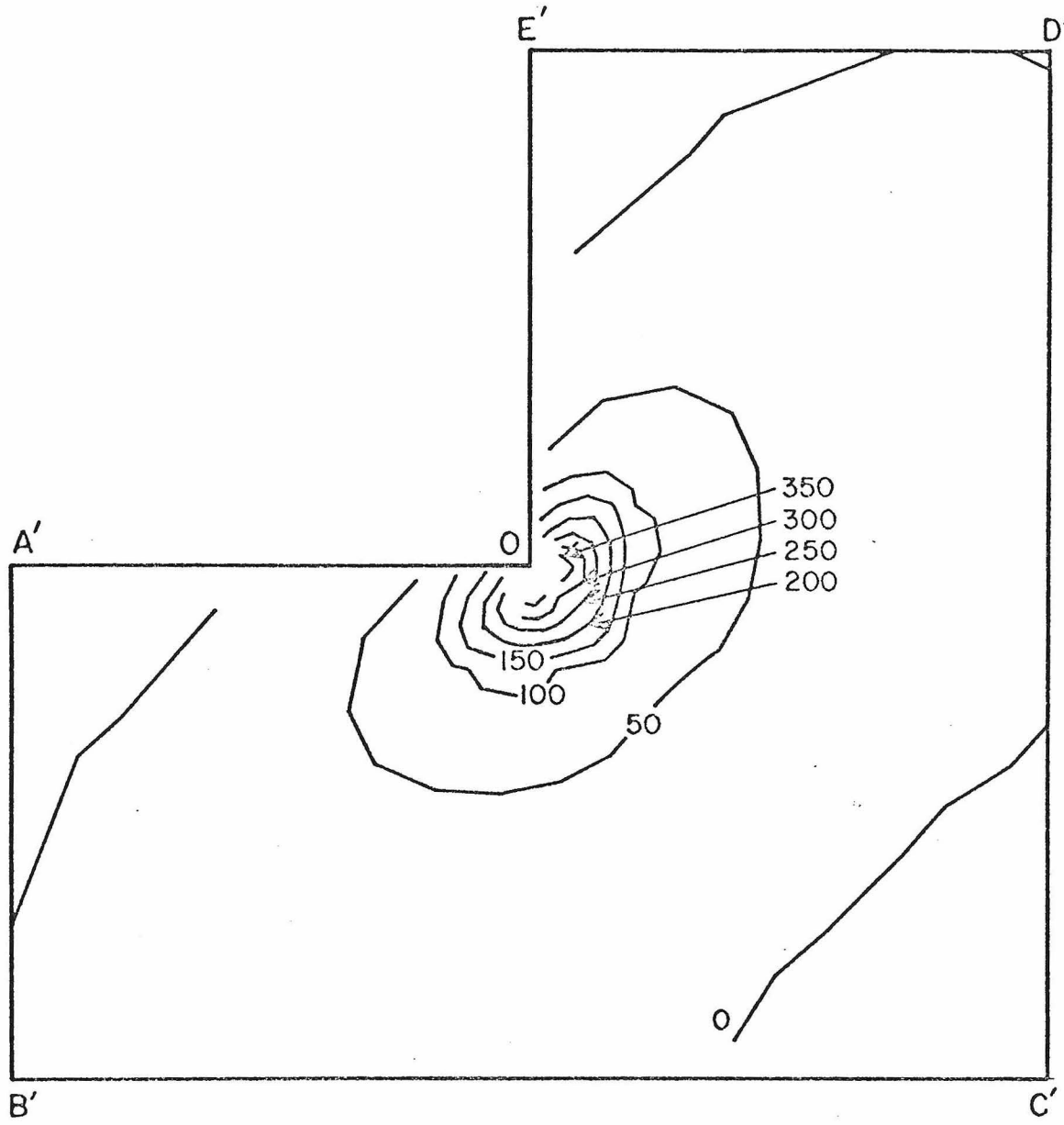Fig. VI.3   Finite Element Configuration
Used in Preliminary Example.

Fig. VI.4 Major Principal Stress Contour
in the Shaded Portion of Fig. 3.
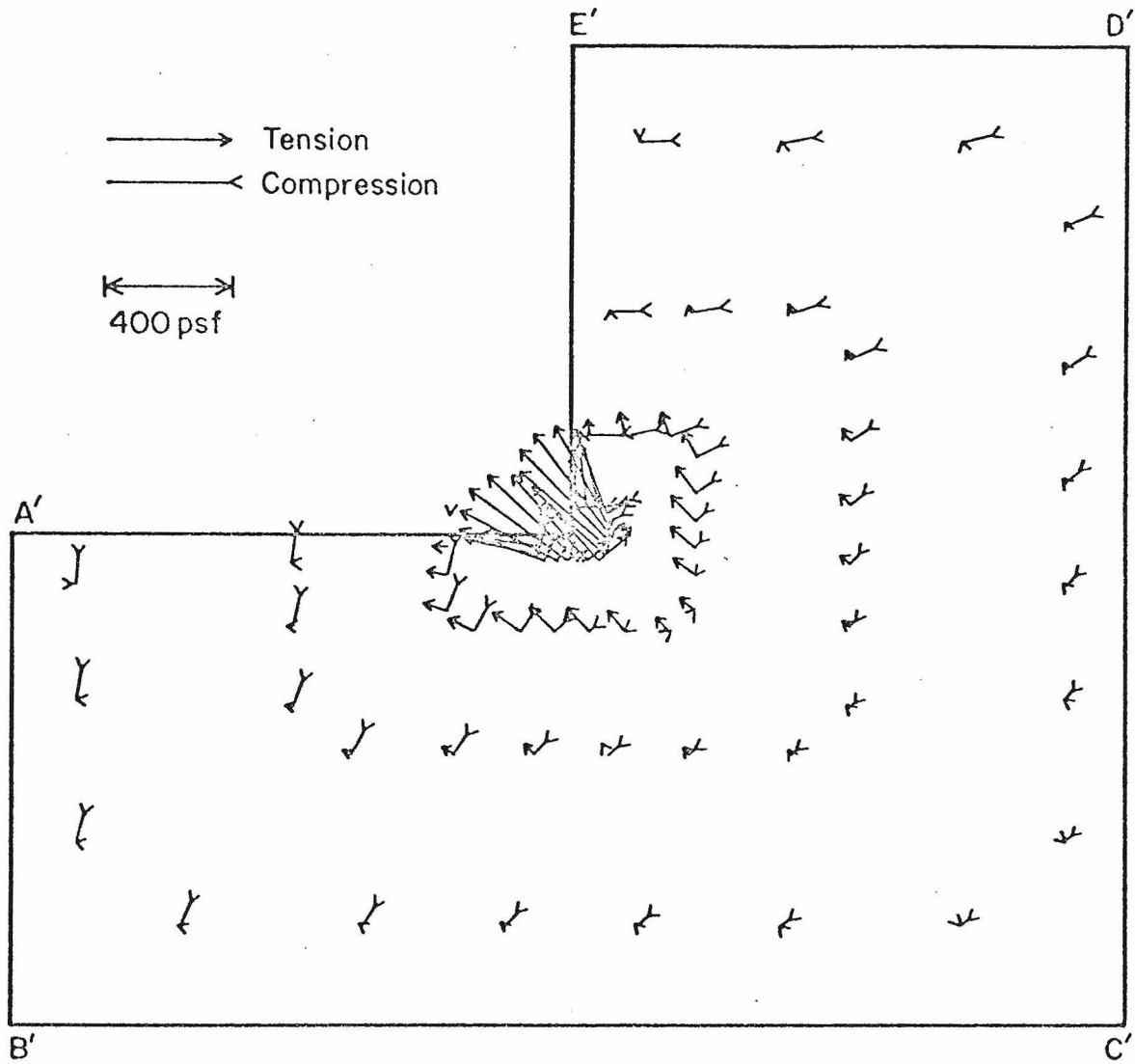
Fig. VI.5 Principal Stresses (Magnitude
and Direction) Plot in the
Shaded Portion of Fig. 3.
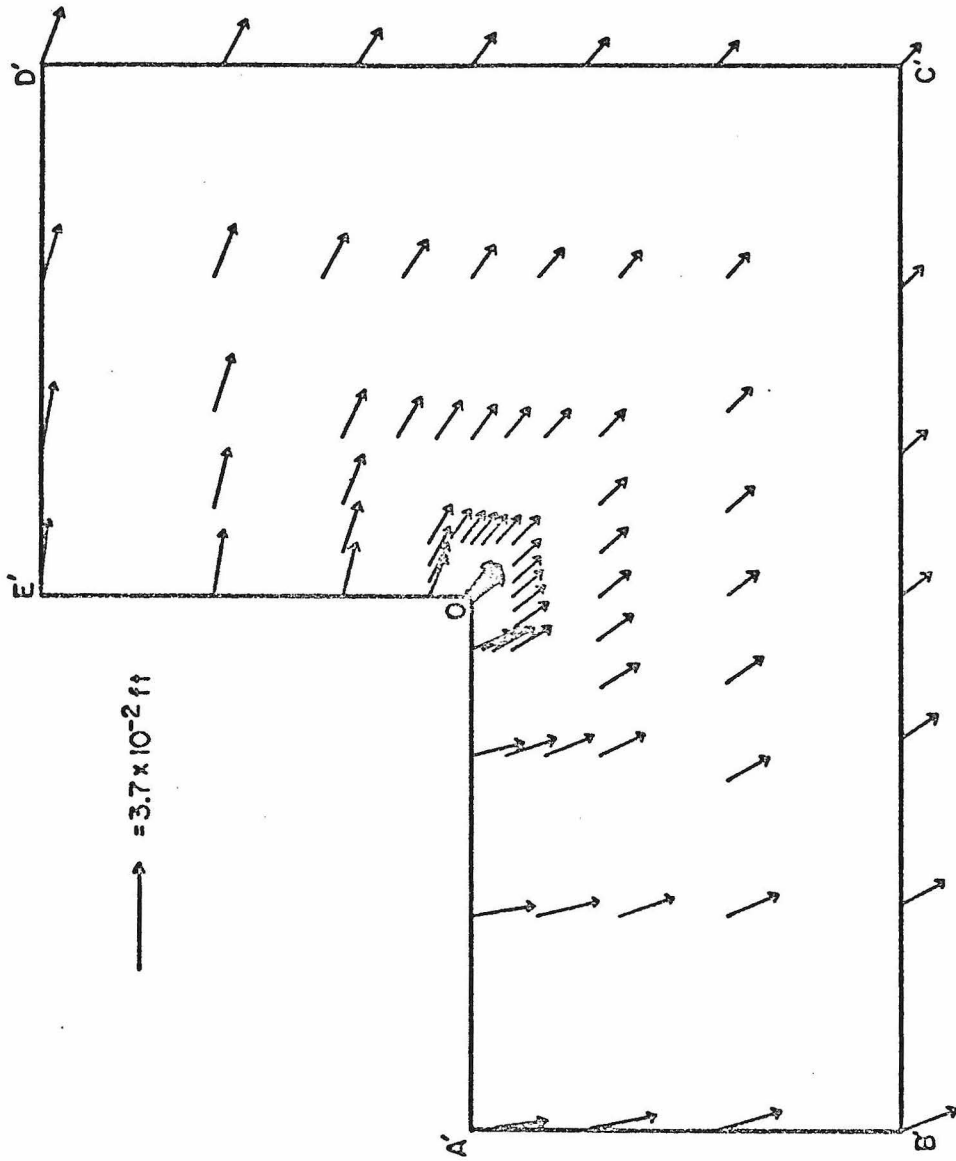
Fig. VI.6 Displacement Plot in the Shaded Portion of Fig. 3.
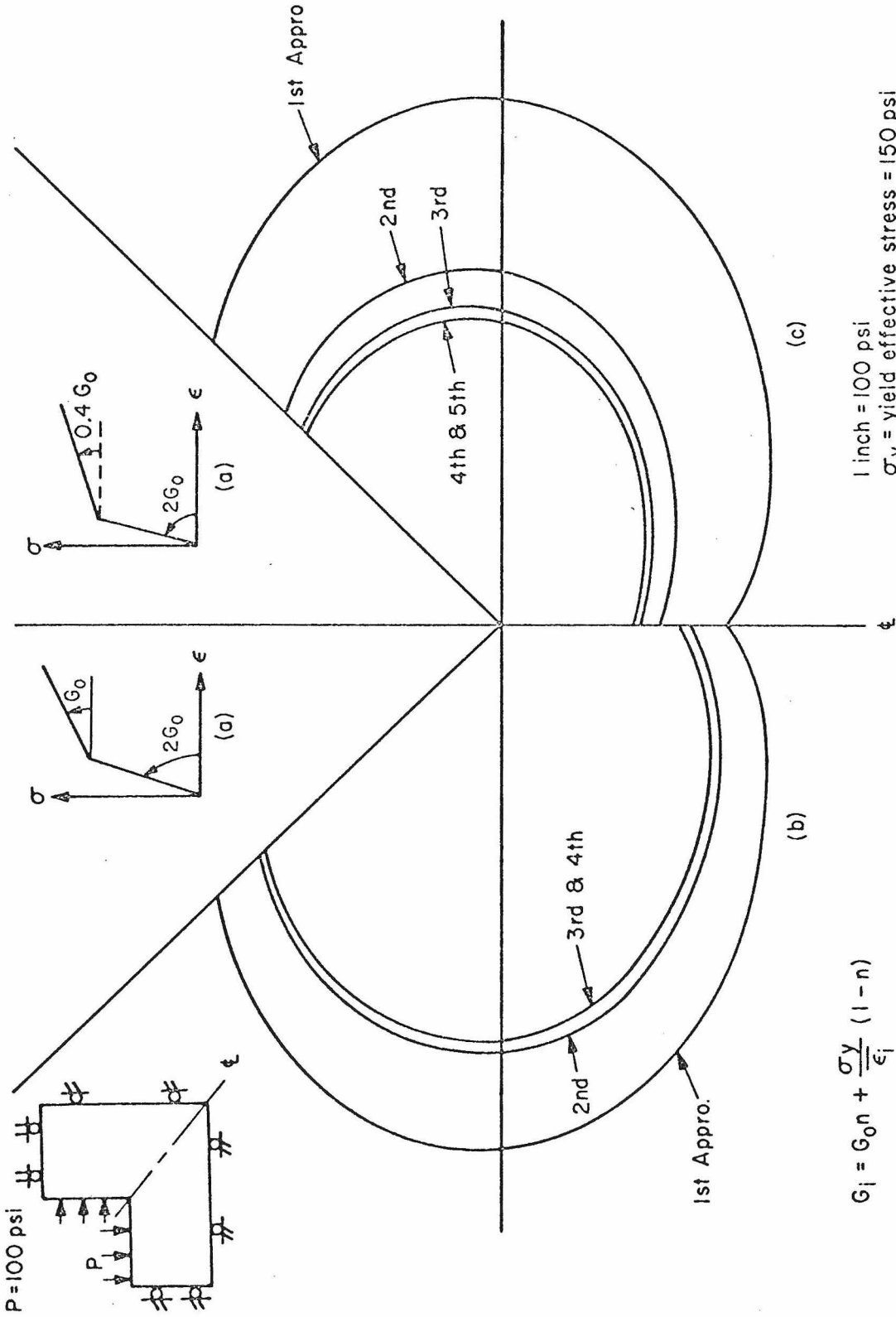
Fig. VI.7 Convergency of Bilinear Pro-
gramming — Magnitude of Major
Principal Stress Around the
Corner Elements Near Toe.

CHAPTER VII

RESULTS AND CONCLUSIONS OF THE PROBLEMS TREATED
BY BILINEAR FINITE ELEMENT ANALYSIS

VII.1. Stress Distribution Around Two-Dimensional Cracks.

VII.1.1 Linear Analysis and Results of Griffith Cracks.

In fracture theory, the concentration of stress and development of failure near the tip of a crack is of importance. In the past, only cracks with simple shapes have been solved analytically by the linear theory of elasticity [24]. For cracks with more complicated shapes and boundary conditions, conventional linear elasticity theory fails to provide solutions. Here the finite element method can be usefully employed. For this type of problem it is necessary that the elements near the corner of a crack be very small in comparison with the size of the crack. Previous investigators [22] have usually neglected this point. The size of the elements they have employed near the tip of a crack or toe of a slope has been too large to indicate the stress concentration correctly. Together with the boundary conditions in some investigations, this has caused failure to develop in regions other than the toe of the slope or the corner of a crack [22]. Before setting up the finite element grid for the crack problem, it is advisable to investigate the nature of the stress distribution in the vicinity of

a crack. It is also preferable to start with a simple crack problem whose solution has been obtained analytically. The simplest case to start with is a two-dimensional Griffith crack [24], [113]. A Griffith crack of length $2L_c$ is shown in Fig. VII.1(a).

If the crack is subjected to uniform internal pressure P_0, the maximum shearing stress at point $P(r, \theta)$, has been found to be [24], [113]

$$\tau_{max} = P_0 \; \frac{r \sin\theta}{L_c} \left(\frac{L_c^2}{r_1 r_2} \right)^{3/2} \tag{7.1}$$

in polar coordinates as shown in Fig. VII.1(a). From Eq.(7.1) it can be seen that the maximum shear stress is roughly inversely proportional to the square of the radial distance from the tip of the crack. Therefore, the size of the finite elements near the tip of the crack should be selected to reflect this and were arranged similar to the configuration in Fig. VI.3. It is logical to arrange these elements in such a fashion that the distance between the center of gravity of each element and the tip of the crack increases proportionally with the square of the order of sequence.

The solution of problems by finite element analysis requires a large digital computer. The number of elements is usually limited by economic reason and limitations in computer storage. In other words, the total number of elements has to be small enough to be economic and within the computational capacity, and yet large enough to provide good solution. Although tedious to set up, a graded network of elements best meets this requirement in the

present problem.

The next step is to establish the influence of the size of the grid on the accuracy of the solution, to determine the optimal grid size for obtaining solutions with reasonable accuracy. Due to its simplicity, the maximum shear stress obtained from the analytical solution and expressed in Eq.(7.1) was used for comparison purposes in this study. A convenient way of visualizing its distribution in the vicinity of a crack and hence of comparing the analytical and computed maximum shear stresses consists of plotting the $\tau(x,y) = \alpha P_0$ where α is a parameter. Since they appear as fringes in photoelastic analyses, these curves are called "isochromatics." By letting $\alpha = \tau(x,y)/P_0$ and changing to Cartesian coordinates, Eq.(7.1) can be rewritten

$$\alpha = \frac{\dfrac{y}{L_c}}{\left[\left(\dfrac{x}{L_c}-1\right)^2 + \left(\dfrac{y}{L_c}\right)^2\right]^{3/4} \left[\left(\dfrac{x}{L_c}+1\right)^2 + \left(\dfrac{y}{L_c}\right)^2\right]^{3/4}} \qquad (7.2)$$

(Note that in Sneddon's paper (1946) and book (1969), the expressions for α are not all correct). From Eq.(7.2) the isochromatic lines in the vicinity of a Griffith crack can be plotted. Due to the symmetry of the problem, only the lines in a quarter of the whole region are shown in Fig.VII.2. From this figure it can be seen that all isochromatic lines pass through the very tip of the crack. This means, of course, that the maximum shear stress is infinite at the tip. Different sizes of finite element grids were set up and solved by linearly elastic analysis. Figs.VII.3, VII.4 and VII.5

show the results. In these figures, (a) shows the finite element configuration, (b) shows the corresponding isochromatic lines in the vicinity of the crack, and (c) shows the comparison between the results of theoretical and finite element solutions along a radius sequence from the crack tip.

VII.1.2 Conclusions of Linear Analysis on Griffith Cracks.

From the above results, the following conclusions can be made:

1. For a finite element analysis, the computed stresses everywhere are finite. However, as shown in series (c) of Figs. VII.3, VII.4, and VII.5 the general trend of stress concentration at the tip of the crack is strongly indicated.

2. In comparing the isochromatic lines from theoretical and finite element solutions, it is seen that the average deviation in maximum shear stress for a grid size $8L_c$ by $8L_c$ is about $0.05P_0$; the results may therefore be taken to be 5% in error. For practical engineering purposes, this would be acceptable. If higher accuracy is desired, it would probably require a grid size of $20L_c$ by $20L_c$ to reach an accuracy of 1%. If this conclusion is extended to the problem of stress and deformation distribution in a semi-infinite slope, it would seem that the boundary should be established fairly far away. A distance at least of 4 or 5 times the height of the slope would be required to reach a meaningful representation of a semi-infinite medium.

3. The smaller the overall size of the grid the less accurate is the solution. Moreover, a lower degree of stress concentration is indicated around the tip of the crack for the smaller grid because of the influence of the boundary constraint.

4. Because of the stress concentration at the tips of the crack, plastic flow occurs in this region even for small pressures P_0. If the failure criterion is taken to be that of Tresca (maximum shear stress), the linearly elastic isochromatic contour can serve as a rough indication of the size of the failure zone. At first glance it would seem that if the yield stress is high or if P_0 is small, the region of plastic strain would be small and would not appreciably affect the distribution of the stresses in regions far away from the tip of the crack. However, due to the tension developed near the crack, the crack extends in practice and the above observation may not necessarily be true. This point will be discussed further in the study that follows.

VII.1.3 Bilinear Analysis, Results and Conclusions of Griffith Cracks.

The next step is the investigation of the effect of plastic strain on the redistribution of stress in the vicinity of a crack. If the bilinear finite element scheme and the Von Mises yield criterion as shown in Eq. (6.2) are applied to the crack problem, the extent of yielding can be found. The size of the yield zone and the stress redistribution in the unyielded area depend on the load, the yield stress value and the characteristics of the bilinear stress-strain

relation. From the bilinear finite element solution it is obvious that the stress in the yielded zone is reduced while the stress in the unyielded zone increases in comparison with the solution from the linear scheme. Fig. VII.6 shows the yield zone with elastic ratio $n = 0.5$ and yield stress $= 2.0P_0$. It can be seen from this figure that even though the yield zone is small, a large part of unyielded region has increased 5% or more in major principal stress (as indicated by the shaded area in Fig. VII.6). A more significant change can be observed if either the elastic ratio n or the yield stress is reduced.

It may be noted at this stage that a sizeable zone of tensile stress has developed as shown in Fig. VII.7. For soils, tensile cracks will open in these zones but this aspect of material behavior is neglected in this study. If this local failure in the tensile zone is considered, the degree of stress redistribution will be even more severe.

VII.1.4 Analysis and Results of Cracks with Various Opening Angles.

The last step in investigating a crack problem is to study the stress distribution around a crack with a shape other than that of a Griffith crack. Various shapes of cracks have been investigated as an extension of Griffith crack theory [119], [120], [121]. For a Griffith crack, the tips can be idealized as the intersection point of two almost parallel straight lines. If the tip angle opens up slightly, the degree of stress concentration will be less than that of a

Griffith crack. However, the quantitative analytical relationship is still to be established. In this study, the effect of different crack angles is investigated by the finite element method. The actual problem of interest would be an infinite crack with different angles of opening as shown in Fig. VII. 8(a). Due to computational limitations, it was not feasible to tackle this problem. Since the stress concentration and stress distribution in the vicinity of a crack tip are the main interest in this study, a crack problem as shown in Fig. VII. 8(b) was instead solved by the finite element method. The stress concentration in the lower corner (L in Fig. VII. 8(b)) does not materially contribute to the stress concentration in the immediate vicinity of the crack tip (T in Fig. VII. 8(b)). Thus, the problem shown in Fig. VII. 8(a) can be related to the results of the problem of Fig. VII. 8(b). This assumption is probably adequate if the finite element grid in the lower corner is not chosen to be too fine. The finite element grid for a crack with 30° opening angles is constructed by cutting a 15° triangular wedge section from the grid shown in Fig. VII. 5(a), and is illustrated in Fig. VII. 8(a). (Only a quarter of the region is employed due to symmetry). The grids for other crack opening angles can be constructed in similar fashion. The results for various crack openings are represented by a plot of isochromatic lines to indicate the stress level and concentration in the vicinity of the crack tips, and are shown in Figs. VII. 9, VII. 10 and VII. 11.

VII.1.5 Conclusion on the Results of Stress Distribution of Crack with Various Opening Angles.

VII. 2   Distribution of Stresses in Slopes and Embankments.

The state of initial stress in a natural slope or in the earth's surface prior to construction of an embankment is an important factor in the deformation and stability of a slope.

This has been taken into account, to a limited extent, in a previous study [22]. For an earth structure under gravity, only a few idealized configurations may be analyzed exactly [112]; for practical cases, some approximate techniques must be employed [122], [123]. It is not difficult to apply the linear finite element analysis to calculate the states of stress and deformation for this type of problem, but interpretation of the results requires some care. To examine the effect of the stresses at the toe of the slope on the stability of the slope for this study, a simple finite slope with a finite element grid as shown in Fig. Vii. 13(a), was established for linear finite element analysis. Fig. VII.13(b) shows the resulting plot for isochromatic lines under gravity loading. From the results, it is evident that there exists a stress concentration around the toe of the slope. It can also be noticed that the region near the bottom boundary is in a state of relatively high stress. If a failure is to develop, it would be initiated in the region of stress concentration and high stress near the bottom boundary. It is the subject of the following study.

VII. 3   Development of Failure and Stability Analysis.

VII. 3. 1   Prelude

It is well known that the final state of stress in an artificial slope or embankment depends upon the manner in which the final configuration is reached [21], [22]. To analyze the state of stress in an artificially-c nstructed slope or embankment, the incremental loading (built-up) or unloading (cut-down) cases must be simulated. This point has long been recognized by various investigators [21], [22]. By the employment of the finite element method, the cases of built-up slopes can be easily simulated. For the cases of cut-down slopes, it has been shown that if the material is homogeneous and linearly elastic, the removal to the final stage may be made in one step and it is unnecessary to simulate the excavation procedure [122]. However, due to the concentration of stress at the toe of every excavation stage, linear elasticity can no longer be expected to apply. In each excavation stage, a toe region progresses down-ward through the material which in the region adjacent to the toe goes through successive stages of stressing, relaxation, and relief of stress. A correct analysis requires the use of an incremental constitutive relation such as the one derived in Part I, which des-cribes completely the stress-strain relationship for the loading, unloading and reloading process. This point is totally neglected by most investigators.

The bilinear scheme used in this study is valid only if a monotonic increase of the state of stress exists. Therefore, it cannot be used to simulate the cut-down process to study the development of failure around an excavated slope. However, the stability of a slope can still be studied qualitatively by considering

the slope as a whole without simulating the cut-down or build-up process. Instead of varying the height of a slope, the gravitational force (unit weight, γ) can be gradually increased to study the development of failure by bilinear finite element analysis.

VII.3.2 Analysis, Results and Conclusions

(a) Homogeneous slopes and embankment.

For slope stability analysis, a dimensionless stability factor (S_f), which is defined as the ratio of the product of unit weight γ and the slope height H to the cohesion c of the material, is usually used as a comparison parameter. By gradually varying the unit weight γ and fixing all other related parameters, the failure zone for various S_f values can be investigated. In this study, the specific slope with finite element configuration as shown in Fig. VII.13(a) was investigated by bilinear analysis. Ideally, Poisson's ratio should be taken to be 0.5. However, the finite element formulation used in this study cannot be used for the $\nu = 0.5$ case. Instead, the ν value was taken as close to 0.5 as possible without generating unreliable results. Some results showing the yield zone for different S_f values applied to the configuration of Fig. VII.13(a) are shown in Figs. VII.14 and VII.15 for $\phi = 0$ and $10°$ respectively. From these results, the following remarks can be made:

1. When S_f is small, the yield zone is first developed as expected, at the toe of the slope due to the stress concentration there. As S_f is gradually increased the toe yield zone spreads.

From these results, the following comments can be made.

1. In the isochromatic plots, it seems that the stress concentration at the tip of the crack is of the same order of magnitude for different openings. If, again, a Tresca failure criterion is used, the yield zones for different openings would also be about the same size. Therefore, if a bilinear representation is employed, the nature of the redistribution of the maximum shear stress would be quite similar for different crack openings. However, if the major principal stress for each corner element around the tip of the crack is plotted for different openings, as shown in Fig. VII.12, it can be seen that the Griffith crack has a much more severe stress concentration. A crack with a larger opening angle has less stress concentration than a crack with a smaller opening angle. If a von Mises-Mohr-Coulomb yield criterion, as in Eq. (6.3) is considered, then a crack with a smaller opening angle would have a larger yield zone. Therefore, it can be speculated that a fracture, beginning as a Griffith crack, will gradually be changed into a wider opening at the tip to plastic strain and the degree of stress concentration will become less.

2. As shown in Figs. VII.9, VII.10, and VII.11, the stress concentration for the upper corners with different openings is clearly determined. However, around the lower corners, the isochromatic lines show a much smaller degree of stress concentration. This occurs because the grid used in the latter region was not fine enough to represent the stress concentration adequately.

With a further increase in S_f a portion near the bottom boundary yields due to the high principal stress difference induced there by gravitational loading. This depends on the value of Poisson's ratio chosen in the problem, as demonstrated below.

2. If a conventional slope stability analysis is applied to a 90° slope as in this case, the critical S_f values are 3.85 and 4.6 [11] for ϕ values of 0° and 10° respectively. However, a substantial region of the slope is seen to be yielding for S_f values well below the critical S_f values by this analysis for both ϕ angle values.

3. The above remarks can be explained as follows. The stress level in the soil increases with depth under gravitational loading. In elastic theory, the vertical stress in an isotropic and homogeneous semi-infinite medium under its own weight has the value of γz where z is the depth from ground surface. For a plane strain case, the principal stress in the other two directions are

$$\sigma_2 = \sigma_3 = \sigma_1 \frac{\nu}{1-\nu} \tag{7.3}$$

According to Drucker and Prager [116], the Von Mises-Coulomb criterion states that a material yields when the following condition is reached:

$$J_2^{1/2} = \frac{3c}{\sqrt{9+12\tan^2\phi}} + \frac{\tan\phi}{\sqrt{9+12\tan_1^2\phi}} (\sigma_1 + \sigma_2 + \sigma_3) \tag{7.4}$$

where

$$J_2 = \frac{1}{6}\left[(\sigma_1 - \sigma_2)^2 + (\sigma_2 - \sigma_3)^2 + (\sigma_3 - \phi_1)^2 \right] \qquad (7.5)$$

From Eqs.(7.3), (7.4) and (7.5), the yield criterion can be restated as:

$$\frac{\sigma_1}{c} = \frac{3}{(\frac{1-2\nu}{1-\nu})\sqrt{3+4\tan^2\phi} - (\frac{1+\nu}{1-\nu})\tan\phi} \qquad (7.6)$$

In other words, yield will occur if the major principal stress reaches the value obtained from Eq.(7.6). It has to be noticed that the denominator in the right-hand side of Eq.(7.6) should be positive in order to have a yield mechanism. If the demonimator is negative or zero then yield will never occur. From Eq.(7.6), it can be seen that yield will not occur in an incompressible semi-infinite medium ($\nu = 0.5$) bounded by a horizontal surface. For a slope on a semi-infinite space, the stress level in the region sufficiently far away from the slope is similar to the above situation. The σ_1 stress in this region would be equal to γz where z is the vertical distance from the crest of the slope. Setting $\gamma_1 = \gamma z$ into Eq.(7.6), the region beneath the critical depth level z_c where $\gamma z_c/c$ is equal to the right-hand side of Eq.(7.6), would presumably yield. However, due to the influence of the slope and the boundary conditions imposed on the finite element grid, the $\gamma z_c/c$ values might not be the same as the values calculated from Eq.(7.6) as shown in Figs.VII.14 and VII.15. The redistribution of stress in

the yield region causes a large portion of the slope to yield at lower S_f value than expected. If the lower boundary in the finite element configuration shown in Fig. VII.13(a) is set further from the ground surface, it can be expected that a larger portion of this configuration would yield at an even lower S_f value.

In dealing with the failure problem, the conventional slope stability methods have proved satisfactory in practice. Yet it is found that a lower S_f value would probably be reached at failure of the slope for small ϕ angles by the bilinear finite element analysis. The conventional analysis, which assumes a soil whose strength does not vary with depth, thus probably gives satisfactory results in a real field situation because the cohesion for normally consolidated and over-consolidated clay soils increases with the increase of depth beneath the ground surface.

In other words, it appears from this analysis that the conventional failure calculation overestimates (is unconservative) the height of slope which will fail for a soil which truly exhibits a constant strength/depth profile. However, soils increase in strength with depth and the increase is sufficient to support the greater slope height predicted by the theory.

(b) Non-homogeneous slope and embankments

In the above analysis, it can be seen that the yield region has not yet reached the crest of the slope. Although a large portion of the slope has yielded, no toe failure mechanism is obtained. A toe failure

mechanism for a slope must have a yield zone extended from the toe of a slope to the crest. If the soil is assumed homogeneous, the above analysis showed that the redistribution of stresses in the yield region near the bottom boundary causes a large portion of the slope to yield before a toe failure mechanism is reached.

In order to reach a toe failure mechanism, this influence due to the redistribution of stress near the bottom boundary must be eliminated. One way of achieving this is to increase the strength with the increase of depth beneath the ground surface. In the following study, the finite element configuration shown in Fig. VII.13(a) is also used but the yield stress is assumed to increase linearly with depth from the ground level OA to the bottom boundary BC (Fig. VII.13(a)).

Fig. VII.16 shows the results for the case in which the yield stress increases linearly by a factor of six from the level OA to the bottom boundary BC. It can be seen that toe failure mechanism is reached at the value $\gamma H/C = 5.5$ for $\phi = 0^\circ$. This $\gamma H/C$ value is considerably higher than the S_f value (3.85) obtained from the conventional stability analysis.

From the above results, it can be noticed that bilinear finite element analysis creates a rather confusing picture in dealing with the problems of slope stability. A bilinear generalization of soil behavior is far from being desirable. The application of a more rigorous constitutive relation such as the one proposed in Part I is strongly recommended.

To ∞

∞

To ∞

T_c O T_c Line of Symmetry

L_c L_c

Line of Symmetry

To ∞

y

(a)
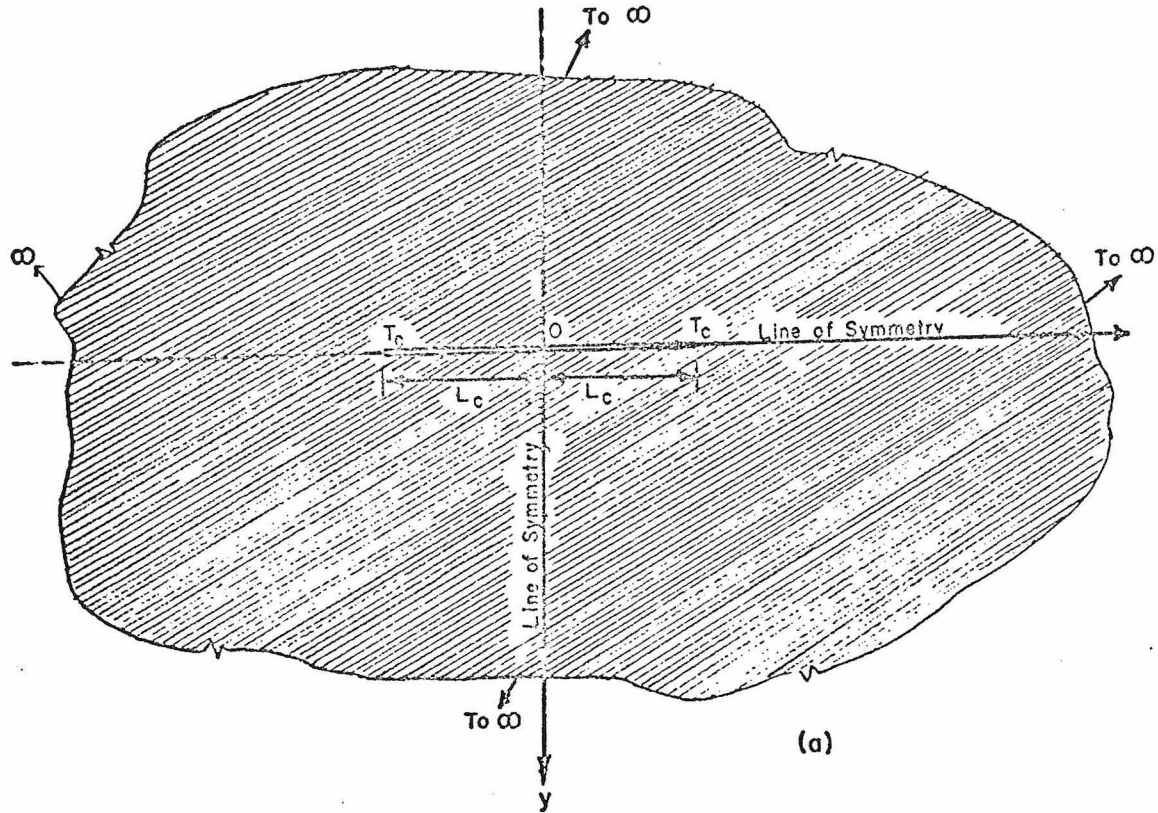
Normal pressure on crack surface = P_0

(b)

T_c O T_c X

θ_2 θ θ_1

r r_1

r_2

P

y
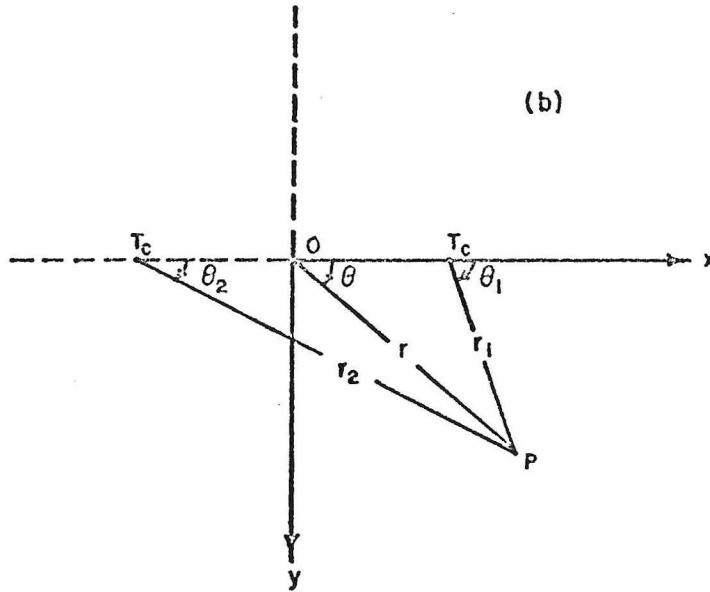
Fig. VII.1 Griffith Crack
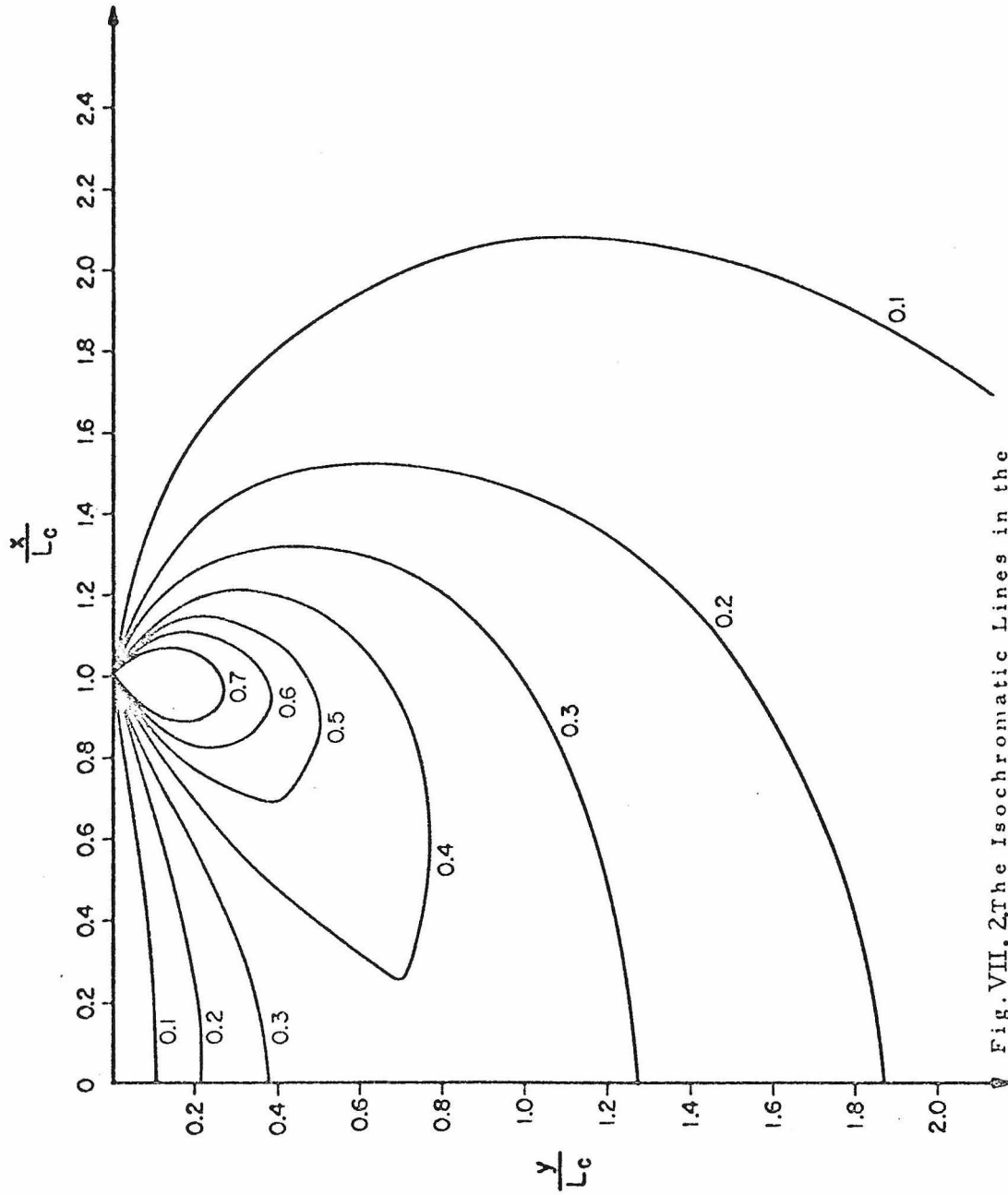
Fig. VII. 2 The Isochromatic Lines in the Vicinity of a Griffith Crack by Classical Theory of Elasticity.

(a) Finite Element Configuration
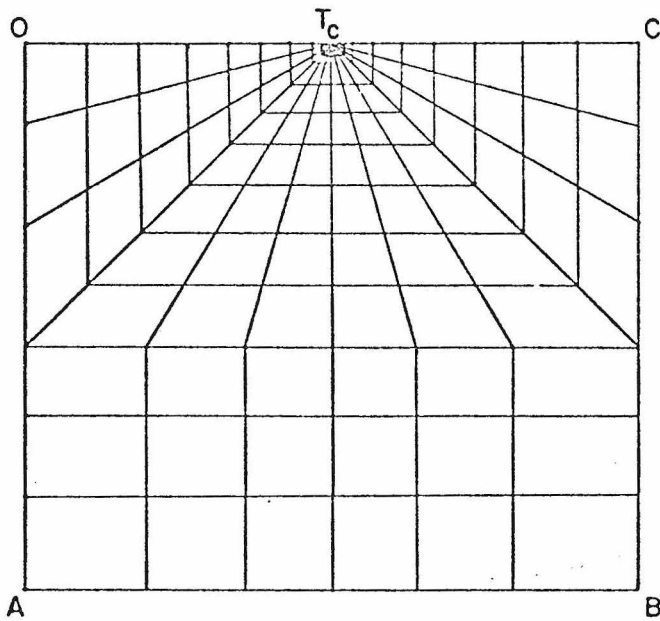
$E = 2 \times 10^6$ psf
$\nu = 0.3$

$\frac{1}{2}$ Crack length = OT_c = 90 ft
$O\,T_c\,C$ = 180 ft
  AB = 180 ft
  OA = BC = 160 ft
No. of Nodal points = 151
No. of Elements = 126

Boundary conditions
(a) Along OA, BC: No horizontal
        displacement
(b) Along AB, CT_c: No vertical
        displacement
(c) On OT_c: Nominal pressure P_o
       = 100 psf
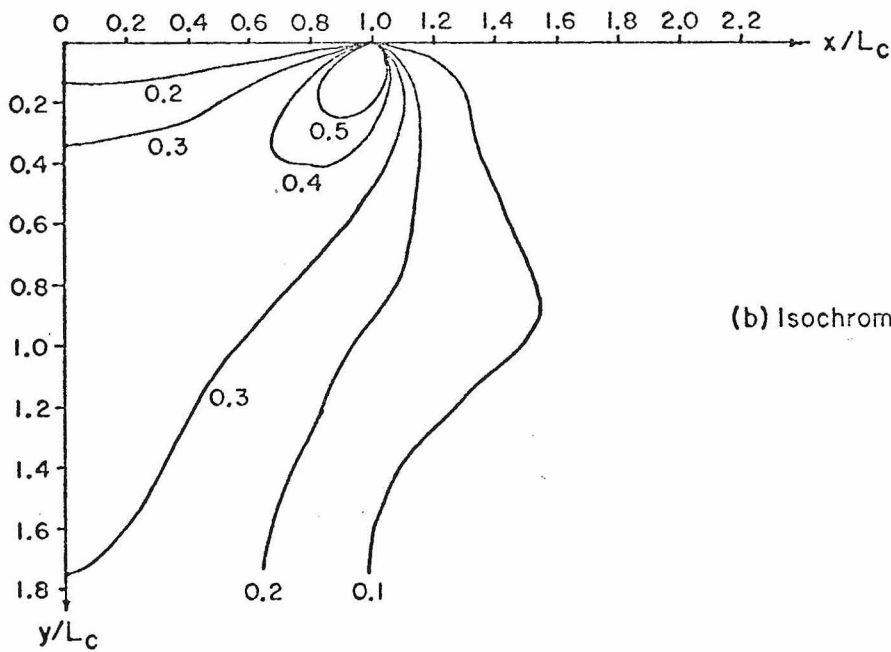
(b) Isochromatic Lines

Fig. VII.3 $1.8\,L_c$ by $2\,L_c$ Finite Element
Configuration and Results.
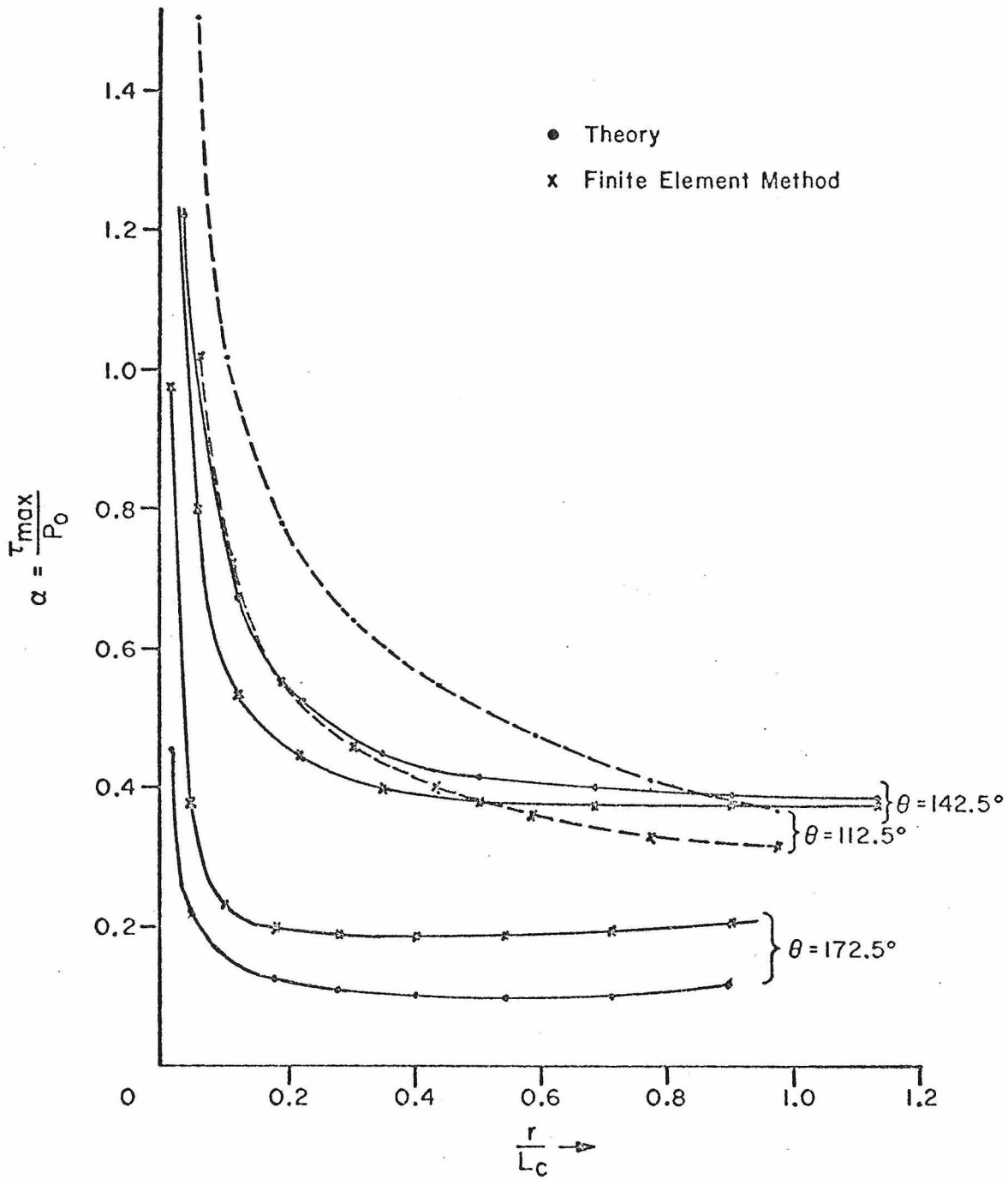
Fig.VII.3(c) Comparison of Maximum Shear Stress
by Finite Element Method and Classical
Theory of Elasticity.

$\frac{1}{2}$ Crack Length = L$_c$ = 0 T$_c$ = 90 ft
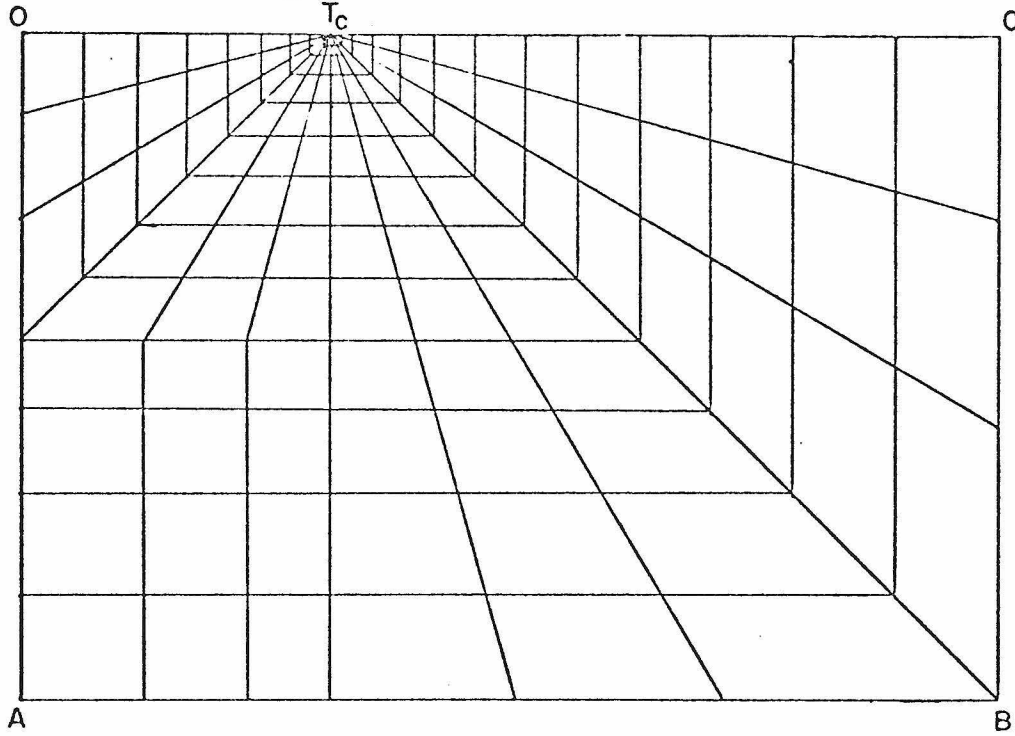
(a) Finite Element Configuration
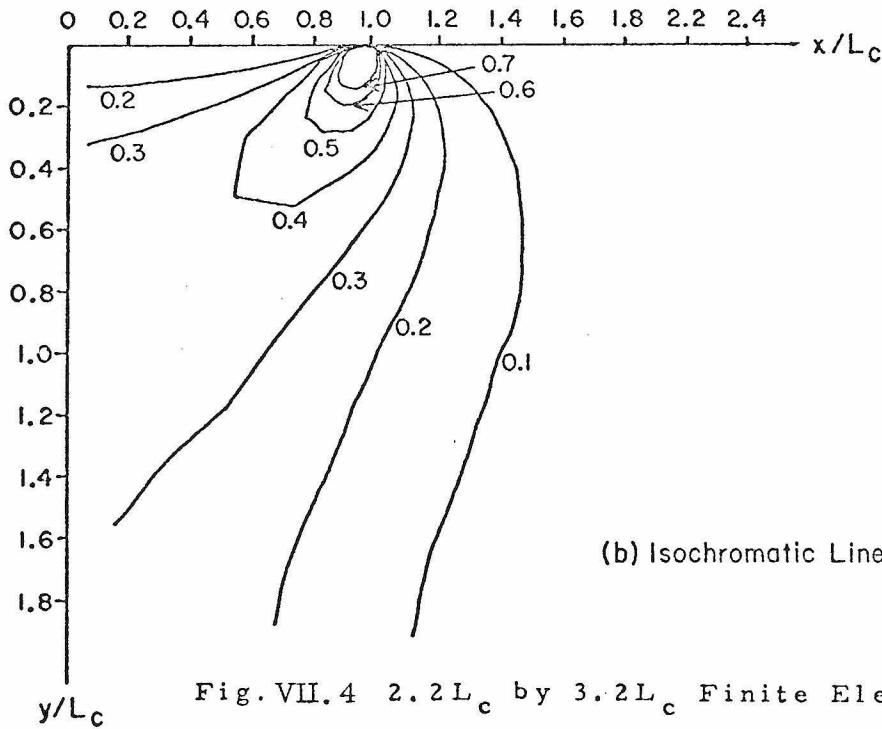
(b) Isochromatic Lines

Fig. VII.4 2.2 L$_c$ by 3.2 L$_c$ Finite Element
Configuration and Results.
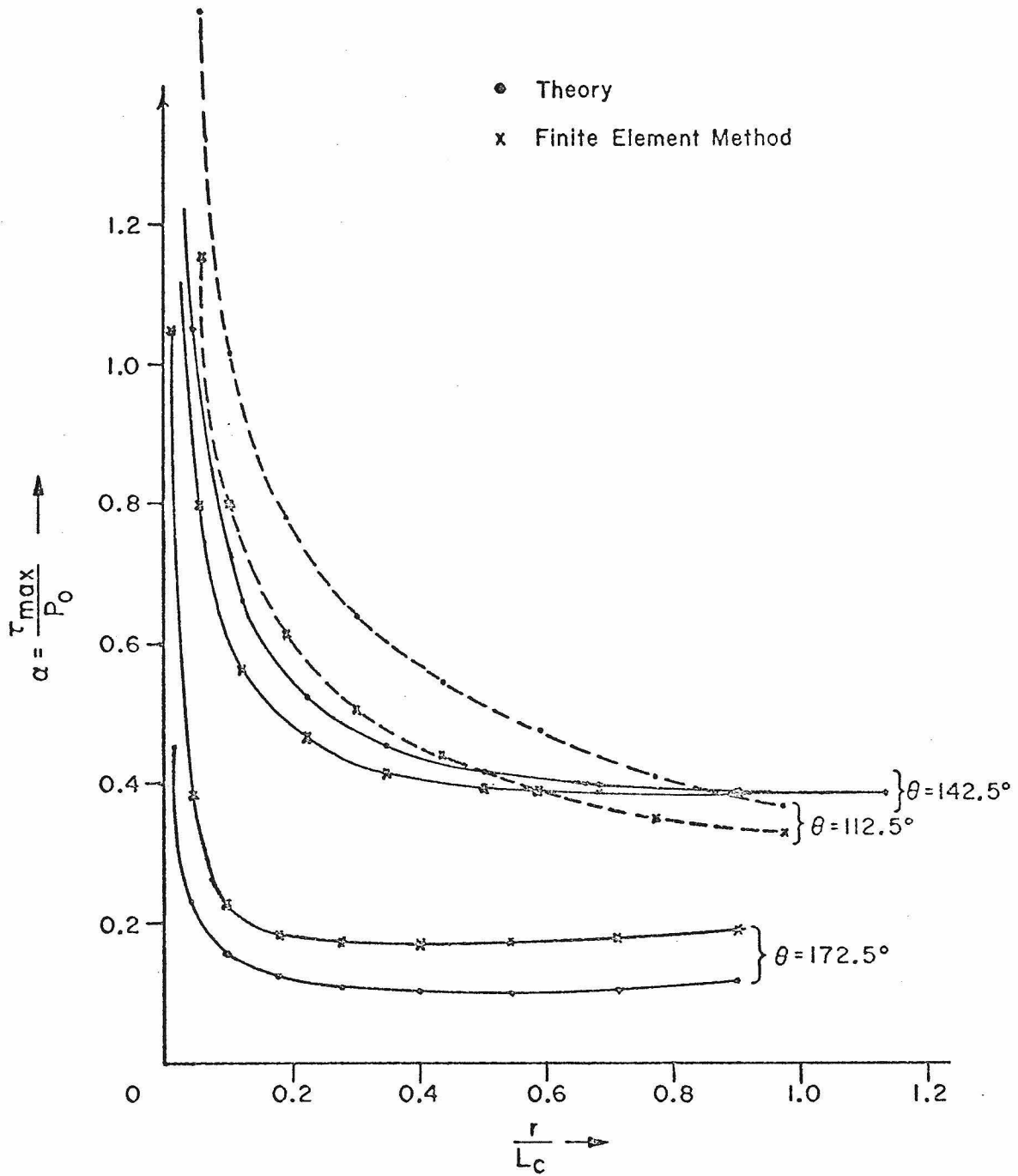
Fig. VII. 4(c) Comparison of Maximum Shear Stress by
Finite Element Method and Classical
Theory of Elasticity.

$\frac{1}{2}$ Crack length = OT_c

= L_c = 90 ft

Material properties and
boundary conditions are
the same as Fig. 10(a)

(a)

(b) Isochromatic Lines
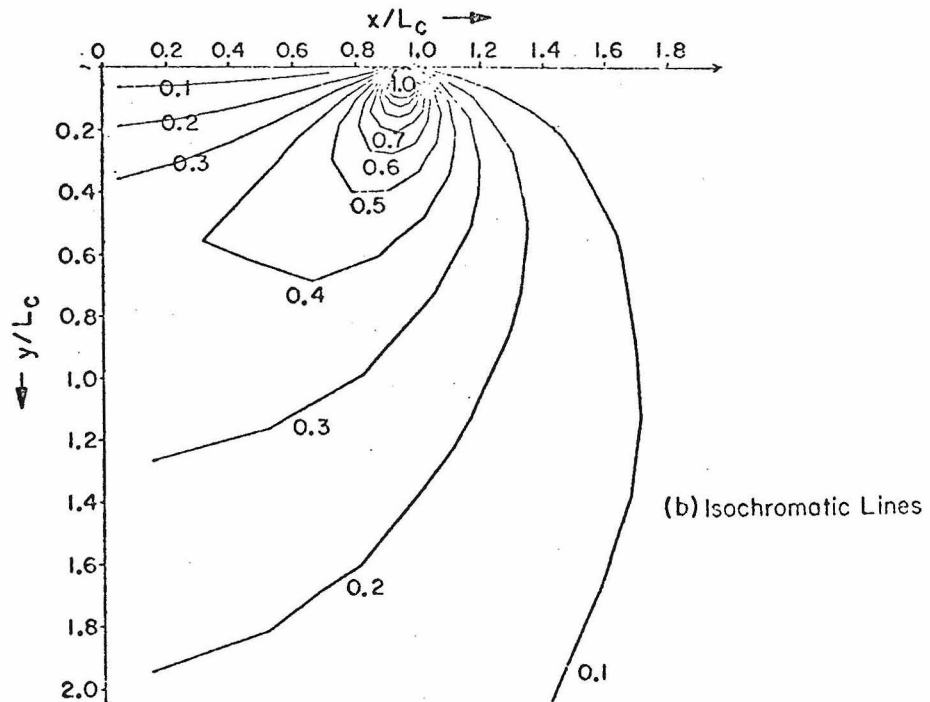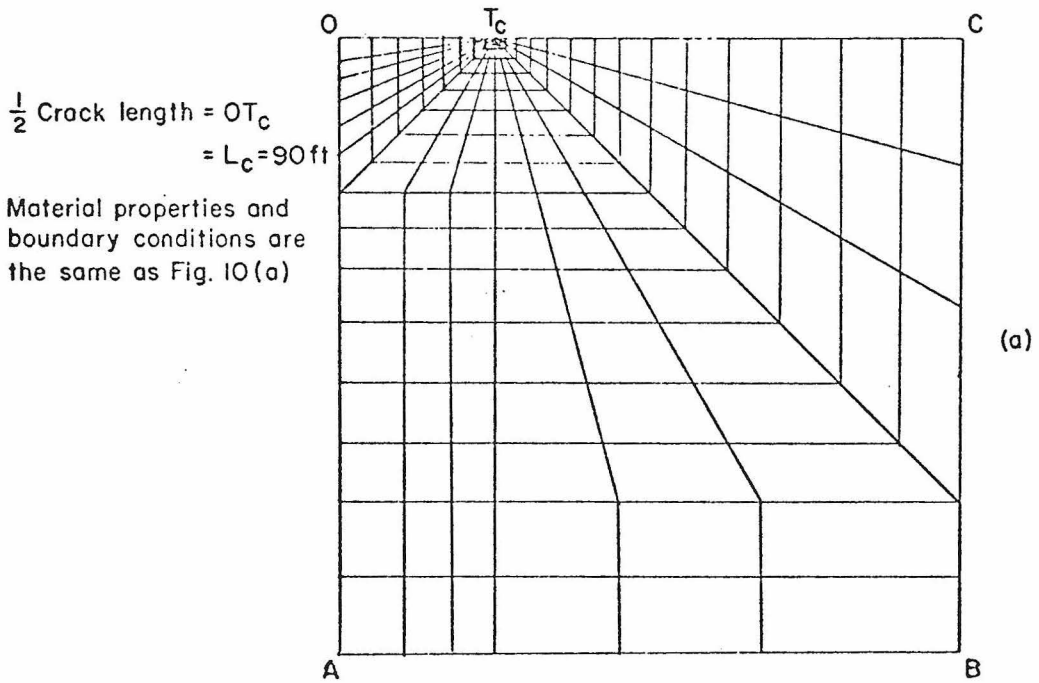
Fig. VII. 5 $4L_c$ by $4L_c$ Finite Element

Configuration and Results.
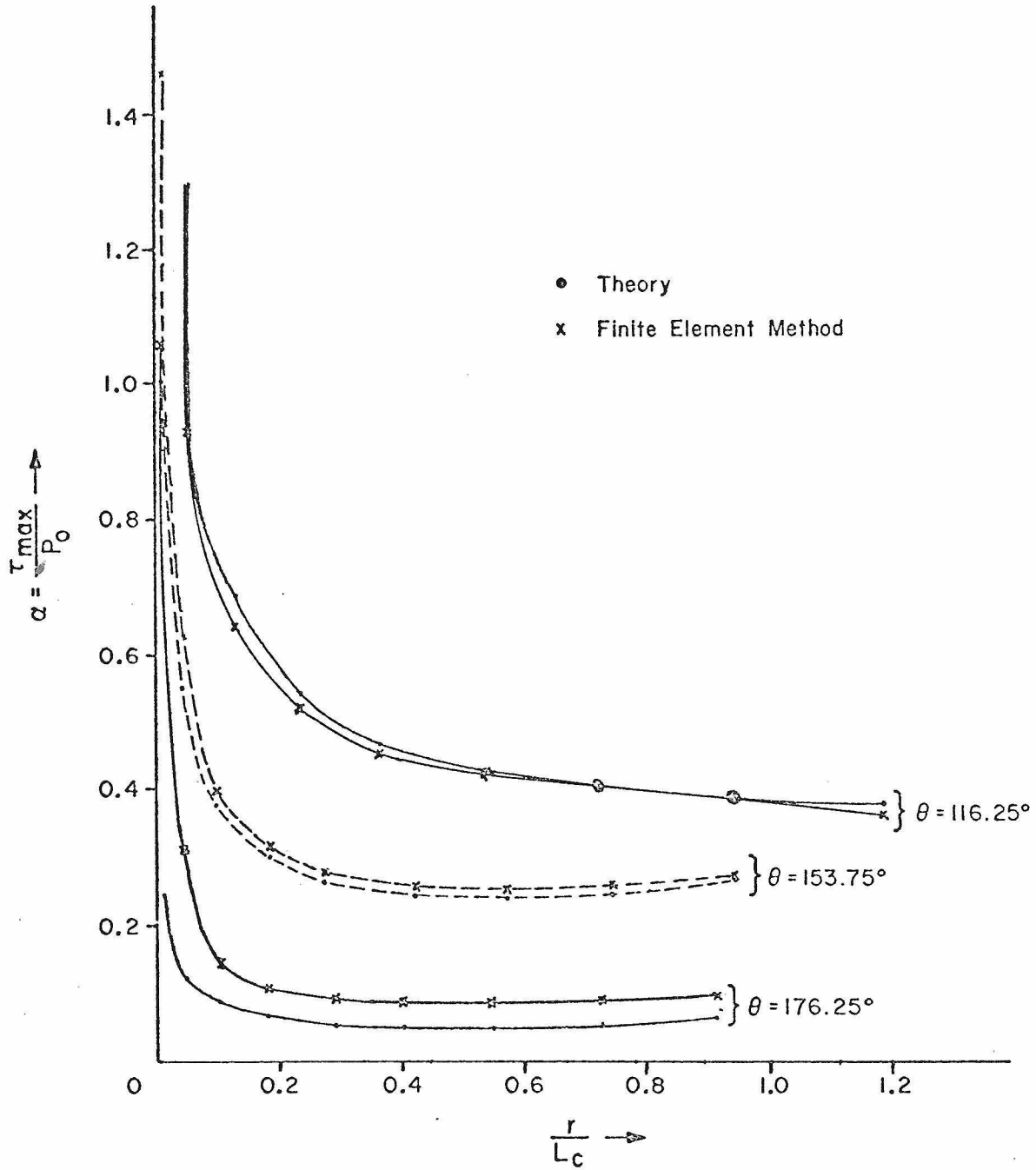
Fig. VII. 5(c) Comparison of Maximum Shear Stress by Finite Element Method and Classical Theory of Elasticity.

n = 0.5
$G_0 = 77 \times 10^5$ psf
$\nu = 0.3$
$P_0 = 100$ psf
$\sigma_y = 200$ psf

Yield zone

Shaded area indicates a redistribution of major principal stress with 5% or more change
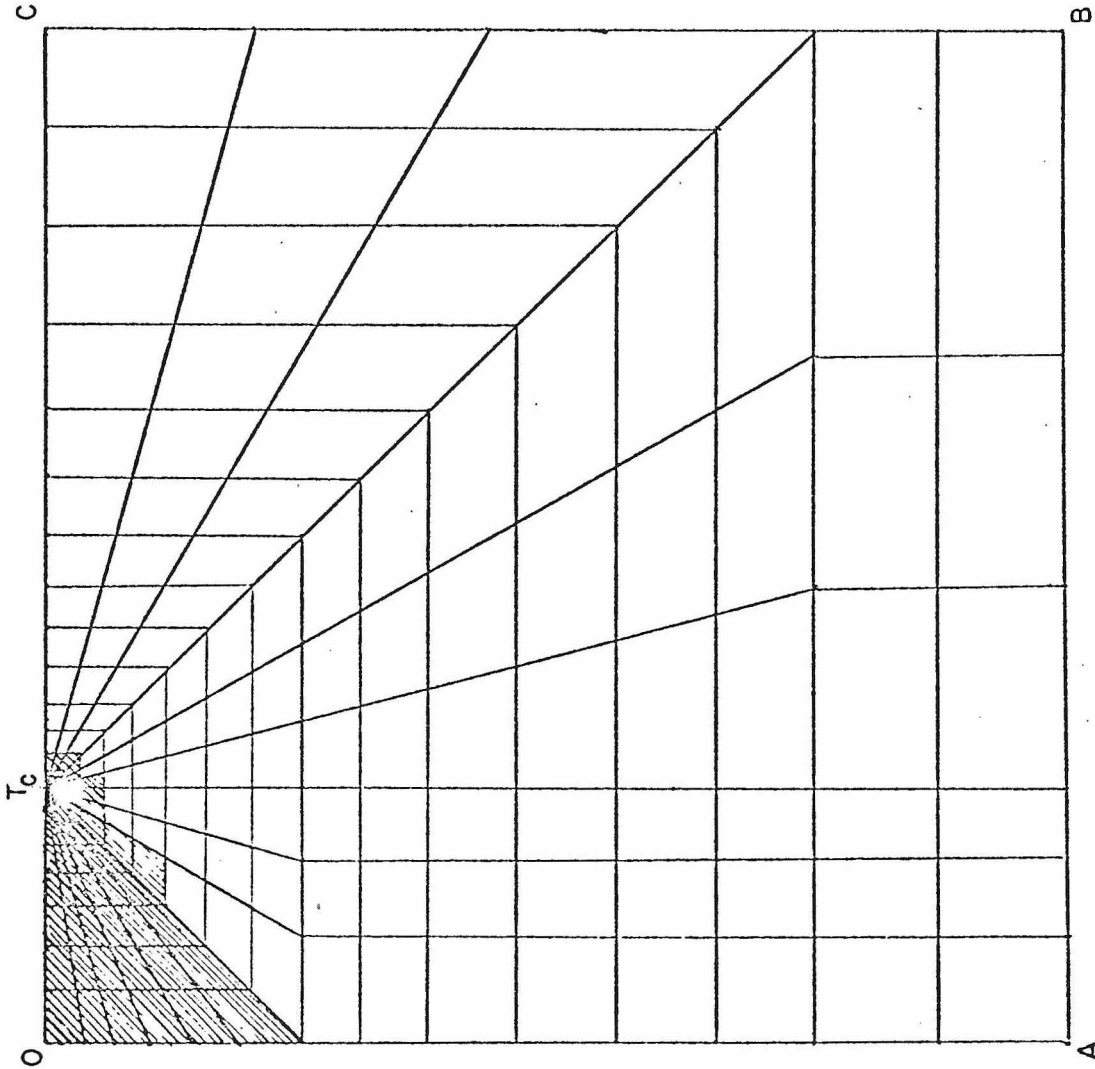
Fig. VII.6 Yield Zone and Stress Redistri- bution of a Griffith Crack.
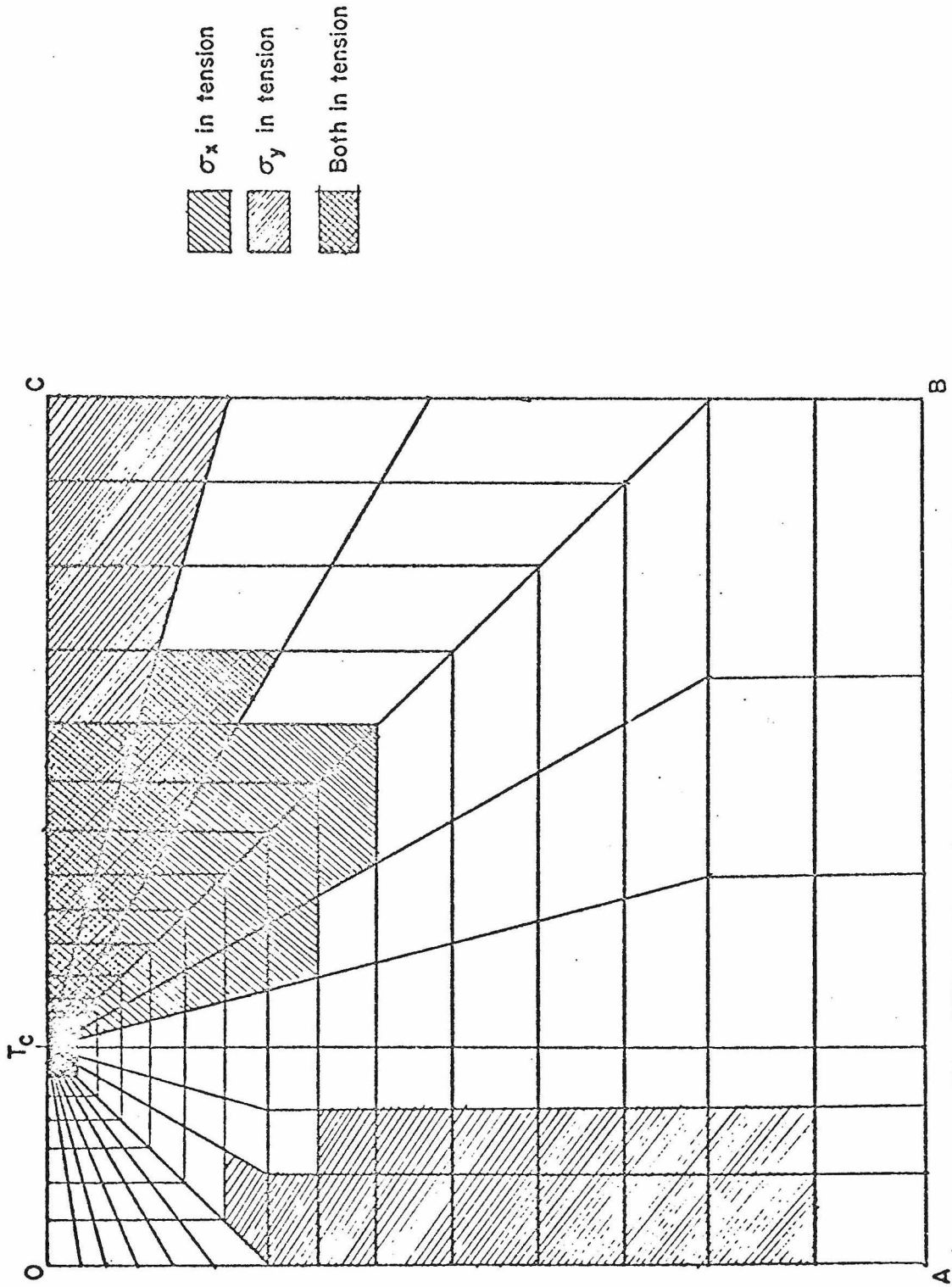
Fig. VII.7 Tension Zone in a Griffith Crack.

(a) Problem of interest
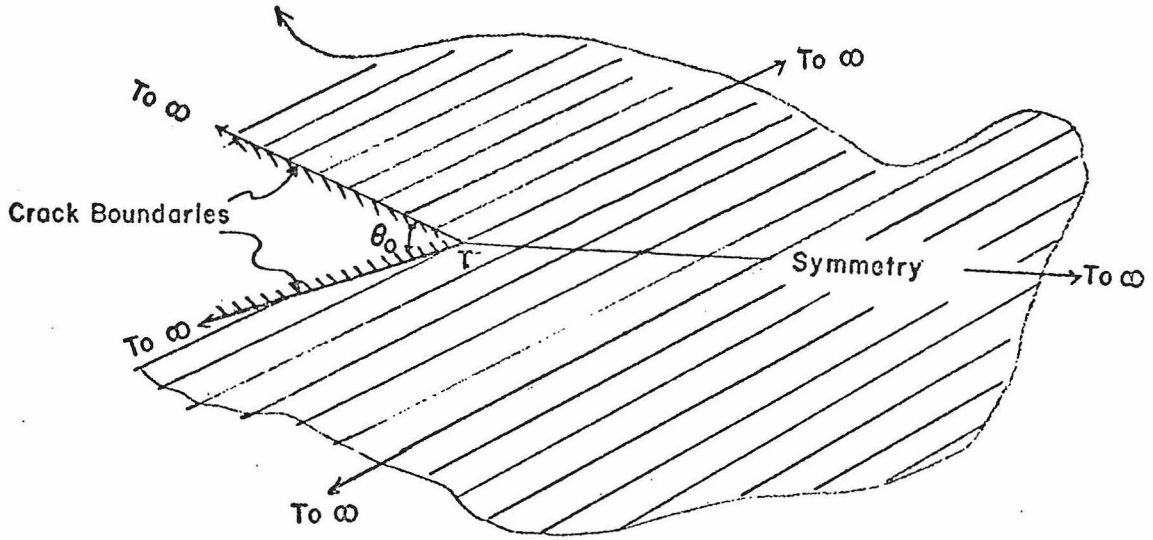
Region covers the full space
Uniform normal pressure on crack boundaries

Fig. VII.8 Cracks with Various Opening
Angles.

(b) Problem solved

No. of Nodal points = 214
No. of Elements = 183

$E_0 = 2 \times 10^6$ psf

$G_0 = 0.77 \times 10^5$ psf

$\nu = 0.3$

Boundary conditions

(a) Along OA, BC: No horizontal
displacement

(b) Along AB, CT_c : No vertical
displacement

(c) On OT_c : Normal pressure P_0
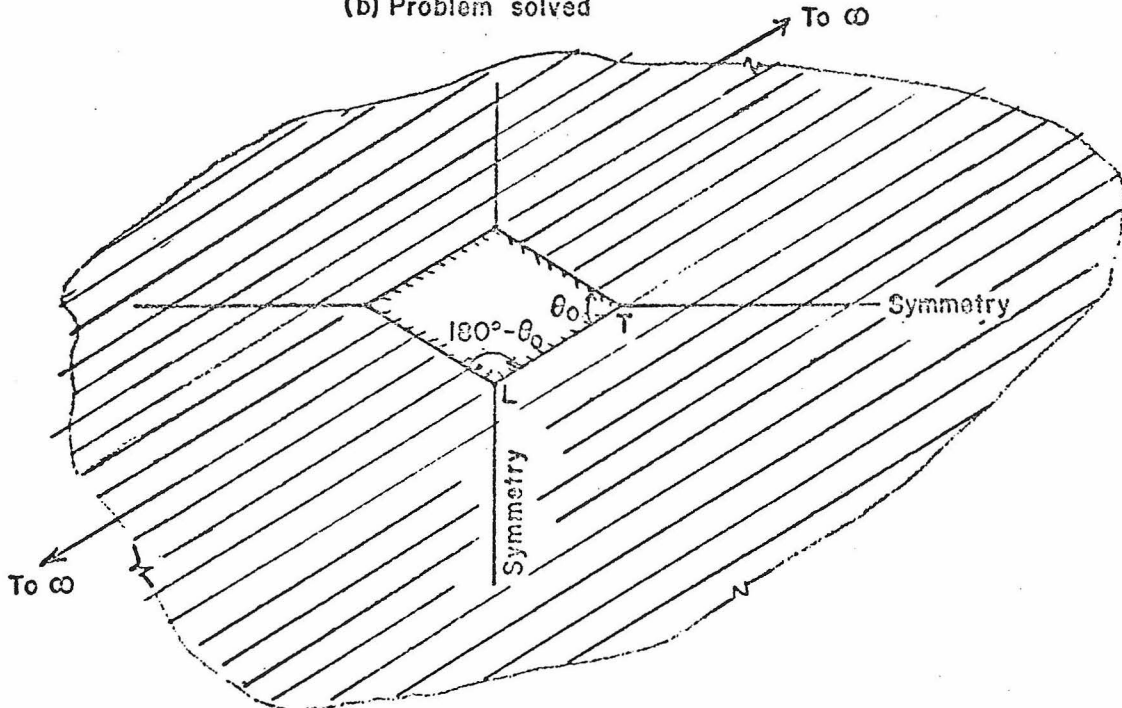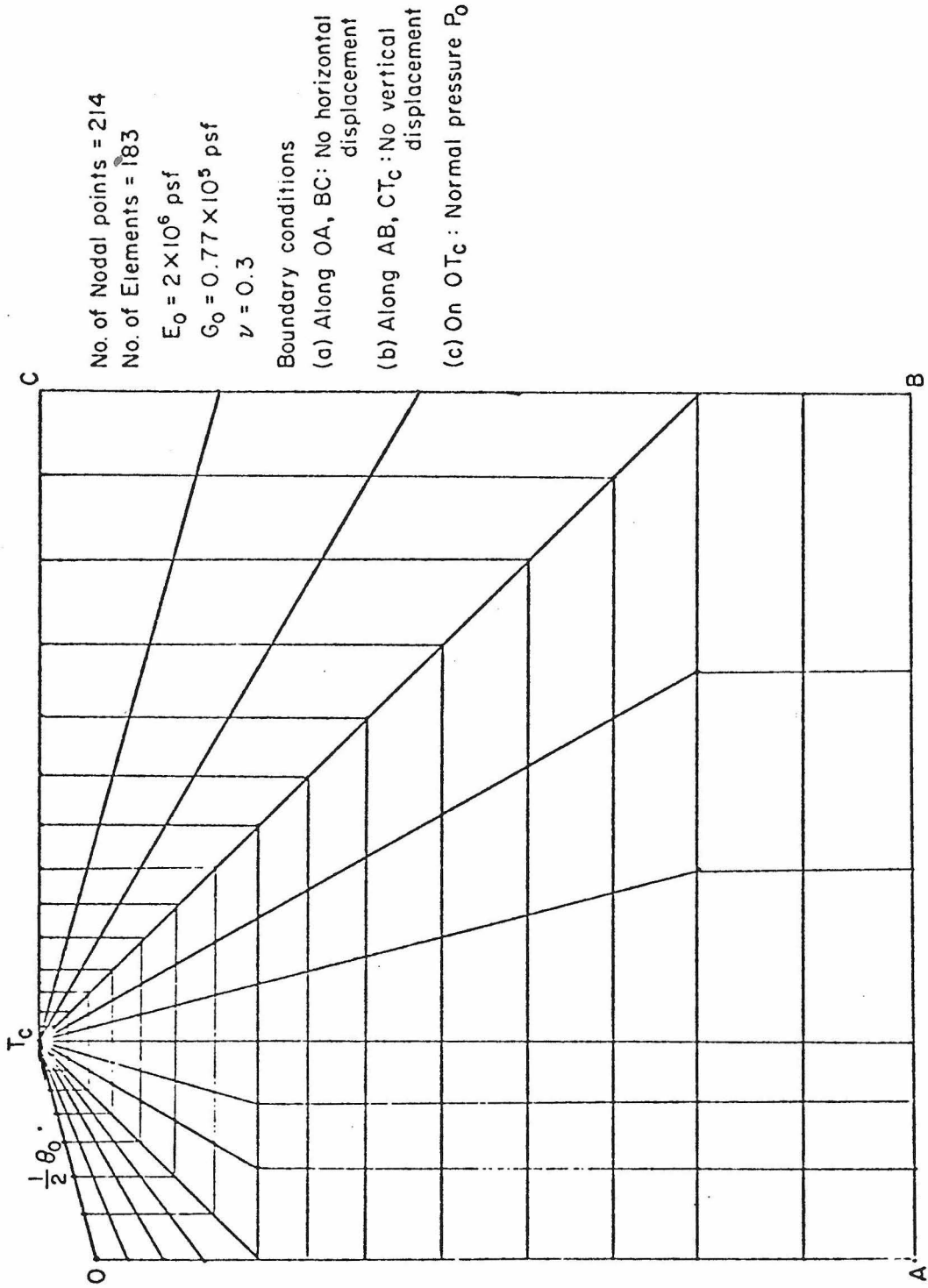
Fig. VII.8(c) Finite Element Configuration
for a 30° Opening Crack.
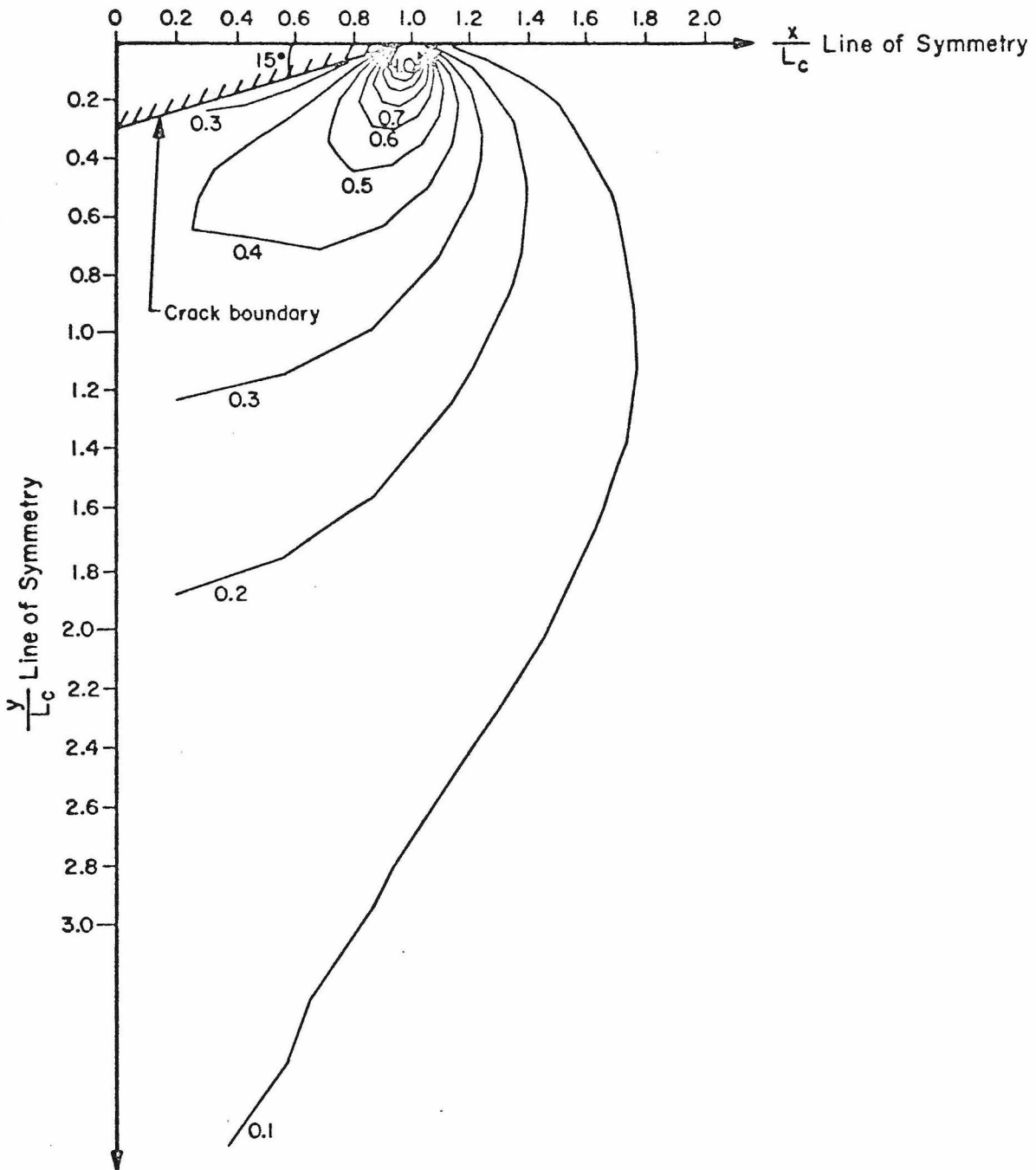
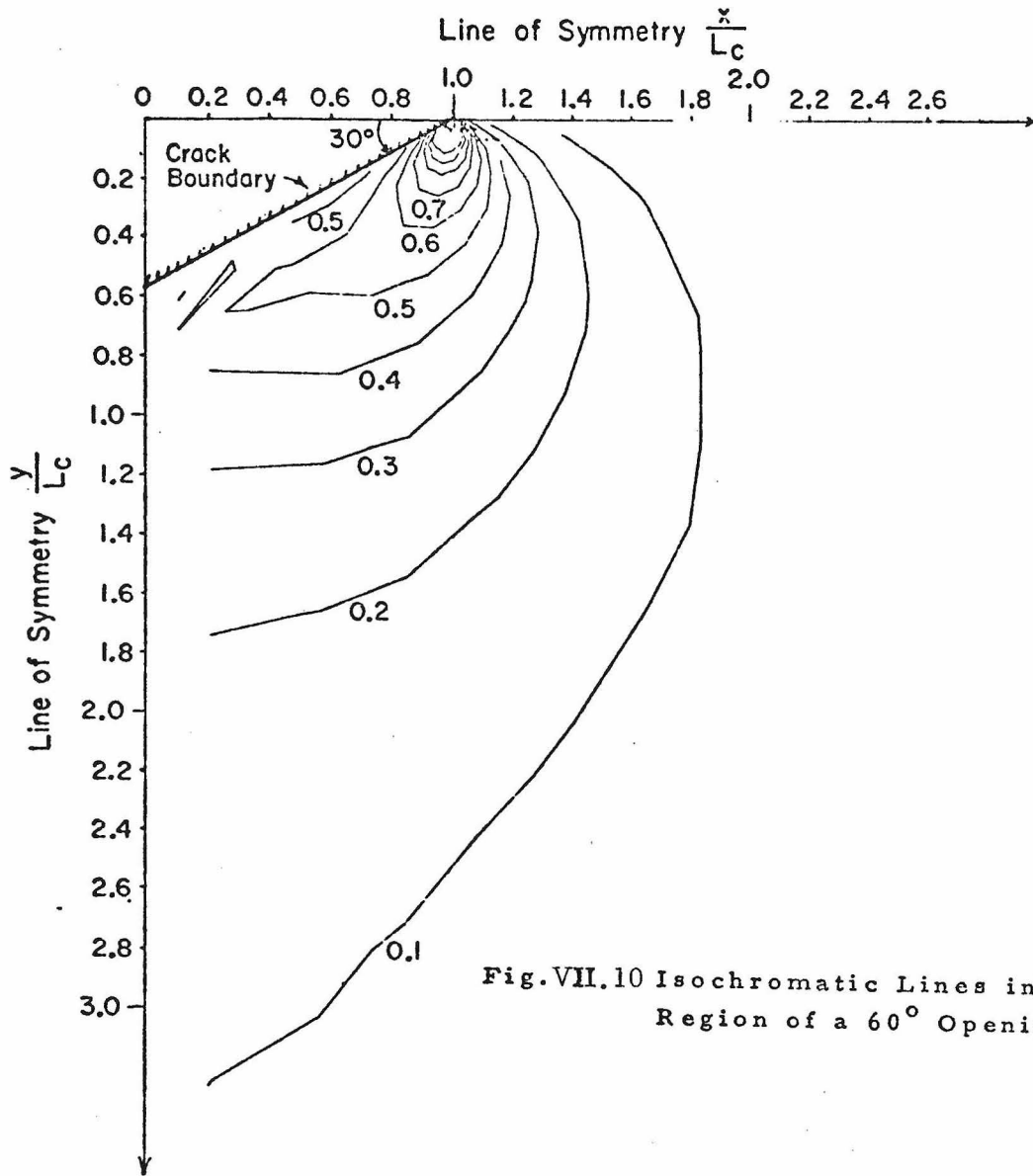Fig. VII. 9   Isochromatic Lines in 1/4
Region of a 30° Opening Crack.

Fig.VII.10 Isochromatic Lines in 1/4
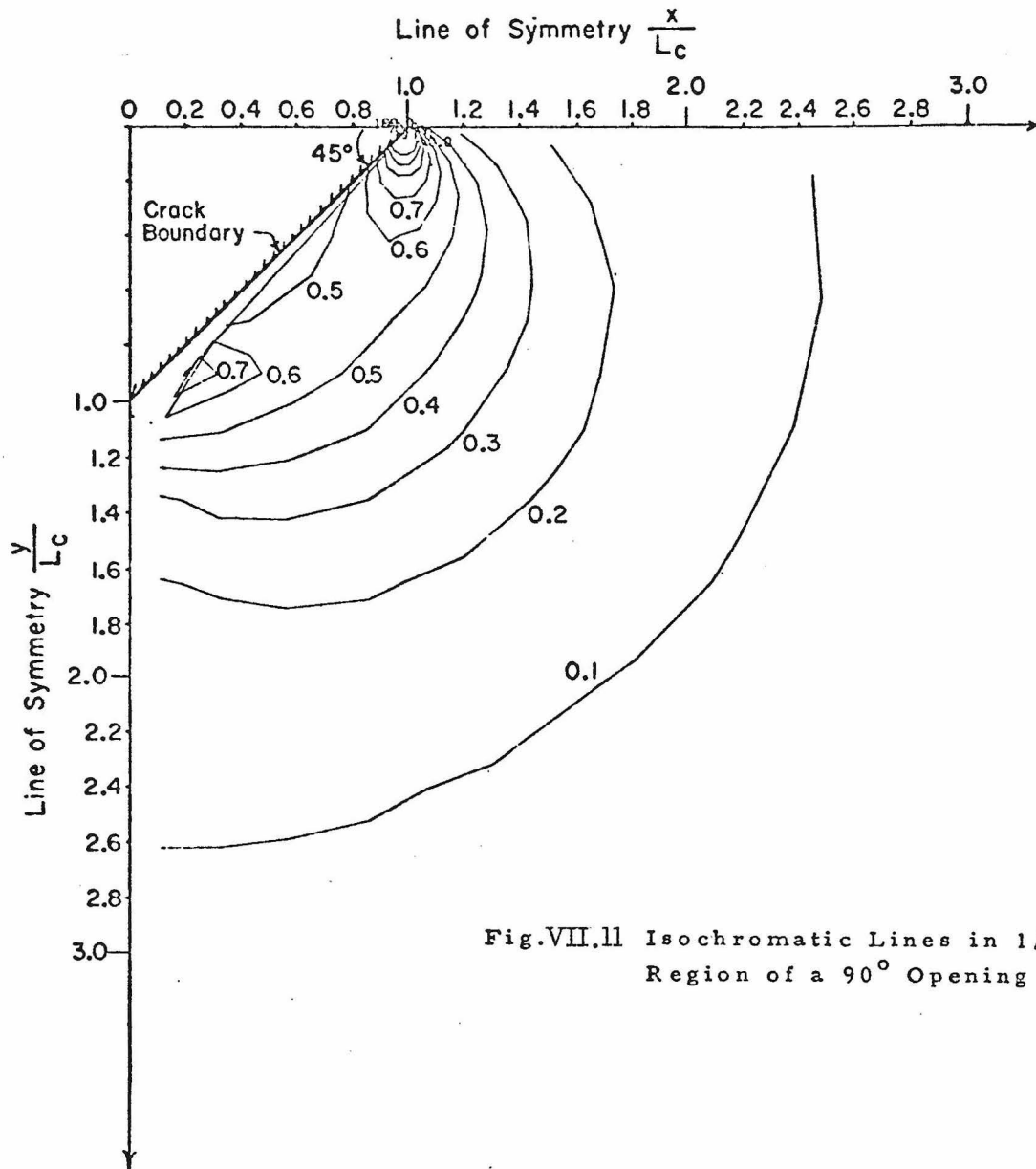Region of a 60° Opening Crack.

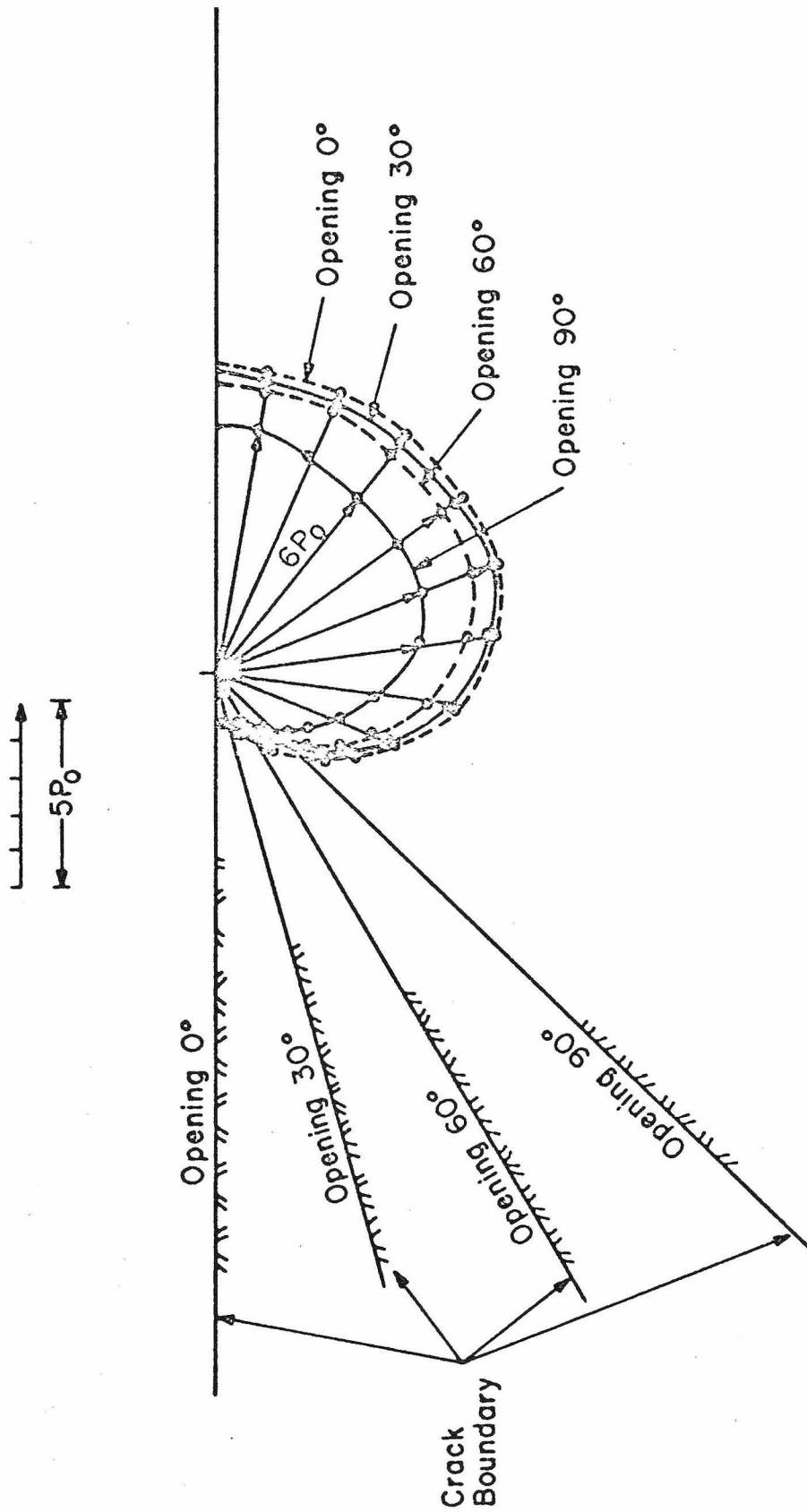Fig.VII.11 Isochromatic Lines in 1/4
Region of a 90° Opening Crack.

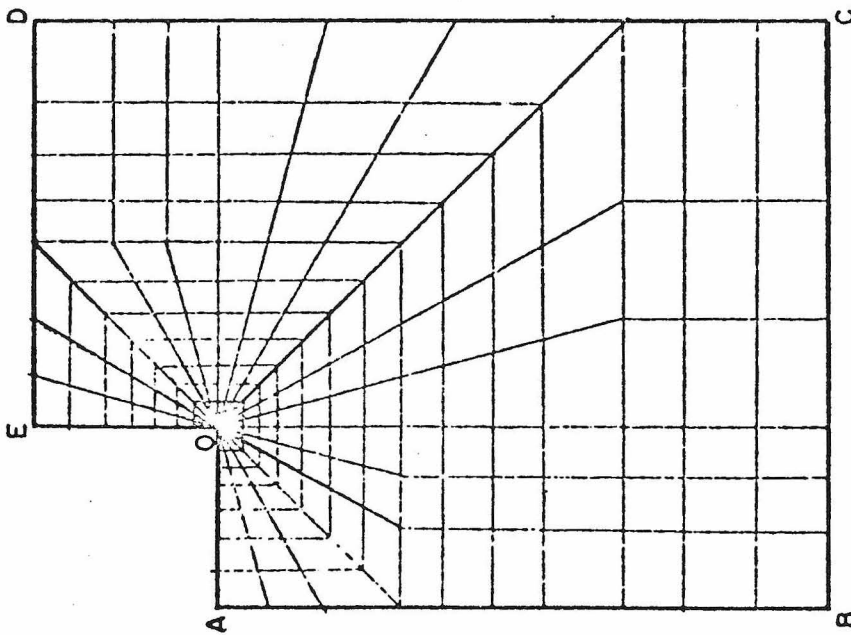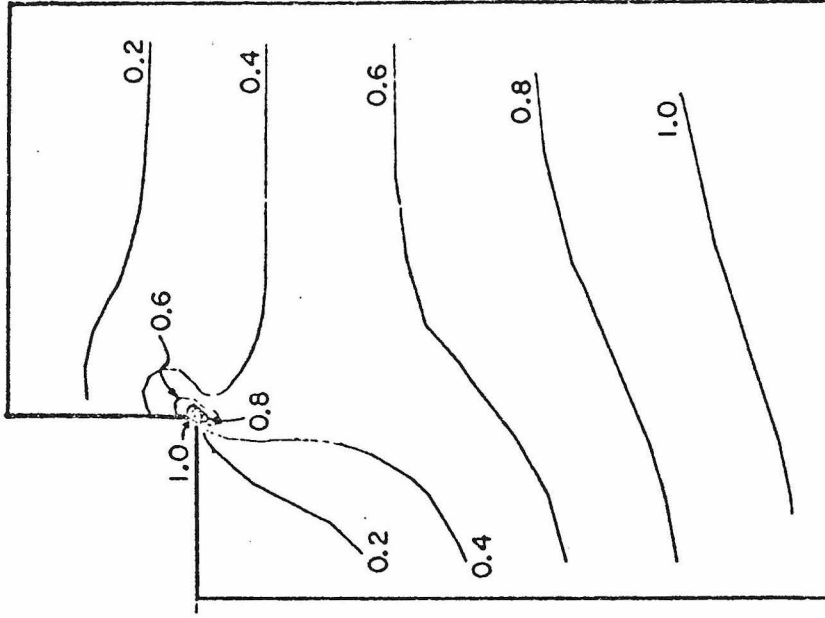Fig. VII.12 Major Principal Stress Distri-
bution in Corner Elements
Around Tips of Cracks with
Various Opening Angles.
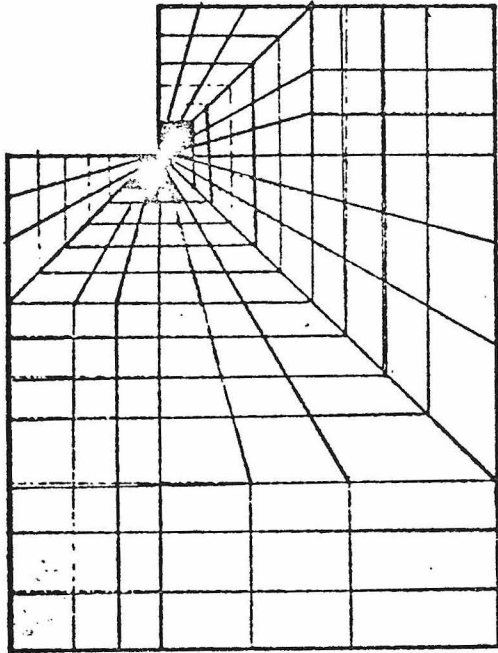
No. of Elements = 228
No. of Nodal points = 263
$E = 2 \times 10^7$ psf
$\nu = 0.3$

$\overline{OA} = EO = 90$ ft
$\overline{AB} = 300$ ft
$\overline{BC} = 290$ ft
$\overline{CD} = 390$ ft
$\overline{DE} = 200$ ft

Boundary conditions
Along $\overline{AB}$ and $\overline{CD}$:
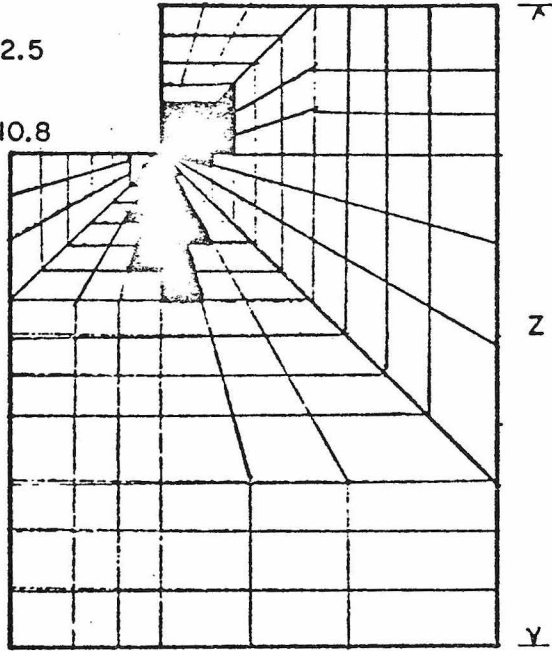   No horizontal disp.
Along $\overline{BC}$: No vertical disp.

(b) Isochromatic Lines

(a) Finite Element Configuration

Fig. VII.13 Finite Element Configuration
and Stress Distribution in a 90°
Slope Under Gravity.

$$\frac{\gamma H}{c} = 2.5$$

$$\frac{\gamma Z}{c} = 10.8$$

(a) Linear Solution

$$(n = 0.1, \ \nu = 0.45, \ \frac{\gamma Z_c}{c} = 9.53)$$

(b) Bilinear Solution

$$(n = 0.1, \ \nu = 0.45, \ \frac{\gamma Z_c}{c} = 9.53)$$
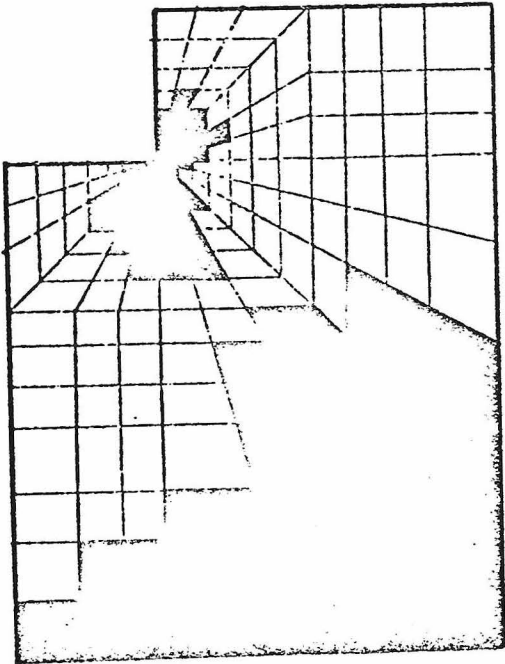
$$\frac{\gamma H}{c} = 3.5$$

$$\frac{\gamma Z}{c} = 15.2$$

Fig.VII.14 Development of Failure in a 90°
Slope with Various S_f Values
for $\phi = 0°$ Case.

$$\frac{\gamma H}{c} = 3.5$$

$$\frac{\gamma Z}{c} = 15.2$$

(a) Linear Solution
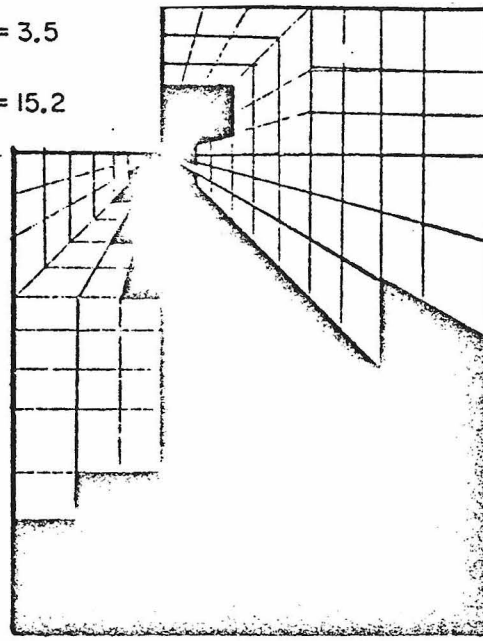
$(n = 0.1, \ \nu = 0.4, \ \frac{\gamma Z c}{c} = 15.5)$

(b) Bilinear Solution

$(n = 0.1, \ \nu = 0.4, \ \frac{\gamma Z c}{c} = 15.5)$

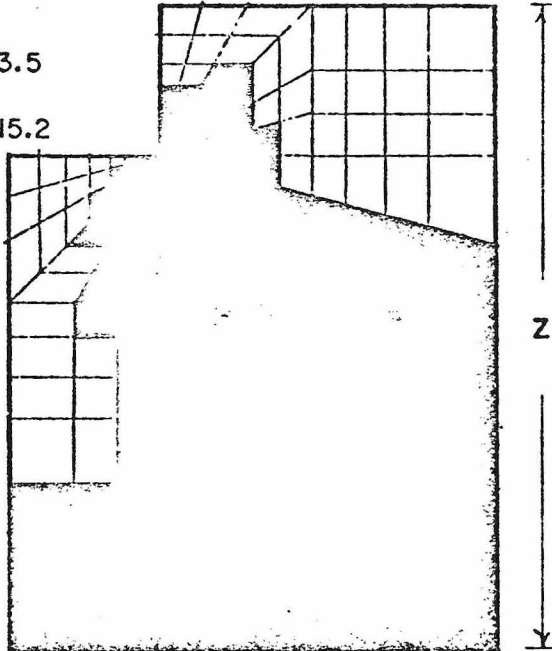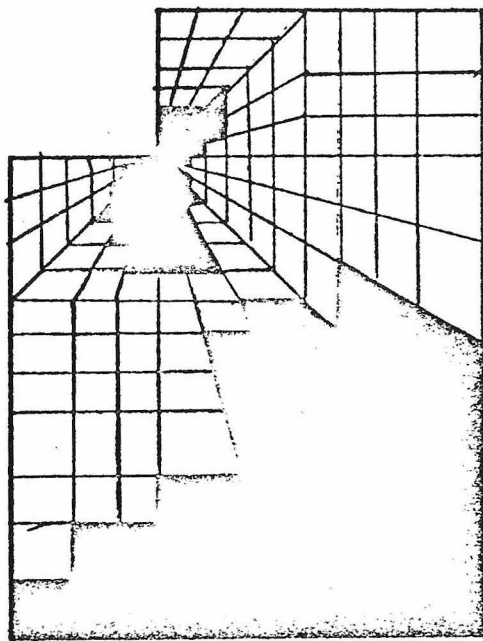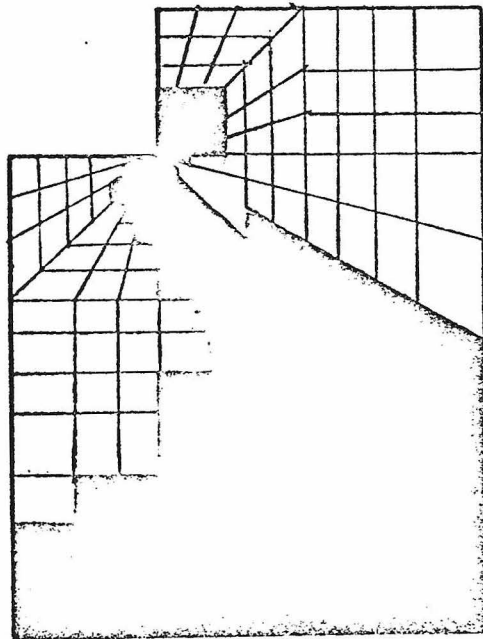$$\frac{\gamma H}{c} = 4.5$$

$$\frac{\gamma Z}{c} = 19.5$$
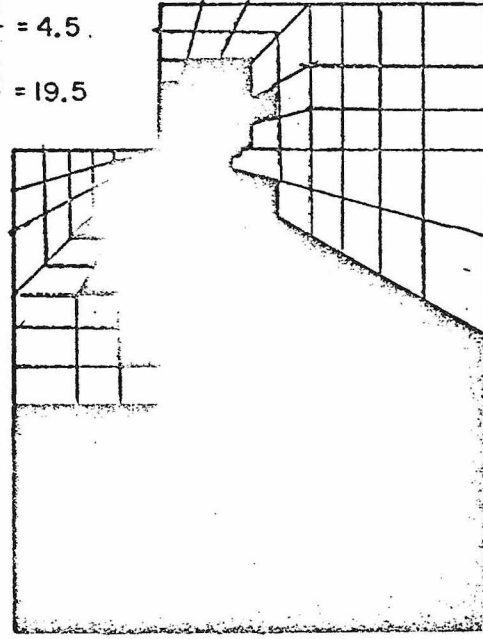
Fig. VII.15 Development of Failure in a 90° Slope with Various S_f Values for $\phi = 10^0$ Case.

(a) Linear Solution
(n = 0.1, ν = 0.4)
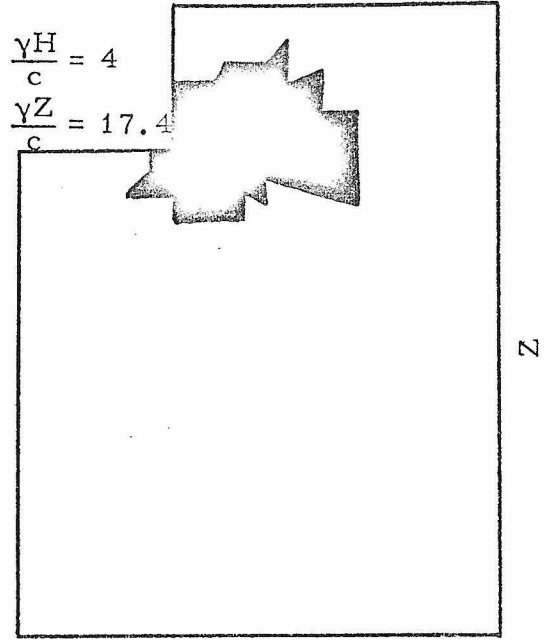
(b) Bilinear Solution
(n = 1, ν = 0.4)

$$\frac{\gamma H}{c} = 4$$

$$\frac{\gamma Z}{c} = 17.4$$

$$\frac{\gamma H}{c} = 5.5$$

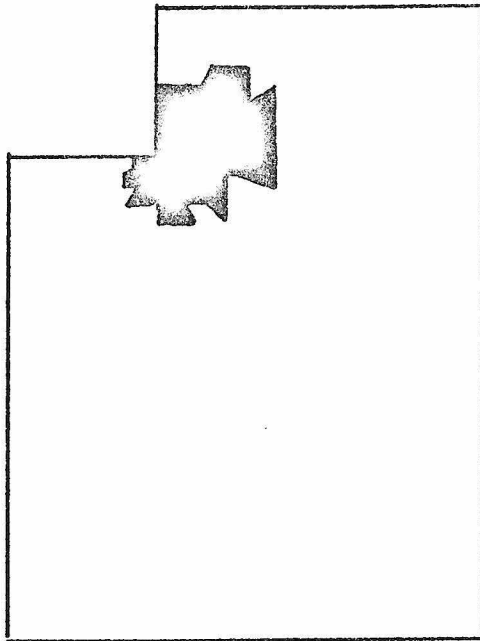$$\frac{\gamma Z}{c} = 23.9$$
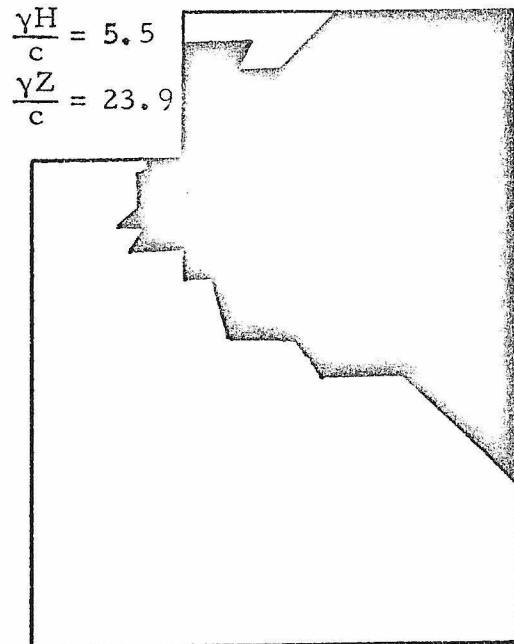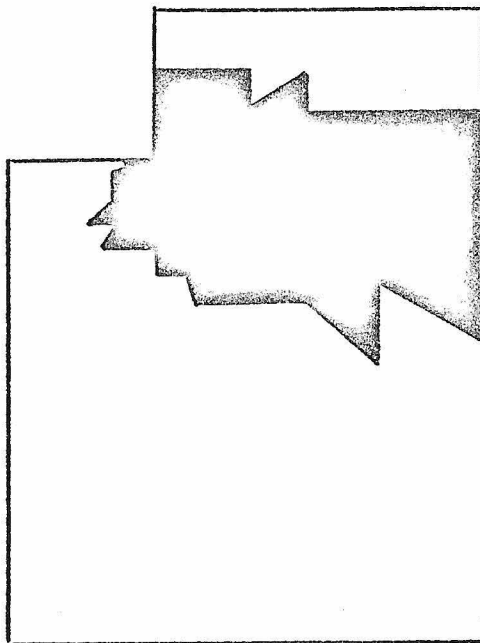
Note: Ratio of yield stress at bottom boundary to yield stress at ground surface = 6.

Fig. VII.16. Development of Failure in a 90° Non-homogeneous Slope with Various s_f Values for $\phi = 0°$ Case

REFERENCES

1. Timoshenko, S., and Goodier, J. N., Theory of Elasticity, McGraw Hill, New York, 1951.

2. Terzaghi, K., Theoretical Soil Mechanics, John Wiley and Sons, New York, 1943.

3. Drucker, D. C., "Some Implications of the Work-hardening and Ideal Plasticity," Q. Appl. Math., vol. 7, 1950.

4. Biot, M. A., "Theory of Deformation of a Porous Visco-Elastic Anisotropic Solid," Jour. Applied Physics, vol. 27, 1956.

5. Shield, R. T., "Mixed Boundary Value Problems in Soil Mechanics," Q. Applied Math., vol. 11, 1953.

6. Drucker, D. C., Gibson, R. E. and Henkel, D. J., "Soil Mechanics and Work-hardening Theories of Plasticity," Trans. ASCE, vol. 122, 1957.

7. Drucker, D. C., "A Definition of Stable Inelastic Material," Jour. Applied Mech., Series E, vol. 26, 1959.

8. Holubec, I., "Elastic Behavior of Cohesionless Soils," Jour. of Soil Mech. and Found. Eng., ASCE, SM5, vol. 94, 1968.

9. Chang, T. Y., Ko, H. Y., Scott, R. F. and Westmann, R. A., "An Integrated Approach to Stress Analysis of Granular Materials," Calif. Inst. of Tech. Soil Mechanics Lab. Report, 1967.

10. Smith, I. M., and Kay, S., "Stress Analysis of Contractive or Dilative Soil," Jour. Soil Mech. and Found. Div., ASCE, SM7, vol. 97, July 1971.

11. Scott, R. F., Principles of Soil Mechanics, Addison-Wesley, Reading, Mass., 1963.

12. Whitman, R. V. and Miller, E. T., "Yielding and Locking of Confined Sand," Jour. Soil Mech. and Found. Div., ASCE, SM4, vol. 90, 1964.

13. Reynolds, O., "On the Dilatancy of Media Composed of Rigid Particles in Contact," Phil. Mag. Series 5, vol. 20, pp. 469, 885.

14. Scott, R. F. and Ko, H. Y., "Deformation of Sand in Shear," Jour. of Soil Mech. and Found. Eng., ASCE, SM5, vol. 93, 1967.

15. Bell, J. M., "Stress-Strain Characteristics of Cohesionless Granular Material Subjected to Statically Applied Homogeneous Loads in an Open System," Ph.D. Thesis, Calif. Inst. of Tech., Pasadena, Calif., 1965.

16. Ko, H. Y., "Static Stress-Deformation Characteristics of Sand," Ph.D. Thesis, Calif. Inst. of Tech., Pasadena, Calif., 1966.

17. Masson, R. M., "Non-linear Characterization and Stress Analysis in a Granular Material," University of Colorado, Boulder, Colorado, 1971.

18. Iwan, W. D., "A Distributed-Element Model for Hysteresis and Its Steady-State Dynamic Response," Jour. of Applied Mech., vol. 33, No. 4, Trans. ASME, vol. 88, Series E, pp. 893-900, Dec. 1966.

19. Iwan, W. D., "On a Class of Models for the Yielding Behavior of Continuous and Composite Systems," Jour. Applied Mech., Paper No. 67-APM-S, Sept. 1967.

20. Wilson, E. L., "Finite Element Analysis of Two-Dimensional Structures," Ph.D. Thesis, Univ. of Calif., Berkeley, Calif., 1963.

21. Brown, C. B. and King, I. P., "Automatic Embankment Analysis: Equilibrium and Instability Conditions," Geotechnique, vol. 16, Sept. 1966.

22. Dunlop, P. and Duncan, J., "Development of Failure Around the Excavated Slope," Jour. of Soil Mech. and Found. Div., ASCE, SM2, vol. 96, 1970.

23. Sneddon, I. N., "The Distribution of Stress in the Neighborhood of a Crack in an Elastic Solid," Proc. Roy. Soc., Series A, 187, 1946.

24. Sneddon, I. N. and Lowengrub, M., Crack Problems in the Classical Theory of Elasticity, John Wiley and Sons, New York, 1969.

25. Barden L. and Khayat, A. J., "Incremental Stress-strain Relations for Sand," Research Report No. 5, Dept. of Civil Eng., Univ. of Manchester, March 1968.

26. Frydman, S., "The Effect of Stress History on the Stress-deformation Behavior of Sand," M.S. Thesis, Israel Inst. of Tech., Haifa, Israel, Jan. 1968.

27. Scott, R. F. and Ko, H. Y., "Stress-deformation and Strength Characteristics," Proc. 7th Int. Conf. Soil Mech. and Found. Engrg., State of the Art Report, pp. 1-47, Mexico, 1969.

28. Slichter, G. S., "Theoretical Investigation of the Motion of Ground Water," U.S. Geol. Survey, 19th Annual Report, 1899.

29. Smith, W. O., Foote, P. D. and Busang, P. E., "Packing of Homogeneous Spheres," Phys. Rev., vol. 34, pp. 1271-1274, 1929.

30. Filep, L., "Egyen lo gombokbol allo halmazok," Vizugyi Kozlemenyek, Budapest, 1936.

31. Mindlin, R. D. and Deresiewicz, H., "Elastic Spheres in Contact under Various Oblique Forces," Jour. Appl. Mech., vol. 20, pp. 327-344, 1953.

32. Iida, K., "Velocity of Elastic Waves in a Granular Substance," Bull. Earthquake Res. Inst., Japan, vol. 17, pp. 738-808, 1939.

33. Takahashi, T. and Sato, Y., "On the Theory of Elastic Waves in Granular Substance," Bull. Earthquake Res. Inst., Japan, vol. 28, pp. 37-43, 1950.

34. Gassmann, F., "Elastic Waves Through a Packing of Spheres," Geophysics, vol. 16, pp. 673-685, 1951.

35. Mindlin, R. D., "Compliance of Elastic Bodies in Contact," Jour. of Applied Mech., vol. 16, pp. 259-268, 1949.

36. Lubkin, J. L., "The Torsion of Elastic Spheres in Contact," Jour. of Applied Mech., vol. 18, pp. 183-187, 1951.

37. Mindlin, R. D., Mason, W. P., Osner, T. F. and Deresiewicz, H., "Effect of an Oscillating Tangential Force on the Contact Surface of Elastic Spheres," Proc. 1st U.S. Nat. Cong. of Applied Mech., pp. 203-208, 1951.

38. Mindlin, R. D., "Mechanics of Granular Media," Proc. 2nd U.S. Nat. Cong. of Applied Mech., pp. 13-20, Ann Arbor, 1954.

39. Duffy, J., and Mindlin, R. D., "Stress-Strain Relations and Vibrations of a Granular Medium," Jour. of Applied Mechanics, vol. 24, pp. 583-593, 1957.

40. Deresiewiez, H., "Stress–Strain Relations for a Simple Model of a Granular Medium," Jour. of Applied Mech., vol. 25, pp. 402-406, 1958.

41. Thurston, C. W. and Deresiewicz, H., "Analysis of Compression Test of a Face-Centered Cubic Array of Elastic Spheres," Jour. of Applied Mech., vol. 26, pp. 251-258, 1959.

42. Ko, H. Y. and Scott, R. F., "Deformation of Sand in Hydrostatic Compression," Jour. Soil Mech. and Found. Div., ASCE, SM3, vol. 93, March 1967.

43. Gudehus, G., "Rheological and Statistical Models for Dry Granular Materials," Vortrage and Diskussionen anlaβlich eines Colloquium uber das Stoffverhatten Korniger Medien, pp. 41-54, Karlsrube, 1970.

44. Horne, M. R., "The Behavior of an Assembly of Rotund, Rigid, Cohesionless Particles," Part I and II, Proc. Roy. Soc., Series A, vol. 286, pp. 62-87, 1965.

45. Neuber, H., "Beitrage zur Statistchen Mechanik der Lockerund Festgesteine," Fortschr. Geol. Rheinld. u. Westf., vol. 15, pp. 181-244, 1968.

46. Murayama, S., "A Theoretical Consideration on a Behavior of Sand," Rheology and Soil Mechanics, IUTAM Sum., pp. 146-159, Grenoble, 1964.

47. Hess, M. S. and Stoll, R. D., "Interparticle Sliding in Granular Materials," Research Report No. 1, The Donald M. Burmister Lab. of Soil Mech., Columbia Univ., N. Y., 1966.

48. Litwiniszyn, J., "New Theoretical and Experimental Research in the Mechanics of Loose Bodies Treated as Media Characterized by Stochastic Equation," Rev. Appl. Mech., vol. 6, pp. 255-262, 1961.

49. Litwiniszyn, J., "An Application of Random Walk Argument to the Mechanics of Granular Media," Rheology and Soil Mech. Symp., IUTAM, pp. 81-89, Grenoble, 1964.

50. Marsal, R. J., "Stochastic Processes in the Grain Skeleton of Soils," Proc. 6th Int. Conf. Soil Mech. and Found. Engrg., vol. 1, pp. 303-307, Toronto, Canada, 1965.

51. Smottczyk, H. D., "Stress Computation in Soil Media," Jour. of Soil Mech. and Found. Div., ASCE, SM2, vol. 93, pp. 101-124, 1967.

52. Marsal, R. J., "Suelos Granulares: Modelo Estadistico Teoria de Fally Y Relaciones Esfuerzo-Deformacion," Research Report, Inst. de Ing., Uni. Nacional Automoma de Mexico, Mexico City, July 1971.

53. Winterkorn, H. F., "Macromeritic Liquids," ASTM Symposium on Dynamic Testing of Soils, Special Tech. Pub. No. 156, pp. 77-89, 1953.

54. Kezdi, A., "Contribution to the Investigations of Granular Systems," Rheology and Soil Mechanics Symp., IUTAM, pp. 165-178, Grenoble, 1964.

55. Rowe, P. W., "The Stress-Dilatancy Relation for Static Equilibrium of an Assembly of Particles in Contact," Proc. Roy. Soc., Series A, vol. 269, pp. 500-527, 1962.

56. Rowe, P. W., "Stress-Dilatancy, Earth Pressure and Slopes," Jour. Soil Mech. and Found. Div., ASCE, vol. 89, pp. 37-61, 1963.
    Discussions by: 1. Gibson, R. E. and Morgenstein, N., Jour. of Soil Mech. and Found. Div., ASCE, vol. 89, pp. 127-128, 1963.
    2. Trollope and Parkin, Jour. of Soil Mech. and Found. Div., ASCE, vol. 89, p. 129, 1963.
    3. Scott, Jour. of Soil Mech. and Found. Div., vol. 90, pp. 133-135, 1964.
    4. Roscoe and Schofield, Jour. of Soil Mech. and Found. Div., ASCE, vol. 90, pp. 136-, 1964.

57. Horne, M. R., "The Behavior of an Assembly of Rotund, Rigid, Cohesionless Particles," Part III, Proc. Roy. Soc., Series A, vol. 90, pp. 21-34, 1969.

58. Barden, L. and Khayatt, A. J., "Incremental Strain Ratio and Strength of Sand in the Triaxial Test," Geotechnique, vol. 16, pp. 338-357, 1966.

59. Lee, K. L. and Seed, H. B., "Drained Strength Characteristics of Sands," Jour. of Soil Mech. and Found. Div., ASCE, SM6, vol. 93, 1967.

60. Zienkiewicz, O. C., The Finite Element Method in Engineering Sciences, McGraw-Hill, London, 1971.

61. Clough, R. W. and Woodward, R. J., "Analysis of Embankment Stresses and Deformations," Jour. of Soil Mech. and Found. Div., ASCE, vol. 93, pp. 529-549, 1967.

62. Girijavallabham, C. V. and Reese, R. C., "Finite Element Method for Problems in Soil Mechanics," Jour. of Soil Mechanics and Found. Div., ASCE, vol. 93, pp. 94, pp. 473-496, 1968.

63. Proc. Symp. on Applications of Finite Element Method in Geotechnical Engrg., U.S. Army Engr. Waterway Experiment Station, Vicksburg, Miss., 1972.

64. Duncan, J. M. and Chang, C. Y., "Nonlinear Analysis of Stress and Strain in Soils," Jour. of Soil Mech. and Found. Div., ASCE, vol. 96, pp. 1629-1653, 1970.

65. Konder, R. L. and Zelasko, J. S., "A Hyperbolic Stress-Strain Formulation for Sands," Proc. 2nd Pan-Am. Conf. on Soil Mech. and Found. Engrg., vol. VI, pp. 289-324, Brazil, 1963.

66. Sternberg, E., "Nonlinear Theory of Elasticity with Small Strain Deformation," Trans., ASME, vol. 68, part 2, pp. A53-A60, 1946.

67. Eringen, A. L., Nonlinear Theory of Continuous Media, McGraw-Hill, New York, 1962.

68. Drucker, D. C., Introduction to Mechanics of Deformable Solids, McGraw-Hill, New York, 1967.

69. Ko, H. Y. and Scott, R. F., "Deformation of Sand at Failure," Jour. of Soil Mech. and Found. Div., ASCE, vol. 94, pp. 883-898, 1968.

70. Ko, H. Y. and Scott, R. F., "A New Soil Testing Apparatus," Geotechnique, vol. 17, pp. 40-57, 1967.

71. Meissner, von H., "Nichtlinears Kraft-Verformungs-verhalten Zylindrischer Korper uns Rolligen Erdstoff," Veroffentlichungen, Heft 45, Int. Bodenmech. Felsmech., Univ. Fridericiana, Harlsruke, 1971.

72. Chang, T. Y., "A Polynomial Plasticity Law of Granular Soils Under Loading Condition," TRW System Paper No. 67-3341.1-198, Los Angeles, Nov. 1967.

73. Coon, M. D. and Evans, R. J., "Recoverable Deformation of Cohesionless Soils," Jour. of Soil Mech. and Found. Div., ASCE, vol. 97, pp. 375-391, 1971.

74. Truesdell, C., "Hypo-elasticity," Jour. Rat. Mech. Analysis, vol. 4, No. 83, pp. 83-133 and pp. 1019-1020, 1955.

75. Bernstein, B., "Hypoelasticity and Elasticity," Arch. Rat. Mech. Analysis, vol. 6, No. 90, pp. 90-104, 1960.

76. Hill, R., Mathematical Theory of Plasticity, Oxford University Press, London, 1950.

77. Reuss, A., "Beruchsichtigung der elastieschen Formanderung in der Plastizitatstheorie," Zeits. angew. Math. Mechanik, vol. 10, pp. 266-274, 1930.

78. Drucker, D. C. and Pragev, W., "Soil Mechanics and Plasticity Analysis for Limited Design," Quarterly of App. Math., vol. 10, No. 2, pp. 157-165, 1952.

79. Shield, R. T., "Mixed Boundary Value Problem in Soil Mechanics," Jour. of Math. Physics of Solids, vol. 4, pp. 144-156, 1955.

80. Drucker, D. C., "Limit Analysis of Two and Three Dimensional Soil Mechanics Problems," Jour. of the Mech. and Phy. of Solids, vol. 1, pp. 217-226, 1953.

81. Shield, R. T., "Stress and Velocity Field in Soil Mechanics," Jour. of Math. Phy., vol. 33, pp. 144-156, 1954.

82. Shield, R. T., "On Coulomb's Law of Failure in Solids," Jour. of the Mech. and Phy. of Solids, vol. 4, pp. 10-16, 1955.

83. Prager, W., Introduction to Plasticity, Addison-Wesley, Reading, Mass., 1959.

84. Paul, B., "A Modification of the Coulomb-Mohr Theory of Fracture," Jour. of App. Mech., vol. 28, pp. 258-268, 1961.

85. Haythornthwaite, R. M., "Range of Yield Condition in Ideal Plasticity," Trans., ASCE, vol. 127, part I, pp. 1252-1267, 1962.

86. Paul, B., "Generalized Pyramidal Fracture and Yield Criteria," Int. Jour. of Solid and Mech., vol. 4, pp. 175-196, 1968.

87. Bishop, A. W., "The Strength of Soils as Engineering Materials," Sixth Rankine Lecture, Geotechnique, vol. 16, 1966.

88. Drucker, D. C., "A More Fundamental Approach to Plastic Stress-Strain Relations," Proc. 1st U.S. National Congress of Applied Mech., ASME, pp. 487-491, 1962.

89. Drucker, D. C., Gibson, R. E. and Henkel, D. C., "Soil Mechanics and Work-hardening Theories of Plasticity," <u>Trans.</u>, ASCE, vol. 122, pp. 338-346, 1957.

90. Roscoe, K. H. and Schofield, A. N., "Mechanical Behavior of an Idealized "Wet Clay"," Proc. European Conf. Soil Mech., vol. 1, pp. 47-54, Wiesbaden, 1963.

91. Roscoe, K. H., Schofield, A. N. and Thurrairajah, A., "Yielding of Clays Wetter than Critical," <u>Geotechnique</u>, vol. 13, pp. 211-240, 1963.

92. Nelson, J., Baron, M. L. and Sandler, I., "Mathematical Models for Geological Materials for Wave Propagation Studies," Proc. 17th Sagamore Army Materials Research Conf. on Shock Waves and Mechanical Properties of Solids, Sept. 1970.

93. Baron, M. L., Nelson, I. and Sandler, I., "Investigation of Air Induced Ground Shock Effect Resulting from Various Explosive Sources - Report 2 - Influence of Constitutive Models on Ground Motion Predictions," Report 5-71-10, Contract DA CA 39-69-0022, Paul Weidlinger, Consulting Engineer, U.S. Army Waterways Experimental Station, Vicksburg, Miss., 1971.

94. Koiter, W. T., "Stress-strain Relations, Uniqueness and Variational Theorems for Elastic-Plastic Materials with a Singular Yield Surface," <u>Quar. of Applied Math.</u>, vol. XI, no. 3, pp. 350-354, 1963.

95. Prager, W., "The Theory of Plasticity: A Survey of Recent Achievements," (James Clayton Lecture), Proc. of the Inst. of Mech. Engrg., London, vol. 169, p. 41, 1955.

96. Weidler, J. B. and Paslay, P. R., "Constitutive Relations for Inelastic Granular Medium," <u>Jour. of Engrg. Mech. Div.</u>, ASCE, vol. 96, EM4, pp. 395-406, Aug. 1970.

97. Weidler, J. B. and Paslay, P. R., "Analytical Description of Behavior of Granular Media," <u>Jour. of Engrg. Mech. Div.</u>, ASCE, vol. 95, EM3, April 1969.

98. de Jong, G. de J., Response to Roscoe's Discussion on de Jong's Paper, "Lower Bound Collapse Theorem and Lack of Normality of Strain Rate to Yield Surface for Soils," IUTAM Symp. on Rheology and Soil Mech., Grenoble, 1964.

99. de Jong, G de J., "Lower Bound Collapse Theorem and Lack of Normality of Strain Rate to Yield Surface for Soils," IUTAM Symp. on Rheology and Soil Mech., Grenoble, 1964.

100. Weidler, J. B., "The Flow Behavior of Sand at Failure," Brown University, Div. of Engrg. Report ARPA E59, August, 1968.

101. Poorooshasb, H. B., Holubec, I. and Sherbourne, A. N., "Yielding and Flow of Sand in Triaxial Compression," Canadian Geotechnical Jour., vol. 3, pp. 178-190, 1966.

102. Barden, L. and Khayatt, A. J., "Incremental Strain Rate Ratios and Strength of Sand in the Triaxial Test," Geotechnique, vol. 16, pp. 338-357, 1966.

103. Paslay, P. R. and Weidler, J. B., "Analysis of Triaxial Test for Granular Soils," Jour. of Engrg. Mech. Div., ASCE, EM5, pp. 587-609, June 1969.

104. Smoltezyk, H. V., Written Contribution to Proc. 5th Int. Conf. Soil Mech. and Found. Engrg., vol. III, p. 137, Paris, 1961.

105. Brown, E. H., "A Theory for the Mechanical Behavior of Sand," Proc. 11th Int. Cong. of Applied Mech. (Henry Gurtler, ed.), Munich, 1964.

106. Palmer, A. C., "Stress-strain Relation for Soils," Brown University Technical Report GP1115/19, Providence, 1965.

107. Chang, J. Y., "On Elasto-Plastic Constitutive Relations of Soil," TRW System, Paper No. 68-3341.3-47, April 1968, Los Angeles, Calif.

108. Wells, C. H., and Paslay, P. R., "A Small-Strain Plasticity Theory for Planar Slip Material," Jour. of Applied Mech., Paper No. 69-APM-4, March 1969.

109. Yandell, W. O., "The Effect of Repeated Rolling of Elasto-plastic Roads," Australian Road Research, vol. 3, No. 7, Sept. 1968.

110. Yandell, W. O., "Prediction of the Behavior of Elasto-plastic Roads During Repeated Rolling Using the Mechano-Lattice Analogy," Highway Research Record, No. 374, 1971.

111. Lu, T. D., A Theoretical Study on the Problems of Slope Stability, Soil Mechanics Series No. 10, Duke University, 1967.

112. Sternberg, E. and Koiter, W. T., "The Wedge Under a Concentrated Couple: A Paradox in Two-Dimensional Theory of Elasticity," Trans., Jour. of Applied Mechanics, ASME, 1958.

113. Silverman, I. K., "Approximate Stress Functions for Triangular Wedges," Jour. of Applied Mechanics, ASME, 1955.

114. Irwin, G. R., Fracture Mechanics, ONR First Symposium on Naval Structural Mechanics, New York, Pergamon Press, 1958.

115. Zienkiewicz, O. C. and Cheung, Y. K., The Finite Element Method in Structural and Continuum Mechanics, McGraw-Hill, New York and London, 1967.

116. Drucker, P. C. and Prager, W., "Soil Mechanics and Plastic Analysis or Limited Design," Q. App. Math., vol. 10, pp. 157-165, 1952.

117. Zienkiewicz, O. C., Valliappan, S. and King, I. P., "Elasto-Plastic Solutions of Engineering Problems 'Initial Stress,' Finite Element Approach," Inter. Jour. for Numerical Methods in Engineering, vol. 1, 1969.

118. Westmann, R. A., "Pressurized Star Crack," Jour. Math. Phys., vol. 43, 1965.

119. Williams, M. L., "The Stresses Around a Fault or Crack in Dissimilar Media," Bull. Seismo. Soc. Amer., vol. 49, 1959.

120. Perlman, A. B. and Sih, G. C., "Elastostatic Problems of Curvelinear Cracks in Bonded Dissimilar Material," Int. Jour. Engrg. Sciences, vol. 5, 1967.

121. Goodman, L. E. and Brown, C. B., "Dead Load Stresses and the Instability of Slopes," Jour. of Soil Mech. and Found. Engrg., ASCE, vol. 89, SM3, 1963.

122. Richards, R. Jr. and Schmid, W. E., "Body-Force Stresses in Gravity Structures," Jour. of Soil Mech. and Found. Engrg., ASCE, vol. 94, SM1, 1968.

123. Lorenz, H., Neumeuer, H. and Gudehus, G., "Test Concerning Compaction and Displacements Performed on Samples of Sand in the State of Plane Deformation," Proc. 6th Int. Conf. Soil Mech. and Found. Engrg., vol. 4, pp. 293-297, 1965.

124. Hambly, E. C., "A New True Triaxial Apparatus, Tech. Note, Geotechnique, vol. 19, 1969.